ISSN 2500-316X (Online)

RUSSIAN TECHNOLOGICAL JOURNAL

РОССИЙСКИЙ ТЕХНОЛОГИЧЕСКИЙ ЖУРНАЛ

Information systems.
Computer sciences.
Issues of information security

Multiple robots (robotic centers) and systems.
Remote sensing and nondestructive testing

Modern radio engineering and telecommunication systems

Micro- and nanoelectronics.
Condensed matter physics

Analytical instrument engineering and technology

Mathematical modeling

Economics of knowledge-intensive and high-tech enterprises and industries.
Management in organizational systems

Product quality management. Standardization

Philosophical foundations of technology and society

12+
www.rtj-mirea.ru

13(1) 2025

ISSN 2500-316X (Online)

RUSSIAN TECHNOLOGICAL JOURNAL

РОССИЙСКИЙ ТЕХНОЛОГИЧЕСКИЙ ЖУРНАЛ

- Information systems. Computer sciences. Issues of information security
- Multiple robots (robotic centers) and systems. Remote sensing and nondestructive testing
- Modern radio engineering and telecommunication systems
- Micro- and nanoelectronics. Condensed matter physics
- Analytical instrument engineering and technology
- Mathematical modeling
- Economics of knowledge-intensive and high-tech enterprises and industries. Management in organizational systems
- Product quality management. Standardization
- Philosophical foundations of technology and society

- Информационные системы. Информатика. Проблемы информационной безопасности
- Роботизированные комплексы и системы. Технологии дистанционного зондирования и неразрушающего контроля
- Современные радиотехнические и телекоммуникационные системы
- Микро- и наноэлектроника. Физика конденсированного состояния
- Аналитическое приборостроение и технологии
- Математическое моделирование
- Экономика наукоемких и высокотехнологичных предприятий и производств. Управление в организационных системах
- Управление качеством продукции. Стандартизация
- Мировоззренческие основы технологии и общества

Russian Technological Journal
2025, Vol. 13, No. 1

Russian Technological Journal
2025, том 13, № 1

https://www.rtj-mirea.ru

https://doi.org/10.32362/2500-316X

ISSN 2500-316X (Online)

Russian Technological Journal
2025, Vol. 13, No. 1

Publication date January 30, 2025.

The peer-reviewed scientific and technical journal highlights the issues of complex development of radio engineering, telecommunication and information systems, electronics and informatics, as well as the results of fundamental and applied interdisciplinary researches, technological and economical developments aimed at the development and improvement of the modern technological base.

Periodicity: bimonthly.
The journal was founded in December 2013. The titles were «Herald of MSTU MIREA» until 2016 (ISSN 2313-5026) and «Rossiiskii tekhnologicheskii zhurnal» from January 2016 until July 2021 (ISSN 2500-316X).

Founder and Publisher:
Federal State Budget
Educational Institution of Higher Education
«MIREA – Russian Technological University»
78, Vernadskogo pr., Moscow, 119454 Russia.

The journal is included into the List of peer-reviewed science press of the State Commission for Academic Degrees and Titles of Russian Federation. The Journal is included in Russian Science Citation Index (RSCI), Russian State Library (RSL), Science Index, eLibrary, Directory of Open Access Journals (DOAJ), Directory of Open Access Scholarly Resources (ROAD), Google Scholar, Ulrich's International Periodicals Directory.

The registration number ПИ № ФС 77 - 81733 was issued in August 19, 2021 by the Federal Service for Supervision of Communications, Information Technology, and Mass Media of Russia.

The subscription index of *Pressa Rossii*: **79641**.

Russian Technological Journal
2025, том 13, № 1

Дата опубликования 30 января 2025 г.

Научно-технический рецензируемый журнал освещает вопросы комплексного развития радиотехнических, телекоммуникационных и информационных систем, электроники и информатики, а также результаты фундаментальных и прикладных междисциплинарных исследований, технологических и организационно-экономических разработок, направленных на развитие и совершенствование современной технологической базы.

Периодичность: один раз в два месяца.
Журнал основан в декабре 2013 года. До 2016 г. издавался под названием «Вестник МГТУ МИРЭА» (ISSN 2313-5026), а с января 2016 г. по июль 2021 г. под названием «Российский технологический журнал» (ISSN 2500-316X).

Учредитель и издатель:
федеральное государственное бюджетное образовательное учреждение высшего образования «МИРЭА – Российский технологический университет»
119454, РФ, г. Москва, пр-т Вернадского, д. 78.

Журнал входит в Перечень ведущих рецензируемых научных журналов ВАК РФ, в которых должны быть опубликованы основные научные результаты диссертаций на соискание ученой степени кандидата наук и доктора наук, входит в RSCI, РГБ, РИНЦ, eLibrary, Directory of Open Access Journals (DOAJ), Directory of Open Access Scholarly Resources (ROAD), Google Scholar, Ulrich's International Periodicals Directory.

Регистрационный номер и дата принятия решения о регистрации СМИ ПИ № ФС 77 - 81733 от 19.08.2021 г. СМИ зарегистрировано Федеральной службой по надзору в сфере связи, информационных технологий и массовых коммуникаций (Роскомнадзор).

Индекс по объединенному каталогу «Пресса России» **79641**.

https://www.rtj-mirea.ru

Editorial Board

Редакционная коллегия

Contents

Содержание

Information systems. Computer sciences. Issues of information security
Информационные системы. Информатика. Проблемы информационной безопасности

UDC 621.311.1
https://doi.org/10.32362/2500-316X-2025-13-1-7-15
EDN DUNSTG

RESEARCH ARTICLE

Improving Smart Grid security: Spectral and fractal analysis as tools for detecting cyberattacks

Sergey V. Kochergin [@], Svetlana V. Artemova, Anatoly A. Bakaev, Evgeny S. Mityakov, Zhanna G. Vegera, Elena A. Maksimova

MIREA – Russian Technological University, Moscow, 119454 Russia
[@] Corresponding author, e-mail: kochergin_s@mirea.ru

Abstract

Objectives. Cyberattacks are major potential sources of disturbances in modern electrical networks (Smart Grid). However, distinguishing between the various kinds of harmonic distortions and malicious interventions can be challenging. The objective of this work is to develop an effective tool for detecting and quantifying the differences between harmonic and anomalous signals. This will permit the identification of cyberattacks associated with harmonic signal distortions to provide a more accurate classification of patterns characteristic of malicious impacts.

Methods. A comparative analysis of various anomaly detection methods was conducted, including fractal analysis, multifractal analysis, Shannon entropy calculation, and power spectral density (PSD) analysis.

Results. Harmonic distortions and anomalous signals caused by cyberattacks may share similar fractal and multifractal characteristics, making it harder to distinguish between them. The use of the Shannon entropy method does not fully capture the complexity and uncertainty of harmonic and anomalous signals. To gain a deeper understanding of the nature of these signals, a comprehensive approach was applied, including analysis of their frequency characteristics and the use of other uncertainty assessment methods, such as multifractal analysis and PSD. Use of the PSD method revealed significant differences in energy distribution between these signals, permitting a more accurate identification of cyberattacks.

Conclusions. For the effective detection of cyberattacks associated with harmonic signal distortions in power systems, a comprehensive approach is required, including time series analysis, frequency analysis, and machine learning methods. This approach not only detects anomalies in signals but also provides their quantitative assessment to improve the accuracy of classifying malicious impacts. The integration of these methods enhances the reliability and security of power systems, making them less vulnerable to cyberattacks.

Keywords: Smart Grid, harmonic distortion, cyberattacks, multifractal analysis, spectral power density (PSD), anomaly detection

• **Submitted:** 12.09.2024 • **Revised:** 15.11.2024 • **Accepted:** 03.12.2024

For citation: Kochergin S.V., Artemova S.V., Bakaev A.A., Mityakov E.S., Vegera Zh.G., Maksimova E.A. Improving Smart Grid security: Spectral and fractal analysis as tools for detecting cyberattacks. *Russian Technological Journal.* 2025;13(1):7–15. https://doi.org/10.32362/2500-316X-2025-13-1-7-15, https://elibrary.ru/DUNSTG

Financial disclosure: The authors have no financial or proprietary interest in any material or method mentioned.

The authors declare no conflicts of interest.

НАУЧНАЯ СТАТЬЯ

Повышение безопасности смарт-сетей: спектральный и фрактальный анализ как инструменты выявления кибератак

С.В. Кочергин [@],
С.В. Артемова,
А.А. Бакаев,
Е.С. Митяков,
Ж.Г. Вегера,
Е.А. Максимова

МИРЭА – Российский технологический университет, Москва, 119454 Россия
[@] Автор для переписки, e-mail: kochergin_s@mirea.ru

Резюме

Цели. В статье рассматриваются гармонические искажения и кибератаки как основные источники нарушений в смарт-сетях (Smart Grid). Цель работы – разработка эффективного инструмента для выявления и численной оценки различий между гармоническими и аномальными сигналами, что позволит обнаруживать кибератаки, связанные с искажением гармонических сигналов, и для более точной классификации паттернов, характерных для вредоносных воздействий.

Методы. Проведен сравнительный анализ различных методов обнаружения аномалий, таких как фрактальный анализ, мультифрактальный анализ, расчет энтропии Шеннона и плотности спектральной мощности (power spectral density, PSD).

Результаты. Полученные результаты показывают, что гармонические искажения и аномальные сигналы, вызванные кибератаками, обладают схожими фрактальными и мультифрактальными характеристиками, что затрудняет их различение. Использование метода энтропии Шеннона не позволило в полной мере оценить сложность и неопределенность гармонических и аномальных сигналов. Для более глубокого понимания природы этих сигналов был применен комплексный подход, включающий анализ их частотных характеристик и применение других методов оценки неопределенности, таких как мультифрактальный анализ и метод PSD. В результате метод PSD выявил значительные различия в распределении энергии между этими сигналами, что позволяет более точно идентифицировать кибератаки.

Выводы. Для эффективного обнаружения кибератак, связанных с искажением гармонических сигналов в энергетических системах, необходим комплексный подход, включающий методы анализа временных рядов, частотный анализ и методы машинного обучения. Такой подход позволяет не только выявлять аномалии в сигналах, но и проводить их численную оценку, что повышает точность классификации вредоносных воздействий. Интеграция этих методов обеспечивает повышение надежности и безопасности энергетических систем, делая их менее уязвимыми к кибератакам.

Ключевые слова: Smart Grid, гармонические искажения, кибератаки, мультифрактальный анализ, спектральная плотность мощности, обнаружение аномалий

• **Поступила:** 12.09.2024 • **Доработана:** 15.11.2024 • **Принята к опубликованию:** 03.12.2024

Для цитирования: Кочергин С.В., Артемова С.В., Бакаев А.А., Митяков Е.С., Вегера Ж.Г., Максимова Е.А. Повышение безопасности смарт-сетей: спектральный и фрактальный анализ как инструменты выявления кибератак. *Russian Technological Journal*. 2025;13(1):7–15. https://doi.org/10.32362/2500-316X-2025-13-1-7-15, https://elibrary.ru/DUNSTG

Прозрачность финансовой деятельности: Авторы не имеют финансовой заинтересованности в представленных материалах или методах.

Авторы заявляют об отсутствии конфликта интересов.

INTRODUCTION

Today's cyber threats pose a serious risk to smart energy grids, known as smart grids. These threats include malware attacks, phishing, DDoS[1] attacks and targeted cyber operations aimed at disrupting critical elements of the energy infrastructure. As a result of its combination of traditional power systems with digital information and communication technologies, Smart Grid technology becomes more susceptible to various threats. With the growing number of cyberattacks, ensuring Smart Grid security becomes a priority for maintaining the stability and security of the power system [1–6].

A characteristic feature of modern power supply is the presence of a large number of consumers with nonlinear power supplies, which cause distortion of the sinusoidal characteristic of voltage and current. This leads to negative consequences, worsening the quality of electrical energy, causing additional losses, and in some cases resulting in various resonance phenomena [7–9]. Moreover, cyberattacks on the electric grid can masquerade as natural distortions and thus remain undetected. This complicates the process of detecting such anomalies, making it much more difficult to identify and distinguish cyberattacks from normal operating modes and posing a serious threat to the overall stability and security of the electric grid.

STUDY AND CLASSIFICATION OF HARMONIC DISTORTION AND ANOMALOUS SIGNALS IN THE CONTEXT OF CYBERSECURITY

In order to implement the research, an artificial dataset was created, including 100 electrical signals with harmonic distortions (depicted by a solid line in Fig. 1) caused by the operation of nonlinear power supplies predominantly characterized by harmonic multiples of three (inverters, power supplies, etc.). 100 signals with random anomalous distortions were additionally created, whose main characteristics are random bursts (in Fig. 1 depicted by a dashed line) distinguishable from repetitive signals of natural origin.

Anomalous distortions differ from harmonic distortions not only in terms of their shape, but also the nature of changes; however, their unpredictable and chaotic nature also complicates their detection and classification. As can be seen from the diagram (Fig. 1), while both signals have similar elements, the anomalous distortion is more pronounced and can differ significantly in amplitude and phase from harmonic distortion.

Due to the fact that harmonic distortions in electrical networks often demonstrate complex dynamics and self-similarity, we will evaluate these signals using fractal methods.

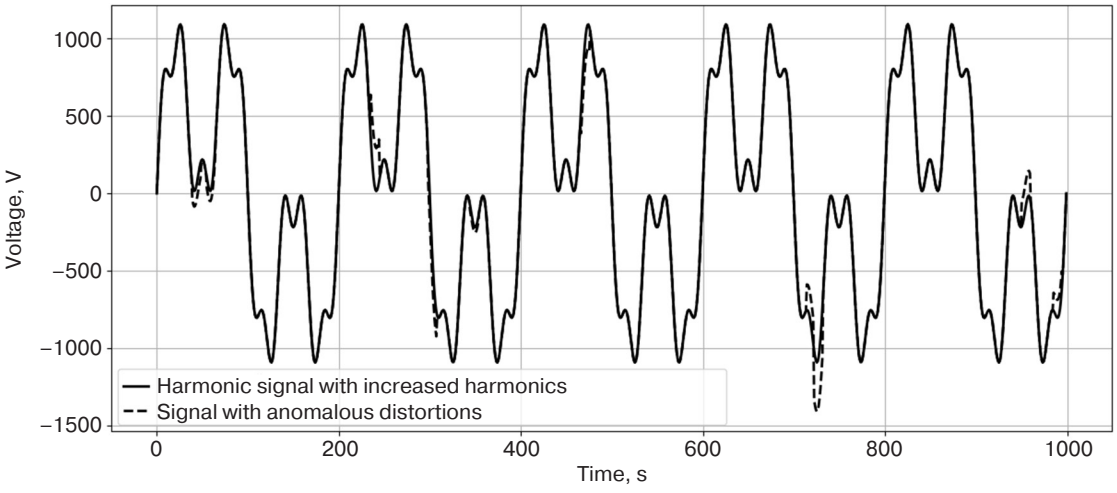

Fig. 1. Comparison of harmonic signal and signal with anomalies

[1] Distributed denial of service is a distributed attack that creates a load on the server and leads to a system failure.

Let us calculate the fractal dimension and the Hurst coefficient, which together allow us to quantify the degree of complexity, self-similarity and correlation structure of the signal. One of the most common methods for determining the fractal dimension is the box-counting method [10]. For a one-dimensional time series, the fractal dimension D is determined by the following formula:

$$D = \lim_{\varepsilon \to 0} \frac{\ln N(\varepsilon)}{\ln(1/\varepsilon)}, \quad (1)$$

where $N(\varepsilon)$ is the number of boxes (segments of length ε) required to cover the entire signal curve.

The Hurst coefficient H is an important fractal parameter that characterizes the degree of long-term dependence and correlation in the signal. It is calculated by the formula:

$$H = \frac{\ln(R/S)}{\ln n}, \quad (2)$$

where R is the range of the accumulated deviation of the signal from the average value; S is the standard deviation; n is the sample size.

The results of calculating (Table) fractal characteristics for harmonic and anomalous signals shows that both types of signals have similar values of both fractal dimensionality and Hurst coefficient. The average value of the Hurst coefficient for the anomalous signals was found to be slightly higher, which may indicate a more pronounced autocorrelation or "memorization" in these signals compared to the harmonic signals. However, this difference is minimal and may be insufficient for a clear distinction between the two types of signals.

The analysis of fractal dimensionality showed that both types of signals have similar values, indicating that they have a similar structure on small scales. This can complicate the task of distinguishing between harmonic and anomalous distortions on the basis of fractal parameters alone.

Table. Comparison of fractal characteristics for harmonic and anomalous signals

Parameter	Type of the signal	Average value
Hurst coefficient	Harmonic signals	0.643
	Anomalous signals	0.652
Fractal dimension	Harmonic signals	0.988
	Anomalous signals	0.988

The results of the study show that, despite the differences in the nature of the signals, their fractal characteristics turned out to be very similar, making it difficult to distinguish them accurately. For a more accurate classification of anomalous and harmonic distortions, it is necessary to conduct a multifractal analysis [11, 12]. The choice of multifractal spectrum is explained by its ability to more deeply characterize complex and heterogeneous signal structures, which are not sufficiently described by traditional monofractal methods.

The performed calculation of the multifractal spectrum resulted in the dependence (Fig. 2), which displays the Hurst exponent $H(q)$ as a function of the scaling parameter q.

In order to achieve this goal, the signal was decomposed into sub-bands using different values of the scaling parameter q, which is related to the signal moments. In the decomposition process, a generalized cumulative function $Z(q, s)$ was calculated according to the definition:

$$Z(q,s) = \sum_{i=1}^{N_s} |X(i,s)|^q, \quad (3)$$

where $X(i, s)$ represents the amplitude of the signal on the scale s, while N_s is the number of elements on this scale.

A scale transformation was performed for each value of q to calculate the dependence of the cumulative function $Z(q, s)$ on the scale s. It was found that for signals with multifractal properties this dependence follows a power law:

$$Z(q,s) \sim s^{\tau(q)}, \quad (4)$$

where $\tau(q)$ is a spectral function describing multifractal characteristics of the signal.

As a result, the values of the Hurst index $H(q)$ were calculated for each value of q using the ratio:

$$H(q) = \frac{\tau(q)}{q}. \quad (5)$$

The results of multifractal analysis (Fig. 2) show that the complexity spectra of harmonic and anomalous signals are very similar, including at different scales. Thus, although the nature of these signals is different, the similarity of their multifractal properties limits the ability to use multifractal analysis to distinguish between harmonic and anomalous signals.

In order to more accurately classify and identify the differences between these types of signals, it becomes necessary to use additional analysis methods. One such

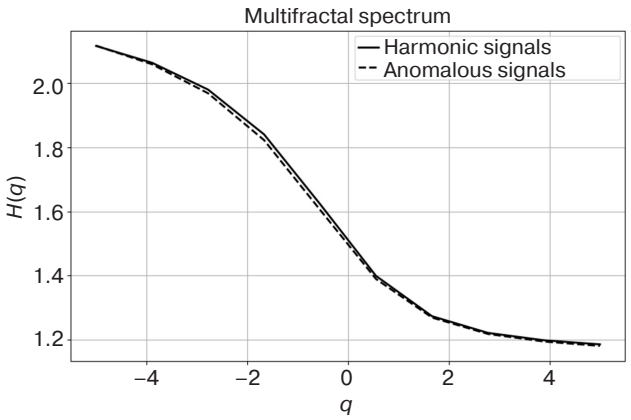

Fig. 2. Dependence of the Hurst index on the scaling parameter

method is Shannon entropy [13, 14], which was chosen for further study due to its ability to quantify the level of uncertainty and complexity in a system. The possibility of using Shannon entropy to analyze the changes in the probability distribution of different events associated with a signal makes it particularly useful in the study of signals with anomalies. In the context of electrical networks, this method can reveal hidden anomalies or instabilities that go undetected when using only multifractal analysis.

In order to compare harmonic and anomalous signals, the Shannon entropy estimation method is used to measure the level of uncertainty in the signal. Shannon entropy H, which shows how uniformly distributed the signal values are, can be calculated by the formula:

$$H = -\sum_{i=1}^{n} p(x_i) \lg p(x_i), \quad (6)$$

where $p(x_i)$ is the probability that the signal takes the value x_i, while n is the number of possible values of the signal.

The diagram (Fig. 3) shows the distribution of Shannon entropy values for two types of signals: harmonic (green color, lines) and anomalous (red color). The frequency f on the ordinate axis shows how often different values of entropy H occur in the data sample. Harmonic signals are characterized by entropy values concentrated in a narrow range around ~5.2 to form a high and narrow peak on the histogram. This indicates a high degree of orderliness and predictability of harmonic signals as reflected in their stable and relatively low entropy values.

In contrast, anomalous signals have a wider entropy distribution, which ranges from 5 to ~5.4 and is combined with a lower and fuzzier peak. This indicates greater randomness and disorder in their structure, resulting in increased entropic variation. The partial overlap of the distributions of harmonic and anomalous signals confirms that some anomalous signals have entropy similar to that of harmonic signals.

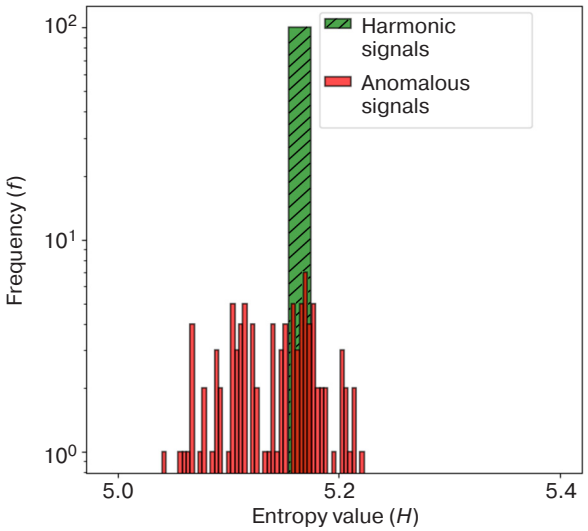

Fig. 3. Shannon entropy (logarithmic scale)

While Shannon entropy provides important information about the degree of uncertainty in a signal, a full understanding of the nature of harmonic and anomalous signals also requires an analysis of their frequency characteristics.

The described method for calculating the power spectral density (PSD) [15, 16] was used in this work to identify key frequency characteristics of signals. This method is suitable for detecting hidden periodicities and anomalies that may remain undetected when analyzing only the temporal characteristics of the signal.

The PSD method gives a more complete picture of the spectral structure of signals by analyzing the energy distribution over frequencies. This is important for differentiation of harmonic and anomalous signals, especially when dealing with complex time series. The application of PSD enables not only qualitative but also quantitative assessment of differences between signals, thus providing more accurate classification and detection of hidden anomalies.

PSD was calculated using the Welch method [17], an improved power spectrum estimation approach that reduces noise by splitting the signal into overlapping segments and averaging their spectra.

The power spectral density $P(\omega)$ of the signals was calculated using the following formula:

$$P(\omega) = \frac{1}{N} \sum_{k=1}^{N} |X_k(\omega)|^2, \quad (7)$$

where ω is the frequency; $X_k(\omega)$ is the discrete Fourier transform of the kth segment of the signal; N is the number of segments.

The Welch method is used to determine the power spectrum more accurately. The signal is divided into several parts, which may overlap. Then Fourier

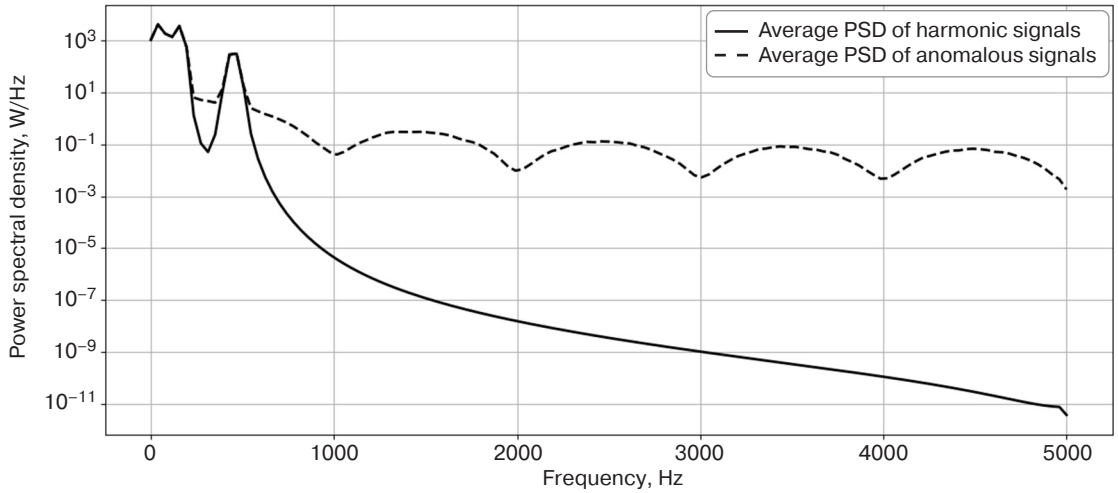

Fig. 4. Comparison of PSD distribution of harmonic and anomalous signals

transform is applied to each part. The average of the power spectra of all segments is then calculated. This reduces the influence of random noise and increases the stability of the estimation:

$$P_{\text{Welch}}(\omega) = \frac{1}{M}\sum_{m=1}^{M} P_m(\omega), \quad (8)$$

where M is the number of segments; $P_m(\omega)$ is the power spectral density for the mth segment.

Figure 4 compares the power spectral density distribution of harmonic and anomalous signals. At low frequencies, harmonic signals show a more concentrated energy distribution. Anomalous signals are characterized by a wider spectrum.

In order to further analyze the spectral characteristics and accurately evaluate the difference between harmonic and anomalous signals, it is necessary to calculate the integral energy of the signals. The integral energy of a signal, which is defined as the area under the PSD curve, serves as a quantitative measure of the total energy distributed across frequencies. It can provide additional insight into the differences between signal types.

The integral energy of the signal E is calculated by integrating the PSD values $P(\omega)$ over the entire frequency range ω:

$$E = \int_{0}^{\omega_{\max}} P(\omega)d\omega, \quad (9)$$

where $\omega_{\max}$ is the maximum frequency up to which the integration is performed.

This transition to integral energy estimation not only reveals how energy is distributed across frequencies, but also quantifies the overall energy content of signals, which is essential to better understand their nature and permit their more accurate classification.

The results of power spectral density calculations revealed a significant difference in the energy distribution between anomalous and harmonic signals in the frequency range of 200–300 Hz. In particular, the energy in this range for the anomalous data was 224.53 units, which is significantly higher than the energy of the harmonic data (27.51 units). This difference indicates that there is a significant increase in energy in the anomalous data in the 200–300 Hz range, which may indicate the presence of additional frequency components or increased activity characteristic of anomalous signals.

The increase in energy can be caused by additional noise, non-harmonic components, or other factors that are not present in harmonic signals. This emphasizes the importance of frequency analysis, especially the PSD method, for detecting anomalies that may not be noticeable when analyzing signals in the time domain.

CONCLUSIONS

The results of this study demonstrate that the PSD method is an effective tool for identifying and numerically evaluating the differences between harmonic and anomalous signals. The described approach can be used to detect cyberattacks involving distortion of harmonic signals and more accurately classify patterns characteristic of malicious attacks. The application of this method can contribute to improved security and resilience of power systems, ensuring timely detection and neutralization of threats.

Authors' contributions

S.V. Kochergin—development of the main research concept, formulation of key aims and objectives, conducting a literature review in the relevant field, preparation of research materials, and coordination of experimental studies.

S.V. Artemova—development and optimization of the research methodology, conducting comparative analyses, and participation in editing and preparing the article.

A.A. Bakaev—determination of the research topic, coordination of result discussions, and final stages of article preparation.

E.S. Mityakov—analysis and interpretation of results, preparation of conclusions, and participation in data discussions.

Zh.G. Vegera—mathematical and statistical support, ensuring the accuracy of quantitative analysis methods, and data integrity verification.

E.A. Maksimova—exploration of existing anomaly detection methods and identification of the most promising approaches for comparative analysis.

REFERENCES

1. Ihsanov I.I. Security in the electric power industry: current threats and protective measures. In: *Youth and Knowledge – Guarantee of Success – 2023: Collection of Scientific Articles of the 10th International Youth Scientific Conference*. Kursk, September 19–20, 2023. Kursk: Universitetskaya kniga; 2023. V. 2. P. 472–474 (in Russ.). https://elibrary.ru/tfyddx
2. Papkov B.V., Osokin L.V., Kuchin N.N. Cyber security of distribution facilities electrical networks. *Sel'skii mekhanizator = Selskiy Mechanizator*. 2024;5:3–7 (in Russ.). https://elibrary.ru/tfmvhi
3. Kolosok I.N., Korkina E.S. Analysis of cybersecurity of power facilities taking into account the mechanism and kinetics of undesirable processes. *Energetik*. 2024;2:3–8 (in Russ.). http://doi.org/10.34831/EP.2024.60.27.001, https://elibrary.ru/ecxvjp
4. Abdrakhmanov I.I. Dangers and threats to cybersecurity in the electric power industry: analysis of modern threats and protection mechanisms. *Nauchnyi Aspekt*. 2024;31(3):3970–3973 (in Russ.). https://elibrary.ru/lrouni
5. Gurina L.A. Assessment of cyber resilience of the operational dispatch control system of EPS. *Voprosy kiberbezopasnosti = Cybersecurity Issues*. 2022;3(49):23–31 (in Russ.). https://elibrary.ru/sapiyh
6. Gurina L.A., Aizenberg N.I. Search for an effective solution to protect microgrid community with interconnected information systems against cyber threats. *Voprosy kiberbezopasnosti = Cybersecurity Issues*. 2023;3(55):37–49 (in Russ.). https://www.elibrary.ru/qguytv
7. Semenov A.S., Bebikhov Yu.V., Egorov A.N., Fedorov O.V. Effect of higher harmonics on electric power quality in supply systems in mines. *Gornyi Zhurnal = Mining Journal*. 2024;2:84–91 (in Russ.). https://doi.org/10.17580/gzh.2024.02.14, https://www.elibrary.ru/nmssyq
8. Voronin M.S. The influence of higher harmonics in the power supply network of an enterprise on the quality of electricity. In: *Technologies, Machines and Equipment for the Design and Construction of Agricultural Facilities: collection of scientific articles of the 2nd International Scientific and Technical Conference of Young Scientists, Graduate Students, Masters and Bachelors.* Kursk: Universitetskaya kniga; 2024. P. 440–442 (in Russ.). https://www.elibrary.ru/wxelva
9. Ovechkin I.S., Puzina E.Yu. Development of technical solutions to reduce the distortion of the sinusoidal voltage curve of overhead lines supplying automatic blocking devices. *Sovremennye tekhnologii. Sistemnyi analiz. Modelirovanie = Modern Technologies. System Analysis. Modeling*. 2023;3(79):112–123 (in Russ.). https://www.elibrary.ru/smcqdv
10. Iannaccone P.M., Khokha M. *Fractal Geometry in Biological Systems: An Analytical Approach.* CRC Press; 1996. 366 p. ISBN 978-0-8493-7636-8.
11. Basarab M.A., Stroganov I.S. Anomaly detection in information processes based on multifractal analysis. *Voprosy kiberbezopasnosti = Cybersecurity Issues*. 2014;4(7):30–40 (in Russ.). https://www.elibrary.ru/tcssen
12. Shelukhin O.I., Pankrushin A.V. Detection of anomalous in real time by methods of multifractal analysis. *Nelineinyi mir = Nonlinear World*. 2016;14(2):72–82 (in Russ.). https://www.elibrary.ru/vtznth
13. Dobrovol'skii G.A., Todoriko O.A. Application of Shannon entropy for voice activity detection in noisy sound recordings. *Vestnik Khersonskogo natsional'nogo tekhnicheskogo universiteta = Bulletin of the Kherson National Technical University.* 2016;3(58):218–223 (in Russ.). https://www.elibrary.ru/xdsiyx
14. Shannon K. *Raboty po teorii informatsii i kibernetike* (*Works on Information Theory and Cybernetics*). Moscow: IL; 1963. 829 p. (in Russ.).
15. Goldenberg L.M., Matyushkin B.D., Polyak M.N. *Tsifrovaya obrabotka signalov*: Spravochnik (*Digital Signal Processing*: Handbook). Moscow: Radio i svyaz'; 1985. 256 p. (in Russ.).
16. Bespalov A.D., Mishagin K.G. Calculation of the spectral power density of phase noise with the allocation of discrete spectral components. In: *Proceedings of the 26th Scientific Conference on Radiophysics dedicated to the 120th anniversary of M.T. Grekhova: Conference materials.* Nizhny Novgorod: N.I. Lobachevsky National Research Nizhny Novgorod State University; 2022. P. 208–211 (in Russ.). https://www.elibrary.ru/xwykrc
17. Welch P.D. The use of Fast Fourier Transform for the estimation of power spectra: A method based on time averaging over short, modified periodograms. *IEEE Transactions on Audio and Electroacoustics.* 1967;15(2):70–73. https://doi.org/10.1109/TAU.1967.1161901

СПИСОК ЛИТЕРАТУРЫ

1. Ихсанов И.И. Безопасность в электроэнергетике: актуальные угрозы и защитные меры. *Юность и знания – гарантия успеха –2023: Сборник научных статей 10-й Международной молодежной научной конференции*. Курск, 19–20 сентября 2023 года. Курск: Университетская книга; 2023. Т. 2. С. 472–474. https://elibrary.ru/tfyddx

2. Папков Б.В., Осокин Л.В., Кучин Н.Н. Кибербезопасность объектов распределительных электрических сетей. *Сельский механизатор*. 2024;5:3–7. https://elibrary.ru/tfmvhi
3. Колосок И.Н., Коркина Е.С. Анализ кибербезопасности объектов энергетики с учетом механизма и кинетики нежелательных процессов. *Энергетик*. 2024;2:3–8. http://doi.org/10.34831/EP.2024.60.27.001, https://elibrary.ru/ecxvjp
4. Абдрахманов И.И. Опасности и угрозы для кибербезопасности в электроэнергетике: анализ современных угроз и механизмов защиты. *Научный аспект*. 2024;31(3):3970–3973. https://elibrary.ru/lrouni
5. Гурина Л.А. Оценка киберустойчивости системы оперативно-диспетчерского управления ЭЭС. *Вопросы кибербезопасности*. 2022;3(49):23–31. https://elibrary.ru/sapiyh
6. Гурина Л.А., Айзенберг Н.И. Поиск эффективного решения по обеспечению защиты от киберугроз сообщества микросетей со взаимосвязанными информационными системами. *Вопросы кибербезопасности*. 2023;3(55):37–49. https://www.elibrary.ru/qguytv
7. Семенов А.С., Бебихов Ю.В., Егоров А.Н., Федоров О.В. Влияние высших гармоник на качество электроэнергии в системах электроснабжения горнодобывающих предприятий. *Горный журнал*. 2024;2:84–91. https://doi.org/10.17580/gzh.2024.02.14, https://www.elibrary.ru/nmssyq
8. Воронин М.С. Влияние высших гармоник в сети электроснабжения предприятия на качество электроэнергии. В сб.: *Технологии, машины и оборудование для проектирования, строительства объектов АПК: сборник научных статей 2-й Международной научно-технической конференции молодых ученых, аспирантов, магистров и бакалавров*. Курск: ЗАО «Университетская книга»; 2024. С. 440–442. https://www.elibrary.ru/wxelva
9. Овечкин И.С., Пузина Е.Ю. Разработка технических решений по уменьшению искажения синусоидальности кривой напряжения воздушных линий, питающих устройства автоблокировки. *Современные технологии. Системный анализ. Моделирование.* 2023;3(79):112–123. https://www.elibrary.ru/smcqdv
10. Iannaccone P.M., Khokha M. *Fractal Geometry in Biological Systems: An Analytical Approach.* CRC Press; 1996. 366 p. ISBN 978-0-8493-7636-8.
11. Басараб М.А., Строганов И.С. Обнаружение аномалий в информационных процессах на основе мультифрактального анализа. *Вопросы кибербезопасности*. 2014;4(7):30–40. https://www.elibrary.ru/tcssen
12. Шелухин О.И., Панкрушин А.В. Обнаружение аномальных выбросов в реальном масштабе времени методами мультифрактального анализа. *Нелинейный мир*. 2016;14(2):72–82. https://www.elibrary.ru/vtznth
13. Добровольский Г.А., Тодорико О.А. Использование энтропии Шеннона для детекции голосовой активности в зашумленных звукозаписях. *Вестник Херсонского национального технического университета*. 2016;3(58):218–223. https://www.elibrary.ru/xdsiyx
14. Шеннон К. *Работы по теории информации и кибернетике*. М.: ИЛ; 1963. 829 с.
15. Гольденберг Л.М., Матюшкин Б.Д., Поляк М.Н. *Цифровая обработка сигналов*: Справочник. М.: Радио и связь; 1985. 256 с.
16. Беспалов А.Д., Мишагин К.Г. Расчет спектральной плотности мощности фазового шума с выделением дискретных спектральных компонент. В: *Труды XXVI научной конференции по радиофизике, посвященной 120-летию М.Т. Греховой: Материалы конференции*. Нижний Новгород: Национальный исследовательский Нижегородский государственный университет им. Н.И. Лобачевского; 2022. С. 208–211. https://www.elibrary.ru/xwykrc
17. Welch P.D. The use of Fast Fourier Transform for the estimation of power spectra: A method based on time averaging over short, modified periodograms. *IEEE Transactions on Audio and Electroacoustics.* 1967;15(2):70–73. https://doi.org/10.1109/TAU.1967.1161901

About the authors

Sergey V. Kochergin, Cand. Sci. (Eng.), Associate Professor, Information Protection Department, Institute of Cybersecurity and Digital Technologies, MIREA – Russian Technological University (78, Vernadskogo pr., Moscow, 119454 Russia). E-mail: kochergin_s@mirea.ru. https://orcid.org/0000-0002-3598-8149

Svetlana V. Artemova, Dr. Sci. (Eng.), Associate Professor, Head of Information Protection Department, Institute of Cybersecurity and Digital Technologies, MIREA – Russian Technological University (78, Vernadskogo pr., Moscow, 119454 Russia). E-mail: artemova_s@mirea.ru. Scopus Author ID 6508256085, RSCI SPIN-code 3775-6241, https://orcid.org/0009-0006-8374-8197

Anatoly A. Bakaev, Dr. Sci. (Hist.), Cand. Sci. (Juri.), Associate Professor, Director of the Institute of Cybersecurity and Digital Technologies, MIREA – Russian Technological University (78, Vernadskogo pr., Moscow, 119454 Russia). E-mail: bakaev@mirea.ru. Scopus Author ID 57297341000, RSCI SPIN-code 5283-9148, https://orcid.org/0000-0002-9526-0117

Evgeny S. Mityakov, Dr. Sci. (Econ.), Professor, Acting Head of the Department "Subject-Oriented Information Systems," Institute of Cybersecurity and Digital Technologies, MIREA – Russian Technological University (78, Vernadskogo pr., Moscow, 119454 Russia). E-mail: mityakov@mirea.ru. Scopus Author ID 55960540500, RSCI SPIN-code 5691-8947, https://orcid.org/0000-0001-6579-0988

Zhanna G. Vegera, Cand. Sci. (Phys.-Math.), Associate Professor, Head of the Department of Higher Mathematics, Institute of Cybersecurity and Digital Technologies, MIREA – Russian Technological University (78, Vernadskogo pr., Moscow, 119454 Russia). E-mail: vegera@mirea.ru. Scopus Author ID 57212931836, RSCI SPIN-code 9076-5678, https://orcid.org/0000-0001-7312-3341

Elena A. Maksimova, Dr. Sci. (Phys.-Math.), Associate Professor, Head of Department "Intelligent Information Security Systems," Institute of Cybersecurity and Digital Technologies, MIREA – Russian Technological University (78, Vernadskogo pr., Moscow, 119454 Russia). E-mail: maksimova@mirea.ru. Scopus Author ID 57219701980, RSCI SPIN-code 6876-5558, https://orcid.org/0000-0001-8788-4256

Об авторах

Кочергин Сергей Валерьевич, к.т.н., доцент, кафедра КБ-1 «Защита информации», Институт кибербезопасности и цифровых технологий, ФГБОУ ВО «МИРЭА – Российский технологический университет» (119454, Россия, Москва, пр-т Вернадского, д. 78). E-mail: kochergin_s@mirea.ru, https://orcid.org/0000-0002-3598-8149

Артемова Светлана Валерьевна, д.т.н., доцент, заведующий кафедрой КБ-1 «Защита информации», Институт кибербезопасности и цифровых технологий, ФГБОУ ВО «МИРЭА – Российский технологический университет» (119454, Россия, Москва, пр-т Вернадского, д. 78). E-mail: artemova_s@mirea.ru. Scopus Author ID 6508256085, SPIN-код РИНЦ 3775-6241, https://orcid.org/0009-0006-8374-8197

Бакаев Анатолий Александрович, д.и.н., к.ю.н., доцент, директор Института кибербезопасности и цифровых технологий, ФГБОУ ВО «МИРЭА – Российский технологический университет» (119454, Россия, Москва, пр-т Вернадского, д. 78). E-mail: bakaev@mirea.ru. Scopus Author ID 57297341000, SPIN-код РИНЦ 5283-9148, https://orcid.org/0000-0002-9526-0117

Митяков Евгений Сергеевич, д.э.н., профессор, и.о. заведующего кафедрой КБ-9 «Предметно-ориентированные информационные системы», Институт кибербезопасности и цифровых технологий, ФГБОУ ВО «МИРЭА – Российский технологический университет» (119454, Россия, Москва, пр-т Вернадского, д. 78). E-mail: mityakov@mirea.ru. Scopus Author ID 55960540500, SPIN-код РИНЦ 5691-8947, https://orcid.org/0000-0001-6579-0988

Вегера Жанна Геннадьевна, к.ф.-м.н., доцент, заведующий кафедрой высшей математики, Институт кибербезопасности и цифровых технологий, ФГБОУ ВО «МИРЭА – Российский технологический университет» (119454, Россия, Москва, пр-т Вернадского, д. 78). E-mail: vegera@mirea.ru. Scopus Author ID 57212931836, SPIN-код РИНЦ 9076-5678, https://orcid.org/0000-0001-7312-3341

Максимова Елена Александровна, д.т.н., доцент, заведующий кафедрой КБ-4 «Интеллектуальные системы информационной безопасности», Институт кибербезопасности и цифровых технологий, ФГБОУ ВО «МИРЭА – Российский технологический университет» (119454, Россия, Москва, пр-т Вернадского, д. 78). E-mail: maksimova@mirea.ru. Scopus Author ID 57219701980, SPIN-код РИНЦ 6876-5558, https://orcid.org/0000-0001-8788-4256

Translated from Russian into English by Lyudmila O. Bychkova
Edited for English language and spelling by Thomas A. Beavitt

Information systems. Computer sciences. Issues of information security

Информационные системы. Информатика. Проблемы информационной безопасности

UDC 001.18:004.94:530.1
https://doi.org/10.32362/2500-316X-2025-13-1-16-27
EDN DUUBKW

RESEARCH ARTICLE

Percolation and connectivity formation in the dynamics of data citation networks in high energy physics

Sergey O. Kramarov [1, 2], Oleg R. Popov [3], Ismail E. Dzhariev [2, @], Egor A. Petrov [2]

[1] *MIREA – Russian Technological University, Moscow, 119454 Russia*
[2] *Surgut State University, Surgut, 628408 Russia*
[3] *Academy of Informatization of Education, Rostov-on-Don, 344065 Russia*
[@] *Corresponding author, e-mail: ismail.silver@yandex.ru*

Abstract

Objectives. The object of the research is to study citation information networks structured on the basis of a sample from the arXiv database related to theoretical high energy physics (high energy physics, HEP). Since 1974, this database has indexed more than 500000 articles, including their complete citation trees. The paper proposes a method for detecting percolation transitions in the dynamics of cluster formation of articles with similar content. Improving the accuracy of information cycles in knowledge networks can help resolve applied problems related to the quality of scientometrics and its indicators.

Methods. An optimized algorithm for dynamic network separation in the *Pajek* software environment was applied, in order to detect the emergence of a largest component equivalent to a percolation transition. This approach enables a detailed study of dynamic and general parameters to be carried out in each reduced network with a given time step. The clustering algorithm combines citation structure and temporal information about data.

Results. It was found that a percolation transition occurs in the HEP network. The indicator of this transition is the formation of a largest component near the critical point which occurs at the 10th month of the time sample interval. At the same time, a generalized conclusion about the behavior of network parameters shows a positive trend in the growth of connectivity for the entire time period (from 1991 to 2003). Furthermore, a generalized analysis of citation distribution reveals eleven laureates of highly cited articles who set the basic vector for development in the field of HEP. It is worth noting that the prominent scientists from the top three in terms of citations are linked by a shared field of research: string theory. Verification of this fact confirms that our citation evaluation method is effective. Determining the characteristics of the HEP (high-energy physics) network enables an important indicator of the researcher's activity and behavior to be identified.

Conclusions. In the column of authors linked by co-authorship, of the 9200 authors in the HEP physics community, 7304 belong to a single connected component. The temporal nature of citations indicates a rapid uptake and understanding of relevant new work. Percolation transitions, which are indicators of sudden conceptual shifts in citation networks, allow us to identify and link articles into research schemes which form clusters of new ideas and theories.

Keywords: information network, citation network, high energy physics, HEP, percolation, percolation transition, connectivity, largest component, cluster, dynamics

• **Submitted:** 23.07.2024 • **Revised:** 20.09.2024 • **Accepted:** 12.11.2024

For citation: Kramarov S.O., Popov O.R., Dzhariev I.E., Petrov E.A. Percolation and connectivity formation in the dynamics of data citation networks in high energy physics. *Russian Technological Journal.* 2025;13(1):16–27. https://doi.org/10.32362/2500-316X-2025-13-1-16-27, https://elibrary.ru/DUUBKW

Financial disclosure: The authors have no financial or proprietary interest in any material or method mentioned.

The authors declare no conflicts of interest.

НАУЧНАЯ СТАТЬЯ

Перколяция и формирование связности в динамике сетей цитирования данных по физике высоких энергий

С.О. Крамаров [1, 2],
О.Р. Попов [3],
И.Э. Джариев [2, @],
Е.А. Петров [2]

[1] *МИРЭА – Российский технологический университет, Москва, 119454 Россия*
[2] *Сургутский государственный университет, Сургут, 628408 Россия*
[3] *Академия информатизации образования, Ростов-на-Дону, 344065 Россия*
[@] *Автор для переписки, e-mail: ismail.silver@yandex.ru*

Резюме

Цели. Объектом исследования выступают информационные сети цитирования, структурированные на основе выборки в arXiv базы данных, связанной с теоретической физикой высоких энергий (high energy physics, HEP), индексирующей с 1974 г. более 500000 статей, включая их полное дерево цитирования. Предлагается методика обнаружения перколяционного перехода в динамике образования кластеров статей, имеющих схожее содержание и тесно связанных друг с другом. Повышение точности количественной оценки информационных циклов в сетях знаний может быть использовано в решении прикладных задач качества наукометрии и ее индикаторов.

Методы. Применен оптимизированный алгоритм по динамическому разделению сети в программной среде *Pajek* с целью обнаружения появления в ней гигантского компонента, эквивалентного перколяционному переходу. Данный подход позволяет с заданным временным шагом реализовать детальное исследование динамических и общих параметров для каждой новой сокращенной сети. Используемый алгоритм кластеризации объединяет структуру цитирования и темпоральную информацию о данных.

Результаты. Обнаружено, что в сети HEP происходит перколяционный переход, индикатором которого является образование вблизи локальной критической точки (10-го месяца интервала временной выборки) гигантского компонента. В то же время обобщенный вывод поведения параметров сетей свидетельствует о положительной динамике в росте связности исследуемой сети для всей временной выборки (с 1991 г. по 2003 г.). Обобщенный анализ распределения цитируемости обнаруживает 11 лауреатов высокоцитируемых статей, которые задавали базовый вектор развития в разделе HEP. Примечательно, что выдающиеся ученые из главной «тройки» цитирования связаны единой динамичной областью исследования – теорией струн. Верификация

вышеуказанного факта подтверждает то, что предложенный метод оценки цитируемости – рабочий. Определение характеристик сети HEP позволяет определить важный для исследователя показатель и его поведение.
Выводы. В графе авторов, связанных отношениями соавторства, 7304 из 9200 авторов научного сообщества физиков HEP относятся к одному связному компоненту. Временной характер цитирования указывает на быстрое понимание и использование соответствующих новых работ. Перколяционный переход, являясь индикатором внезапных концептуальных изменений в сетях цитирования, позволяет выявлять и связывать статьи в исследовательскую схему, составляющую кластер новых идей или теорий.

Ключевые слова: информационная сеть, сеть цитирования, физика высоких энергий, HEP, перколяция, перколяционный переход, связность, гигантский компонент, кластер, динамика

• **Поступила:** 23.07.2024 • **Доработана:** 20.09.2024 • **Принята к опубликованию:** 12.11.2024

Для цитирования: Крамаров С.О., Попов О.Р., Джариев И.Э., Петров Е.А. Перколяция и формирование связности в динамике сетей цитирования данных по физике высоких энергий. *Russian Technological Journal.* 2025;13(1):16–27. https://doi.org/10.32362/2500-316X-2025-13-1-16-27, https://elibrary.ru/DUUBKW

Прозрачность финансовой деятельности: Авторы не имеют финансовой заинтересованности в представленных материалах или методах.

Авторы заявляют об отсутствии конфликта интересов.

INTRODUCTION

A distinct category of complex networks, together with social, biological, and technological networks, is represented by information networks, also referred to as *knowledge networks*.

Newman defines an information network as "consisting of data elements linked together in some way" [1]. Two of the most studied information networks are citation networks of scientific publications and text page networks of the World Wide Web [2–5]. In them, the vertices are articles or web pages, and the directed edges are citations of one article in another article or hyperlinks.

Certain other information networks have been studied to a lesser extent. For example, the network of citations between patents which in some respects are similar to citations between academic research articles.

Keyword index networks are closely related to networks of web pages and academic documents. They are different from direct link networks between documents. An index is a bipartite network of links between a record of keywords and the document which they indicate. They are used, for example, as the basis for search engine algorithms which try to find documents or pages that are similar to each other.

The network of relations between classes of words in a thesaurus, which has been studied in a number of works [4, 6, 7], can also be regarded as informational. Thesaurus users move through the network from one word to another in search of a specific term which perfectly reflects the idea they have in mind.

Semantic links between terms and mental constructs used for semantic representation of a special scientific language represent conceptual or terminological networks. In [8], the parameters of the dynamics of link formation dynamics in networks structured on the basis of dictionaries of model predictive terms thematically related to promising information technologies were studied.

The network of citation references between scientific publications, the structure of which quite accurately reflects the structure of information stored in its vertices—articles, corresponds well to the concept of *information network*.

Citation analysis can identify articles and link them into a research pattern which forms a cluster defined by the research specialty. An indicator of sudden conceptual changes resulting from new theories or ideas is sudden changes in the citation network.

There are two basic areas of network analysis of citation references, reflecting the gradual development of knowledge in dynamics.

A widespread method is main path analysis method [9, 10], which represents citation networks as a system of channels carrying scientific knowledge or information. Main path analysis calculates the extent to which a particular citation or article is used as a reference. This is called a traversal count. Paths or components from the source vertex to the destination vertex with the highest traversal weight, assumed to define the main information flow, are extracted. Analysis of their dynamics over time reflects the integration or specialization of the scientific community.

Analyses of this kind related to data fragmentation also include approaches based on the identification of key routes, islands, and probabilistic flows [11].

These methods focus on localization, highlighting highly cited articles and leaving out a large stratum of the entire data set expressed in weak long-range network correlations [12, 13].

Another trend of simulation and analysis of information processes occurring in networks with irregular structure is related to the application of methods of percolation theory known in solid-state physics [14–19], capable of answering important applied questions. Percolation theory is successfully applicable in applications which provide protection of technological networks from virus attacks [20], nanotechnology for the design of virus-like particles [17], and algorithms for monitoring and predicting the evolution of information in sociotechnical systems [21].

Percolation in social networks by the analysis of knowledge networks or information percolation is a relevant, popular and developing trend at the intersection of scientific concepts. A coherent theory of this area, including the conceptual range, is just being formed. Its elements are being collated within the framework of a number of works by domestic and foreign authors [21–24], in order to reflect different sides of a complex multidimensional phenomenon. A more universal view of the analysis of the critical behavior of percolation transitions shows the need to take into account global information about network connectivity, resolved by artificial intelligence and machine learning algorithms [24].

Percolation theory from statistical physics focuses on patterns of network connectivity, namely the clusters of nodes which can be reached from each other. The main interest is the relative size of the largest cluster, i.e. the fraction of nodes in the largest (giant) component P_∞, which acts as a measure of functionality.

With regard to more complete coverage of network processes, it is important that long-range correlations control the percolation transition, as in the case of thermal phase transitions. Another significant factor is that the corresponding quantities near the critical point p_c are described by the formulas of power laws and critical indices.

The structure of clusters formed by elements of citation networks from the same section of theoretical high-energy physics is a significant factor in the detection of percolation phase transitions [25, 26].

This is important in the development of network science and its applications [18]:

- in terms of heterogeneous interaction models of the components which make up complex networked systems;
- as a paradigm of random and semi-random connectivity of components of networked systems;
- as a confirmation of the principle of universality of phase transitions in a large variety of physical and socio-technical systems.

Understanding percolation theory facilitates the understanding of network systems and can be used to quantify and resolve some basic problems in applied informatics and scientometrics. It can in particular help with the detection of clusters of articles with similar content and which are closely related to each other. This approach to analyzing the links between scientific publications improves the accuracy of information cycle assessment in scientometrics and the quality of indicators.

Thus, identifying and understanding the topological properties of the clusters formed, as well as the distribution of cluster sizes and the average distance between network elements belonging to the same cluster is of interest.

Simulation of clusters formed by elements of citation networks, which reflect both nonlinear processes occurring in a certain scientific field and a wide variety of its complex systems, enables their dynamics, reveal hidden connections, correlations, and cycles to be predicted.

The object of the study is the international information networks structured on the basis of the Stanford Linear Accelerator Center SPIRES-HEP database. Since 1974, the literature on theoretical high-energy physics (HEP) has been comprehensively cataloged online and more than 500000 articles, including their full citation tree, have been indexed.

TOOLS AND METHODS

The basic research methodology proceeds from mapping the dynamics of formation of a complex associated structure of the studied citation network with nodes, links taking into account the weight of various elements according to three basic criteria: degree of nodes, distance, and strength of links between nodes.

In the most general form, regardless of the physical nature and model of the system, percolation theory answers the following question: what is the probability that there exists an open path from zero to infinity (or whether there exists an infinite cluster of interconnected pores or nodes)? Thus, the problem boils down to whether such paths exist for a given probability p. Basically, the theory is concerned with the existence of such a cluster and its structure with respect to the probability of filling p.

Unlike thermal or magnetic phase transitions, the percolation transition is a geometric phase transition and is characterized by the structural properties of clusters near the critical probability p_c.

The measure of functionality is the probability that a node (or link) belongs to an infinite cluster. At $p < p_c$ there are only finite clusters and $P_\infty = 0$. At $p > p_c$ P_∞ behaves similarly to the density below the critical temperature T_c and increases with increasing p according to the power law:

$$P_\infty \sim (p - p_c)^\beta. \quad (1)$$

The linear size of the finite clusters below and above p_c is characterized by the correlation length ξ. The correlation length is defined as the average distance between two nodes in the same finite cluster. When p approaches p_c, ξ increases with the same degree v below and above the threshold:

$$\xi \sim (p - p_c)^{-v}. \quad (2)$$

The average number of nodes (mass) of a finite cluster S also diverges from the index γ above and below p_c:

$$S \sim (p - p_c)^{-\gamma}. \quad (3)$$

The indices β, v and γ describe the critical behavior of typical quantities associated with the percolation transition and are called critical indices.

These degree indices are universal and depend neither on the structural details of the lattice (e.g., square or triangular), nor on the type of percolation (node, link, or continuum). They depend only on the dimensionality of the space (see the table). Dimensionless quantities are used in network science.

Table. Estimates of critical percolation indicators

	Space dimensionality				
	$d = 2$	$d = 3$	$d = 4$	$d = 5$	$d \geq 6$
β	5/36	0.417 ± 0.003	0.5	0.7	1.0
v	48/36	0.875 ± 0.008	0.7	0.6	0.5
γ	86/36	1.795 ± 0.005	1.8	1.6	1.0

From the point of view of forming a coherent information network, structural parameters such as distance between nodes, network diameter, clustering and intermediacy indices are of great importance.

Since the structure of percolation clusters is well described by the fractal concept [27], let us pay attention to the fractal dimensions d_f, d_{min} and d_l which describe the distance between vertices.

The fractal dimension d_f describes $M(r)$, i.e., the way in which, on average, the mass M of a cluster inside a sphere of radius r scales with r. Dimension d_{min} describes the self-similarity and structure on the shortest path between two arbitrary nodes A and B, while d_l describes $M(l)$, i.e., how M at the shortest distance l from a given node scales with l. They are related to each other:

$$d_l = \frac{d_f}{d_{min}}. \quad (4)$$

The concept of shortest distance (or optimal distance) also plays an important role in describing dynamical phenomena in disordered systems, such as the spread of wildfires or epidemics spreading along the shortest path from the source. In [27], it is shown that the rate of propagation of a fire front or epidemic is related to the measure of degree v. In a knowledge network, the shortest or optimal paths are important because they tell us how information will propagate with the highest probability.

Based on the well-known and tested [9, 28] *Pajek*[1] software environment, we can propose an optimized algorithm for dynamic network partitioning to detect the appearance of a largest component in the network, equivalent to a percolation transition.

The following factors are emphasized therein:

1. We select the source network, either complete or containing some subnet, with which we are going to work further. In our case, the network parameter (.net) represents the citation graph of the part of the arXiv[2], database corresponding to HEP. The vertices of the graph are arXiv article identifiers in the form of nodes. Relationships between these entities, such as article citations, are represented by links between the entities, i.e., X cites Y. The vector parameter (vec) represents a temporal data series (dates of article data release) with different time step (day, month, year);
2. In order to extract a part of the network, i.e., to create a localized representation, the sets (or classes) of vertices to be extracted need to be determined. We divide the vertices of the original network into a certain number of mutually exclusive subsets (clusters) with a given time threshold (initial state) and step;
3. Computation and a detailed study of dynamic and general parameters for each new reduced network [29]. Particular attention is paid to the dynamics of the largest component, measured as percentage. The splits (steps) end when this parameter in the new network is no longer significant, i.e. from the minimum value to the maximum value;
4. Processing and visualization of the obtained data of time dependencies of link parameters in citation networks.

There is currently considerable interest in the problem of how the largest component in networks is formed and whether it is possible to predict this process. A methodology involving detailed analysis in citation networks can be applied to a much wider range of disciplines: from chemistry, physics and biology to the social sciences. The approach proposed uses a clustering algorithm which combines citation structure and data information. The proposed methodology is expected to identify clusters relevant to promising scientific trends.

[1] http://mrvar.fdv.uni-lj.si/pajek/. Accessed April 20, 2024.
[2] https://arxiv.org/archive/hep-th. Accessed April 20, 2024.

RESULTS AND DISCUSSION

For the purpose of this analysis, the high energy physics citation network from August 1, 1991 to May 12, 2003 in the arXiv[2] database, which contains 27770 publications of articles in High Energy Physics—Theory (HEP or hep-th) at the time of data collection, is considered.[3]

Transformed into *Pajek*[1] format, the files allow us to conduct a study using this citation network. The first file hep-th-new.net is a network file with 27770 vertices and 352807 graphs. A vector file called date-new.vec contains the dates of the articles converted to the number of days since August 1, 1991. The number of days is broken down into months, in order to visualize the results of the study.

The description of the graphs of time dependencies and citation distribution begins with a detailed analysis of the dependence of the largest component on the time interval. The abscissa axis shows time t in months, where 0 is March 1993, month 28 is July 1995.

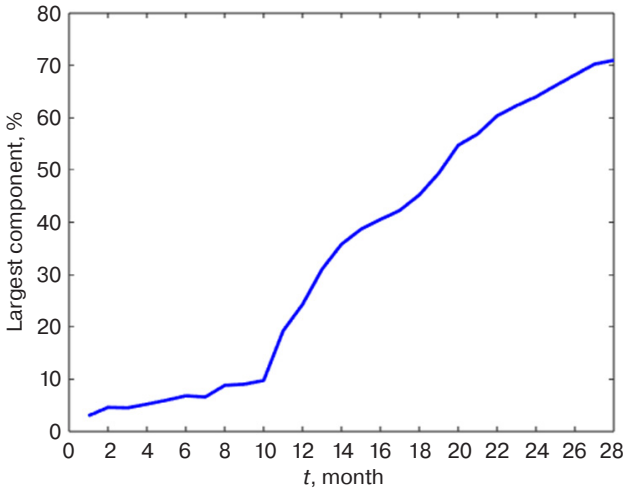

Fig. 1. Time dependence of the largest component

In Fig. 1, a sharp increase in the largest component is observed in the interval between 1993–1994, indicating the presence of a largest component. At a certain critical value, the dependence graph shows a sharp increase from a very small value to a finite fraction of the whole system, characteristic of a percolation phase transition. The graph ceases to be linear, signaling the formation of the largest component at a certain point in time equal to 10 months. The key moment for the percolation transition, found by the study, is a speech at a string theory conference in 1994 made by Edward Witten who proposed M-theory. In the months following Witten's statement, hundreds of new papers appeared on the Internet confirming that the new theory plays an important role in HEP. Today, this flurry of papers is known as the second superstring revolution. After a while, five superstring theories (type I, type IIA, type IIB, HO, and HE) became considered as different limits of the unified M-theory.

Observing the sharp increase in the size of the largest component in month 10, is can be assumed that the formation of the largest component is caused by the large publication activity in HEP during this period. However, when conducting a detailed study, it was found out that the peak of publications falls in the period between 1997–1998. The dependence graph confirming this fact is shown at the end of the article.

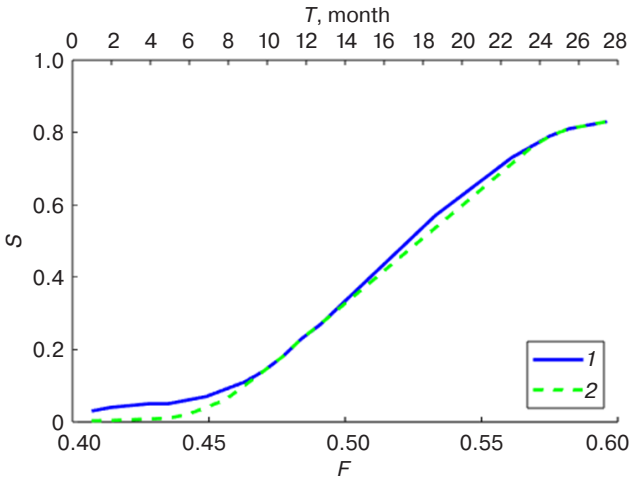

Fig. 2. Largest component size as a function of probability in network growth dynamics: (*1*) normalized daily dependence of the presented algorithm; (*2*) normalized stepwise dependence based on simulation data [30]

In Fig. 2, the size of the largest component S is de-dimensionalized and expressed in fractions. The normalized daily dependence (curve *1*) of the algorithm presented herein bears a strong positive correlation with the normalized stepwise dependence on the percolation probability F (curve *2*) in the dynamic opinion model (non-consensus opinion, NCO) obtained in [30]. The phase transition in the NCO model was found to belong to the same universality class as the invasion penetration with capture.

It was also found that in [30], the formation of a largest component can be observed in the interval of 0.4–0.6 simulation steps. The simulation step is understood as a fraction of the probability F of the network reaching a stable state. This interval coincides with the data at time interval T of 28 months obtained in this study. Due to the identity of the input datasets for HEP, the relationship of these dependencies is expected.

In order to understand why percolation occurs at this moment, let us study the general and dynamic parameters of the investigated network in the time

[3] http://vlado.fmf.uni-lj.si/pub/networks/data/. Accessed April 15, 2024.

interval. Figures 3–6 show the series of dependencies of the main network characteristics for HEP.

The average distance parameter is responsible for the average path length among all reachable pairs of nodes in the network [29]. From Fig. 3a, it can be seen that the average distance in the network increases with time, which contributes to the next parameter in Fig. 3b, the diameter of the network. The network diameter is the maximum eccentricity among all vertices of the network.

Figure 4 shows the dependence of clustering coefficients on time in months. The transitivity coefficient is responsible for the average probability that two vertices which are network neighbors of the same other vertex will themselves be neighbors. A sharp increase in the parameter indicates an increase in the probability of two different vertices being neighbors in the period from months 1 to 7, then the situation stabilizes and the coefficient varies around 0.1.

An unweighted average known as the Watts–Strogatz clustering coefficient is also used, although it does not give the exact proportion of closed dual parts. In Fig. 4b, the coefficient increases to 0.18 at month 10 and stabilizes at a value of 0.13 after month 18.

Figure 5a shows a positive linear increase in the total link strength parameter, confirmed by the growth of citations in articles throughout the entire study interval. The average degree parameter is responsible for the structural cohesion of the network. Its increase indicates that the number of links per node is increasing.

The last dynamic parameter in the study is the betweenness centralization. It determines the frequency of interval values between vertices in the network divided by the maximum possible value in a network of the same

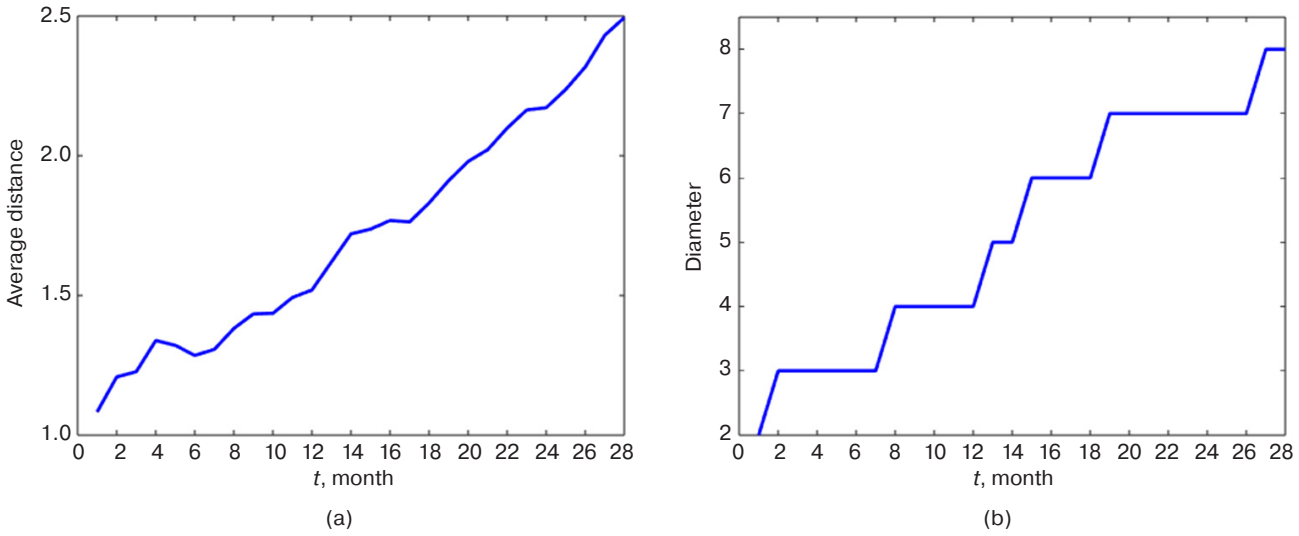

Fig. 3. Dependence of average distance to the top (a) and network diameter (b) on time

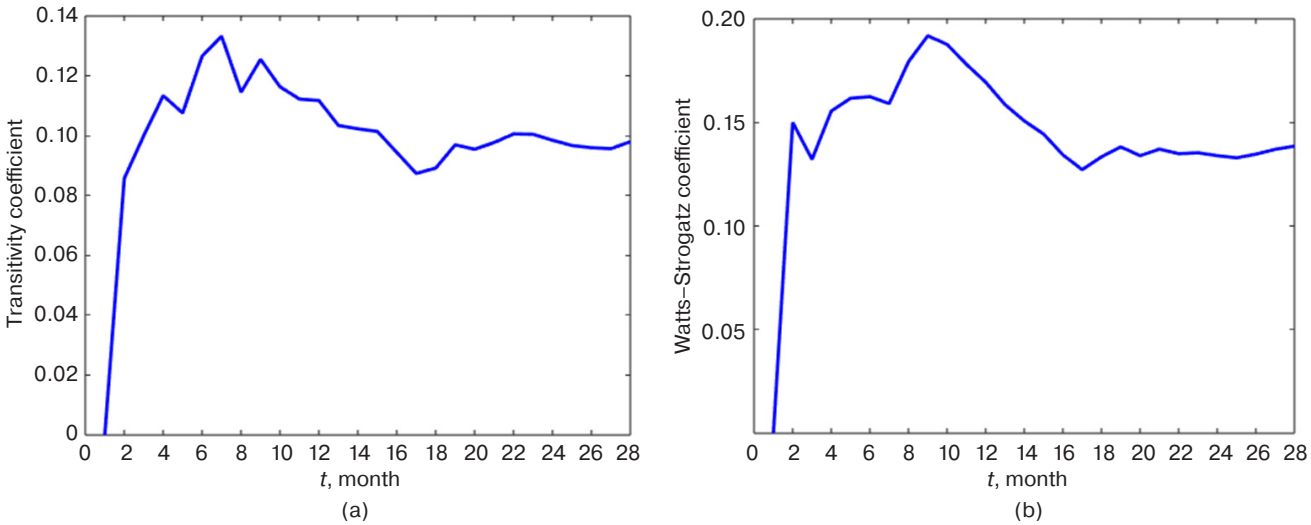

Fig. 4. Time dependence of clustering coefficients:
(a) transitivity coefficient; (b) Watts–Strogatz coefficient

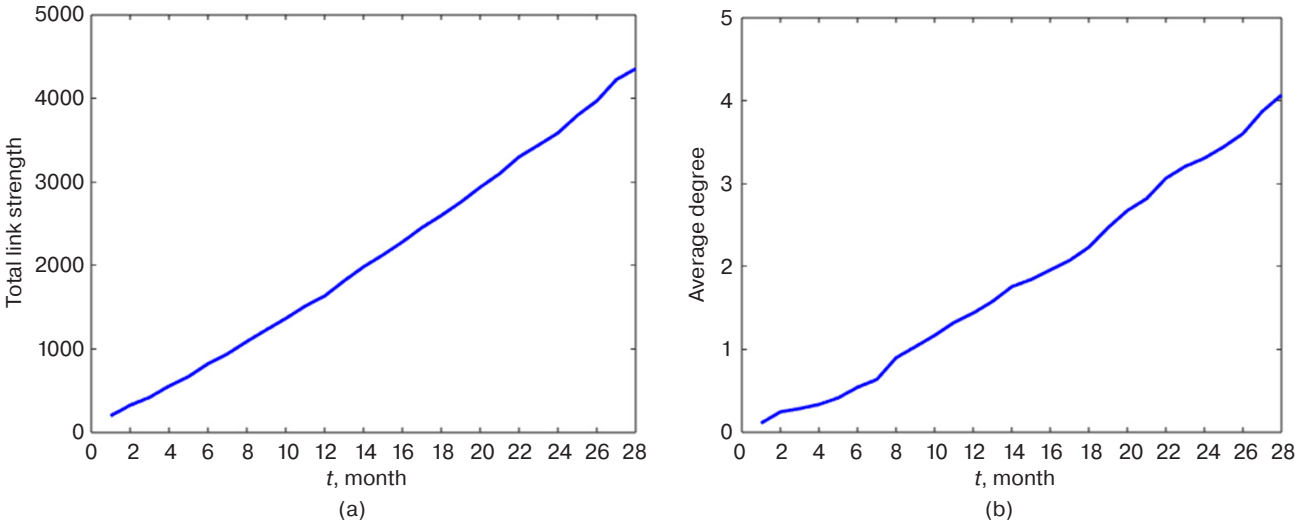

Fig. 5. Dependence of the total link strength in the network (a) and average degree of all vertices (b) on time

size. In other words, it is a measure of how central some vertices in the network are when compared to others. In Fig. 6, an increase in this parameter indicates that elements with an increased number of intermediate links are formed in the network, further indicating an increase in its connectivity. The significance of the betweenness centralization and average distance which determine the degree of information transmission without loss and distortion, is obvious [29].

Analysis of the behavior of dynamic and general network parameters for each time sample over the entire study interval enabled us to find that the HEP network contains a largest component. Each of the analyses performed contributes to the general understanding of the processes of dynamics of conceptual changes in the field of theoretical high-energy physics. This could not be achieved without a detailed study of individual network properties.

The final step of this study is to analyze the citation distribution from 1991 to 2003.The overall structure of the subgraph is examined to identify influential authors. Finally, potential laureates of the prize for theoretical high-energy physics can be predicted.

Authors who submitted articles to arXiv from 1991 to 2003 were ranked according to the number of citations. Next, a dependence of the share of citations of authors on the number of articles was built (Fig. 7). Based on the results of the study, 11 laureates of highly cited articles were found, establishing the vector of development in the HER section. For clarity, the graph lists the articles from the main "top three". The list is headed by Juan Martin Maldacena, Edward Witten, and Steven Scott Gubser [31–33]. It is worth noting that the validity of the results in this dependence is confirmed by the fact that these outstanding scientists are related by a single field of research: string theory. In addition,

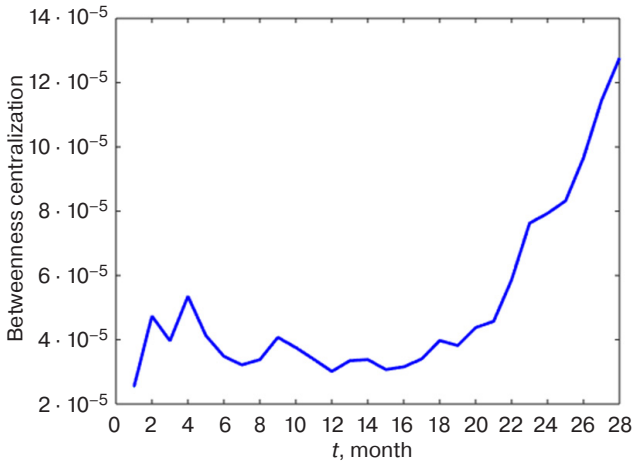

Fig. 6. Time dependence of the betweenness centralization between vertices of the network

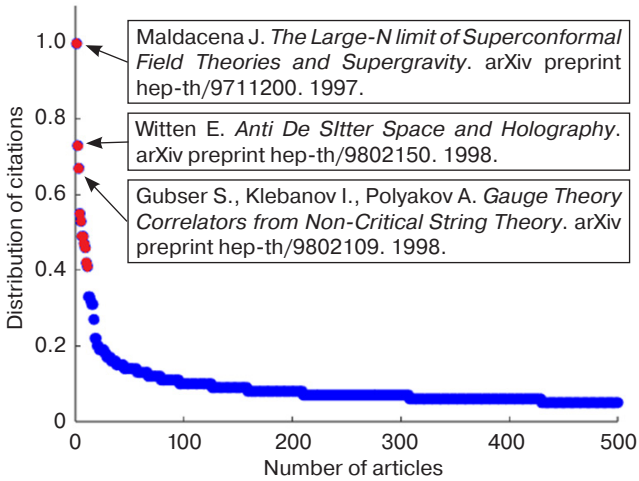

Fig. 7. Distribution of citations of HEP research articles between 1992 and 2003

verification of the above fact confirms that the proposed method works.

Thus, the characterization of the HER network enables a new method for citation evaluation to be introduced. In this study, the first step is to create a user-friendly database from the uploaded network. The second step is to determine the parameters of the source file. Then, in practice, the construction of a series of dependencies of parameters will allow us to determine the importance for the researcher indicator of the network and its behavior.

The practical application of this method allows us to discover non-trivial dependencies of different networks, the study of which leads to the discovery of new results. For specialists in a narrowly focused field, there is a need to find valuable information from a large amount of data of a certain network. The methodology proposed will allow us to identify not only the moment of time when this information appeared, but also the very area in which it is located.

CONCLUSIONS

The study finds that percolation results partially reflect the connective properties of networks and thus can be used as an algorithm to identify special subsets of networks, identifying communities of agents holding the same conceptual opinion.

In the steady state, nodes adhering to the same state exhibit a phase transition from small clusters to large linking clusters when citation concentration increases. Percolation transition, as an indicator of sudden conceptual changes in citation networks, allows us to identify and link articles into a research scheme which constitutes a cluster of new ideas or theories.

In the column of authors linked by co-authorship relationships, of the 9200 authors, 7304 belong to one cohesive component. The citation and authorship networks reflect the structure of close communication through formal and informal scientific literature. The HEP physics community publishes a large number of papers, and the temporal nature of citations indicates rapid understanding and utilization of relevant new work.

Percolation is a common model of disordered systems, and its close connection with the fractal concept, from self-similarity to multifractality, is emphasized. The behavior of the dynamic and general parameters of the real information network for each time sample over the entire study interval, shows that the HEP network contains a largest component. However, analysis of the degree of self-similarity of random processes, their stationarity or non-stationarity is an area for further study. In this regard, the logical continuation of the work is the fractal analysis of time series of information flows in HEP.

Authors' contribution. All authors equally contributed to the research work.

REFERENCES

1. Newman M.E.J. *Networks: An Introduction*. Oxford; NY: Oxford University Press; 2010. 772 p.
2. Lande D.V., Snarskii A.A., Bezsudnov I.V. Internet: Navigation in complex networks: models and algorithms. *Mezhdunarodnyi zhurnal prikladnykh i fundamental'nykh issledovanii = International Journal of Applied and Fundamental Research*. 2011;7:98–99 (in Russ.).
3. Doreian P., Batagelj V., Ferligoj A. (Eds.). *Advances in Network Clustering and Blockmodeling*. John Wiley & Sons; 2020. 432 p.
4. Newman M.E.J. The structure and function of complex networks. *SIAM Rev.* 2003;45(2):167–256. https://doi.org/10.1137/S003614450342480
5. Maltseva D.V., Pavlova I.A., Kapustina L.V., Vashchenko V.A., Fiala D. Comparative analysis of the capabilities of WoS and eLibrary for analyzing bibliographic networks. *Sotsiologiya: metodologiya, metody, matematicheskoe modelirovanie* (*Sotsiologiya:4M*) = *Sociology: Methodology, Methods, Mathematical Modeling* (*Sociology:4M*). 2023;56:7–68 (in Russ.). https://doi.org/10.19181/4m.2023.32.1.1
6. Kinouchi O., Martinez A.S., Lima G.F., Lourenco G.M., Risau-Gusman S. Deterministic walks in random networks: An application to thesaurus graphs. *Phys. A*. 2002;315(3–4):665–676. https://doi.org/10.1016/S0378-4371(02)00972-X
7. Motter A.E., de Moura A.P., Lai Y.-C., Dasgupta P. *Topology of the conceptual network of language*. arXiv preprint cond-mat/0206530. 2002. https://arxiv.org/abs/cond-mat/0206530v1, https://doi.org/10.48550/arXiv.cond-mat/0206530
8. Kramarov S.O., Popov O.R., Dzhariev I.E., Petrov E.A. Dynamics of link formation in networks structured on the basis of predictive terms. *Russian Technological Journal*. 2023;11(3):17–29. https://doi.org/10.32362/2500-316X-2023-11-3-17-29
9. De Nooy W., Mrvar A., Batagelj V. *Exploratory Social Network Analysis with Pajek: Revised and Expanded Edition for Updated Software*. 3rd ed. Ser.: Structural Analysis in the Social Sciences. Cambridge: Cambridge University Press; 2018. 455 p. https://doi.org/10.1017/9781108565691
10. Batagelj V., Doreian P., Ferligoj A., Kejžar N. *Understanding Large Temporal Networks and Spatial Networks: Exploration, Pattern Searching, Visualization and Network Evolution*. Chichester, West Sussex: John Wiley & Sons; 2014. 464 p. https://doi.org/10.1002/9781118915370

11. Maltseva D., Batagelj V. Journals publishing social network analysis. *Scientometrics*. 2021;126:3593–3620. https://doi.org/10.1007/s11192-021-03889-z
12. Kozlov A.S., Pyko S.A., Bogachev M.I. Statistical analysis of object parameters identified during multi-threshold processing of random fields with long-range correlation. *Nauka nastoyashchego i budushchego = Science: Present and Future*. 2021;2:164–167 (in Russ.).
13. Sun H., Radicchi F., Kurths J., et al. The dynamic nature of percolation on networks with triadic interactions. *Nat. Commun*. 2023;14:1308. https://doi.org/10.1038/s41467-023-37019-5
14. Broadbent S.R., Hammersley J.M. Percolation processes: I. Crystals and mazes. *Math. Proc. Cambridge Philos. Soc.* 1957;53(3):629–641. https://doi.org/10.1017/S0305004100032680
15. Stauffer D., Aharony A. *Introduction to Percolation Theory*. 2nd revised ed. London: Taylor & Francis; 2003. 180 p.
16. Dashko Yu.V., Kramarov S.O., Zhdanov A.V. Sintering of polycrystalline ferroelectrics and the percolation problem in stochastically packed networks. *Ferroelectrics*. 1996;186(1–4):85–88. https://doi.org/10.1080/00150199608218039
17. Brunk N.E., Twarock R. Percolation Theory Reveals Biophysical Properties of Virus-like Particles. *ACS Nano*. 2021;15(8):12988–12995. https://doi.org/10.1021/acsnano.1c01882
18. Li M., Liu R.-R., Lu L., Hu M.-B., Xu S., Zhang Y.-C. Percolation on complex networks: Theory and application. *Phys. Rep*. 2021;907:1–68. https://doi.org/10.1016/j.physrep.2020.12.003
19. Mondal S., Pachhal S., Agarwala A. Percolation transition in a topological phase. *Phys. Rev. B*. 2023;108(22): L220201. https://doi.org/10.1103/PhysRevB.108.L220201
20. Lesko S.A., Alyoshkin A.S., Filatov V.V. Stochastic and Percolating Models of Blocking Computer Networks Dynamics during Distribution of Epidemics of Evolutionary Computer Viruses. *Rossiiskii tekhnologicheskii zhurnal*. 2019;7(3):7–27 (in Russ.). https://doi.org/10.32362/2500-316X-2019-7-3-7-27
21. Zhukov D.O., Khvatova T.Yu., Saltzman A.D. Modeling of stochastic dynamics of changes in node states and percolation transitions in social networks with self-organization and memory. *Informatika i ee primeneniya = Informatics and Applications*. 2021;15:102–110 (in Russ.). https://doi.org/10.14357/19922264210114
22. Perova Yu.P., Lesko S.A., Zhukov D.O., Chechurin A.V. Analysis and modeling of processes in complex social network structures based on the Fokker-Planck equation. *Vestnik Tomskogo gosudarstvennogo universiteta. Upravlenie, vychislitel'naya tekhnika i informatika = Tomsk State University Journal of Control and Computer Science*. 2022;60:32–41 (in Russ.). https://doi.org/10.17223/19988605/60/4
23. Xie J., Meng F., Sun J., Ma X., Yan G., Hu Y. Detecting and modelling real percolation and phase transitions of information on social media. *Nat. Hum. Behav*. 2021;5(9):1161–1168. https://doi.org/10.1038/s41562-021-01090-z
24. Oh S.M., Choi K., Kahng B. Machine learning approach to percolation transitions: global information. *J. Stat. Mech*. (*JSTAT*). 2023;2023(8):083210. http://doi.org/10.1088/1742-5468/aceef1
25. Petrov E.A., Dzhariev I.E., Popov O.R., Sysoev S.M. An approach to prediction of universal dynamic processes: A case-study of modeling electromagnetic effect on gas-hydrate strata. *GIAB. Gornyi informatsionno-analiticheskii byulleten = MIAB. Mining Inf. Anal. Bull.* 2023;6:56–66 (in Russ.). https://doi.org/10.25018/0236_1493_2023_6_0_56
26. Sigov A.S., Zhukov D.O., Novikova O.A. Modeling of memory realization processes and the implementation of information in self-organization in forecasting the new's events using arrays of natural language texts. *Sovremennye informatsionnye tekhnologii i IT-obrazovanie = Modern Information Technologies and IT Education.* 2016;12(1):42–55 (in Russ.).
27. Bunde A., Havlin S. *Fractals and Disordered Systems*. Springer Science & Business Media; 2012. 408 p.
28. Popov O.R., Kramarov S.O. The study of information dissemination in networks arranged from a set of forecasting terms. *Vestnik kibernetiki = Proceedings in Cybernetics.* 2022;1(45): 38–45 (in Russ.). https://doi.org/10.34822/1999-7604-2022-1-38-45
29. Dzhariev I.E., Petrov E.A., Popov O.R., et al. Studying the dynamics of scientific and educational networks using the Monte Carlo method. In: *The Possibilities of Natural and Artificial Intelligence Combining in Educational Systems*. Moscow: RIOR; 2023. P. 91–99 (in Russ.). https://doi.org/10.29039/02124-8
30. Shao J., Havlin S., Stanley H.E. Dynamic opinion model and invasion percolation. *Phys. Rev. Lett*. 2009;103(1):018701. https://doi.org/10.1103/PhysRevLett.103.018701
31. Maldacena J. *The Large-N limit of Superconformal Field Theories and Supergravity*. 1997. https://arxiv.org/abs/hep-th/9711200
32. Witten E. *Anti De SItter Space and Holography*. 1998. https://arxiv.org/abs/hep-th/9802150
33. Gubser S., Klebanov I., Polyakov A. *Gauge Theory Correlators from Non-Critical String Theory*. 1998. https://arxiv.org/abs/hep-th/9802109

СПИСОК ЛИТЕРАТУРЫ

1. Newman M.E.J. *Networks: An Introduction*. Oxford; NY: Oxford University Press; 2010. 772 p.
2. Ландэ Д.В., Снарский А.А., Безсуднов И.В. Интернетика: Навигация в сложных сетях: модели и алгоритмы. *Международный журнал прикладных и фундаментальных исследований*. 2011;7:98–99.
3. Doreian P., Batagelj V., Ferligoj A. (Eds.). *Advances in Network Clustering and Blockmodeling*. John Wiley & Sons; 2020. 432 p.
4. Newman M.E.J. The structure and function of complex networks. *SIAM Rev.* 2003;45(2):167–256. https://doi.org/10.1137/S003614450342480

5. Мальцева Д.В., Павлова И.А., Капустина Л.В., Ващенко В.А., Фиала Д. Сравнительный анализ возможностей WoS и eLIBRARY для анализа библиографических сетей. *Социология: методология, методы, математическое моделирование* (*Социология:4М*). 2023;56:7–68. https://doi.org/10.19181/4m.2023.32.1.1
6. Kinouchi O., Martinez A.S., Lima G.F., Lourenco G.M., Risau-Gusman S. Deterministic walks in random networks: An application to thesaurus graphs. *Phys. A*. 2002;315(3–4):665–676. https://doi.org/10.1016/S0378-4371(02)00972-X
7. Motter A.E., de Moura A.P., Lai Y.-C., Dasgupta P. *Topology of the conceptual network of language*. arXiv preprint cond-mat/0206530. 2002. https://arxiv.org/abs/cond-mat/0206530v1, https://doi.org/10.48550/arXiv.cond-mat/0206530
8. Крамаров С.О., Попов О.Р., Джариев И.Э., Петров Е.А. Динамика формирования связей в сетях, структурированных на основе прогностических терминов. *Russian Technological Journal.* 2023;11(3):17–29. https://doi.org/10.32362/2500-316X-2023-11-3-17-29
9. De Nooy W., Mrvar A., Batagelj V. *Exploratory Social Network Analysis with Pajek: Revised and Expanded Edition for Updated Software*. 3rd ed. Ser.: Structural Analysis in the Social Sciences. Cambridge: Cambridge University Press; 2018. 455 p. https://doi.org/10.1017/9781108565691
10. Batagelj V., Doreian P., Ferligoj A., Kejžar N. *Understanding Large Temporal Networks and Spatial Networks: Exploration, Pattern Searching, Visualization and Network Evolution*. Chichester, West Sussex: John Wiley & Sons; 2014. 464 p. https://doi.org/10.1002/9781118915370
11. Maltseva D., Batagelj V. Journals publishing social network analysis. *Scientometrics*. 2021;126:3593–3620. https://doi.org/10.1007/s11192-021-03889-z
12. Козлов А.С., Пыко С.А., Богачев М.И. Статистический анализ параметров объектов, выделяемых при многопороговой обработке случайных полей с дальней корреляцией. *Наука настоящего и будущего*. 2021;2:164–167.
13. Sun H., Radicchi F., Kurths J., et al. The dynamic nature of percolation on networks with triadic interactions. *Nat. Commun*. 2023;14:1308. https://doi.org/10.1038/s41467-023-37019-5
14. Broadbent S.R., Hammersley J.M. Percolation processes: I. Crystals and mazes. *Math. Proc. Cambridge Philos. Soc.* 1957;53(3):629–641. https://doi.org/10.1017/S0305004100032680
15. Stauffer D., Aharony A. *Introduction to Percolation Theory*. 2nd revised ed. London: Taylor & Francis; 2003. 180 p.
16. Dashko Yu.V., Kramarov S.O., Zhdanov A.V. Sintering of polycrystalline ferroelectrics and the percolation problem in stochastically packed networks. *Ferroelectrics*. 1996;186(1–4):85–88. https://doi.org/10.1080/00150199608218039
17. Brunk N.E., Twarock R. Percolation Theory Reveals Biophysical Properties of Virus-like Particles. *ACS Nano*. 2021;15(8):12988–12995. https://doi.org/10.1021/acsnano.1c01882
18. Li M., Liu R.-R., Lu L., Hu M.-B., Xu S., Zhang Y.-C. Percolation on complex networks: Theory and application. *Phys. Rep*. 2021;907:1–68. https://doi.org/10.1016/j.physrep.2020.12.003
19. Mondal S., Pachhal S., Agarwala A. Percolation transition in a topological phase. *Phys. Rev. B*. 2023;108(22): L220201. https://doi.org/10.1103/PhysRevB.108.L220201
20. Лесько С.А., Алёшкин А.С., Филатов В.В. Стохастические и перколяционные модели динамики блокировки вычислительных сетей при распространении эпидемий эволюционирующих компьютерных вирусов. *Российский технологический журнал*. 2019;7(3):7–27. https://doi.org/10.32362/2500-316X-2019-7-3-7-27
21. Жуков Д.О., Хватова Т.Ю., Зальцман А.Д. Моделирование стохастической динамики изменения состояний узлов и перколяционных переходов в социальных сетях с учетом самоорганизации и наличия памяти. *Информатика и ее применения*. 2021;15(1):102–110. https://doi.org/10.14357/19922264210114
22. Перова Ю.П., Лесько С.А., Жуков Д.О., Чечурин А.В. Анализ и моделирование процессов в сложных социальных сетевых структурах на основе уравнения Фоккера-Планка. *Вестник Томского государственного университета. Управление, вычислительная техника и информатика*. 2022;60:32–41. https://doi.org/10.17223/19988605/60/4
23. Xie J., Meng F., Sun J., Ma X., Yan G., Hu Y. Detecting and modelling real percolation and phase transitions of information on social media. *Nat. Hum. Behav*. 2021;5(9):1161–1168. https://doi.org/10.1038/s41562-021-01090-z
24. Oh S.M., Choi K., Kahng B. Machine learning approach to percolation transitions: global information. *J. Stat. Mech*. (*JSTAT*). 2023;2023(8):083210. http://doi.org/10.1088/1742-5468/aceef1
25. Петров Е.А., Джариев И.Э., Попов О.Р., Сысоев С.М. Подход к прогнозированию универсальных динамических процессов на примере моделирования электромагнитного воздействия на газогидратные пласты. *Горный информационно-аналитический бюллетень*. 2023;6:56–66. https://doi.org/10.25018/0236_1493_2023_6_0_56
26. Сигов А.С., Жуков Д.О., Новикова О.А. Моделирование процессов реализации памяти и самоорганизации информации при прогнозировании новостных событий с использованием массивов естественно-языковых текстов. *Современные информационные технологии и ИТ-образование*. 2016;12(1):42–55.
27. Bunde A., Havlin S. *Fractals and Disordered Systems*. Springer Science & Business Media; 2012. 408 p.
28. Попов О.Р., Крамаров С.О. Исследование распространения информации в сетях, структурированных из набора прогностических терминов. *Вестник кибернетики*. 2022;1(45):38–45. https://doi.org/10.34822/1999-7604-2022-1-38-45
29. Джариев И.Э., Петров Е.А., Попов О.Р. и др. Исследование динамики научно-образовательных сетей с помощью моделирования методом Монте-Карло. В кн.: *Возможности сочетания естественного и искусственного интеллектов в образовательных системах*. М.: Издательский Центр РИОР; 2023. С. 91–99. https://doi.org/10.29039/02124-8
30. Shao J., Havlin S., Stanley H.E. Dynamic opinion model and invasion percolation. *Phys. Rev. Lett*. 2009;103(1):018701. https://doi.org/10.1103/PhysRevLett.103.018701

31. Maldacena J. *The Large-N limit of Superconformal Field Theories and Supergravity*. 1997. https://arxiv.org/abs/hep-th/9711200
32. Witten E. *Anti De SItter Space and Holography*. 1998. https://arxiv.org/abs/hep-th/9802150
33. Gubser S., Klebanov I., Polyakov A. *Gauge Theory Correlators from Non-Critical String Theory*. 1998. https://arxiv.org/abs/hep-th/9802109

About the authors

Sergey O. Kramarov, Dr. Sci. (Phys.-Math.), Professor, Advisor to the President of the University, MIREA – Russian Technological University (78, Vernadskogo pr., Moscow, 119454 Russia); Chief Researcher, Surgut State University (22, Energetikov ul., Surgut, 628408 Russia). E-mail: maoovo@yandex.ru. Scopus Author ID 56638328000, ResearcherID E-9333-2016, RSCI SPIN-code 2821-6380, https://orcid.org/0000-0003-3743-6513

Oleg R. Popov, Cand. Sci. (Eng.), Associate Professor, Expert-Analyst, Southern Branch of the Academy of Informatization of Education (124/5, Dneprovskii per., Rostov-on-Don, 344065 Russia). E-mail: cs41825@aaanet.ru. ResearcherID AAT-8018-2021, RSCI SPIN-code 1041-0680, http://orcid.org/0000-0001-6209-3554

Ismail E. Dzhariev, Junior Researcher, Postgraduate Student, Department of Automated Information Processing and Management Systems, Polytechnic Institute, Surgut State University (22, Energetikov ul., Surgut, 628408 Russia). E-mail: dzhariev2_ie@edu.surgu.ru. ResearcherID GZB-1868-2022, RSCI SPIN-code 1667-2152, https://orcid.org/0000-0003-4068-1050

Egor A. Petrov, Junior Researcher, Postgraduate Student, Department of Automated Information Processing and Management Systems, Polytechnic Institute, Surgut State University (22, Energetikov ul., Surgut, 628408 Russia). E-mail: petrov2_ea@edu.surgu.ru. ResearcherID GZG-8857-2022, SPIN-код РИНЦ 4847-1445, https://orcid.org/0000-0002-4151-197X

Об авторах

Крамаров Сергей Олегович, д.ф.-м.н., профессор, советник президента университета, ФГБОУ ВО «МИРЭА – Российский технологический университет» (119454, Россия, Москва, пр-т Вернадского, д. 78); главный научный сотрудник, БУ ВО «Сургутский государственный университет» (628408, Россия, Сургут, ул. Энергетиков, д. 22). E-mail: maoovo@yandex.ru. Scopus Author ID 56638328000, ResearcherID E-9333-2016, SPIN-код РИНЦ 2821-6380, https://orcid.org/0000-0003-3743-6513

Попов Олег Русланович, к.т.н., доцент, эксперт-аналитик, Южное отделение МОО «Академия информатизации образования» (344065, Россия, Ростов-на-Дону, пер. Днепровский, д. 124/5). E-mail: cs41825@aaanet.ru. ResearcherID AAT-8018-2021, SPIN-код РИНЦ 1041-0680, http://orcid.org/0000-0001-6209-3554

Джариев Исмаил Эльшан оглы, младший научный сотрудник, аспирант, кафедра автоматизированных систем обработки информации и управления, Политехнический институт, БУ ВО «Сургутский государственный университет» (628408, Россия, Сургут, ул. Энергетиков, д. 22). E-mail: dzhariev2_ie@edu.surgu.ru. ResearcherID GZB-1868-2022, SPIN-код РИНЦ 1667-2152, https://orcid.org/0000-0003-4068-1050

Петров Егор Аркадьевич, младший научный сотрудник, аспирант, кафедра автоматизированных систем обработки информации и управления, Политехнический институт, БУ ВО «Сургутский государственный университет» (628408, Россия, Сургут, ул. Энергетиков, д. 22). E-mail: petrov2_ea@edu.surgu.ru. ResearcherID GZG-8857-2022, SPIN-код РИНЦ 4847-1445, https://orcid.org/0000-0002-4151-197X

Translated from Russian into English by Lyudmila O. Bychkova
Edited for English language and spelling by Dr. David Mossop

Information systems. Computer sciences. Issues of information security

Информационные системы. Информатика. Проблемы информационной безопасности

UDC 519.95:621.3
https://doi.org/10.32362/2500-316X-2025-13-1-28-37
EDN BUGTUV

RESEARCH ARTICLE

Probabilistic characteristics analysis of virus attack effect on digital substations

Alexander S. Leontyev,
Dmitry V. Zhmatov @

MIREA – Russian Technological University, Moscow, 119454 Russia
@ *Corresponding author, e-mail: zhmatov@mirea.ru*

Abstract

Objectives. This study aims to create analytical methods for evaluating the probabilistic safety characteristics of information and software elements in digital substations in order to ensure security in different virus scenarios.

Methods. The methods of reliability theory, random process theory, and recovery theory were used.

Results. The derived integral ratios were further used to estimate the probability characteristics of information processing security when performing functional tasks in various scenarios of attacks on digital substations, as well as multiple technologies used for protection against such threats. Numerical studies of safe information processing probability of different intensities of attacks and times of their activation were conducted, in order to consider the frequency of diagnostics of the system by the service personnel and customer requirements for the safe operation of the system in a certain period. We performed calculations for various protection technologies against similar attacks on digital substations. A protection technology with system diagnostic deterministic frequency can support customer requirements in the event of accidental and relatively rare virus attacks. Security technologies consider different maintenance personnel operation modes to ensure customer fulfillment requirements for safe information processing probability and the case of deliberate attacks on digital substations in each period.

Conclusions. The technologies considered herein for information protection from attacks on digital substations can provide the necessary level of information security system operation for all types of threats. These technologies can be applied when the system diagnostics frequency increases from twice an hour to at least once every 25 minutes. Our findings underline the importance of timely monitoring of ever-changing attack environments for digital substations.

Keywords: digital substations, flow characteristic, viruses, safe operation probability, information, and computer systems

• **Submitted:** 12.04.2024 • **Revised:** 12.09.2024 • **Accepted:** 21.11.2024

For citation: Leontyev A.S., Zhmatov D.V. Probabilistic characteristics analysis of virus attack effect on digital substations. *Russian Technological Journal.* 2025;13(1):28–37. https://doi.org/10.32362/2500-316X-2025-13-1-28-37, https://elibrary.ru/BUGTUV

Financial disclosure: The authors have no financial or proprietary interest in any material or method mentioned.

The authors declare no conflicts of interest.

НАУЧНАЯ СТАТЬЯ

Анализ вероятностных характеристик воздействия вирусных атак на цифровые подстанции

А.С. Леонтьев,
Д.В. Жматов [@]

МИРЭА – Российский технологический университет, Москва, 119454 Россия
[@] *Автор для переписки, e-mail: zhmatov@mirea.ru*

Резюме

Цели. Цель данного исследования заключается в создании аналитических методов для оценки вероятностных характеристик безопасности информационных и программных элементов цифровых подстанций. Эти методы направлены на обеспечение кибербезопасности в условиях различных сценариев воздействия вирусов.

Методы. Использованы методы, базирующиеся на теории надежности, теории случайных процессов и теории восстановления.

Результаты. Выведены интегральные соотношения, которые позволяют оценить вероятностные характеристики безопасности обработки информации при выполнении функциональных задач в различных сценариях атак на цифровые подстанции, а также при использовании различных технологий защиты от подобных угроз. Проведены численные исследования вероятности безопасной обработки информации при различной интенсивности атак и времени их активации с учетом частоты проведения диагностики системы обслуживающим персоналом и требований заказчика к безопасному функционированию системы в определенный период времени. Расчеты выполнены для различных технологий защиты от подобных атак на цифровые подстанции. Показано, что технология защиты с детерминированной частотой диагностики системы может обеспечить требования заказчика к безопасности только при случайных и относительно редких вирусных атаках. Технологии защиты, учитывающие различные режимы работы обслуживающего персонала, могут обеспечить выполнение требований заказчика по вероятности безопасной обработки информации в заданный период времени и при преднамеренных атаках на цифровые подстанции.

Выводы. Рассмотренные технологии защиты информации от атак на цифровые подстанции могут обеспечить необходимый уровень безопасности функционирования информационной системы для всех видов угроз при условии увеличения частоты диагностики системы с 2 раз в 1 ч до не реже 1 раза в 25 мин. Это подчеркивает важность активной мониторинговой политики в условиях постоянно меняющейся среды атак для цифровых подстанций.

Ключевые слова: цифровые подстанции, характеристика потоков, вирусы, вероятность безопасного функционирования, информационно-вычислительные системы

• **Поступила:** 12.04.2024 • **Доработана:** 12.09.2024 • **Принята к опубликованию:** 21.11.2024

Для цитирования: Леонтьев А.С., Жматов Д.В. Анализ вероятностных характеристик воздействия вирусных атак на цифровые подстанции. *Russian Technological Journal.* 2025;13(1):28–37. https://doi.org/10.32362/2500-316X-2025-13-1-28-37, https://elibrary.ru/BUGTUV

Прозрачность финансовой деятельности: Авторы не имеют финансовой заинтересованности в представленных материалах или методах.

Авторы заявляют об отсутствии конфликта интересов.

INTRODUCTION

Modern information computer systems (ICS) are part of the control loop of socioeconomic and sociopolitical processes. They enable the main stages of analysis of the current situation to be automated, the emergence and development of crisis situations to be identified, and recommendations for their elimination and prevention to be formed. ICSs also provide analytically processed and summarized information for supporting the decision-making process [1]. Therefore, such systems are subject to increased requirements for timeliness and reliability of the information processed.

The software and hardware tools of an ICS should provide support for document preparation processes, taking into account possible interferences, including the impact of viruses, failures, malfunctions, and information distortion [2]. The integrated use of analytical methods to study virus threats and modeling on their basis the processes of virus impact on the information system with the help of the *KOK* tool-modeling software complex was considered for the first time in the work of A.I. Kostogryzov and G.A. Reznikov [3]. In order to facilitate the joint use of the original multilevel network analytical models of TDF research taking into account distortions in the input information [2] and analytical models that take into account information distortion by viruses, it seems reasonable to extend the class of models considered in [3] using recovery theory methods, as demonstrated in [4].

The studies [2, 5, 6] consider issues of evaluating the probabilistic-temporal characteristics of information processing taking into account failures, malfunctions, and distortions of input information under the limitations on the service time set by the customer. These studies also evaluate the reliability characteristics of ICS hardware, software and networks, which are the source of information for situation centers. At present, insufficient attention is paid to assessing the impact of viruses on the probabilistic-temporal characteristics of information processing, taking into account customer requirements for the security of system operation and the range of information protection technologies used by service personnel. Therefore, the analytical evaluation of probabilistic characteristics of information and software resources security under various scenarios of virus impact and information protection technologies appears a relevant research task.

The works [7–11] address computer viruses and their impact on data security, the main ways of virus penetration into the system, as well as a comparative analysis of antivirus programs. The articles [12–15] propose analytical models for an accurate determination of the intensity of virus attacks. The results obtained can be used as initial data for the development of a higher-level information security model, considered in the present article.

Data security is acquiring particular significance in the modern digital world, where information technology plays a key role in managing various systems, including energy networks. One of the main challenges in this context is the protection of digital substations from malicious impacts such as viruses.

For effective protection against viruses in digital substations, evaluation models that can predict the probabilistic characteristics of the possible impact of viruses on computer systems are needed. Such models can be useful in developing protection strategies and making decisions about the security of the information infrastructure.

One of the key elements of evaluation models is to consider the probability of viruses affecting digital substations. This requires an analysis of various attack scenarios and evaluation of the probability of their occurrence. In addition, it is important to consider the probability of detection and removal of viruses, as well as their potential impact on system operation.

Another important aspect to consider is the temporal aspect of attacks. Viruses may be active at specific time intervals or may be continuous. In order to properly assess risks and develop appropriate countermeasures, evaluation must take into account such temporal parameters. The various defense technologies which can be applied to prevent and detect virus attacks on digital substations must also be considered. Evaluation models should employ the effectiveness of these technologies and their ability to secure the system.

1. MAJOR CYBERATTACKS ON DIGITAL POWER SUBSTATIONS

Digital substations are a critical part of modern infrastructure, providing reliable transmission and distribution of electricity. However, as technology advances, digital substations are becoming more vulnerable to cyberattacks.

Table 1 presents the names of the main virus attacks on digital power substations.

The type of virus attack can impact various aspects of a digital power substation, including:

- *System functionality*. Virus attacks can disrupt the normal functioning of control, monitoring, and protection systems, thus leading to system failure or malfunction.
- *Data security*. Some types of viruses can be directed to steal or destroy data stored in a digital substation, thus leading to leaks of sensitive information or loss of important data.
- *System integrity*. Virus attacks can damage hardware or software components of a substation, thus resulting in loss of or damage to equipment and interruption of operations.

- *System availability*. Some virus attacks may cause denial of service or overload network resources, thus resulting in temporary system unavailability to process requests to operators.
- *Personnel safety*. Virus attacks can create dangerous situations for personnel working at the substation, for example by changing system parameters without their knowledge or possibly causing physical damage to equipment.
- *Financial losses*. A successful virus attack can cause significant financial losses associated with system restoration, lost revenue due to equipment downtime, and consumer reimbursements.

Threats from internal users, such as employees of energy companies, also pose a serious risk to the security of digital substations. Unauthorized access to systems, loss of confidential information or malicious actions within the company can have disastrous consequences.

Measures for preventing potential consequences of virus attacks include:

- regular updates of software and protection systems;
- introduction of multi-level authentication for access to substation control systems;
- training personnel on the basics of cybersecurity and identification of phishing attacks;
- monitoring network activity in order to detect suspicious behavior;
- implementation of clear security policies and access control to critical systems.

Table 1. Virus attacks on digital power substation

Name of attack	Description	Potential consequences
SQL-injection	Introduction of malicious SQL code into an application or database through incorrect processing of the user input	Gaining unauthorized access to data, changing or deleting information in the database
Malicious software	Installing malicious software on substation computers or devices for the purpose of stealing the data, interrupting operations, or controlling the system	Substation disruption, loss of data confidentiality, interruption of power supply
Phishing	Sending fake emails to deceive substation personnel, to gain access to systems or confidential information	Unauthorized access to systems, leakage of confidential data
DDos-attack[1]	Overloading the network or substation servers by sending a large number of requests, in order to disrupt operations	Failure of service, temporary or prolonged interruption of substation operation
GOOSE-messages[2] spoofing	Gaining unauthorized access to substation systems through the use of stolen credentials	Potential change of system operation parameters, disruption of system operation, threat to power supply security
Ransomware	Infection of the system with malicious program code, blocking access to data, demanding a ransom in order to restore access	Data loss, substation interruption, financial losses
Man-in-the-Middle	Intercept and alter communications between substation devices such that an attacker can manipulate data	Possibility of data manipulation and distortion, interruption of information exchange
Zero-Day Exploit	Exploitation of a vulnerability in software that has not yet been discovered and fixed by the developers	Unauthorized access, malware introduction, potential threat to system security
Spoofing (falsification)	Forging addresses or identities to create a false perception of authenticity or authorization	Breach of authentication, possible misleading of the control system
Attack on the hardware	Attempting to affect substation hardware, such as power transformers or circuit breakers	Potential damage to equipment, interruption of power supply

[1] Distributed denial of service.
[2] Generic object-oriented substation event is a protocol designed for communication between relay protection devices by transmitting data digitally over Ethernet.

Cyberattacks on digital power substations pose a serious threat to the energy infrastructure. Understanding the main types of attacks and taking appropriate measures for their prevention is an important task in ensuring the safety and reliability of substations in the face of ever-increasing cyber threats.

2. FORMULATION AND SOLUTION OF THE PROBLEM OF EVALUATING PROBABILISTIC SAFETY CHARACTERISTICS FOR DIGITAL SUBSTATIONS

Preventive diagnostic tools are assumed to be able to detect all infiltrated viruses and traces of their impact. Recovery tools are assumed to be able to fully restore the violated integrity of information and program resources of the *i*th type. As a result of diagnostics, viruses are eliminated. The integrity of information and program resources is then restored if distortions are detected, and interrupted requests can be processed again after restoration of system integrity. Evaluation using analytical approaches is based on the application of random process recovery theory methods [4].

In order to perform the necessary analytical transformations, it is required to set the following parameters:

$V_{imp}(t)$, distribution function (DF) of time between virus impacts on the system;

$V_{act}(t)$, DF of the virus activation time after it has entered the system;

$F_{diag}(t)$, DF of time between diagnostics;

$G_i(t)$, the DF of information processing time of the *i*th type, including waiting time in the queue and processing time itself.

The distribution functions used are approximated in analytical models by two-parameter Erlangian or hyperexponential DFs within the framework of second-order theory on mathematical expectations and variance [4].

DF moments $G_i(t)$ (mathematical expectation and variance) are estimated using multilevel models which describe information processing processes in the digital substation system. These models are formalized with the multilevel analytical nested models (mass service networks), using technological processing operations, emerging hardware and software failures [2]. This approach is original in terms of the temporal characteristics of request processing in nested hardware-level network models. Such an approach is relatively independent of the type of DFs which characterize the flows of requests at this level and the type of flows in the network model of the software level. This allows the flows at the hardware level to be approximated by Poisson flows. The approach enables not only the hardware-level network model to be decomposed, but also the multilevel model into network models of different levels. These can then be investigated by analytical methods. In particular, the hardware-level model is analyzed using the analytical methods of intermediate mass service theory. The software-level network model, which uses the approximation of real distributions by Erlang for the first two points, and hyperexponential distributions using the Erlang stage method, is reduced to an equivalent Markovian model. This is then assessed using well-known analytical methods.

We consider a regeneration process in which the regeneration points correspond to the start time of the next antivirus diagnosis of digital substations.

Let $\{t_n\}_{n=1}^{\infty}$ be the recovery process, moments t_n of which correspond to the time of the next antivirus diagnostics of the system.

If the intervals between diagnostics τ are the same, then the following formula is valid:

$$\xi_i(t) = \int_0^{t_{n+1}-t} V_{imp}(t - t_n - \theta) V_{act}(\theta) dG_i(\theta), \quad (1)$$

wherein $\xi_i(t)$ is the probability that during the processing of the *i*th type of request the processed information will be infected with viruses on the time interval $t_n \le t \le t_{n+1}$, $n \ge 1$.

In accordance with the basic properties of recovery processes and the limit theorem of recovery theory, the probability of information distortion by viruses $P_{vir(i)}$ is defined by relation (2), and the probability that information is not distorted is estimated by formula (3):

$$P_{vir(i)} = \frac{1}{F_{diag}^{(1)}} \int_0^{\infty} \left\{ \left[1 - F_{diag}(t) \right] \int_0^{\tau - t} V_{imp}(t - \theta) V_{act}(\theta) dG_i(\theta) \right\} dt, \quad (2)$$

$$P_{imp(i)} = 1 - P_{vir(i)}. \quad (3)$$

Over a given period of time T_{giv} from the moment of the last prophylaxis under the condition $T_{giv} < F_{diag}^{(1)}$, the probability of the hazardous impact absence is defined by the ratio:

$$P_{imp(i)}(T_{giv}) = 1 - \int_0^{T_{giv}} V_{imp}(T_{giv} - \theta) V_{act}(\theta) d\theta. \quad (4)$$

We use formula (4) to estimate the probability of the absence of dangerous effects without any diagnostics. It assumes that by the onset of the period T_{giv}, the integrity of information resources is ensured.

3. TECHNOLOGIES FOR PROTECTING INFORMATION SYSTEMS FROM HAZARDOUS IMPACTS

When implementing information technologies in digital substations, the frequency of routine diagnostics by maintenance personnel depends significantly on the frequency of exposure to threat sources, such as viruses. When making calculations, we will consider different scenarios of threats (viruses) impact on digital substations and different scenarios of routine diagnostics by maintenance personnel. Due to insufficient statistics concerning the impact of viruses on digital substations, we will assume that different digital substations use the same virus protection technologies.

Routine diagnostics and system integrity control of information and software resources are performed at certain intervals during implementation of protection technologies. The system integrity is restored using the methods provided for the purpose of detection of inactivated sources of danger (viruses) or traces of their impact.

We examine the probability of secure information processing at different levels of intensity of viruses and their activation time, different frequency of system diagnostics by maintenance personnel, and given customer requirements for the probability of secure system operation.

The following designations for the initial data are used in the calculations:

j is an index of scenario variant and protection method;

$\sigma_j = \frac{1}{V_{\text{imp}}^{(1)}}$ is the frequency of impact on the system for virus introduction;

$\beta_j = F_{\text{act}}^{(1)}$ is the average activation time of the infiltrating virus in jth scenario;

$T_{\text{int.}j} = F_{\text{diag.}j}^{(1)}$ is the average time interval between the end of the previous diagnosis and the beginning of the next one in jth scenario;

$T_{\text{diag.}j}$ is the duration of diagnostics, including restoration of system integrity (set in advance).

The customer should impose requirements on the following parameters:

$P_{\text{giv.}j}$ is the minimum permissible probability of safe operation of the system (predefined by the customer).

The following indicators are evaluated:

$P_{\text{imp.}j}$ is a probability of absence of hazardous impact during a specified period $T_{\text{giv.}j}$ in jth scenario.

From the user point of view, the system is assumed to be safe for a given time T_{giv} = 1 day, if no hazardous impact occurs during this time or if all sources of danger are detected immediately when they enter the system. Moreover, these models assume that after diagnostics, as well as after integrity restoration, the system remains in a completely safe state.

The average time required for a diagnostic procedure, including repair work, is estimated to be 60 s. The initial data for calculations is presented in Table 2.

Given insufficient statistics on the impact of viruses on digital substations, virus exposure scenarios, including virus intensity and activation time, were chosen according to the data presented in [3]. Estimation calculations were performed using exponential distribution functions. In this asymptotic case, the analytical relations obtained using recovery theory methods and the analytical formulas presented in [3] give the same results. Therefore, as in [3], the tool-modeling complex for assessing the quality of functioning of *KOK* information systems was used for the preliminary assessment calculations of the impact of viruses on electric substations. In the future, as in [4], real distributions will be approximated by two-parameter Erlangian or hyperexponential distributions for the first two moments.

Figure 1 presents the calculation results of the safe operation probability of digital substations in a variety of threat impact scenarios, and the routine diagnostics scenarios of the information integrity and program resources by maintenance personnel $(j = \overline{1,10})$ in accordance with the given initial data (Table 2).

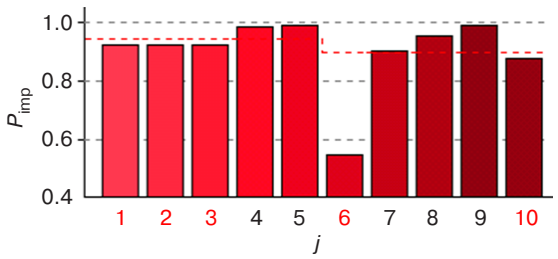

Fig. 1. Probability of safe operation of the information system in different threat scenarios $(j = \overline{1,10})$ for a digital substation

Based on the above preliminary assessment calculation and the data presented in Table 2, the following conclusions can be drawn.

1. Protection of digital substations from deliberate threats with the frequency of impact once a day is provided by diagnostics of information and program resources at least once every 6 h (Fig. 4, j = 7, 8, 9).
2. At the same time, for threats occurring on average once every 1 h, the probability of no dangerous virus exposure during a day would be 0.88 at a diagnostic frequency of once every 30 min, less than the specified 0.9.

We examine the question concerning when diagnostic modes of information and software resources of digital substations can provide the required security of digital substations for the most dangerous scenario of virus attacks. These are when new viruses penetrate the system on average once every 1 h with their activation time of 1 h.

Table 2. Security evaluations of information system operation at a digital substation

Threat characteristics			Characteristics of the substation service device			Customer's requirements
j	σ_j	β_j	$T_{int,j}$	$T_{diag,j}$	$T_{giv,j}$	$P_{giv,j}$
1	1 week^{-1}	6 h	1 week	1 min	1 day	0.95
2	1 week^{-1}	6 h	3 days	1 min	1 day	0.95
3	1 week^{-1}	6 h	1 day	1 min	1 day	0.95
4	1 week^{-1}	6 h	6 h	1 min	1 day	0.95
5	1 week^{-1}	6 h	3 h	1 min	1 day	0.95
6	1 day^{-1}	3 h	1 day	1 min	1 day	0.90
7	1 day^{-1}	3 h	6 h	1 min	1 day	0.90
8	1 day^{-1}	3 h	3 h	1 min	1 day	0.90
9	1 day^{-1}	3 h	1 h	1 min	1 day	0.90
10	1 h^{-1}	1 h	30 min	1 min	1 day	0.90

Figures 2–5 show the dependencies of the probability of the absence of dangerous impacts on information resources of digital substations for the most dangerous scenario of deliberate virus impacts $P_{imp.10}$ ($j = 10$). These are in the event of changes in the intensity of threat impacts, average virus activation time, interval between diagnostics and probabilistic-time requirements of the customer.

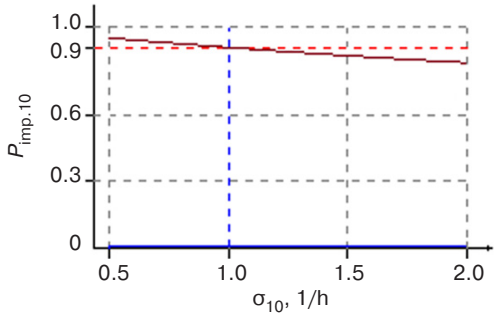

Fig. 2. Dependence of the value of $P_{imp.10}$ on the frequency of exposure to threats

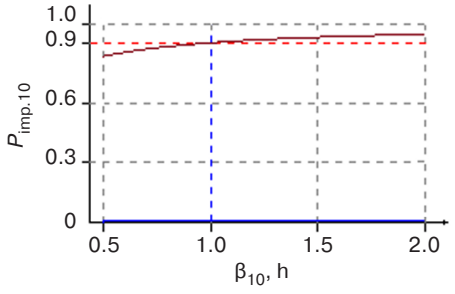

Fig. 3. Dependence of the value of $P_{imp.10}$ on the average time of threat activation

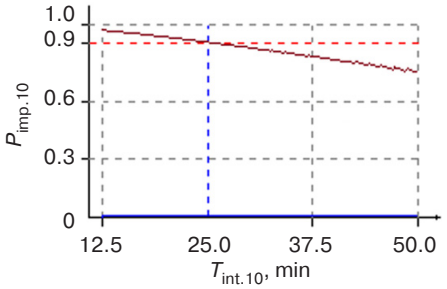

Fig. 4. Dependence of the value of $P_{imp.10}$ on the average interval between diagnostics

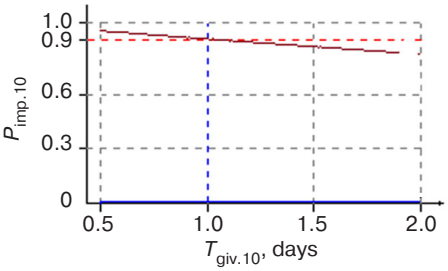

Fig. 5. Dependence of the value of $P_{imp.10}$ on the time set by the customer $T_{giv.10}$

The calculation results presented in Figs. 2–5 show that the system security decreases noticeably with increasing virus intensity. In all the scenarios considered, an increase in the virus activation time leads to an increase in and the system security. When the time of absence of virus influences T_{giv} set by the customer decreases, the system security increases in all threat scenarios and protection methods.

The results obtained indicate that when system diagnostics is implemented every 25 min rather than once every 1 h (shown in Fig. 4), the protection of digital substations from the most dangerous scenarios of virus impact can provide the required security of information resources of digital substations while meeting the specified customer requirements for the probability of safe operation.

These scenarios of virus threats and ways to combat them are general in nature and can be applied to study the security of various digital substations.

CONCLUSIONS

This study provides a review of the main types of cyberattacks on digital power substations, along with their potential consequences and prevention measures.

We established integral relations that allowed us to evaluate the probabilistic characteristics of safe information processing of digital substations under different scenarios of virus exposure, as well as when using different technologies of information protection from dangerous influences. These ratios provide an opportunity to analyze the probability of safe information processing of digital substations in different levels of virus impact intensity, virus activation time, frequency of diagnostics by maintenance personnel and specified customer requirements for the probability of safe operation of the message management system in digital substations.

We conduct calculations for different technologies of the information protection of digital substations from dangerous influences. Particular attention was paid to the most dangerous scenarios of virus impact and to the protection technology which ensures the customer-defined safety of digital substations functioning under all considered threats. An important conclusion is that by implementing this technology and reducing the interval of diagnostics of information resources of digital substations to 25 min, the level of safety of digital substations system operation can be significantly increased.

The results obtained provide practically applicable recommendations to ensure the security of information resources in digital substations using modern technologies of protection against virus attacks. The findings are relevant in the context of the growing complexity of threats and high dynamics of digital technology development, emphasizing the need for effective measures to ensure the security of digital substation information systems.

Authors' contributions

A.S. Leontyev—developed integral equations to assess the probabilistic characteristics of information processing security; conducted numerical studies on the probability of secure information processing under varying attack intensities, activation times, and system diagnostic frequencies; analyzed the impact of a deterministic diagnostic frequency on meeting customer safety requirements under random and infrequent attacks.

D.V. Zhmatov—investigated the effectiveness of various protection technologies against attacks on digital substations; analyzed protection technologies that consider the operating modes of maintenance personnel and their impact on meeting customer requirements; formulated conclusions about the need to increase system diagnostic frequency to ensure security under deliberate attacks; emphasized the importance of an active monitoring policy in the changing threat landscape for digital substations.

REFERENCES

1. Starovoitov A.V., Starikov P.P., Dubitsky K.A., Lukyanov S.E., Pavlov L.P., Simonov V.M., Syedin D.Yu. Computerized complex of federal information systems for supporting decision-making in the field of science and technology. *Informatizatsiya i svyaz' = Informatization and Communication*. 2021;6:7–19 (in Russ.). https://doi.org/10.34219/2078-8320-2021-12-6-7-19
2. Leontyev A.S. Multilevel Analytical and Analytical-Simulation Models for Evaluating the Probabilistic and Temporal Characteristics of Multimachine Computing Complexes with Regard to Reliability. *Mezhdunarodnyi nauchno-issledovatel'skii zhurnal = International Research Journal*. 2023;5(131) (in Russ.). https://doi.org/10.23670/IRJ.2023.131.8
3. Kostogryzov A.I., Reznikov G.Y. Modeling of Hazardous Impact Processes on Protected Information System. *Informatsionnye tekhnologii v proektirovanii i proizvodstve = Information Technologies in Design and Production*. 2004;2:17–27 (in Russ.).
4. Gusev K.V., Leontiev A.S. Theoretical Development of Models for the Assessment of Security against Unauthorized Access and Preservation of the Confidentiality of the Information Used. *IT Standard*. 2021;4(29):38–44 (in Russ.).
5. Akimova G.P., Solovyev A.V., Tarkhanov I.A. Modeling the reliability of distributed information systems. *Informatsionnye tekhnologii i vychislitel'nye sistemy = Journal of Information Technologies and Computing Systems*. 2019;3:70–86 (in Russ.). https://doi.org/10.14357/20718632190307
6. Pavsky V.A., Pavsky K.V. Mathematical Model for Calculating Reliability Indicators of Scalable Computer Systems Considering Switching Time. *Izvestiya YuFU. Tekhnicheskie nauki = Izvestiya SFedU. Engineering Sciences*. 2020;2(212): 134–145 (in Russ.). https://doi.org/10.18522/2311-3103-2020-2-134-145

7. Minitaeva A.M., Sokolov A.V. Main Ways of Penetration and Impact of File Viruses on the System. *Mezhdunarodnyi zhurnal gumanitarnykh i estestvennykh nauk = International Journal of Humanities and Natural Sciences*. 2023;4–3(79):56–60 (in Russ.). https://doi.org/10.24412/2500-1000-2023-4-3-56-60
8. Litvinov P.V. Simulation modeling of information security issues as a tool for assessing security and cost optimization. *Mir komp'yuternoi avtomatizatsii = Computer Automation World*. 2016;1:43–53 (in Russ.).
9. Blazutskaya E.Y., Sharafutdinov A.G. Next Generation Viruses and Antiviruses. *NovaInfo.ru*. 2015;1(35):92–94 (in Russ.).
10. Popov I.O., Marunko A.S., Petrov O.I., Oleinik A.A. Viruses and Antivirus Programs in Information Security. *Nauchnye zapiski molodykh issledovatelei = Scientific Notes of Young Scientists*. 2020;8(4):74–80 (in Russ.).
11. Sidenko G.A., Redko G.V., Beznos O.S. Comparative Analysis of Antivirus Programs. *StudNet*. 2020;9:676–680 (in Russ.).
12. Zavodtsev I.A., Borisov M.A., Bondarenko M.M., Meleshko V.A. Refined Method of Analytical Modeling of Viral Software Propagation Processes for Assessing Security of Informatization Objects. *Computational Nanotechnology*. 2022;9(1):11–20 (in Russ.).
13. Boyko A.A. Method of Analytical Modeling of Viruses Propagation Process in Computer Networks with Different Topology. *Trudy SPIIRAN = SPIIRAS Proceedings*. 2015;5(42):196–211 (in Russ.). https://doi.org/10.15622/sp.42.4
14. Magazev A.A., Tsyrulnik V.F. Investigation of a Markov Model for Computer System Security Threats. *Aut. Control Comp. Sci.* 2018;52(7):615–624. https://doi.org/10.3103/S0146411618070180
[Original Russian Text: Magazev A.A., Tsyrulnik V.F. Investigation of a Markov Model for Computer System Security Threats. *Modelirovanie i analiz informatsionnykh sistem*. 2017;24(4):445–458 (in Russ.). https://doi.org/10.18255/1818-1015-2017-4-445-458]
15. Kotenko I.V., Vorontsov V.V. Analytical Models of Network Worms Propagation. *Trudy SPIIRAN = SPIIRAS Proceedings.* 2007;4:208–224 (in Russ.). https://doi.org/10.15622/sp.4.15

СПИСОК ЛИТЕРАТУРЫ

1. Старовойтов А.В., Стариков П.П., Дубицкий К.А., Лукьянов С.Э., Павлов Л.П., Симонов В.М., Съедин Д.Ю. Комплекс автоматизированных государственных информационных систем поддержки управленческих решений в сфере науки и техники. *Информатизация и связь*. 2021;6:7–19. https://doi.org/10.34219/2078-8320-2021-12-6-7-19
2. Леонтьев А.С. Многоуровневые аналитические и аналитико-имитационные модели оценки вероятностно-временных характеристик многомашинных вычислительных комплексов с учетом надежности. *Международный научно-исследовательский журнал.* 2023;5(131). https://doi.org/10.23670/IRJ.2023.131.8
3. Костогрызов А.И., Резников Г.Я. Моделирование процессов опасного воздействия на защищаемую информационную систему. *Информационные технологии в проектировании и производстве*. 2004;2:17–27.
4. Гусев К.В., Леонтьев А.С. Теоретическое развитие моделей для оценки защищенности от несанкционированного доступа и сохранения конфиденциальности используемой информации. *ИТ Стандарт*. 2021;4(29):38–44.
5. Акимова Г.П., Соловьев А.В., Тарханов И.А. Моделирование надежности распределенных вычислительных систем. *Информационные технологии и вычислительные системы* (*ИТиВС*). 2019;3:70–86. https://doi.org/10.14357/20718632190307
6. Павский В.А., Павский К.В. Математическая модель для расчета показателей надежности масштабируемых вычислительных систем с учетом времени переключения. *Известия ЮФУ. Технические науки*. 2020;2(212):134–145. https://doi.org/10.18522/2311-3103-2020-2-134-145
7. Минитаева А.М., Соколов А.В. Основные способы проникновения и воздействия файловых вирусов на систему. *Международный журнал гуманитарных и естественных наук*. 2023;4–3(79):56–60. https://doi.org/10.24412/2500-1000-2023-4-3-56-60
8. Литвинов П.В. Имитационное моделирование вопросов информационной безопасности как инструмент оценки защищенности и оптимизации затрат. *Мир компьютерной автоматизации.* 2016;1:43–53.
9. Блазуцкая Е.Ю., Шарафутдинов А.Г. Вирусы нового поколения и антивирусы. *NovaInfo.ru*. 2015;1(35):92–94.
10. Попов И.О., Марунько А.С., Петров О.И., Олейник А.А. Вирусы и антивирусные программы в информационной безопасности. *Научные записки молодых исследователей.* 2020;8(4):74–80.
11. Сиденко Г.А., Редько Г.В., Безнос О.С. Сравнительный анализ антивирусных программ. *Научно-образовательный журнал для студентов и преподавателей «StudNet»*. 2020;9:676–680.
12. Заводцев И.А., Борисов М.А., Бондаренко М.М., Мелешко В.А. Уточненный способ аналитического моделирования процессов распространения вирусного программного обеспечения для оценки защищенности объектов информатизации. *Computational nanotechnology*. 2022;9(1):11–20.
13. Бойко А.А. Способ аналитического моделирования процесса распространения вирусов в компьютерных сетях различной структуры. *Труды СПИИРАН*. 2015;5(42):196–211. https://doi.org/10.15622/sp.42.4
14. Магазев А.А., Цырульник В.Ф. Исследование одной марковской модели угроз безопасности компьютерных систем. *Моделирование и анализ информационных систем*. 2017;24(4):445–458. https://doi.org/10.18255/1818-1015-2017-4-445-458
15. Котенко И.В., Воронцов В.В. Аналитические модели распространения сетевых червей. *Труды СПИИРАН*. 2007;4:208–224. https://doi.org/10.15622/sp.4.15

About the authors

Alexander S. Leontyev, Cand. Sci. (Eng.), Senior Researcher, Associate Professor, Department of Mathematical Support and Standardization, Institute of Information Technologies MIREA – Russian Technological University (78, Vernadskogo pr., Moscow, 119454 Russia). E-mail: leontev@mirea.ru. RSCI SPIN-code 5798-9721, https://orcid.org/0000-0003-3673-2468

Dmitry V. Zhmatov, Cand. Sci. (Eng.), Associate Professor, Department of Mathematical Support and Standardization, Institute of Information Technologies, MIREA – Russian Technological University (78, Vernadskogo pr., Moscow, 119454 Russia). E-mail: zhmatov@mirea.ru. Scopus Author ID 56825948100, RSCI SPIN-code 2641-6783, https://orcid.org/0000-0002-7192-2446

Об авторах

Леонтьев Александр Савельевич, к.т.н., старший научный сотрудник, доцент кафедры математического обеспечения и стандартизации информационных технологий, Институт информационных технологий, ФГБОУ ВО «МИРЭА – Российский технологический университет» (119454, Россия, Москва, пр-т Вернадского, д. 78). E-mail: leontev@mirea.ru. SPIN-код РИНЦ 5798-9721, https://orcid.org/0000-0003-3673-2468

Жматов Дмитрий Владимирович, к.т.н., доцент, доцент кафедры математического обеспечения и стандартизации информационных технологий, Институт информационных технологий ФГБОУ ВО «МИРЭА – Российский технологический университет» (119454, Россия, Москва, пр-т Вернадского, д. 78). E-mail: zhmatov@mirea.ru. Scopus Author ID 56825948100, SPIN-код РИНЦ 2641-6783, https://orcid.org/0000-0002-7192-2446

Translated from Russian into English by Lyudmila O. Bychkova
Edited for English language and spelling by Dr. David Mossop

Information systems. Computer sciences. Issues of information security

Информационные системы. Информатика. Проблемы информационной безопасности

UDC 004.855.5:004.622
https://doi.org/10.32362/2500-316X-2025-13-1-38-48
EDN HJHQTR

RESEARCH ARTICLE

Topic modeling in the stream of short messages in Russian

Elena S. Mozaidze @

V.G. Shukhov Belgorod State Technological University, Belgorod, 308012 Russia
@ *Corresponding author, e-mail: mozaidze95@mail.ru*

Abstract

Objectives. This work is devoted to the topic modeling of short messages received through social networks or in another way in the form of a series of short messages. This need arises in public relations systems in state and municipal structures, in public opinion polling centers, as well as in customer service systems and marketing departments. The aim of the work is to develop and experimentally test a set of algorithms for a thematic model for automatically determining the main topics of information exchange and typical messages illustrating these topics.

Methods. The work uses methods of variable statistical distributions applied to collocation statistics and approaches typical for resolving problems of topic modeling of short texts, but applied to successive messages. In this way, online machine learning and topic modeling are considered jointly.

Results. The work considered the construction of a thematic model in which clusters found with the presentation of their typical representatives and current weight can help decision-making in accordance with the subject of these most important messages. The proposed method was experimentally tested on a corpus of real messages. The results of topic modeling (the constructed thematic models) are consistent with the results obtained manually. The messages selected illustrate that the topics with the highest weight are seen as such from the point of view of human experts.

Conclusions. The proposed algorithm of topic modeling allows the most important topics in current communication to be automatically identified. It shows posts that serve as indicators of these topics, and thereby significantly simplifies the solution of the problem.

Keywords: topic modeling, EM-algorithm, hidden placement, streaming renormalization method

• **Submitted:** 25.03.2024 • **Revised:** 30.09.2024 • **Accepted:** 17.11.2024

For citation: Mozaidze E.S. Topic modeling in the stream of short messages in Russian. *Russian Technological Journal.* 2025;13(1):38–48. https://doi.org/10.32362/2500-316X-2025-13-1-38-48, https://elibrary.ru/HJHQTR

Financial disclosure: The author has no financial or proprietary interest in any material or method mentioned.

The author declares no conflicts of interest.

НАУЧНАЯ СТАТЬЯ

Тематическое моделирование в потоке коротких сообщений на русском языке

Е.С. Мозаидзе [@]

Белгородский государственный технологический университет им. В.Г. Шухова, Белгород, 308012 Россия
[@] *Автор для переписки, e-mail: mozaidze95@mail.ru*

Резюме

Цели. Работа посвящена тематическому моделированию коротких сообщений, поступающих посредством социальных сетей или другим способом в виде серии. Такая задача возникает в системах работы с населением в государственных и муниципальных структурах, в центрах опроса общественного мнения, а также в системах обслуживания клиентов и маркетинговых подразделениях. Цель работы – разработка и экспериментальная проверка набора алгоритмов тематической модели для автоматического определения основных тем обмена информацией и типичных сообщений, иллюстрирующих эти темы.

Методы. Используются методы переменных статистических распределений, примененных к статистике коллокаций, и подходы, характерные для решения задач тематического моделирования коротких текстов, но в применении к следующим друг за другом сообщениям. Таким образом, задачи онлайнового машинного обучения и тематического моделирования рассматриваются в совокупности.

Результаты. Рассмотрено построение тематической модели, в которой найденные кластеры с предъявлением их типичных представителей и текущего веса могут помочь человеку в принятии решений в соответствии с тематикой этих наиболее важных сообщений. Предложенный метод был экспериментально протестирован на корпусе реальных сообщений. Результаты тематического моделирования (построенные тематические модели) согласуются с результатами, полученными вручную: выбранные сообщения, иллюстрирующие проблемные темы с наибольшим весом, являются таковыми и с точки зрения экспертов.

Выводы. Предлагаемый алгоритм тематического моделирования позволяет автоматически выявлять наиболее важные темы в текущем общении, показывает посты, служащие индикаторами этих тем, что позволяет существенно упростить решение задачи.

Ключевые слова: тематическое моделирование, EM-алгоритм, скрытое размещение, метод поточной перенормировки

• **Поступила:** 25.03.2024 • **Доработана:** 30.09.2024 • **Принята к опубликованию:** 17.11.2024

Для цитирования: Мозаидзе Е.С. Тематическое моделирование в потоке коротких сообщений на русском языке. *Russian Technological Journal.* 2025;13(1):38–48. https://doi.org/10.32362/2500-316X-2025-13-1-38-48, https://elibrary.ru/HJHQTR

Прозрачность финансовой деятельности: Автор не имеет финансовой заинтересованности в представленных материалах или методах.

Автор заявляет об отсутствии конфликта интересов.

INTRODUCTION

When working with social networks and messengers, the need almost always arises for an automated search for the most important topic in the exchange of messages. This is due to many reasons, including the need for chat moderation, identifying moments when a responsible person needs to intervene, searching for the most important topics of communication at the moment in the context of chat topics.

The case studied in this article relates to information exchange in social networks in the city of Belgorod. The reason for this choice is that the authors were able to obtain this data, however, the proposed methodology is applicable to any research subject of this kind for which there is a sufficient amount of data available.

Topic modeling is a way of training a machine (computer) to identify meaningful topics in texts. For example, by analyzing an array of news and journalistic texts, it is possible to identify certain topics. Of course, computers cannot understand the meaning of articles literally, but if there is a large collection of texts with different topics, then the probabilities of joint use of words enable to identify separate thematic layers.

A topic stratum filtered from a set of texts is simply a set of words characteristic of a topic. Words in such a set are sorted by importance for the topic [1–3]. In terms of cluster analysis, a topic is the result of biclustering, i.e., simultaneous clustering of both words and documents according to their semantic proximity.

In 1998, the scientists K. Papadimitriou, H. Tomaki, S. Vempala, and P. Raghavan were among the first to show interest in the topic of the probabilistic topic model [4]. Their work was devoted to latent semantic indexing (LSI), a method of information retrieval based on spectral analysis of the document database.

Further development of this topic is reflected in the works of foreign scientists.

Thomas Hofmann [5] studied probabilistic latent semantic indexing. Unlike the standard latent semantic indexing using singular value decomposition, the probabilistic variant has a strong statistical foundation and defines a proper generative model of the data. Search experiments on a number of test collections show significant performance gains over direct term matching methods as well as LSI. David Bley [6–8] considered supervised latent Dirichlet allocation (sLDA) or the statistical model of labeled documents. In his papers, he illustrates the advantages of sLDA over modern ordered regression, as well as over unsupervised latent Dirichlet allocation (LDA) analysis followed by a separate regression. Andrew Ng, an American computer scientist, Associate Professor at Stanford University, a researcher into robotics and machine learning, and one of the founders of the online learning platform "Coursera"[1], predicted long ago[2] [3] that natural language recognition would become the main method of human-computer interaction. In his work, he drew attention to reinforcement learning as one of the ways of machine learning.

Russian scientists have also contributed to the development of this topic.

Vorontsov [9] proposed in his work additive regularization of topic models (ARTM), based on maximization of the weighted sum of the logarithm of likelihood and additional criteria: regularizers. This simplifies the combination of topic models and the construction of any complex multi-objective models. Potapenko [10] considered a generalized EM-algorithm[3] with smoothing, sampling and thinning heuristics, enabling both known thematic models and new ones to be obtained at different combinations of these heuristics. Lukashevich [11] and Nokel[4] have presented the results of experiments on adding bigrams to topic models and taking into account the similarity between them and unigrams. They proposed a new algorithm PLSA-SIM, as a modification of the probabilistic latent semantic analysis (PLSA) algorithm for building topic models. The article by Korshunov and Gomzin presents a comparative review of various models, describes ways of estimating their parameters and quality of results, and gives examples of open software implementations [12].

Topic modeling software libraries such as *Mallet*[5], *Gensim*[6], and *BigArtm*[7] have been developed, thus enabling the creation of probabilistic topic modeling.

The active use of large language model (LLM) tools, including for resolving topic modeling problems, began a few years ago. Quite a large number of works in this area have appeared, a number of which are relevant to the objectives of this study. In [13], the authors study key events in news feeds. The problem of their identification and links is considered. The study is based on the use of LLM for retrieval and summarization, while actual topic modeling is done by selecting the top topic with a sliding window algorithm. Despite

[1] https://www.coursera.org. Accessed December 02, 2024.

[2] Ng A.Y. *Shaping and Policy Search in Reinforcement Learning*. Ph.D. Thesis, UC Berkley, 2003.

[3] An expectation–maximization (EM) algorithm is an iterative method used in mathematical statistics to find maximum likelihood estimates of the parameters of probabilistic models when the model depends on some hidden variables.

[4] Nokel M.A. *Methods for improving probabilistic topic models of the text collections based on lexicoterminological information*: Cand. Sci. Thesis (phys.-math.). Moscow, 2015. 20 p. (in Russ.).

[5] http://mallet.cs.umass.edu/topics.php. Accessed December 02, 2024.

[6] https://radimrehurek.com/gensim. Accessed December 02, 2024.

[7] http://bigartm.org. Accessed December 02, 2024.

good results in the stated area, the dynamics of topic distribution is not explicitly taken into account in the work and, in addition, the model is not pre-trained. The article [14] discusses the interpretation of topic model results using the large language model ChatGPT[8]. Interestingly, the result of the study showed that this LLM diverged from human interpretation in almost half of the cases. The purpose of the work was simply to demonstrate the ability of ChatGPT to describe topics and provide useful information, although the LLM did not help in topic modeling itself[9, 10]. The works focus, respectively, on topic modeling of summarized texts and the evaluation of contextualized topic coherence. The first article shows that LLM successfully translates meaning into summarized texts, but topic modeling in them is not always correct: the quality depends on the context. The automatic topic coherence evaluation proposed by the authors of the second paper works well for short documents and is not affected by meaningless but highly rated topics. This result certainly deserves to be considered and used for further research.

The aim of [1] is concentrated on statement of objective and the concept of researching the texts received by the state structures in order to categorize them into structural units of governance corresponding to the topics of the texts. The results were used in the present study.

The objectives of this study are the development and experimental validation of a set of topic modeling algorithms which will lead to the construction of a set of clusters with the presentation of their typical representatives and current weights, subject to the normal normalization and distribution conditions usual for topic modeling.

1. MATERIALS AND METHODS

1.1. Task statement

Let us assume that there is a permanent system which accepts short and medium-length messages (remarks, appeals). It can be a personal page in a social network, a web service for receiving requests, an electronic mailbox with automated text uploading, a customer relationship management system, etc.

Most often, one of two objectives arises for the information collected in this way: 1) to distribute messages into predefined groups (classes); or 2) to group messages into predefined groups (clusters) with similar semantics. Let us consider the second problem on the flow of messages, namely: to each newly arrived message we compare a vector, the coordinates of which represent the probabilities of this message belonging to the clusters formed by this moment.

The above objective is topic modeling or, in other words, soft biclustering. In this formulation, the problem is complicated by the fact that the set of messages is not bounded, and it is necessary either to determine the number of clusters each time, or to fix it and disband unnecessary clusters.

In the case of a satisfactory solution, the described objective can be applied in outreach systems for state and municipal structures, in public opinion polling centers, as well as in CRM (customer relationship management) systems and marketing services of corporations.

1.2. Solution method

Topic modeling methods are usually based on computing frequencies of words in documents, as well as words and documents in topics. The most commonly used methods for topic modeling are the EM-algorithm[11, 12], or hidden Dirichlet placement[13]. The distinguishing features of both are the need to weight all words in messages without taking meaning relations into account. Meanings are recovered from known meanings in large arrays of text. In essence, topic modeling only performs meaning benchmarking.

In the task at hand, working with meaning in the way described (similar to benchmarking) is not possible, because messages are usually short and often contain grammatical errors. In such a case, it is extremely difficult to orient them to a topic by means of benchmarking: this requires a larger block of text.

In [1], a technique of working with messages based on noun–verb pairs is proposed. The set is mapped to each message with at least one such pair. In this study, we will assume that such mapping has already been performed and each message has an identifier and a set of noun–verb pairs corresponding to it.

It is further assumed that:

- messages follow each other and each has an identifier;
- if there are no verbs or nouns in the message, it is considered irrelevant and is not taken into account, but an identifier is assigned to it;

[8] https://chat-gpt.org/. Accessed December 02, 2024.

[9] https://arxiv.org/abs/2403.15112. Accessed December 02, 2024.

[10] https://arxiv.org/abs/2305.14587. Accessed December 02, 2024.

[11] https://pythobyte.com/python-for-nlp-topic-modeling-8fb3d689/?ysclid=lgdpql4ef3963911399 (in Russ.). Accessed December 02, 2024.

[12] https://mathprofi.com/userinfo/14285/ (in Russ.). Accessed December 02, 2024.

[13] https://digitrain.ru/articles/252142/ (in Russ.). Accessed December 02, 2024.

- for the sliding message window, there is a log of noun–verb pairs with the corresponding message ID;
- topics are identified by the nouns included in the messages;
- each noun–verb pair has a probability (a number between 0 and 1) of occurring in a topic such that the sum of the probabilities for the pair across all topics is 1;
- each message has a probability of entering a topic, and the sum of the message probabilities across all topics is 1;
- the maximum number of topics is fixed. Deletion of topics is based on the topic weight indicator, calculated as the product of the average pairing probability in the topic by the number of messages related to the topic.

Such assumptions allow us to use the method of streamline renormalization: regular discarding of elements with small weights.

Next, let us consider one by one the steps of the process of analyzing messages in a moving window.

1.2.1. Preprocessing

The analyzer input receives the messages representing a text in Russian language consisting of one or several sentences. In order to prepare for modeling, the following operations are performed on the message text:

- sentence tokenization (splitting into sentences) by means of *nltk*[14];
- tokenization of words in a sentence by means of *nltk*;
- part-of-speech detection of tokens by means of *nltk*;
- lemmatization of nouns and verbs by means of *pymorphy2*[15];
- composition of noun–verb pairs according to the "nearest neighbors" rule.

All of this is implemented in the *appeals_processing.ipynb*[16] program module and can run in real time in the message stream.

1.2.2. Topic modeling

The output of the *appeals_processing.ipynb* preprocessor is a set of lemmatized nouns and verbs contained in a message box of length A lines, and a .csv or .json file (currently implemented to receive .csv, but reconfiguring to .json is easy), each line of which contains a list of three items:

- a string of the type "[(noun1, verb1), ..., (nounN, verbN)]";
- file number;
- number of the message in the file.

Thus, a set of noun–verb pairs can be nested in a number set on the one hand, and on the other hand unambiguously related to the message upon which it is constructed.

Then, for each pair in each message, the following algorithm is implemented, the steps of which are discussed in more detail in the Results section:

1. If the noun is contained in topics, the pair is included in those topics as well as in newly created topics for this message with equal probabilities.
2. If the noun is not contained in topics but the verb is contained in topics, the pair is included in those topics with probabilities reduced by a multiplier μ (a given constant parameter), and a new topic on the noun is created. The pair is included in it and in the newly created topics for that message with equal probabilities.
3. If neither the noun nor the verb is contained in topics, a new topic on the noun is formed and the pair is included in it, as well as in the newly created topics for this message with equal probabilities.

After all pairs of all messages have been processed by this algorithm, a .json file of the topic model is created. Each topic key (noun) is matched to a .json object with keys (noun–verb pairs), and values—probabilities of occurrence of the pair in the topic.

The result of the topic modeling is a convolved .json object of the topic model. In it, each topic key corresponds to a numerical value of the weight of this topic. Sorted by descending values, this object will give the desired clusters with their weights.

1.3. Materials

The data for this study was prepared from incoming messages which came to the administration of the city of Belgorod. Proper names and other attributes which de-mask personal data were removed. The dataset processed in this way was a .csv file with a header of the form "Date; Time; Question," any message can be reconstructed by date and time of receipt. The questions were the messages (requests) processed for the following purposes: to build a tag cloud (which in this case was a topic cloud) and to identify the most important questions.

The dataset included 3621 messages, some of which were repetitive (people copied the question and resent it). Some of which did not contain noun–verb pairs or were misspelled in such a way that the words were not in the underlying dictionaries.

The dataset review was organized by a sliding window of 300 messages. This is the average volume of messages for a month. Thus, the system analyzed the content of messages for the past month and provided the topics and the most important issues in messages for

[14] https://www.nltk.org/. Accessed December 02, 2024.
[15] https://github.com/pymorphy2/pymorphy2. Accessed December 02, 2024.
[16] https://disk.yandex.ru/d/8LPWy3ZP-7V30Q (in Russ.). Accessed December 02, 2024.

this period. Since the window was sliding, the result of the work could change every day, even with each new message.

Currently, the administration specialists prioritize the consideration of appeals manually. The proposed program system will be able to do this automatically. The study proposes a metric to measure the quality of sorting of appeals by a machine in comparison with sorting by humans.

2. RESULTS

2.1. Computing probabilities in a topic model

There are the following items as inputs to the topic modeling algorithm:

- .csv-file or other referral source containing the date and time the referral was received and the text of the reference;
- dictionaries of Russian nouns and verbs;
- dictionary T_m of the topic model built by this moment (by message number m): the key (noun) finds a dictionary with a key (a noun–verb pair) and a value in the form of the pair's probability of belonging to the topic. At the beginning of the work this dictionary does not yet exist, it is initiated by the first essential (containing a noun and a verb) reference.

In the dictionary of the topic model, the sum of the probability values (hereafter simply values) across all topics for a given pair must equal 1. That is:

$$T_m = \{t : \{s : p_{st}\}\}, \sum_t p_{st} = 1 \ \forall s \in S_m,$$

wherein t is the noun (topic), s are the noun–verb pairs constructed from the set S_m containing m references, p_{st} is the probability that the pair s belongs to topic t.

The output of the algorithm is a new T_{m+1} topic model dictionary which satisfies the same requirement.

Possible cases for each pair of s from reference $m + 1$:

1. If there is already a pair s in T_m, all its values are replaced by the values of $\hat{p}(1 - p_0 n_0)$, where $\hat{p}$ is the current value and p_0, n_0 are the value for the pair s in the new topics and their number, respectively;
2. If there is no pair s in T_m, but there is a topic that matches a noun from the pair s, then s is entered into the dictionary of that topic with a value equal to p_1; in addition, the pair s is entered into all newly created topics with probabilities p_4;
3. If there is no topic matching the noun from s in T_m, but some topics have a pair with the verb from s, then s is entered into the dictionaries of these topics with a value equal to p_2. In addition, the pair s is entered into all newly created topics with probabilities p_5;
4. If neither the noun nor the verb from the pair s is present in T_m, then a new topic (based on the noun from s) is created in T_{m+1}, and s is entered into it with probability p_3. In all other newly created topics, s is entered with the probability p_6.

Thus, we have non-intersecting possibilities for a pair s, and finally the following relations must be satisfied:

Case 1. The sum over all topics containing s, its new values, must be equal to 1:

$$p_0 n_0 + \sum_s \hat{p}_s (1 - p_0 n_0) = 1,$$

which is fulfilled identically. But since p_0 has the sense of probability, then:

$$p_0 \le \frac{1}{n_0},$$

Case 2. The sum of all old and new topics is equal to 1:

$$p_1 n_{\text{noun}} + n_0 p_4 = 1,$$

wherein n_{noun} is the number of available (old) topics with the noun from the pair s. Hence we obtain:

$$p_1 = \frac{1 - n_0 p_4}{n_{\text{noun}}}, \quad p_4 \le \frac{1}{n_0}.$$

Case 3. The sum of all old and new topics is equal to 1:

$$p_2 n_{\text{verb}} + n_0 p_5 = 1,$$

wherein n_{verb} is the number of old topics with a verb from the pair s. Hence we obtain:

$$p_2 = \frac{1 - n_0 p_5}{n_{\text{verb}}}, \quad p_5 \le \frac{1}{n_0}.$$

Case 4. The sum of all new topics is equal to 1:

$$p_3 n_{\text{new}} + (n_0 - n_{\text{new}}) p_6 = 1,$$

wherein n_{new} is the number of new topics with the noun pair s. Hence we obtain:

$$p_3 = \frac{1 - (n_0 - n_{\text{new}}) p_6}{n_{\text{new}}}, \ p_6 \le \frac{1}{n_0 - n_{\text{new}}}.$$

Since all probabilities p_4, p_5, p_6 correspond to the inclusion of a pair in the topic only on the basis of its

presence in one reference, we will assume that they are equal to:

$$p_4 = p_5 = p_6 \equiv q \le \frac{1}{n_0}.$$

We will consider the probabilities p_1 and p_5 to be equal, since they correspond to inclusion in the topic by noun.

We will relate the probability of inclusion in the topic by noun to the probability of inclusion in the topic by verb:

$$p_2 = kp_1.$$

Let us denote $p_1 = p_3 = p$, and now the unit sums are rewritten as:

$$pn_{\text{noun}} + n_0 q = 1,$$

$$kpn_{\text{verb}} + n_0 q = 1,$$

$$pn_{\text{new}} + (n_0 - n_{\text{new}})q = 1.$$

Let us solve this system of equations and determine p, q, k:

$$p = \frac{n_{\text{new}}}{n_{\text{new}} n_0 - n_{\text{noun}} n_0 + n_{\text{noun}} n_{\text{new}}},$$

$$q = \frac{n_{\text{new}} - n_{\text{noun}}}{n_{\text{new}} n_0 - n_{\text{noun}} n_0 + n_{\text{noun}} n_{\text{new}}},$$

$$k = \frac{n_{\text{noun}}}{n_{\text{verb}}},$$

if all n_{verb} and $n_{\text{new}} \cdot n_0 - n_{\text{noun}} \cdot n_0 + n_{\text{noun}} \cdot n_{\text{new}}$ differ from 0.

Let us now consider the cases where one or both of these values are equal to 0.

If $n_{\text{verb}} = 0$, then there are no pairs in the message corresponding to Case 3, and hence there are only two equations. The unknowns are only p and q. The solutions for them have already been found above.

If

$$n_{\text{new}} \cdot n_0 - n_{\text{noun}} \cdot n_0 + n_{\text{noun}} \cdot n_{\text{new}} = 0,$$

then it follows from the equations that $n_{\text{new}} = n_{\text{noun}} = 0$, i.e., this case corresponds to the described Case 1, when the pair s is already contained in T_m, and the parameter p_0 can have any value.

Since the new topics in this case definitely do not contain a noun from s, the pairing probability in them must be less than or equal to the probability of any pairing from a given reference in the old dictionary:

$$\hat{p}_s(1 - p_0 n_0) \le \min_s \hat{p}_s \Big|_{\hat{p}_s \ne 0}.$$

As a result, in order to find a new dictionary T_{m+1} for each pair from the circulation, we need to find the numbers:

$$n_{\text{noun}}, n_0, n_{\text{new}}, n_{\text{verb}}, p_0,$$

and n_0 is the same for all pairs s from a given circulation.

When building a new dictionary T_{m+1}, the following values of probabilities should be used:

$$p_0 = \frac{1}{n_0}\left(1 - \frac{1}{\hat{p}} \min_1 \hat{p}_1 \Big|_{\hat{p}_1 \ne 0}\right),$$

$$p_1 = p_3 = \frac{n_{\text{new}}}{n_{\text{new}} n_0 - n_{\text{noun}} n_0 + n_{\text{noun}} n_{\text{new}}},$$

$$p_2 = \frac{1}{n_{\text{verb}}} \cdot \frac{n_{\text{new}} n_s}{n_{\text{new}} n_0 - n_{\text{noun}} n_0 + n_{\text{noun}} n_{\text{new}}},$$

$$p_4 = p_5 = p_6 = \frac{n_{\text{new}} - n_{\text{noun}}}{n_{\text{new}} n_0 - n_{\text{noun}} n_0 + n_{\text{noun}} n_{\text{new}}}.$$

2.2. Algorithm of topic modeling of appeals represented by sets of “noun–verb” pairs

Input: T_m topic-model dictionary (can be empty) containing at most w different noun–verb pairs (w is the size of the “window”); a reference represented as a list of ordered noun–verb pairs (noun comes first, tokens are lemmatized).

Output: T_{m+1} dictionary containing at most w distinct pairs, in which all pairs from $m + 1$ reference were given probabilities of belonging to topics expressed by nouns.

Procedure:

1. We set $n_0 = n_{\text{new}} = 0$.
2. For all s pairs in a reference.
3. We look through the T_m dictionary and find:

   a) values $\hat{p}_s$ that s has in T_m, and the corresponding topics $t_{sp}^1, ..., t_{sp}^n$;

   b) topics $t_s^1, ..., t_s^{n_{\text{noun}}}$ matching the noun from s, but not containing s in its entirety;

   c) topics $t_{\text{verb}}^1, ..., t_{\text{verb}}^{n_{\text{verb}}}$ not matching the ones in (a) and (b) that have at least one verb from s;
4. If step 3 did not yield any matches, we increase n_0 by 1; if, in addition, there is no noun from s among the new topics already created (or no new topics yet), we increase n_{new} на 1 from it by copying and then work with it. Topic: $t_{\text{new}}^{n_{\text{new}}}$;

5. After viewing of the dictionary T_m is completed, we create a dictionary T_{m+1} from it by copying and then work with it.
6. We find

$$p_0 = \frac{1}{n_0}\left(1 - \frac{1}{\hat{p}} \min_1 \hat{p}_1 \Big|_{\hat{p}_1 \neq 0}\right);$$

7. We write into the topics $t_{sp}^1, ..., t_{sp}^n$ with probabilities p_0 the pairs s found at step 3a).
8. In the topics $t_s^1, ..., t_s^{n_{\text{noun}}}$ we write with probabilities $p = \frac{n_{\text{new}}}{n_{\text{new}} n_0 - n_{\text{noun}} n_0 + n_{\text{noun}} n_{\text{new}}}$ the pairs s found at step 3b).
9. In the topics $t_{\text{verb}}^1, ..., t_{\text{verb}}^{n_{\text{verb}}}$ we write with probabilities $p_2 = \frac{1}{n_{\text{verb}}} p$ the pairs s found at step 3c).
10. In the topics $t_{\text{new}}^1, ..., t_{\text{new}}^{n_{\text{new}}}$ we write:
    a) with probabilities p, which nouns match the topic;
    b) with probabilities
    $$q = \frac{n_{\text{new}} - n_{\text{noun}}}{n_{\text{new}} n_0 - n_{\text{noun}} n_0 + n_{\text{noun}} n_{\text{new}}}$$
    all other pairs of the reference.
11. If the number of pairs W in the dictionary is greater than w, we find the topic with the lowest weight and remove all or $(W - w)$ pairs (whichever is less) from it. We do this until all $(W - w)$ redundant pairs have been removed from the dictionary.
12. We compute the weights of the remaining topics and sort them.

Following this algorithm, we will obtain in each iteration the most weighted topics sorted by weight.

2.3. Results of topic modeling

In order to test the algorithm, the previously mentioned dataset was selected. Repetitive messages and messages that did not contain nouns with verbs were removed. The working dataset contained about 2700 messages sent to the mayor of Belgorod and city departments over a year. The data was anonymized. The window size (in pairs simultaneously in the dictionary) was assumed to be $w = 300$.

The figure shows a graph of the change in the weight of the top vocabulary topics throughout the year.

In general, the topics selected by the model correspond to the most important issues of concern to citizens over a certain period of time. This is not seen directly in the topics, because the topic in the context of this paper is a single word (noun). It is difficult to assess the importance of messages. However, a topic is a key

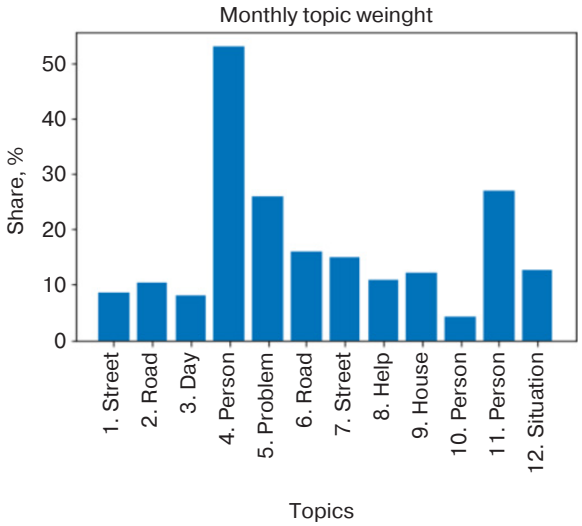

Figure. The most popular topics in references to the Mayor's Office of the city of Belgorod

to a set of messages and if that set is such, and changes in such a way that the weight of the topic increases, then the messages in the set are worthy of attention. The administration worked on the posts grouped around the topic leaders, and then other topics came to the top. This means that the people (administration) and the machine (proposed system) reacted correctly to the mood in the city. Otherwise there would have been topics that remained at the top for a long time. According to the assessment of the city administration specialists, the topic modeling was carried out correctly.

Metrics can be used to quantify the quality of topic modeling, such as the BCubed metric[17] [15], the use of which is justified by the construction of the algorithm. If we denote by $p_{ts.mon}$ the probability that a message s related to month *mon* belongs to topic t $\left(\sum_t p_{ts.mon} = 1\right)$, then BC precision (*BCP*) and BC recall (*BCR*) for the topic t in month *mon* will be defined by the formulae:

$$BCP(t, mon) = \frac{\sum_s p_{ts.mon}}{\sum_{s,k} p_{tsk}},$$

$$BCR(t, mon) = \frac{\sum_s p_{ts.mon}}{\sum_{r,k} p_{rsk}}.$$

For the dataset from the experiment, the first metric of top topics always exceeded 55%, while the second metric ranged from 27% to 83% (respectively the weight of topics shown in the figure). Given that the number of

[17] The BCubed family of metrics is implemented in the library https://pypi.org/project/bcubed-metrics/. Accessed December 02, 2024.

topics per month was never less than 70, the quality of the clustering can be recognized as high for the metric as well: random selection would result in a rate of about 1.5%.

CONCLUSIONS

In this study, we proposed a topic modeling method and algorithm for short messages. Clustering of short messages is a challenging task because such messages are very difficult to map to any context, i.e., large corpora of text on which the model can be trained do not usually provide satisfactory descriptions of topics.

The work is based on a previously proposed methodology of message meaning contour extraction in Russian texts based on noun–verb pairs.

Using the proposed methodology, a topic model was built and simulated on real data. The constructed clustering showed a relatively high level of quality by BCubed metric. At the same time, the result is also visible in qualitative evaluation. If a topic is calculated as a top topic in a particular period, the issues raised in it deserve to be prioritized and acted upon by people. In the example dataset used in the experiment, such a correlation (between the suggested set of messages for prioritized response and the messages people selected) was greater than 70%. However, even without quantification, the employees of the organization owning the dataset expressed their willingness to use the software built on the proposed algorithm as a decision support system (more precisely, an advising system for priority response to messages). In their opinion, this would greatly reduce message processing time.

ACKNOWLEDGMENTS

This work was realized in the framework of the Priority 2030 Program using the equipment of High Technology Center at the V.G. Shukhov Belgorod State Technological University.

REFERENCES

1. Brusentsev A.G., Zueva E.S. Thematic models and tools for processing the natural language in application to the problems of municipal structures. In: *Actual Theoretical and Applied Issues of the Socio-Economic Systems Management: Proc. Second International Scientific and Practical Conference.* Moscow; 2020. V. 2. P. 262–269 (in Russ.). https://elibrary.ru/fkgyxn
2. Zueva E.S. Probabilistic classification of incoming calls based on a controlled recurrent neurons algorithm. In: *Proc. International Scientific and Technical Conference of Young Scientists of V.G. Shukhov BSTU.* Belgorod: V.G. Shukhov BSTU; 2021. P. 3564–3575 (in Russ.). https://www.elibrary.ru/nhlzpv
3. Polyakov V.M., Mozaidze E.S. Collaborative filtering algorithm as a possible tool for detecting a dangerous tweet (short message) in social networks of a representative office of the government of the Belgorod region. In: *Modern Issues of Sustainable Development of Society in the Era of Transformation Processes*: *Collection of Materials of the 4th International Scientific and Practical conference*. Moscow; 2022. P. 136–148 (in Russ.). https://doi.org/10.34755/IROK.2022.14.90.027, https://www.elibrary.ru/mzrsgm
4. Papadimitriou C.H., Tamaki H., Raghavan P., Vempala S. Latent semantic indexing: A probabilistic analysis. In: *Proceedings of the Seventeenth ACM SIGACT-SIGMOD-SIGART Symposium on Principles of Database Systems.* ACM; 1998. P. 159–168. https://doi.org/10.1145/275487.275505
5. Hofmann T. Probabilistic latent semantic indexing. In: *Proceedings of the 22nd Annual International ACM SIGIR Conference on Research and Development in Information Retrieval.* ACM; 1999. P. 50–57. https://doi.org/10.1145/312624.312649
6. Blei D., McAuliffe J. Supervised topic models. In: *Advances in Neural Information Processing Systems 20* (*NIPS 2007*). 2008. P. 121–128.
7. Blei D.M., Lafferty J.D. Dynamic topic models. In: *Proceedings of the 23rd International Conference on Machine learning* (*ICML '06*). ACM; 2006. P. 113–120. https://doi.org/10.1145/1143844.1143859
8. Blei D.M. Probabilistic topic models. *Communications of the ACM*. 2012;55(4):77–84. https://doi.org/10.1145/2133806.2133826
9. Vorontsov K.V. Additive regularization for topic models of text collections. *Dokl. Math.* 2014;89(3):301–304. https://doi.org/10.1134/S1064562414020185
   [Original Russian Text: Additive regularization for topic models of text collections. *Doklady Akademii Nauk*. 2014;456(3): 268–271 (in Russ.). https://doi.org/10.7868/S0869565214090096]
10. Vorontsov K.V., Potapenko A.A. EM-like algorithms for probabilistic topic modeling. *Mashinnoe obuchenie i analiz dannykh = Machine Learning and Data Analysis*. 20131(6):657–686 (in Russ).
11. Nokel M.A., Lukashevich N.V. Topic Models: Adding Bigrams and Taking Account of the Similarity between Unigramsand Bigrams. *Vychislitel'nye metody i programmirovanie = Numerical Methods and Programming*. 2015;16(2):215–234 (in Russ.). https://doi.org/10.26089/NumMet.v16r222
12. Korshunov A., Gomzin A. Topic modeling in natural language texts. *Trudy Instituta sistemnogo programmirovaniya RAN* (*Trudy ISP RAN*) = *Proceedings of the Institute for System Programming of the RAS* (*Proceedings of ISP RAS*). 2012;23: 215–240 (in Russ.). https://doi.org/10.15514/ISPRAS-2012-23-13

13. Nakshatri N., Liu S., Chen S., Roth D., Goldwasser D., Hopkins D. Using LLM for Improving Key Event Discovery: Temporal-Guided News Stream Clustering with Event Summaries. *Findings of the Association for Computational Linguistics: EMNLP*. 2023:4162–4173. https://doi.org/10.18653/v1/2023.findings-emnlp.274
14. Rijcken E., Scheepers F., Zervanou K., Spruit M., Mosteiro P., Kaymak U. Towards Interpreting Topic Models with ChatGPT. *2023. Paper presented at The 20th World Congress of the International Fuzzy Systems Association*, Daegu, Republic of Korea. 2023. V. 5. Available from URL: https://pure.tue.nl/ws/portalfiles/portal/300364784/IFSA_InterpretingTopicModelsWithChatGPT.pdf
15. Amigo E., Gonzalo J., Artiles J., Verdejo F. A comparison of extrinsic clustering evaluation metrics based on formal constraints. *Information Retrieval*. 2009;12(4):461486.

СПИСОК ЛИТЕРАТУРЫ

1. Брусенцев А.Г., Зуева Е.С. Тематические модели и инструменты обработки естественного языка в применении к задачам муниципальных структур. В сб.: *Актуальные теоретические и прикладные вопросы управления социально-экономическими системами: материалы II Международной научно-практической конференции.* М.: Институт развития дополнительного профессионального образования; 2020. Т. 2. С. 262–269. https://elibrary.ru/fkgyxn
2. Зуева Е.С. Вероятностная классификация входящих обращений на основе алгоритма управляемых рекуррентных нейронов. В сб.: *Материалы Международной научно-технической конференции молодых ученых БГТУ им. В.Г. Шухова.* Белгород: БГТУ им. В.Г. Шухова; 2021. С. 3564–3575. https://www.elibrary.ru/nhlzpv
3. Поляков В.М., Мозаидзе Е.С. Алгоритм коллаборативной фильтрации как возможный инструмент выявления опасного твита (короткого сообщения) в социальных сетях представительства органа государственной власти Белгородской области. В сб.: Современные вопросы устойчивого развития общества в эпоху трансформационных процессов: *материалы IV международной научно-практической конференции.* М.: ООО «ИРОК»; 2022. С. 136–148. https://doi.org/10.34755/IROK.2022.14.90.027, https://www.elibrary.ru/mzrsgm
4. Papadimitriou C.H., Tamaki H., Raghavan P., Vempala S. Latent semantic indexing: A probabilistic analysis. In: *Proceedings of the Seventeenth ACM SIGACT-SIGMOD-SIGART Symposium on Principles of Database Systems.* ACM; 1998. P. 159–168. https://doi.org/10.1145/275487.275505
5. Hofmann T. Probabilistic latent semantic indexing. In: *Proceedings of the 22nd annual international ACM SIGIR conference on Research and development in information retrieval.* ACM; 1999. P. 50–57. https://doi.org/10.1145/312624.312649
6. Blei D., McAuliffe J. Supervised topic models. In: *Advances in Neural Information Processing Systems 20* (*NIPS 2007*). 2008. P. 121–128.
7. Blei D.M., Lafferty J.D. Dynamic topic models. In: *Proceedings of the 23rd International Conference on Machine learning* (*ICML '06*). ACM; 2006. P. 113–120. https://doi.org/10.1145/1143844.1143859
8. Blei D.M. Probabilistic topic models. *Communications of the ACM*. 2012;55(4):77–84. https://doi.org/10.1145/2133806.2133826
9. Воронцов К.В. Аддитивная регуляризация тематических моделей коллекций текстовых документов. *Доклады академии наук*. 2014;456(3):268–271. https://doi.org/10.7868/S0869565214090096
10. Воронцов К.В., Потапенко А.А. Модификации EM-алгоритма для вероятностного тематического моделирования. *Машинное обучение и анализ данных*. 2013;1(6):657–686.
11. Нокель М.А., Лукашевич Н.В. Тематические модели: добавление биграмм и учет сходства между униграммами и биграммами. *Вычислительные методы и программирование*. 2015;16(2):215–234. https://doi.org/10.26089/NumMet.v16r222
12. Коршунов А., Гомзин А. Тематическое моделирование текстов на естественном языке. *Труды Института системного программирования РАН* (*Труды ИСП РАН*). 2012;23:215–242. https://doi.org/10.15514/ISPRAS-2012-23-13
13. Nakshatri N., Liu S., Chen S., Roth D., Goldwasser D., Hopkins D. Using LLM for Improving Key Event Discovery: Temporal-Guided News Stream Clustering with Event Summaries. *Findings of the Association for Computational Linguistics: EMNLP*. 2023:4162–4173. https://doi.org/10.18653/v1/2023.findings-emnlp.274
14. Rijcken E., Scheepers F., Zervanou K., Spruit M., Mosteiro P., Kaymak U. Towards Interpreting Topic Models with ChatGPT. *2023. Paper presented at The 20th World Congress of the International Fuzzy Systems Association*, Daegu, Republic of Korea. 2023. V. 5. URL: https://pure.tue.nl/ws/portalfiles/portal/300364784/IFSA_InterpretingTopicModelsWithChatGPT.pdf
15. Amigo E., Gonzalo J., Artiles J., Verdejo F. A comparison of extrinsic clustering evaluation metrics based on formal constraints. *Information Retrieval*. 2009;12(4):461486.

About the author

Elena S. Mozaidze, Postgraduate Student, Department of Computer Software and Automated Systems, V.G. Shukhov Belgorod State Technological University (46, Kostyukova ul., Belgorod, 308012 Russia). E-mail: mozaidze95@mail.ru. https://orcid.org/0000-0002-7919-7963

Об авторе

Мозаидзе Елена Сергеевна, аспирант, кафедра программного обеспечения вычислительной техники и автоматизированных систем, ФГБОУ ВО «Белгородский государственный технологический университет им. В.Г. Шухова» (308012, Россия, Белгород, ул. Костюкова, д. 46). E-mail: mozaidze95@mail.ru. https://orcid.org/0000-0002-7919-7963

Translated from Russian into English by Lyudmila O. Bychkova
Edited for English language and spelling by Dr. David Mossop

Information systems. Computer sciences. Issues of information security
Информационные системы. Информатика. Проблемы информационной безопасности

UDC 681.3
https://doi.org/10.32362/2500-316X-2025-13-1-49-58
EDN JQICRJ

RESEARCH ARTICLE

Technical and economic analysis of servers as computing system modules of the warehouse scale computer class

Grigory V. Petushkov @, **Alexander S. Sigov**

MIREA – Russian Technological University, Moscow, 119454 Russia
@ *Corresponding author, e-mail: petushkov@mirea.ru*

Abstract

Objectives. The work set out to technically and economically analyze servers as computing modules of computing systems of the warehouse scale computer (WSC) class.

Methods. The research was carried out using the methods of mathematical analysis and modeling.

Results. The article provides a technical and economic analysis of computing modules or servers. Servers are created on the basis of Xeon (Intel) class microprocessors and the like. An overview of the microprocessor subclasses is given along with an indication of server organization options, as well as their main components and primary areas of use. Server reliability is a complex property that may include durability, maintainability and persistence, or certain combinations of these properties depending on the purpose of the object and the conditions of its use. To ensure maximum reliability, backup elements, including arrays of disks and power supplies, as well as backup servers, are used alongside special solutions, including the use of hot swapping and connection, checking and correction of random access memory errors, and temperature control of server compartments.

Conclusions. The review of options for organizing servers and their main components allows permits the conclusion that their operation is sufficiently reliable. However, servers integrated into the WSC class have special requirements, namely, continuity of operation in 24/7 mode for long periods of time. This requires the development of methods for assessing the reliability of such highly reliable systems, including backup elements, in relation to hardware and software failures, as well as methods for predicting failures and measures to combat their consequences.

Keywords: reliability, backup elements, MP subclasses, error checking and correction, error correction, disk array, WSC class

• **Submitted:** 18.10.2024 • **Revised:** 22.11.2024 • **Accepted:** 09.12.2024

For citation: Petushkov G.V., Sigov A.S. Technical and economic analysis of servers as computing system modules of the warehouse scale computer class. *Russian Technological Journal*. 2025;13(1):49–58. https://doi.org/10.32362/2500-316X-2025-13-1-49-58, https://www.elibrary.ru/JQICRJ

Financial disclosure: The authors have no financial or proprietary interest in any material or method mentioned.

The authors declare no conflicts of interest.

НАУЧНАЯ СТАТЬЯ

Технико-экономический анализ серверов как вычислительных модулей вычислительных систем класса WSC

Г.В. Петушков [@], **А.С. Сигов**

МИРЭА – Российский технологический университет, Москва, 119454 Россия
[@] *Автор для переписки, e-mail: petushkov@mirea.ru*

Резюме

Цели. Целью работы является технико-экономический анализ серверов как вычислительных модулей вычислительных систем (ВС) класса WSC (warehouse scale computer).

Методы. Основные результаты работы получены с использованием методов математического анализа и моделирования.

Результаты. Проведен технико-экономический анализ вычислительных модулей или серверов на базе микропроцессоров класса Xeon (Intel, США) и им подобных. Приведен обзор подклассов микропроцессоров с указанием основных областей их использования, а также вариантов организации серверов и их основных составляющих. Надежность – комплексное свойство, которое, в зависимости от назначения объекта и условий его применения, может включать безотказность, долговечность, ремонтопригодность и сохраняемость или определенные сочетания этих свойств. Для обеспечения максимальной надежности сервера используют как резервирующие элементы – массивы дисков и блоков питания, так и резервные серверы, и специальные решения: использование горячей замены и подключения, методы повышения надежности оперативной памяти Error Checking and Correction для коррекции ошибок модулей оперативной памяти, контроль температурных режимов отсеков сервера.

Выводы. Проведенный обзор вариантов организации серверов и их основных составляющих позволяет сделать вывод о достаточно высокой надежности их функционирования. От серверов, объединенных в ВС класса WSC, как от системы, требуется непрерывность функционирования в режиме 24/7 в течение длительного времени. Это требует разработки методик оценки надежности таких высоконадежных систем, включающих резервные элементы, по отношению к отказам аппаратуры и программного обеспечения, а также методик прогнозирования отказов и мер борьбы с их последствиями.

Ключевые слова: надежность, резервирующие элементы, подклассы микропроцессоров, error checking and correction , коррекция ошибок, массив дисков, класс WSC

• **Поступила:** 18.10.2024 • **Доработана:** 22.11.2024 • **Принята к опубликованию:** 09.12.2024

Для цитирования: Петушков Г.В., Сигов А.С. Технико-экономический анализ серверов как вычислительных модулей вычислительных систем класса WSC. *Russian Technological Journal*. 2025;13(1):49–58. https://doi.org/10.32362/2500-316X-2025-13-1-49-58, https://www.elibrary.ru/JQICRJ

Прозрачность финансовой деятельности: Авторы не имеют финансовой заинтересованности в представленных материалах или методах.

Авторы заявляют об отсутствии конфликта интересов.

INTRODUCTION

A server has many characteristics such as reliability, performance, form factor, power consumption, etc., which are in turn made up of a set of properties of the individual nodes that make up the server [1].

Performance, which is primarily determined by the amount and speed of computation, also depends on the type of tasks performed. As the required amount of computation increases, the performance of components, especially the processor, should also be increased.

Significant reductions in power consumption, as well as improved power efficiency and infrastructure flexibility, can be achieved using the modular design principles of blade server architecture [2].

Server power consumption is primarily affected by its available resources, such as the number of processors (and cores), their clock speeds, the amount of random access memory (RAM), the performance and capacity of the storage subsystem, as well as the performance of the network interfaces.

Depending on the task, the choice of hardware selection can include increases in available resources for improved performance or their decrease as a means of saving energy. Up to a certain point, resources may be increased by increasing memory capacity and performance, as well as the number of processors. However, after reaching this limit, further performance increases by such means becomes inefficient and uneconomical. In such cases, resources may be increased by other methods, for example, by parallelizing tasks between several servers or application optimization. Reductions in server resources are usually aimed at reducing the size and power consumption of installations [3].

PROCESSOR

Processor key characteristics [4] include performance, power consumption, and energy efficiency (the average amount of energy consumed per instruction executed).

Processor performance is defined as the execution speed of program code instructions, i.e., the number of instructions processed per unit time (instructions per second, IPS). This can be expressed mathematically as follows:

$$\text{Perfomance} = \frac{\text{Number of instructions}}{\text{Time of execution}} = \text{IPS}. \quad (1)$$

Instead of the number of instructions per time unit, it is more convenient to consider the number of program code instructions executed per processor clock (instructions per cycle, IPC).

$$\text{Perfomance} = \frac{\text{Number of instructions}}{\text{Number of clocks}} \times \times \frac{\text{Number of clocks}}{\text{Execution time}} = \text{IPC}. \quad (2)$$

Processor performance is directly related to both the clock frequency F and the number of instructions executed per IPC clock.

Thus, there are two main approaches to improving processor performance [5]: the first is to increase the clock frequency, while the second is to increase the number of instructions executed per clock. In practice, both approaches are usually applied simultaneously, since clock frequency parameters and the number of instructions executed per clock are interrelated.

The dependence of processor power consumption on its clock frequency appears as follows:

$$\text{Power} = CU^2F, \quad (3)$$

where C is the dynamic capacitance of the processor; U is the processor supply voltage; F is the processor operating frequency.

In other words, the power consumed by the processor is proportional to the clock frequency, the square of the processor's supply voltage and its dynamic capacitance. Since the clock frequency is directly related to the supply voltage, the power consumption varies nonlinearly with the processor frequency. Consequently, processor performance and power consumption are also related in a nonlinear manner.

Increasing the clock frequency gives only a marginal increase in performance and is accompanied by a much larger increase in processor power consumption [6].

Currently, the focus in improving processor performance has shifted from increasing clock frequency to achieving high performance levels with minimal energy consumption. The key indicator [7] in this context is the processor energy efficiency (energy per instruction, EPI), which is measured as the average amount of energy consumed per executed instruction:

$$\text{EPI} = \frac{\text{Power (J)}}{\text{Number of instructions}}. \quad (4)$$

Processor performance per 1 watt of power consumed will be as follows:

$$\frac{\text{Perfomance}}{\text{Power}} = \frac{\left(\frac{\text{Number of instructions}}{\text{Time}}\right)}{\left(\frac{\text{Power}}{\text{Time}}\right)} = = \frac{\text{Number of instructions}}{\text{Power}} = \frac{1}{\text{EPI}}. \quad (5)$$

Consequently:

$$EPI = \frac{Power}{Perfomance}. \quad (6)$$

One of the approaches to creating a power-efficient processor is to use multicore architecture [8]. This increases performance by increasing the number of instructions executed per clock without increasing and sometimes even decreasing the clock frequency. Theoretically, when increasing the number of cores from 1 to 2, it is possible to maintain the same performance by reducing the clock frequency of each core by a factor of 2.

The performance gain in this case can be estimated as a reduction of the program execution time when using a multicore processor *tn* compared to its execution time on a single-core processor *t*1. Thus, the performance gain will be equal to [9]:

$$\frac{t1}{tn} = 1 - p\left(1 - \frac{1}{n}\right), \quad (7)$$

where p is the share of program code instructions that can be executed in parallel; n is the number of the processors.

The graphical dependence of performance gain on the number of processor cores is shown in Fig. 1.

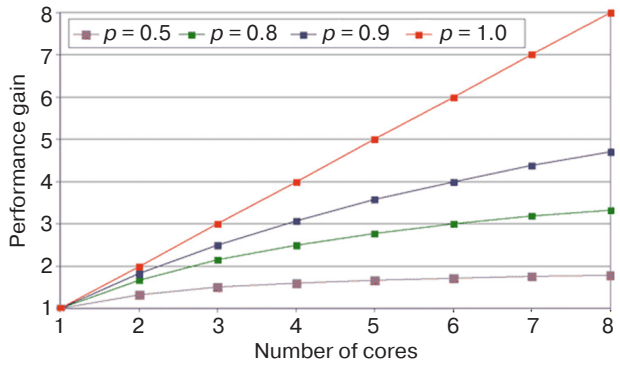

Fig. 1. Dependence of performance gain on the number of processor cores

Multicore architecture significantly improves performance, especially when running multiple applications simultaneously. Under perfect conditions, each application can run on a separate processor core.

Intel Xeon microprocessors

Intel Xeon class microprocessors (Intel, USA) [10] are built on the same microarchitectures as desktop processors (x86), but with the addition of server-specific features.

The design and implementation of server processors is characterized by considerable complexity as compared to desktop systems due to the required implementation of many specific features. Due to the increasing complexity and development time of new architectures using the 10-nm process technology, process technologies used with different processor families such as Xeon, Opteron (AMD, USA) and Baikal-T1 (Baikal Electronics, Russia) are tending to converge.

Crystalwell technology can help to overcome the limitations of low system memory bandwidth and demonstrate improved results in HD video processing and math operations. With Broadwell processors, 4368 HD video streams can be executed simultaneously, representing a 40% increase over the 3120 streams on their Haswell processors.

Intel Xeon E3 v6 processors are available in 8 models, none of which offer reduced power consumption. In this lineup, the use of embedded dynamic random access memory (DRAM) has also been abandoned. However, as before, processors with index 1xx5 v6 are equipped with their own graphics cores.

The main changes include the transition to the Kaby Lake architecture while retaining the 14-nm process technology. In addition, the maximum memory bandwidth has been increased to 37.5 GB/s and frequencies have been increased to DDR4-2400 and DDR3L-1866.

The performance gain when switching from E3 to E5 processors and using two E5 processors is shown in Fig. 2.

Intel tests show the following result: performance increases 1.5 times when switching from E3 to E5 processors and another 2 times when doubling the number of processors. Switching to a 4-processor system provides similar linear performance gains. Performance improves similarly with new processor generations, for example, when switching from E3 v5 or v6 to E5 v4.

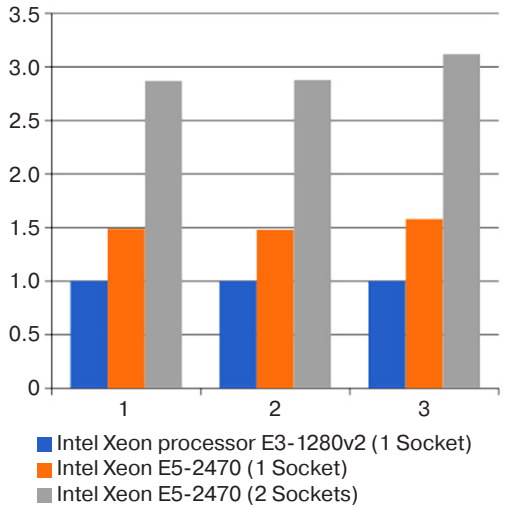

Fig. 2. Change in performance when switching from E3 to E5: (1) SPECint_ratebase 2006, (2) SPECfp*ratebase 2006, (3) SPECjbb*2005

In the future, Broadwell-EX processors will be replaced by Skylake Purley. These new processors will feature 6-channel DDR4 RAM controllers (instead of the current generation's 4-channel), AVX-512 instruction set, Omni-Path bus, Cannonlake graphics support, and embedded field-programmable gate arrays (FPGAs). Embedded FPGAs enable the processor configuration to be optimized for specific tasks, which configuration is not available in the Skylake architecture.

Intel Xeon D processors

Intel Xeon D processors [11] are the successors to the Atom line, but are designed for lightweight server solutions. These processors are systems-on-a-chip and include x86 computing cores, 10G network card, I/O ports (including PCIe[1]), DDR4 controller and SATA interfaces. They are manufactured using a 14nm process technology.

Intel Xeon D-15xx, whose main application area is networking, cloud storage and enterprise storage systems, offer new opportunities to optimize diverse workloads and infrastructures.

AMD Opteron server processors

Server processors from AMD are represented by five series: Opteron 3000, 4000, and 6000, A-series based on ARM-architecture, as well as hybrid processors X-series [12]. These processors, which are primarily designed for web hosting, are characterized by their affordable price. They support DDR3-1866 MHz memory.

Generally, the Opteron line of processors combine good performance, a large number of cores, and a competitive price. Rather than using hyperthreading technology analogs, the performance of Opteron processors is increased by adding more physical cores.

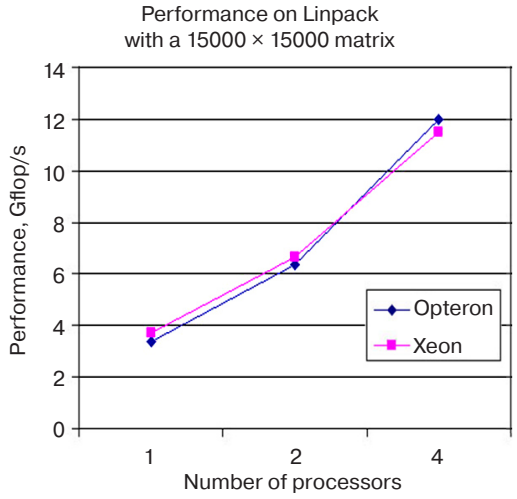

Fig. 3. Performance comparison of Intel Xeon and AMD Opteron processors

Based on the X2150 processor, the X2170 hybrid processor is a fully integrated x86 architecture unit that includes a CPU, graphics processor and I/O controller. It features low power consumption to reduce the total cost of ownership of data centers and adapt to the requirements of high-performance server platforms.

The main tasks for which these server processors are designed include organizing delivery and distribution networks, video preprocessing, console desktop clients, rendering, transcoding, and video streaming.

Combining CPU and GPU technologies in an ultra-dense form factor can result in large performance-per-watt gains over traditional solutions.

Baikal-T1 processor

The Baikal-T1 processor [13], which is based on 2 computing cores having a clock frequency of 1.2 GHz, is implemented on a 28-nm process belonging to the MIPS Warrior P5600 r5 family of Imagination Technologies (United Kingdom). It uses the MIPS32 architecture with support for the extraordinary instruction execution paradigm and the ability to combine up to 6 cores into a single cluster. The P5600 r5 cores support OmniShield hardware zonal data protection technology and 128-bit SIMD-commands[2] for high-speed parallel processing, especially in multimedia applications.

The processor is equipped with 1 MB of high-performance coherent cache memory and an integrated RAM controller with DDR3-1600 support. It includes integrated interfaces: 1 × 10 Gbit Ethernet, 2 × 1 Gbit Ethernet, PCIe Gen.3 x4, SATA 3.0, and USB 2.0. Due to the processor's low power consumption at less than 5 watts, it may be used to develop quiet systems that do not require active cooling.

The main anticipated applications for this processor are industrial automation, embedded systems, and communications.

RANDOM ACCESS MEMORY

Server memory differs from desktop memory due to its inclusion of parity and error correction code (ECC) modules. This type of memory includes additional functionality to provide greater stability, such as the use of register buffered memory. Thus, server memory is manufactured according to different standards than desktop systems.

A key characteristic of server RAM is fault tolerance. Many servers are designed to run mission-critical applications that place high demands on memory. The level of fault tolerance is provided both through

[1] Peripheral component interconnect express is a computer bus that provides point-to-point connectivity using a high-performance serial communications protocol.

[2] Single instruction, multiple data—a principle of computer computing that enables parallelism at the data level.

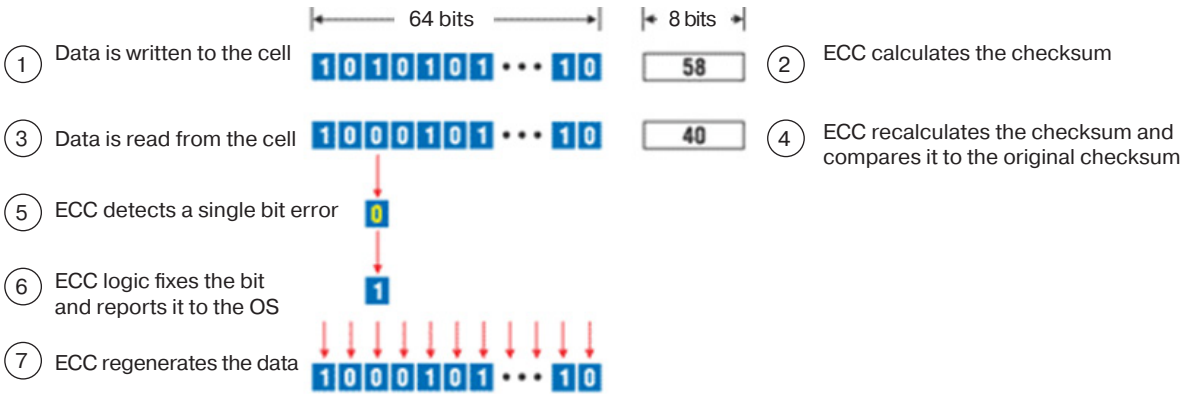

Fig. 4. Single-bit error detection and correction diagram. OS—operating system

improvements in the chip manufacturing process and through the use of memory error protection technologies such as ECC [14].

There are two main ways to protect against memory errors:

1. Module testing, i.e., regular checking of memory status to detect and correct problems.
2. Use of error detection and correction technologies, i.e., the introduction of technologies for automatically detecting and correcting memory errors.

ECC technology, which significantly reduces the probability of memory errors, provides single-bit error detection and correction, along with multibit error detection. This is an important feature for server RAM where reliability and error tolerance are critical. The corresponding operational mechanism is demonstrated in Fig. 4.

Memory errors can also cause significant downtime in database server applications. If an error occurs, database recovery can take several hours due to the need to recover data from transaction log entries that have not yet been entered into the database.

Advanced ECC technology, which is designed to correct multibit errors on a single DRAM chip, significantly increases system reliability by supporting data recovery even in case of failure of the entire chip.

Since four bits from each chip are distributed to four ECC devices (one bit for each ECC device), an error in one chip can correct up to four single-bit errors (Fig. 5).

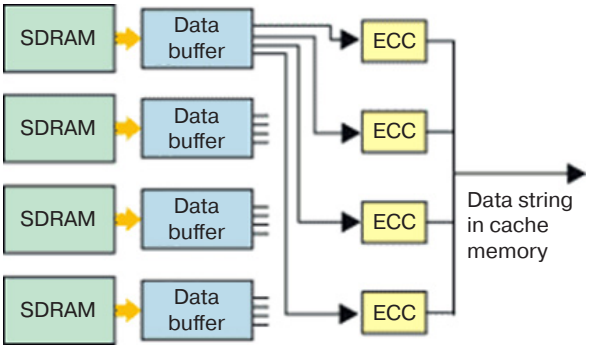

Fig. 5. Advanced ECC operation diagram

The Chipkill mechanism is used to deal with multibit errors on individual chips, including failure of all data bits. This mechanism provides higher protection and reliability compared to traditional methods.

DDR4 DRAM is currently the most advanced and widely used RAM technology. However, DDR5 DRAM is already under development. DDR5 is expected to provide twice the capacity of DDR4 modules, as well as increased bandwidth. DDR5 memory, which is to be manufactured using a 10-nm process, will initially be available in capacities ranging from 1 GB to 4 GB.

STORAGE SUBSYSTEM

An important aspect is availability of drives: server drives must remain functional and active at all times, while desktop PC drives can be placed in standby mode when access is not required [15].

For reliability and performance, redundant arrays of independent disks are often used to combine multiple disk drives for increased fault tolerance and performance. Important factors that influence drive selection include the connection interface, capacity, and drive structure. Here, the expected data to be stored, as well as its importance and the requirements of the installed applications, also play a significant role.

Hard disk drives (HDD), which represent the classic storage solution, provide an acceptable level of reliability; their performance depends on factors such as rotation speed, interface and cache size. HDDs range from 7200 to 15000 rpm depending on performance requirements. However, higher rotational speeds result in higher power consumption and higher cooling requirements. An additional potential problem consists in vibration due to the varying speeds of the disks, which can be disruptive if the disks are in different write cycles. To prevent such problems, it is recommended to use disks with the same rotation speed within the same server. It is also worth noting that the service life of hard disks is limited by their mechanical wear and tear.

Solid state drives (SSDs) have no moving parts, eliminating mechanical wear and vibration. They use flash memory to store data, allowing them to achieve I/O performance that can be hundreds of times faster than HDDs. SSDs, which do not require power for the electric motor, consume about one-fifth of the power of HDDs.

When selecting a drive, it is important to keep in mind that SSDs have a limited data retention period when turned off. If the SSD is used for backup storage, the information will be available for a maximum of 10 years. However, this period may be shortened due to heavy use and exposure to ambient temperatures.

A promising direction in the development of data storage systems is the transition to non-volatile memory of the NAND[3] type. Such memory eliminates the main causes of delays in the data exchange channel between the system and the solid-state drive. Using the PCIe bus directly, without additional adapters (SATA, SAS, etc.), reduces latency at the controller level. Selecting NVMe[4] helps to eliminate latency at the software level (both in the controller firmware and system drivers) as well as significantly increasing the level of parallelism when exchanging data streams over the bus.

The NVMe interface is a key benefit for server applications, especially when processing large numbers of requests simultaneously. Switching to NVMe can significantly improve disk array efficiency by scaling the number of queues and commands.

The evolution of storage systems continues with the development of new storage technologies, such as pulse code modulation and other promising solutions, which may lead to significant improvements in access speed and overall performance in the future.

Crossbar estimates that resistive random-access memory (RRAM) modules will deliver write speeds 20 times faster than NAND flash memory, reaching 140 MB/s compared to NAND's 7 MB/s. Read speeds for RRAM will be around 17 MB/s. An additional advantage of RRAM is the longevity of data storage, which can be up to 20 years, as compared to only 1–3 years for NAND.

Magnetoresistive random-access memory is also being considered as an alternative to NAND flash memory. It stands out for its high data access speed and reliability under unfavorable environmental conditions. Magnetoresistive memory can operate at very high temperatures, making it particularly suitable for extreme environments such as military and space applications.

CONCLUSIONS

The review of server organization options and their main components allows us to conclude the sufficient reliability of their operation. However, servers combined in the WSC class as a system additionally require continuous operation in 24/7 mode for long periods of time. This, in turn, requires the development of methods for assessing the reliability of such highly reliable systems, including redundant elements to compensate for hardware and software failures, as well as methods for predicting failures and measures to combat their consequences.

Authors' contribution
All authors equally contributed to the research work.

[3] Not AND is a universal two-input logic element, Schaeffer stroke.

[4] NVM Express is non-volatile memory host controller interface specification—access interface to solid state drives connected via PCI Express bus.

REFERENCES

1. Henessey J.L., Patterson D.A. *Komp'yuternaya arkhitektura. Kolichestvennyi podkhod* (*Computer Architecture. A Quantitative Approach*): transl. from Engl. 5th ed. Moscow: Tekhnosfera; 2016. 936 p. (in Russ.).
[Henessey J.L., Patterson D.A. *Computer Architecture. A Quantitative Approach.* 5th ed. Morgan Kaufmann; 2011. 856 p.]
2. Sugak E.V. *Prikladnaya teoriya nadezhnosti. Praktikum* (*Applied Reliability Theory. The Workshop. Textbook*). Moscow: Lan; 2023. 312 p. (in Russ.). ISBN 978-5-507-47014-3
3. Tengaikin E.I. *Organizatsiya setevogo administrirovaniya. Setevye operatsionnye sistemy, servery, sluzhby i protokoly. Prakticheskie raboty* (*Organization of Network Administration. Network Operating Systems, Servers, Services and Protocols. Practical Work*). St. Petersburg: Lan; 2022. 100 p. (in Russ.). ISBN 978-5-8114-9783-6
4. Kovalenko S.M., Platonova O.V. Analysis of the operational efficiency of complex automation systems and the calculation of their reliability on the basis of continuous models. *Izvestiya vysshikh uchebnykh zavedenii. Mashinostroenie = BMSTU J. Mechanical Engineering.* 2014;8(653):75–89 (in Russ.). http://doi.org/10.18698/0536-1044-2014-8-75-79
5. Voevodin V.V., Voevodin Vl.V. *Parallel'nye vychisleniya* (*Parallel Computing*). St. Petersburg: BHV-Petersburg; 2002. 608 p. (in Russ.).
6. Orlov S.A., Tsil'ker B.Ya. *Organizatsiya EVM i system* (*Organization of Computers and Systems*). St. Petersburg: Piter; 2016. 688 p. (in Russ.).
7. Polovko A.M., Gurov S.V. *Osnovy teorii nadezhnosti* (*Fundamentals of Reliability Theory*). St. Petersburg: BHV-Petersburg; 2006. 702 p. (in Russ.). ISBN 5-94157-541-6
8. Cherkesov G.N. *Nadezhnost' apparatno-programmnykh kompleksov* (*Reliability of Hardware and Software Complexes*). St. Petersburg: Piter; 2005. 479 p. (in Russ.). ISBN 5-469-00102-4
9. Sapozhnikov V.V., Sapozhnikov V.V., Efanov D.V. *Osnovy teorii nadezhnosti i tekhnicheskoi diagnostiki* (*Fundamentals of Reliability Theory and Technical Diagnostics*). St. Petersburg: Lan; 2019. 588 p. (in Russ.). ISBN 978-5-8114-3453-4
10. Podgorny Y.V., Antonovich A.N., Petrushin A.A., Sigov A.S., Vorotilov K.A. Effect of metal electrodes on the steady-state leakage current in PZT thin film capacitors. *J. Electroceram.* 2022;49:15–21. https://doi.org/10.1007/s10832-022-00288-5
11. Abdullaev D.A., Milovanov R.A., Volkov R.L., Borgardt N.I., Lantsev A.N., Vorotilov K.A., Sigov A.S. Ferroelectric memory: state-of-the-art manufacturing and research. *Rossiiskii tekhnologicheskii zhurnal*. 2020;8(5):44–67 (in Russ.). https://doi.org/10.32362/2500-316X-2020-8-5-44-67
12. Konyukhova O.V., Kravtsova E.A., Lukyanov P.V. *Tekhnicheskoe i programmnoe obespechenie vychislitel'nykh mashin i system* (*Technical and Software Support of Computers and Systems*). Moscow, Vologda: Infra-Inzheneriya; 2023. 200 p. (in Russ.). ISBN 978-5-9729-1186-8
13. Zhuravlev A.A. *Organizatsiya i arkhitektura EVM. Vychislitel'nye sistemy* (*Organization and Architecture of Computers. Computer Systems*). St. Petersburg: Lan; 2022. 144 p. (in Russ.). ISBN 978-5-507-48089-0
14. Gelbukh C.A. *Seti EVM i telekommunikatsii. Arkhitektura i organizatsiya* (*Computer Networks and Telecommunications. Architecture and Organization*). St. Petersburg: Lan; 2019. 208 p. (in Russ.). ISBN 978-5-8114-3474-9
15. Andreev A.M., Mozharov G.P., Syuzev V.V. *Mnogoprotsessornye vychislitel'nye sistemy. Teoreticheskii analiz, matematicheskie modeli i primenenie* (*Multiprocessor Computing Systems. Theoretical Analysis, Mathematical Models and Applications*). Moscow: Bauman Press; 2011. 336 p. (in Russ.). ISBN 978-5-7038-3439-6

СПИСОК ЛИТЕРАТУРЫ

1. Хенесси Д.Л., Паттерсон Д.А. *Компьютерная архитектура. Количественный подход*. 5-е изд. М.: Техносфера; 2016. 936 с.
2. Сугак Е.В. *Прикладная теория надежности. Практикум.* М.: Лань; 2023. 312 с. ISBN 978-5-507-47014-3
3. Тенгайкин Е.И. *Организация сетевого администрирования. Сетевые операционные системы, серверы, службы и протоколы*. *Практические работы*. СПб.: Лань; 2022. 100 с. ISBN 978-5-8114-9783-6
4. Коваленко С.М., Платонова О.В. Анализ задачи эффективной эксплуатации комплексов систем автоматизации и расчеты надежности на основе непрерывных моделей. *Известия вузов. Машиностроение*. 2014;8(653):75–89. http://doi.org/10.18698/0536-1044-2014-8-75-79
5. Воеводин В.В., Воеводин Вл.В. *Параллельные вычисления*. СПб.: БХВ-Петербург; 2002. 608 с.
6. Орлов С.А., Цилькер Б.Я. *Организация ЭВМ и систем*. СПб.: Питер; 2016. 688 с.
7. Половко А.М., Гуров С.В. *Основы теории надежности*. СПб.: БХВ-Петербург; 2006. 702 с. ISBN 5-94157-541-6
8. Черкесов Г.Н. *Надежность аппаратно-программных комплексов*. СПб.: Питер; 2005. 479 с. ISBN 5-469-00102-4
9. Сапожников В.В., Сапожников В.В., Ефанов Д.В. *Основы теории надежности и технической диагностики*. СПб.: Лань; 2019. 588 с. ISBN 978-5-8114-3453-4
10. Podgorny Y.V., Antonovich A.N., Petrushin A.A., Sigov A.S., Vorotilov K.A. Effect of metal electrodes on the steady-state leakage current in PZT thin film capacitors. *J. Electroceram.* 2022;49:15–21. https://doi.org/10.1007/s10832-022-00288-5
11. Абдуллаев Д.А., Милованов Р.А., Волков Р.Л., Боргардт Н.И., Ланцев А.Н., Воротилов К.А., Сигов А.С. Сегнетоэлектрическая память: современное производство и исследования. *Российский технологический журнал*. 2020;8(5):44–67. https://doi.org/10.32362/2500-316X-2020-8-5-44-67

12. Конюхова О.В., Кравцова Э.А., Лукьянов П.В. *Техническое и программное обеспечение вычислительных машин и систем.* М., Вологда: Инфра-Инженерия; 2023. 200 с. ISBN 978-5-9729-1186-8
13. Журавлев А.А. *Организация и архитектура ЭВМ. Вычислительные системы*. СПб.: Лань; 2022. 144 с. ISBN 978-5-507-48089-0
14. Гельбух С.А. *Сети ЭВМ и телекоммуникации. Архитектура и организация*. СПб.: Лань; 2019. 208 с. ISBN 978-5-8114-3474-9
15. Андреев А.М., Можаров Г.П., Сюзев В.В. *Многопроцессорные вычислительные системы. Теоретический анализ, математические модели и применение*. М.: Издательство МГТУ им. Н.Э. Баумана; 2011. 336 с. ISBN 978-5-7038-3439-6

About the authors

Grigory V. Petushkov, Vice-Rector, MIREA – Russian Technological University (78, Vernadskogo pr., Moscow, 119454 Russia). E-mail: petushkov@mirea.ru. https://orcid.org/0009-0006-0801-429X

Alexander S. Sigov, Academician at the Russian Academy of Sciences, Dr. Sci. (Phys.–Math.), Professor, President, MIREA – Russian Technological University (78, Vernadskogo pr., Moscow, 119454 Russia). E-mail: sigov@mirea.ru. Scopus Author ID 35557510600, ResearcherID L-4103-2017, RSCI SPIN-code 2869-5663, https://www.researchgate.net/profile/A_Sigov

Об авторах

Петушков Григорий Валерьевич, проректор, ФГБОУ ВО «МИРЭА – Российский технологический университет» (119454, Россия, Москва, пр-т Вернадского, д. 78). E-mail: petushkov@mirea.ru. https://orcid.org/0009-0006-0801-429X

Сигов Александр Сергеевич, академик Российской академии наук, д.ф.-м.н., профессор, президент ФГБОУ ВО «МИРЭА – Российский технологический университет» (119454, Россия, Москва, пр-т Вернадского, д. 78). E-mail: sigov@mirea.ru. Scopus Author ID 35557510600, ResearcherID L-4103-2017, SPIN-код РИНЦ 2869-5663, www.researchgate.net/profile/A_Sigov

Translated from Russian into English by Lyudmila O. Bychkova
Edited for English language and spelling by Thomas A. Beavitt

Modern radio engineering and telecommunication systems

Современные радиотехнические и телекоммуникационные системы

UDC 621.314.1+681.586.7
https://doi.org/10.32362/2500-316X-2025-13-1-59-67
EDN APNAQO

RESEARCH ARTICLE

Method for designing DC/DC converters based on Zeta topology

Vladimir K. Bityukov,
Aleksey I. Lavrenov @

MIREA – Russian Technological University, Moscow, 119454 Russia
@ *Corresponding author, e-mail: lavrenov@mirea.ru*

Abstract

Objectives. The work set out to develop a new design method for DC/DC converters based on the Zeta topology to calculate the ratings of inductors and capacitors of the Zeta converter with magnetically coupled inductors and verify the accuracy of the ultimate continuous mathematical model and design method based on it using SPICE simulation in the *Multisim* computer-aided design (CAD) system.

Methods. The proposed method analyzes an ultimate continuous mathematical model to calculate the ratings of coupled inductors and capacitors of the converter.

Results. The simulation of the Zeta converter with coupled inductors was carried out using the *Multisim* CAD system, during which the load and transfer characteristics of the converter were obtained. These characteristics show the dependencies of the currents flowing through the coupled inductors and voltages across the capacitors on the input voltage, as well as the dependence of the output voltage on the load current. The presented design method is shown to be accurate and in full agreement with the simulation results. A correlation between the transfer and load characteristics of currents and voltages obtained by simulation and calculation is established. The differences between the values calculated using the ultimate continuous mathematical model and the results of simulation in the *Multisim* CAD system are comparable to measurement errors.

Conclusions. The proposed design method is used calculate element ratings for the Zeta topology both with and without taking the inductive coupling into account. The method can also be used to calculate the steady-state values and ripple currents of the inductors and voltages across the capacitors. The design method for DC/DC converters presented in the paper can be used for both preliminary evaluation calculations and more detailed calculations, including analysis of the device operation under various input voltages and load resistances.

Keywords: DC/DC converter, buck-boost converter, Zeta topology, ultimate continuous mathematical model, design method, simulation

• **Submitted:** 24.04.2024 • **Revised:** 28.08.2024 • **Accepted:** 03.12.2024

For citation: Bityukov V.K., Lavrenov A.I. Method for designing DC/DC converters based on Zeta topology. *Russian Technological Journal*. 2025;13(1):59–67. https://doi.org/10.32362/2500-316X-2025-13-1-59-67, https://elibrary.ru/APNAQO

Financial disclosure: The authors have no financial or proprietary interest in any material or method mentioned.

The authors declare no conflicts of interest.

НАУЧНАЯ СТАТЬЯ

Метод проектирования DC/DC-преобразователей, построенных по Zeta-топологии

В.К. Битюков,
А.И. Лавренов @

МИРЭА – Российский технологический университет, Москва, 119454 Россия
@ *Автор для переписки, e-mail: lavrenov@mirea.ru*

Резюме

Цели. Цели работы – разработка нового метода проектирования DC/DC-преобразователей, построенных по топологии Zeta с возможным учетом магнитной связи дросселей, проведение расчетов по предложенной методике номиналов дросселей и конденсаторов Zeta-преобразователя с индуктивно связанными дросселями и проверка достоверности предельной непрерывной математической модели и метода проектирования, основанного на ней, с помощью SPICE-моделирования в системе автоматизированного проектирования *Multisim*.

Методы. Поставленные задачи решены при помощи аналитического анализа предельной непрерывной математической модели. Предложенным методом выполнен расчет номиналов связанных дросселей и конденсаторов преобразователя.

Результаты. С помощью системы автоматизированного проектирования *Multisim* проведено моделирование Zeta-преобразователя со связанными дросселями, в ходе которого получены нагрузочные и передаточные характеристики преобразователя, показывающие зависимости токов, протекающих в связанных дросселях, и напряжений на конденсаторах от входного напряжения, а также зависимость выходного напряжения от тока нагрузки. Показано, что представленный метод проектирования достоверен и полностью соответствует результатам моделирования. Установлена корреляция передаточных и нагрузочных характеристик токов и напряжений, полученных моделированием и расчетным путем. Отличия рассчитанных с помощью предельной непрерывной математической модели значений от результатов моделирования в системе автоматизированного проектирования *Multisim* сопоставимы с погрешностью измерений.

Выводы. Предложенный метод проектирования позволяет рассчитать номиналы элементов Zeta-топологии как с учетом индуктивной связи дросселей, так и без него. Кроме того, с помощью данного метода возможно рассчитать постоянные значения и пульсации токов дросселей и напряжений на конденсаторах. Приведенный в статье метод проектирования DC/DC-преобразователей можно использовать как для предварительного оценочного расчета, так и для более детального расчета с анализом работы устройства при различных входных напряжениях и сопротивлениях нагрузки.

Ключевые слова: DC/DC-преобразователь, понижающе-повышающий преобразователь, топология Zeta, предельная непрерывная математическая модель, метод проектирования, моделирование

• **Поступила:** 24.04.2024 • **Доработана:** 28.08.2024 • **Принята к опубликованию:** 03.12.2024

Для цитирования: Битюков В.К., Лавренов А.И. Метод проектирования DC/DC-преобразователей, построенных по Zeta-топологии. *Russian Technological Journal*. 2025;13(1):59–67. https://doi.org/10.32362/2500-316X-2025-13-1-59-67, https://elibrary.ru/APNAQO

Прозрачность финансовой деятельности: Авторы не имеют финансовой заинтересованности в представленных материалах или методах.

Авторы заявляют об отсутствии конфликта интересов.

INTRODUCTION

DC/DC converters of various topologies [1–3] are used in space [4], aerospace [5], medical equipment [6], and a wide range of mobile devices [7, 8]. The general trend towards miniaturization of DC/DC converters and autonomous design of radio-electronic devices is driving the need for new methods of DC/DC converter design. The main difficulty in designing DC/DC converters for such devices is associated with the typically low voltages and absorbed currents. At currents below 0.5 A, the efficiency of the DC/DC converter starts to drop sharply[1], requiring a rigorous evaluation of the device operation in different modes using more advanced calculation methods [6, 7, 9–11].

The design of DC/DC converters is based on appropriate mathematical models [11], as is the design of any other radio-electronic device. They provide the basis for a uniform methodical approach to developing, designing and investigating devices. The method for designing unipolar DC/DC converters built according to the Zeta topology, taking into account the inductive coupling of the inductors, is also based on such a model [12, 13].

1. DETERMINING THE RATINGS OF ZETA CONVERTER RADIO ELEMENTS WITH ALLOWANCE FOR MAGNETIC COUPLING OF INDUCTORS

The circuit diagram of a DC/DC converter based on the Zeta topology is shown in Fig. 1. It has two inductors, two capacitors, an electronic key, typically in the form of a field effect transistor, and a control unit (CU) that determines the transistor mode [2]. The inductors L1 and L2 perform the function of energy storage and transfer by electromagnetic induction. The capacitor C1 is present in the circuit to decouple the input and output of the converter. The separating capacitor C1, which is sometimes referred to as a "flying capacitor", not only separates but also stores and transfers energy. Capacitor C2 is the output smoothing capacitor.

The method for calculating the Zeta converter taking into account the magnetic coupling of the inductors is based on the corresponding mathematical model [11–13]. The design of the Zeta converter on coupled inductors significantly reduces the current ripple [14]. The mathematical model is used to obtain expressions for the constant and variable values of the inverter currents and voltages. By analyzing the obtained expressions, equations are derived to determine the rated electrical values of the electric radio elements, ERE. The following parameters are required for calculating the ERE ratings of the DC/DC converter:

- constant output voltage U_{C2};
- constant input voltage range from $U_{\text{in min}}$ to $U_{\text{in max}}$;
- switching period of the power switch T;
- maximum ripple amplitudes of voltages u_{C1}, u_{C2} and currents i_{L1}, i_{L2} are Δu_{C1}, Δu_{C2} Δi_{L1}, and Δi_{L2} respectively;
- range of load resistance variation from $R_{\text{l min}}$ to $R_{\text{l max}}$ (or load currents from $I_{\text{l min}}$ to $I_{\text{l max}}$);
- coupling coefficient of inductors k_c.

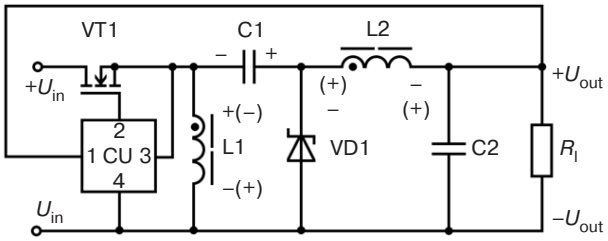

Fig. 1. Circuit diagram of the buck-boost converter based on the Zeta topology. Here and in the following figures, the designations of the circuit elements correspond to those adopted in GOST 2.710-811[2]. R_l is load resistance, U_{in} is input voltage, U_{out} is output voltage

The optional parameters are the active winding resistances of the coupled inductors L1 and L2, which are r_1 and r_2. The resistances r_1 and r_2 are taken into account in the construction of the mathematical model in order to clarify the calculation and to simplify the derivation of the inductor current equations due to the peculiarities in the construction of the limit continuous mathematical models.

For the calculation, it is necessary to determine the input voltage $U_{\text{in }0.5}$ with duty factor $D_{0.5}$ equal to 0.5 and the minimum load resistance $R_{\text{l min}}$ using the following equation:

[1] Datasheet TPS40200 Wide Input Range Non-Synchronous Voltage Mode Controller datasheet (Rev. G). Texas Instruments. SLUS659G – FEBRUARY 2006–REVISED NOVEMBER 2014.

[2] GOST 2.710-81. Interstate Standard. *Unified system for design documentation. Alpha-numerical designations in electrical diagrams*. Moscow: Izd. Standartov; 1985 (in Russ.).

$$U_{\text{in}\,0.5}=\frac{\left(-U_{\text{C2}}D_{0.5}^2+2U_{\text{C2}}D_{0.5}-U_{\text{C2}}\right)r_2-U_{\text{C2}}D_{0.5}^2r_2-R_{\text{l av}}U_{\text{C2}}D_{0.5}^2+2R_{\text{l av}}U_{\text{C2}}D_{0.5}-R_{\text{l av}}U_{\text{C2}}}{R_{\text{l av}}D_{0.5}^2-R_{\text{l av}}D_{0.5}},\qquad(1)$$

where $R_{\text{l av}}=\frac{R_{\text{l min}}+R_{\text{l max}}}{2}$ is the average load resistance.

In addition, the minimum and maximum duty factors D_{min} and D_{max} should be calculated using the following equations:

$$D_{\text{min}}=\frac{\sqrt{-\left(4U_{\text{C2}}^2r_1r_2\right)+\left(R_{\text{l min}}^2U_{\text{in max}}^2-4R_{\text{l min}}U_{\text{C2}}^2r_1\right)}-2U_{\text{C2}}r_2-\left(2R_{\text{l min}}U_{\text{C2}}+R_{\text{l min}}U_{\text{in max}}\right)}{-2U_{\text{C2}}r_2-2U_{\text{C2}}r_1-\left(2R_{\text{l min}}U_{\text{C2}}+2R_{\text{l min}}U_{\text{in max}}\right)},\qquad(2)$$

$$D_{\text{max}}=\frac{\sqrt{-\left(4U_{\text{C2}}^2r_1r_2\right)+\left(R_{\text{l min}}^2U_{\text{in min}}^2-4R_{\text{l min}}U_{\text{C2}}^2r_1\right)}-2U_{\text{C2}}r_2-\left(2R_{\text{l min}}U_{\text{C2}}+R_{\text{l min}}U_{\text{in min}}\right)}{-2U_{\text{C2}}r_2-2U_{\text{C2}}r_1-\left(2R_{\text{l min}}U_{\text{C2}}+2R_{\text{l min}}U_{\text{in min}}\right)}.\qquad(3)$$

Since the calculation method is based on the limiting continuous mathematical model of the Zeta converter, the largest discrepancy between the calculated values of the ripple amplitudes and the simulation result is observed at the limits of the duty factor D_{min} and D_{max} according to [15]. The highest agreement observed in the neighborhood of the duty factor D is equal to 0.5. Therefore, it would be reasonable to calculate the converter ratings exactly at $D = 0.5$. For this, it is necessary to obtain the analytical dependence between the maximum current and voltage ripples of the converter and their ripples at $D = 0.5$. Thus, by taking into account (1)–(3), the equations for the conversion factors k_{L1}, k_{L2}, k_{C1} and k_{C2} can be derived. Obviously, the equations for calculating ripples Δi_{L1} and Δi_{L2} are the same [13], so the coefficients k_{L1} and k_{L2} are also identical. It can therefore be further assumed that $k_{\text{L1}} = k_{\text{L2}} = k_{\text{L}}$.

$$k_{\text{L}}=\frac{-\frac{U_{\text{in max}}D_{\text{min}}T\left(k_{\text{c}}\sqrt{L_1L_2}+L_2\right)}{L_2L_1\left(k_{\text{c}}-1\right)\left(k_{\text{c}}+1\right)}+\frac{U_{\text{in max}}D_{\text{min}}^3Tr_1\left(k_{\text{c}}\sqrt{L_1L_2}+L_2\right)}{L_2L_1\left(k_{\text{c}}-1\right)\left(k_{\text{c}}+1\right)\left(\left(D_{\text{min}}^2-2D_{\text{min}}+1\right)r_2+D_{\text{min}}^2r_1+R_{\text{l max}}D_{\text{min}}^2-2R_{\text{l max}}D_{\text{min}}+R_{\text{l max}}\right)}}{-\frac{U_{\text{in}\,0.5}D_{0.5}T\left(k_{\text{c}}\sqrt{L_1L_2}+L_2\right)}{L_2L_1\left(k_{\text{c}}-1\right)\left(k_{\text{c}}+1\right)}+\frac{U_{\text{in}\,0.5}D_{0.5}^3Tr_1\left(k_{\text{c}}\sqrt{L_1L_2}+L_2\right)}{L_2L_1\left(k_{\text{c}}-1\right)\left(k_{\text{c}}+1\right)\left(\left(D_{0.5}^2-2D_{0.5}+1\right)r_2+D_{0.5}^2r_1+R_{\text{l max}}D_{0.5}^2-2R_{\text{l max}}D_{0.5}+R_{\text{l max}}\right)}},\qquad(4)$$

$$k_{\text{C1}}=\frac{\frac{-U_{\text{in min}}D_{\text{max}}^2T\left(D_{\text{max}}-1\right)}{C_1\left(\left(D_{\text{max}}^2-2D_{\text{max}}+1\right)r_2+D_{\text{max}}^2r_1+R_{\text{l min}}D_{\text{max}}^2-2R_{\text{l min}}D_{\text{max}}+R_{\text{l min}}\right)}}{\frac{-U_{\text{in}\,0.5}D_{0.5}^2T\left(D_{0.5}-1\right)}{C_1\left(\left(D_{0.5}^2-2D_{0.5}+1\right)r_2+D_{0.5}^2r_1+R_{\text{l min}}D_{0.5}^2-2R_{\text{l min}}D_{0.5}+R_{\text{l min}}\right)}},\qquad(5)$$

$$k_{\text{C2}}=\frac{\frac{U_{\text{in max}}D_{\text{min}}T^2\left(k_{\text{c}}\sqrt{L_1L_2}+L_1\right)}{8C_2L_1L_2\left(k_{\text{c}}-1\right)\left(k_{\text{c}}+1\right)}+\frac{U_{\text{in max}}D_{\text{min}}^3T^2r_1\left(k_{\text{c}}\sqrt{L_1L_2}+L_1\right)}{8C_2L_1L_2\left(k_{\text{c}}-1\right)\left(k_{\text{c}}+1\right)\left(\left(D_{\text{min}}^2-2D_{\text{min}}+1\right)r_2+D_{\text{min}}^2r_1+R_{\text{l max}}D_{\text{min}}^2-2R_{\text{l max}}D_{\text{min}}+R_{\text{l max}}\right)}}{\frac{U_{\text{in}\,0.5}D_{0.5}T^2\left(k_{\text{c}}\sqrt{L_1L_2}+L_1\right)}{8C_2L_1L_2\left(k_{\text{c}}-1\right)\left(k_{\text{c}}+1\right)}+\frac{U_{\text{in}\,0.5}D_{0.5}^3T^2r_1\left(k_{\text{c}}\sqrt{L_1L_2}+L_1\right)}{8C_2L_1L_2\left(k_{\text{c}}-1\right)\left(k_{\text{c}}+1\right)\left(\left(D_{0.5}^2-2D_{0.5}+1\right)r_2+D_{0.5}^2r_1+R_{\text{l max}}D_{0.5}^2-2R_{\text{l max}}D_{0.5}+R_{\text{l max}}\right)}}.\qquad(6)$$

The above equations include the ERE ratings L1, L2, C1, and C2. Using the *Simplify Mathcad* function[3], the expressions (4)–(6) can be simplified to eliminate variables L_1, L_2, C_1, and C_2, thus obtaining equations that are independent of the inductor and capacitor ratings. However, since the final equations for determining the coefficients k_{L}, k_{C1}, and k_{C2} are quite extensive, they have not been included in the present paper.

[3] https://www.mathcad.com/en. Accessed April 24, 2024.

Using expressions (4)–(6), the equations for the ripple amplitudes of currents and voltages at the duty factor $D = 0.5$ can be written as follows:

$$\Delta i_{\mathrm{L1}\,0.5} = \frac{\Delta i_{\mathrm{L1}}}{k_{\mathrm{L}}},\ \Delta i_{\mathrm{L2}\,0.5} = \frac{\Delta i_{\mathrm{L2}}}{k_{\mathrm{L}}},\ \Delta u_{\mathrm{C1}\,0.5} = \frac{\Delta u_{\mathrm{C1}}}{k_{\mathrm{C1}}},\ \Delta u_{\mathrm{C2}\,0.5} = \frac{\Delta u_{\mathrm{C2}}}{k_{\mathrm{C2}}}. \tag{7}$$

The equations for calculating the ratings of the inductors L1, L2 and capacitors C1, C2 are as follows:

$$L_1 = \frac{\left(\left(D_{0.5}^2 - 2D_{0.5} + 1\right)k_{\mathrm{c}}r_2 + D_{0.5}^2 k_{\mathrm{c}} r_1 + \left(R_{\mathrm{l\,max}} D_{0.5}^2 - 2R_{\mathrm{l\,max}} D_{0.5} + R_{\mathrm{l\,max}}\right)k_{\mathrm{c}}\right)\Delta i_{\mathrm{L2}\,0.5}\sqrt{L_1 L_2}}{\Delta i_{\mathrm{L1}\,0.5}\left(\left(D_{0.5}^2 - 2D_{0.5} + 1\right)r_2 + D_{0.5}^2 r_1 + R_{\mathrm{l\,max}} D_{0.5}^2 - 2R_{\mathrm{l\,max}} D_{0.5} + R_{\mathrm{l\,max}}\right)} +$$
$$+ \frac{\left(U_{\mathrm{in}\,0.5} D_{0.5}^3 - 2U_{\mathrm{in}\,0.5} D_{0.5}^2 + U_{\mathrm{in}\,0.5} D_{0.5}\right)Tr_2 + \left(R_{\mathrm{l\,max}} U_{\mathrm{in}\,0.5} D_{0.5}^3 - 2R_{\mathrm{l\,max}} U_{\mathrm{in}\,0.5} D_{0.5}^2 + R_{\mathrm{l\,max}} U_{\mathrm{in}\,0.5} D_{0.5}\right)T}{\Delta i_{\mathrm{L1}\,0.5}\left(\left(D_{0.5}^2 - 2D_{0.5} + 1\right)r_2 + D_{0.5}^2 r_1 + R_{\mathrm{l\,max}} D_{0.5}^2 - 2R_{\mathrm{l\,max}} D_{0.5} + R_{\mathrm{l\,max}}\right)}, \tag{8}$$

$$L_2 = \frac{\left(\left(D_{0.5}^2 - 2D_{0.5} + 1\right)k_{\mathrm{c}}r_2 + D_{0.5}^2 k_{\mathrm{c}} r_1 + \left(R_{\mathrm{l\,max}} D_{0.5}^2 - 2R_{\mathrm{l\,max}} D_{0.5} + R_{\mathrm{l\,max}}\right)k_{\mathrm{c}}\right)\Delta i_{\mathrm{L1}\,0.5}\sqrt{L_1 L_2}}{\Delta i_{\mathrm{L2}\,0.5}\left(\left(D_{0.5}^2 - 2D_{0.5} + 1\right)r_2 + D_{0.5}^2 r_1 + R_{\mathrm{l\,max}} D_{0.5}^2 - 2R_{\mathrm{l\,max}} D_{0.5} + R_{\mathrm{l\,max}}\right)} +$$
$$+ \frac{\left(U_{\mathrm{in}\,0.5} D_{0.5}^3 - 2U_{\mathrm{in}\,0.5} D_{0.5}^2 + U_{\mathrm{in}\,0.5} D_{0.5}\right)Tr_2 + \left(R_{\mathrm{l\,max}} U_{\mathrm{in}\,0.5} D_{0.5}^3 - 2R_{\mathrm{l\,max}} U_{\mathrm{in}\,0.5} D_{0.5}^2 + R_{\mathrm{l\,max}} U_{\mathrm{in}\,0.5} D_{0.5}\right)T}{\Delta i_{\mathrm{L2}\,0.5}\left(\left(D_{0.5}^2 - 2D_{0.5} + 1\right)r_2 + D_{0.5}^2 r_1 + R_{\mathrm{l\,max}} D_{0.5}^2 - 2R_{\mathrm{l\,max}} D_{0.5} + R_{\mathrm{l\,max}}\right)}, \tag{9}$$

$$C_1 = \frac{-\left(U_{\mathrm{in}\,0.5} D_{0.5}^2 T\left(D_{0.5} - 1\right)\right)}{\Delta u_{\mathrm{C1}\,0.5}\left(\left(D_{0.5}^2 - 2D_{0.5} + 1\right)r_2 + D_{0.5}^2 r_1 + R_{\mathrm{l\,min}} D_{0.5}^2 - 2R_{\mathrm{l\,min}} D_{0.5} + R_{\mathrm{l\,min}}\right)}, \tag{10}$$

$$C_2 = \frac{-\left(U_{\mathrm{in}\,0.5} D_{0.5} T^2 \left(D_{0.5} - 1\right)^2 \left(r_2 + R_{\mathrm{l\,max}}\right)\left(k_{\mathrm{c}}\sqrt{L_1 L_2} + L_1\right)\right)}{8\Delta u_{\mathrm{C2}\,0.5} L_1 L_2 \left(k_{\mathrm{c}} - 1\right)\left(k_{\mathrm{c}} + 1\right)\left(\left(D_{0.5}^2 - 2D_{0.5} + 1\right)r_2 + D_{0.5}^2 r_1 + R_{\mathrm{l\,max}} D_{0.5}^2 - 2R_{\mathrm{l\,max}} D_{0.5} + R_{\mathrm{l\,max}}\right)}. \tag{11}$$

It follows from equations (8) and (9) that the ERE values for coupled inductors are also interdependent. While obtaining the solution to this equation is analytically complicated, it can be taken into account that coupled inductors usually have the same ratings and therefore the same ripple. With this in mind, the equations for determining L_1 and L_2 can be written as follows:

$$L_1 = \frac{\left(-\left(U_{\mathrm{in}\,0.5} D_{0.5}^3\right) + 2U_{\mathrm{in}\,0.5} D_{0.5}^2 - U_{\mathrm{in\,max}} D_{0.5}\right)Tr_2}{\left(1 - k_{\mathrm{c}}\right)\left(\left(D_{0.5}^2 - 2D_{0.5} + 1\right)\Delta i_{\mathrm{L1}\,0.5} r_2 + D_{0.5}^2 \Delta i_{\mathrm{L1}\,0.5} r_1 + \left(R_{\mathrm{l\,min}} D_{0.5}^2 - 2R_{\mathrm{l\,min}} D_{0.5} + R_{\mathrm{l\,min}}\right)\Delta i_{\mathrm{L1}\,0.5}\right)} +$$
$$+ \frac{\left(\left(2R_{\mathrm{l\,min}} U_{\mathrm{in}\,0.5} D_{0.5}^2 - R_{\mathrm{l\,min}} U_{\mathrm{in}\,0.5} D_{0.5}^3 - R_{\mathrm{l\,min}} U_{\mathrm{in}\,0.5} D_{0.5}\right)T - 2U_{\mathrm{in}\,0.5} D_{0.5}^3 Tr_1\right)}{\left(1 - k_{\mathrm{c}}\right)\left(\left(D_{0.5}^2 - 2D_{0.5} + 1\right)\Delta i_{\mathrm{L1}\,0.5} r_2 + D_{0.5}^2 \Delta i_{\mathrm{L1}\,0.5} r_1 + \left(R_{\mathrm{l\,min}} D_{0.5}^2 - 2R_{\mathrm{l\,min}} D_{0.5} + R_{\mathrm{l\,min}}\right)\Delta i_{\mathrm{L1}\,0.5}\right)}, \tag{12}$$

$$L_2 = $$
$$= \frac{\left(U_{\mathrm{in}\,0.5} D_{0.5}^3 - 2U_{\mathrm{in}\,0.5} D_{0.5}^2 + U_{\mathrm{in\,max}} D_{0.5}\right)Tr_2 + \left(R_{\mathrm{l\,min}} U_{\mathrm{in}\,0.5} D_{0.5}^3 - 2R_{\mathrm{l\,min}} U_{\mathrm{in}\,0.5} D_{0.5}^2 + R_{\mathrm{l\,min}} U_{\mathrm{in}\,0.5} D_{0.5}\right)T_1}{\left(1 - k_{\mathrm{c}}\right)\left(\left(D_{0.5}^2 - 2D_{0.5} + 1\right)\Delta i_{\mathrm{L2}\,0.5} r_2 + D_{0.5}^2 \Delta i_{\mathrm{L2}\,0.5} r_1 + \left(R_{\mathrm{l\,min}} D_{0.5}^2 - 2R_{\mathrm{l\,min}} D_{0.5} + R_{\mathrm{l\,min}}\right)\Delta i_{\mathrm{L2}\,0.5}\right)}. \tag{13}$$

Equations (12) and (13) differ only by a summand $-2U_{\text{in }0.5}D_{0.5}^3Tr_1$ in the numerator in (12), which depends on the equivalent resistance of the inductor L1. Therefore, the ratings of L_1 and L_2 are approximately equivalent.

2. EXAMPLE CALCULATION OF ZETA CONVERSION ERE VALUES

The initial parameters for the converter calculation are as follows: $k_c = -0.99$, $U_{C2} = 12$ V, $U_{\text{in max}} = 17.5$ V, $U_{\text{in min}} = 6.5$ V, $\Delta i_{L1} = 330$ mA, $\Delta i_{L2} = 330$ mA, $\Delta u_{C1} = 7$ mV, $\Delta u_{C2} = 1.9$ mV, $R_{\text{l min}} = 50$ Ohm, and $R_{\text{l max}} = 100$ Ohm. By calculating the input voltage $U_{\text{in }0.5}$, the minimum and maximum duty factors $D_{\min}$ and $D_{\max}$ using equations (1)–(3), we obtain $U_{\text{in }0.5} = 12.005$ V, $D_{\min} = 0.407$, and $D_{\max} = 0.649$. Using the above parameters and taking into account equation (7), we obtain $k_L = 1.185$, $k_{C1} = 1.298$, and $k_{C2} = 1.186$. Accordingly, the ripple amplitudes at duty factor $D = 0.5$ are $\Delta i_{L1\,0.5} = 278$ mA, $\Delta i_{L2\,0.5} = 278$ mA, $\Delta u_{C1\,0.5} = 5$ mV, and $\Delta u_{C2\,0.5} = 1.6$ mV.

After calculating the ratings of the elements according to equations (10)–(13), we obtain $L_1 \approx 22$ μHn, $L_2 \approx 22$ μHn, $C_1 \approx 44$ μF, and $C_2 \approx 44$ μF.

3. VALIDATION OF CALCULATION RESULTS IN THE *MULTISIM*[4] MODELING ENVIRONMENT

A SPICE simulation of a Zeta converter with inductively coupled inductors is shown in Fig. 2, where T1 is a block of coupled inductors, each rated at 22 μHn. The coupling coefficient of the inductors is 0.99. This means that the inductors are switched on against each other to suppress current ripple. The resistors r_1 and r_2 simulate the active winding resistances of the coupled inductors, while C1 is a "flying" capacitor, C2 is a smoothing output capacitor, VT1 is a power key that allows the power part to be switched at a given frequency, V1 and V2 are sources of constant voltage and pulse width modulation voltage, and VD1 is an ideal diode. In addition, there are also current and voltage probes used to display current and voltage parameters.

Simulation results in transient analysis mode over 4 ms after onset are shown in Fig. 3. This shows the shapes of the currents through the windings of the inductors L1 and L2, as well as the voltages C_1 and C_2 on the capacitors in stationary operation after the transients have passed. It should be noted that maximum and minimum U_{C2} voltages are midway between each energy storage and transmission stage, as stated in [13].

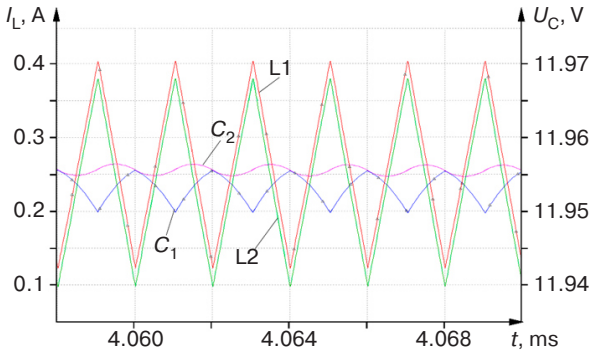

Fig. 3. The graphs of currents and voltages of the Zeta converter in steady state

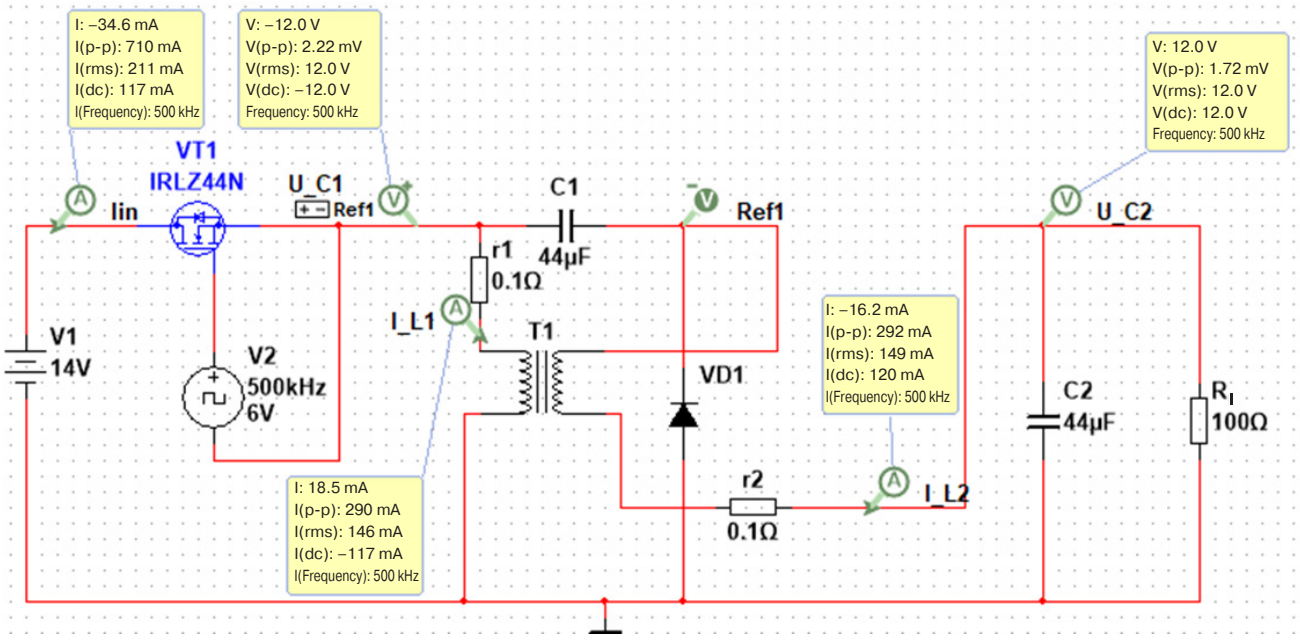

Fig. 2. Simulation scheme for the Zeta converter with inductively coupled inductors

[4] https://www.ni.com/en.html. Accessed April 24, 2024.

The calculated and simulated transfer characteristics of the converter currents and voltages are shown in Figs. 4–7 to demonstrate the accuracy of the calculations.

The transfer characteristic is the dependence of the physical quantity on the converter input voltage. The mathematical model of the converter is used to calculate the values.

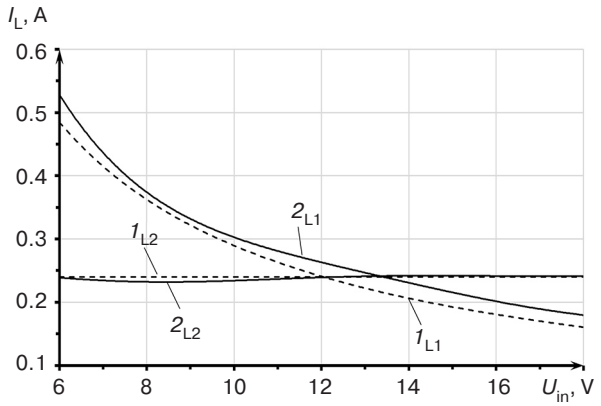

Fig. 4. Transfer characteristics of currents through inductor windings L1 and L2 at a load resistance of 50 Ohm: *1* is the calculated value; *2* is the simulation result

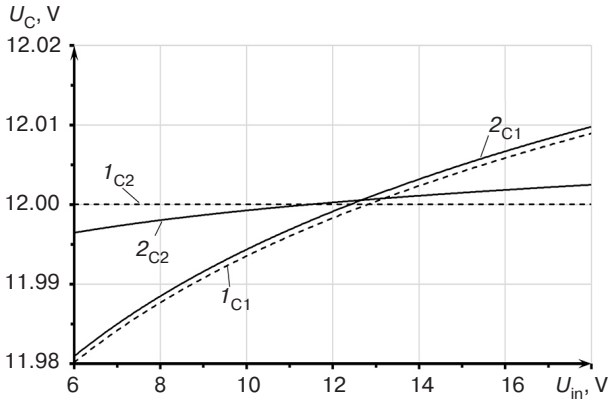

Fig. 5. Transfer characteristics of voltages across capacitors C1 and C2 at a load resistance of 50 Ohm: *1* is the calculated value; *2* is the simulation result

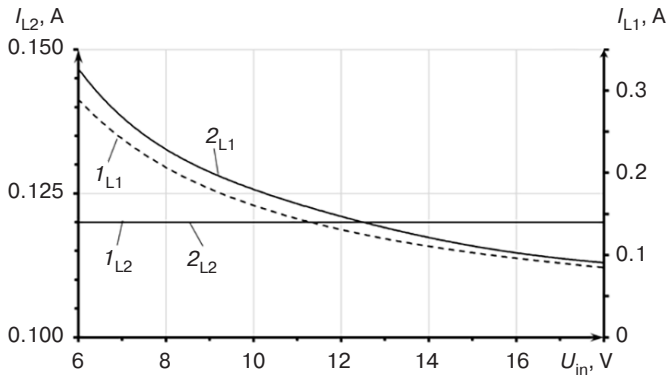

Fig. 6. Transfer characteristics of currents through inductor windings L1 and L2 at a load resistance of 100 Ohm: *1* is the calculated value; *2* is the simulation

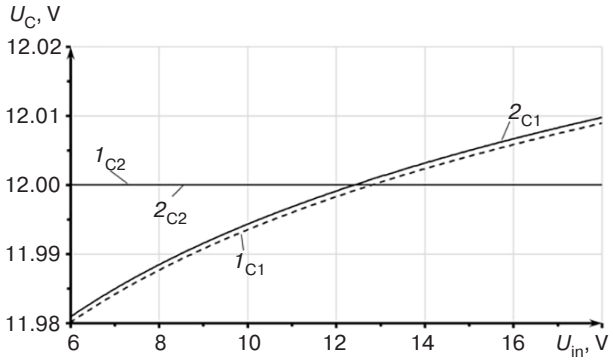

Fig. 7. Transfer characteristics of voltages across capacitors C1 and C2 at a load resistance of 100 Ohm: *1* is the calculated value; *2* is the simulation result

The transfer characteristic graphs show agreement between the calculated values and the simulation results, confirming the reliability of the calculation method. The deviations of the simulated curves from the calculated ones are quite small; for example, the deviation of the current I_{L1} in the simulation from the calculated one ranges from 3.5% to 12%. The deviation ranges similarly from 0% to 3.4% for I_{L2}, from 0% to 0.05% for U_{C1}, and from 0.003% to 0.03% for U_{C2}, demonstrating the reliability of the calculations.

The load characteristics of the converter at input voltages of 6.5, 12, and 17.5 V are shown in Fig. 8. Since the difference between the calculated and simulated output voltages does not exceed one hundredth of a percent, the graphs of the converter load characteristics obtained by calculation and simulation are almost identical. The load characteristics for input voltages of 12 and 17.5 V are plotted in Cartesian coordinates at the bottom and left. The load characteristic at input voltage is plotted in coordinates at the top and right. The information in Fig. 8 shows that the results of calculations using the proposed DC/DC converter design method and mathematical model fully reproduce the load current dependence on the stabilization voltage variation. This demonstrates the reliability of the methods considered in describing the operation of DC/DC converters designed according to the Zeta topology, taking into account the magnetic coupling of the coupled inductors.

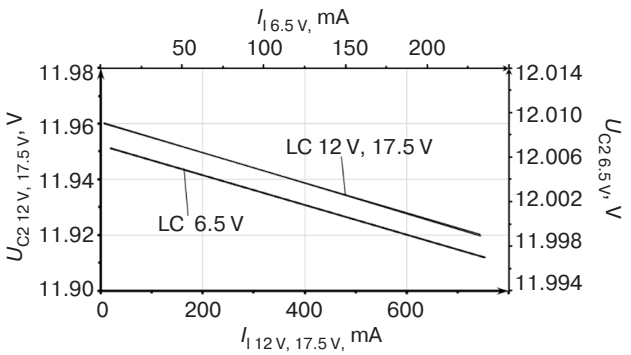

Fig. 8. Load characteristics (LC) at 12 V and 17.5 V, and LC load characteristic at 6.5 V. I_l is load current

CONCLUSIONS

The paper presents a new method for designing DC/DC converters based on the Zeta topology, which allows magnetic coupling of inductors. As well as allowing the capacitor and inductor ratings of the converter power section to be calculated, the presented method takes into account the variable components of the currents flowing through the inductor windings and the voltages across the capacitors.

With the ERE ratings obtained in the design, the simulation is carried out in the *Multisim* computer-aided design system; calculations are performed using the converter limit continuous mathematical model on which the above method is based. The resulting transfer and load characteristics show a high degree of agreement between the mathematical calculations and the *Multisim* simulation results.

Authors' contribution
All authors equally contributed to the research work.

REFERENCES

1. Odinokov A.O., Kremzukov Yu.A. Selecting DC converter topology. SEPIC or Zeta. *Prakticheskaya silovaya elektronika = Practical Power Electronics*. 2022;4(88):44–47 (in Russ.). https://www.elibrary.ru/fayaac
2. Bityukov V.K., Simachkov D.S., Babenko V.P. *Skhemotekhnika elektropreobrazovatel'nykh ustroistv* (*Circuitry of Electrical Converter Devices*). Vologda: Infra-Inzheneriya; 2023. 384 p. (in Russ.). ISBN 978-5-9729-1439-5
3. Erickson R.W., Maksimović D. *Fundamentals of Power Electronics*. NY: Springer; 2020. 1084 p. https://doi.org/10.1007/978-3-030-43881-4
4. Guter R.L. Prospects of multi-functional DC/DC modules development for Space engineering. *Prakticheskaya silovaya elektronika = Practical Power Electronics*. 2023;1(89):37–39 (in Russ.). https://www.elibrary.ru/vcxjlf
5. Vasyukov I.V., Pavlenko A.V., Batishchev D.V. Review and Analysis of Topologies of Converters of Power Supply Systems on Hydrogen Fuel Cells for Unmanned Aerial Vehicles of Kilowatt Power Class. *Izvestiya vysshikh uchebnykh zavedenii. Elektromekhanika = Russian Electromechanics*. 2022;65(2):19–26 (in Russ.).
6. Kramm M.N., Bodin O.N., Bodin A.Y., et al. Constructional Features of a Multielectrode Electrocardiology Screening System. *Biomed. Eng.* 2023;56(5):345–352. https://doi.org/10.1007/s10527-023-10233-7
[Original Russian Text: Kramm M.N., Bodin O.N., Bodin A.Y., Truong T.L.N., Zhikhareva G.V. Constructional Features of a Multielectrode Electrocardiology Screening System. *Meditsinskaya Tekhnika*. 2022;5(335):37–41 (in Russ.). https://www.elibrary.ru/camqob]
7. Lukin A.V., Shaikhutdinov M.V. Accelerated reliability tests of DC/DC switched mode power supplies of the CMB6A series. *Prakticheskaya silovaya elektronika = Practical Power Electronics*. 2022;3(87):26–33 (in Russ.). https://www.elibrary.ru/lbnupb
8. Belov G.A., Petrov K.I. Studying dynamic model of resonant DC-DC voltage converter. *Prakticheskaya silovaya elektronika = Practical Power Electronics*. 2022;2(86):8–13 (in Russ.). https://www.elibrary.ru/efnqkz
9. Tretiakov N.K., Kuzmenko V.P., Solenaya O.Ya. AC voltage sources design employing state-of-the-art solutions. *Prakticheskaya silovaya elektronika = Practical Power Electronics*. 2024;1(93):40–45 (in Russ.). https://www.elibrary.ru/wqmtyd
10. Belov G.A. Time domain analysis of an LLC type DC-DC voltage converter in discontinuous conduction mode. *Prakticheskaya silovaya elektronika = Practical Power Electronics*. 2022;1(85):2–13 (in Russ.). https://www.elibrary.ru/vwnrci
11. Korshunov A.I. Limiting continuous model of a system with periodic high-frequency structure variation. *Silovaya elektronika = Power Electronics*. 2021;5(92):48−51 (in Russ.).
12. Bityukov V.K., Lavrenov A.I., Petrov D.R. Current and voltage pulsations of Zeta converter with inductively coupled inductors (Part 1). *Proektirovanie i tekhnologiya elektronnykh sredstv = Design and Technology of Electronic Means*. 2023;3:36–41 (in Russ.). https://www.elibrary.ru/doawcn
13. Bityukov V.K., Lavrenov A.I., Petrov D.R. Current and voltage pulsations of Zeta converter with inductively coupled inductors (Part 2). *Proektirovanie i tekhnologiya elektronnykh sredstv = Design and Technology of Electronic Means*. 2023;4:27–31 (in Russ.). https://www.elibrary.ru/dspqrt
14. Zhu F., Li Q. Coupled Inductors with an Adaptive Coupling Coefficient for Multiphase Voltage Regulators. *IEEE Transactions on Power Electronics*. 2023;38(1):739–749. https://doi.org/10.1109/TPEL.2022.3203855
15. Bityukov V.K., Lavrenov A.I., Malitskiy D.A. Analysis of the DC/DC Zeta topology converter ripples by applying its limiting continuous mathematical model. *Russian Technological Journal*. 2023;11(4):36–48 (in Russ.). https://doi.org/10.32362/2500-316X-2023-11-4-36-48

СПИСОК ЛИТЕРАТУРЫ

1. Одиноков А.О., Кремзуков Ю.А. Выбор топологии преобразователя постоянного напряжения. SEPIC или Zeta. *Практическая силовая электроника*. 2022;4(88):44–47. https://www.elibrary.ru/fayaac
2. Битюков В.К., Симачков Д.С., Бабенко В.П. *Схемотехника электропреобразовательных устройств*. Вологда: Инфра-Инженерия; 2023. 384 с. ISBN 978-5-9729-1439-5

3. Erickson R.W., Maksimović D. *Fundamentals of Power Electronics*. NY: Springer; 2020. 1084 p. https://doi.org/10.1007/978-3-030-43881-4
4. Гутер Л.Р. Перспективы разработки многофункциональных модулей DC/DC для космической техники. *Практическая силовая электроника*. 2023;1(89):37–39. https://www.elibrary.ru/vcxjlf
5. Васюков И.В., Павленко А.В., Батищев Д.В. Обзор и анализ топологий преобразователей систем электропитания на водородных топливных элементах для беспилотных летательных аппаратов киловаттного класса мощности. *Известия вузов. Электромеханика*. 2022;65(2):19–26.
6. Крамм М.Н., Бодин О.Н., Бодин А.Ю., Чыонг Т.Л.Н., Жихарева Г.В. Особенности построения многоэлектродной системы электрокардиологического скрининга. *Медицинская техника*. 2022;5(335):37–41. https://www.elibrary.ru/camqob
7. Лукин А.В., Шайхутдинов М.В. Ускоренные испытания на надежность импульсных источников питания DC/DC серии CMB6A. *Практическая силовая электроника*. 2022;3(87):26–33. https://www.elibrary.ru/lbnupb
8. Белов Г.А., Петров К.И. Исследование динамической модели резонансного преобразователя постоянного напряжения. *Практическая силовая электроника*. 2022;2(86):8–13. https://www.elibrary.ru/efnqkz
9. Третьяков Н.К., Кузьменко В.П., Соленая О.Я. Проектирование источников переменного напряжения с использованием современных решений. *Практическая силовая электроника*. 2024;1(93):40–45. https://www.elibrary.ru/wqmtyd
10. Белов Г.А. Временной анализ резонансного преобразователя постоянного напряжения типа LLC в режиме прерывистого тока. *Практическая силовая электроника*. 2022;1(85):2–13. https://www.elibrary.ru/vwnrci
11. Коршунов А.И. Предельная непрерывная модель системы с периодическим высокочастотным изменением структуры. *Силовая электроника*. 2021;5(92):48−51.
12. Битюков В.К., Лавренов А.И., Петров Д.Р. Пульсации токов и напряжений Zeta преобразователя с индуктивно связанными дросселями (Часть 1). *Проектирование и технология электронных средств.* 2023;3:36–41. https://www.elibrary.ru/doawcn
13. Битюков В.К., Лавренов А.И., Петров Д.Р. Пульсации токов и напряжений Zeta преобразователя с индуктивно связанными дросселями (Часть 2). *Проектирование и технология электронных средств*. 2023;4:27–31. https://www.elibrary.ru/dspqrt
14. Zhu F., Li Q. Coupled Inductors with an Adaptive Coupling Coefficient for Multiphase Voltage Regulators. *IEEE Transactions on Power Electronics*. 2023;38(1):739–749. https://doi.org/10.1109/TPEL.2022.3203855
15. Битюков В.К., Лавренов А.И., Малицкий Д.А. Анализ пульсаций DC/DC преобразователя, построенного по Zeta топологии, с использованием его предельной непрерывной математической модели. *Russian Technological Journal.* 2023;11(4):36–48. https://doi.org/10.32362/2500-316X-2023-11-4-36-48

About the authors

Vladimir K. Bityukov, Dr. Sci. (Eng.), Professor, Department of Radio Wave Processes and Technology, Institute of Radio Electronics and Informatics, MIREA – Russian Technological University (78, Vernadskogo pr., Moscow, 119454 Russia). E-mail: bitukov@mirea.ru. ResearcherID Y-8325-2018, Scopus Author ID 6603797260, RSCI SPIN-code 3834-5360, https://orcid.org/0000-0001-6448-8509

Aleksey I. Lavrenov, Postgraduate Student, Assistant, Department of Radio Wave Processes and Technology, Institute of Radio Electronics and Informatics, MIREA – Russian Technological University (78, Vernadskogo pr., Moscow, 119454 Russia). E-mail: lavrenov@mirea.ru. RSCI SPIN-code 6048-5027, https://orcid.org/0000-0001-5722-541X

Об авторах

Битюков Владимир Ксенофонтович, д.т.н., профессор, кафедра радиоволновых процессов и технологий, Институт радиоэлектроники и информатики, ФГБОУ ВО «МИРЭА – Российский технологический университет» (119454, Россия, Москва, пр-т Вернадского, д. 78). E-mail: bitukov@mirea.ru. Scopus Author ID 6603797260, ResearcherID Y-8325-2018, SPIN-код РИНЦ 3834-5360, https://orcid.org/0000-0001-6448-8509

Лавренов Алексей Игоревич, аспирант, ассистент, кафедра радиоволновых процессов и технологий, Институт радиоэлектроники и информатики, ФГБОУ ВО «МИРЭА – Российский технологический университет» (119454, Россия, Москва, пр-т Вернадского, д. 78). E-mail: lavrenov@mirea.ru. SPIN-код РИНЦ 6048-5027, https://orcid.org/0000-0001-5722-541X

Translated from Russian into English by K. Nazarov
Edited for English language and spelling by Thomas A. Beavitt

UDC 527.62
https://doi.org/10.32362/2500-316X-2025-13-1-68-75
EDN LSCIAO

RESEARCH ARTICLE

Formation of a database of auxiliary information for positioning in an environment with heterogeneous radio transparency

Mikhail N. Krizhanovsky [@], **Olga V. Tikhonova**

MIREA – Russian Technological University, Moscow, 119454 Russia
[@] *Corresponding author, e-mail: mihakri007@mail.ru*

Abstract

Objectives. A pressing problem for indoor positioning systems in the absence of access to global navigation satellite systems is low positioning accuracy. This is usually associated with uneven coverage of the work area due to its geometric features or the presence of massive obstacles and walls within its boundaries. This problem is frequently resolved by placing an excessive number of positioning system base stations in the work area. This approach generates a high cost for such systems, which in turn prevents their deployment. Therefore, research and development aimed at improving the accuracy of indoor positioning systems using a minimum number of stations is of great relevance. The author previously proposed a method of increasing the accuracy of indoor positioning by taking into account obstacles known at the design stage of the system. Consideration of such obstacles in calculating the location is achieved through the mechanism of preliminary splitting of radio beacons into groups, and the allocation of reference stations of these groups among the base stations. The aim of the work is to improve this algorithm by automating the stage of preparing information about the grouping of stations.

Methods. A computer simulation method was used, in order to confirm the operability of the algorithm to divide the stations of the positioning system into overlapping groups.

Results. The criteria for automatic station grouping and a universal algorithm for dividing stations into groups were developed, enabling the automated preparation of the minimum necessary initial data for a program implementing an algorithm for positioning in a zone of heterogeneous radio transparency.

Conclusions. Modeling of the proposed algorithm has confirmed its operability. The results obtained can be used as a significant addition to the previously proposed algorithm for taking into account obstacles when calculating distances to base stations.

Keywords: indoor positioning systems, station grouping algorithm, RSSI, trilateration

• **Submitted:** 22.12.2023 • **Revised:** 15.07.2024 • **Accepted:** 20.11.2024

For citation: Krizhanovsky M.N., Tikhonova O.V. Formation of a database of auxiliary information for positioning in an environment with heterogeneous radio transparency. *Russian Technological Journal*. 2025;13(1):68–75. https://doi.org/10.32362/2500-316X-2025-13-1-68-75, https://elibrary.ru/LSCIAO

Financial disclosure: The authors have no financial or proprietary interest in any material or method mentioned.

The authors declare no conflicts of interest.

НАУЧНАЯ СТАТЬЯ

Разбиение множества базовых станций локальной системы позиционирования на пересекающиеся группы

М.Н. Крижановский [@], **О.В. Тихонова**

МИРЭА – Российский технологический университет, Москва, 119454 Россия
[@] *Автор для переписки, e-mail: mihakri007@mail.ru*

Резюме

Цели. Актуальной проблемой систем локального позиционирования при отсутствии доступа к глобальным навигационным спутниковым системам является низкая точность позиционирования, связанная, как правило, с неравномерным покрытием рабочей зоны в связи с ее геометрическими особенностями или наличием в ее пределах массивных препятствий и стен. Обычно эта проблема решается путем размещения в рабочей зоне избыточного числа базовых станций системы позиционирования. Подобный подход порождает высокую стоимость таких систем, что в свою очередь препятствует их распространению. Поэтому исследования и разработки, направленные на повышение точности локальных систем позиционирования при использовании минимального числа станций, имеют большую актуальность. Ранее автором был предложен метод повышения точности локального позиционирования путем учета препятствий, известных на этапе проектирования системы. Учет таких препятствий при расчете местоположения реализуется за счет механизма предварительного разбиения радиомаяков на группы и выделения опорных станций этих групп среди базовых станций. Целью работы является усовершенствование этого алгоритма за счет автоматизации этапа подготовки информации о группировке станций.

Методы. Использован метод компьютерного моделирования для подтверждения работоспособности алгоритма разбиения станций системы позиционирования на пересекающиеся группы.

Результаты. Разработаны критерии автогруппировки станций и универсальный алгоритм разбиения станций на группы, позволяющий в автоматизированном режиме подготовить минимально необходимые начальные данные для программы, реализующей алгоритм позиционирования в зоне неоднородной радиопрозрачности.

Выводы. Моделирование предложенного алгоритма подтвердило его работоспособность. Полученные результаты могут использоваться как существенное дополнение к предложенному ранее алгоритму учета препятствий при расчете расстояний до базовых станций.

Ключевые слова: локальные системы позиционирования, алгоритм группировки станций, RSSI, трилатерация

• **Поступила:** 22.12.2023 • **Доработана:** 15.07.2024 • **Принята к опубликованию:** 20.11.2024

Для цитирования: Крижановский М.Н., Тихонова О.В. Разбиение множества базовых станций локальной системы позиционирования на пересекающиеся группы. *Russian Technological Journal*. 2025;13(1):68–75. https://doi.org/10.32362/2500-316X-2025-13-1-68-75, https://elibrary.ru/LSCIAO

Прозрачность финансовой деятельности: Авторы не имеют финансовой заинтересованности в представленных материалах или методах.

Авторы заявляют об отсутствии конфликта интересов.

INTRODUCTION

Positioning objects in confined spaces has become a common issue due to the growing popularity of robotization of various spheres of life. It has been resolved in various ways, using various combinations of components and algorithmic solutions for coordinate determination. As a rule, such systems are implemented on the basis of one of the common wireless data transmission interfaces, such as Wi-Fi [1–3], BLE[1] [4–6], ZigBee [7–9], UWB[2] [10–14], etc.

In indoor positioning, the problem of accuracy improvement is the most pressing, as confirmed by the fact that the largest number of publications is devoted to it. For example, [15] proposes increasing accuracy by purchasing more expensive components which is often not economically feasible for the consumer. In [16] accuracy improvement is provided by using two protocols (Wi-Fi and BLE) and two algorithms for coordinate calculation (trilateration [17] and matching [18]).

Another solution was proposed in [19], which discussed the possibility of reducing the average value of the positioning error by taking into account the loss of signal power when crossing obstacles, where information about the location in the working area is known in advance. It is proposed that at the stage of system development each particular case of the working area in which it is planned to carry out positioning of any objects be approached individually. In order to take obstacles into account, it is proposed that all base stations of the system used for positioning into groups be divided in advance. This is based on the known data on the coordinates of obstacles. Then the reference stations among them can be singled out. The division into groups is based on the principle of finding a group on the same side of the obstacles. A reference station is selected based on its proximity to the geometric center of the area occupied by a particular group of stations, bounded not necessarily by a closed contour of obstacles. According to the algorithm proposed in the paper, the positioning device first compares the signal levels from the reference stations of different groups. After determining the strongest signal in the calculation of distances based on the measurement of the received signal strength indicator (RSSI), the positioning device will be able to decide that all stations belonging to the group whose reference station has the strongest signal are on the same side of the obstacles with the object. Thus, the distance to these stations is calculated as if they were in line of sight.

The distance to the stations in line-of-sight according to the measured RSSI value is calculated according to the following relation:

$$\frac{P_r(d_0)}{P_r(d)} = \frac{d^n}{d_0},$$

wherein d_0 is the calibration distance, which is usually 1 m; $P_r(d_0)$ is the RSSI value determined by the receiver at the calibration distance; $P_r(d)$ RSSI value determined by the receiver during the measurement; d is the measured distance; and n is the coefficient of signal power loss which ranges from 2 to 4 for air, depending on the presence of obstacles.

From this equation, the expected RSSI value at distance d can be obtained as follows:

$$P_r(d) = P_r(d_0) - 10n\lg\left(\frac{d}{d_0}\right) \text{ dBm},$$

$$d = d_0 \cdot 10^{\frac{P_r(d_0)-P_r(d)}{10n}} \text{ m}.$$

For stations belonging to other groups, the distance from the object is calculated in accordance with the Motley–Keenan mathematical model [20]. Then the received power and distance to the signal source will be calculated according to the following formulae:

$$P_r(d) = P_r(d_0) - k_W P_W - 10n\lg\left(\frac{d}{d_0}\right) \text{ dBm},$$

$$d = d_0 \cdot 10^{\frac{P_r(d_0)-k_W P_W - P_r(d)}{10n}} \text{ m},$$

[1] Bluetooth low energy—Bluetooth technology with low power consumption.

[2] Ultra-wide band—A short-range, low-power wireless communication technology that uses ultra-wideband signals with extremely low power spectral density as a carrier.

wherein k_W is the number of the passed single-type obstacles (walls), and P_W is the loss of signal power when passing through a single-type obstacle (wall).

The modeling carried out in [19] confirmed a significant improvement of positioning accuracy by means of the trilateration method. It should be noted that the partitioning into groups and allocation of reference stations were performed "manually" at the developer's discretion.

The objective of this article is to improve the positioning algorithm proposed in [19] for positioning in the zone of inhomogeneous radio transparency by automating the process of dividing base stations into groups, selecting reference stations and introducing additional parameters for the realization of these actions. This objective is also to resolve possible ambiguities when making a decision on line-of-sight with stations which can arise when an object is located on the boundary of two groups of stations.

STATION GROUPING CRITERIA

The criteria for making a decision on combining several stations into one group should ensure the formation of groups consisting of stations located in the area. They should form a convex polygon without obstacles inside it, so that the positioned object located in the area occupied by a particular group of stations has mutual direct visibility with all stations of this group. If we divide the space into non-intersecting sectors occupied by groups, as in Fig. 1, then when using the method of line-of-sight determination as described in [19] (based on stations belonging to the group from whose reference station the signal of the highest amplitude is received) there may be cases of incorrect line-of-sight determination when the object is located on the boundaries of such areas.

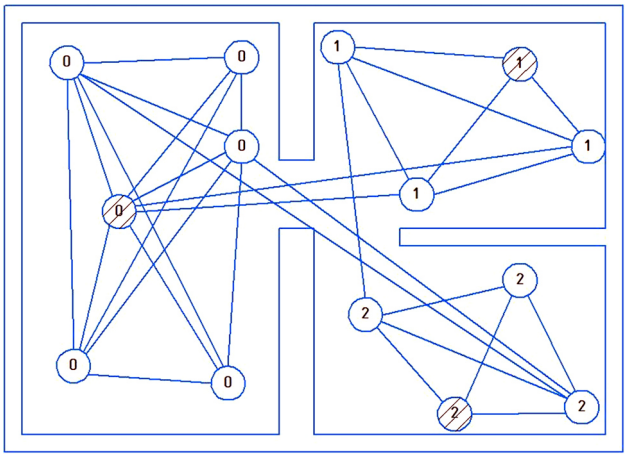

Fig. 1. Case of a work area map with stations divided into groups: shaded stations are reference stations; stations connected by lines are in line of sight

Among the stations from which the strongest signals are received by the object and which participate in the calculation of coordinates, there may be stations from the group for which an incorrect decision about the absence of line-of-sight will be made. An example of such a situation is shown in Fig. 2, where the positioned object located between two groups of stations is designated as PO.

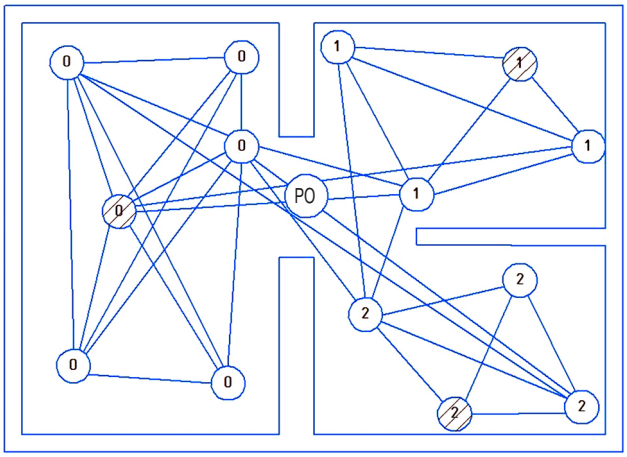

Fig. 2. Case of ambiguity in the definition of line of sight with stations

Figure 2 shows that the closest reference station is the station of group 0, but that the three closest stations are each from three different groups.

In such a situation, the range from some of the stations taken into account in the calculation will be calculated incorrectly. This will lead to significant errors in positioning. The implementation of overlapping groups will eliminate this problem, since it will eliminate the very possibility of the boundary condition. For example, in the situation presented in Fig. 3, this error in positioning will not occur. An additional group "3" appears on the diagram (the designation "3" is marked next to the stations belonging to this group). This group includes the boundary stations from the other three groups, thus eliminating the ambiguity of determining the stations with which there is direct visibility.

It can thus be stated that the condition of station groups located in areas without obstacles within their boundaries is ensured by mutual direct visibility of the said stations. Also, in order for each group to be able to provide positioning of the object independently, it must have at least three stations (for the case of two-dimensional positioning). Two stations in direct line of sight cannot be considered as a group, since it is not always possible to determine the object location unambiguously from the signals from two stations.

With regard to creating conditions for the formation of overlapping groups by the designed algorithm, it was experimentally established that, if a restriction on the

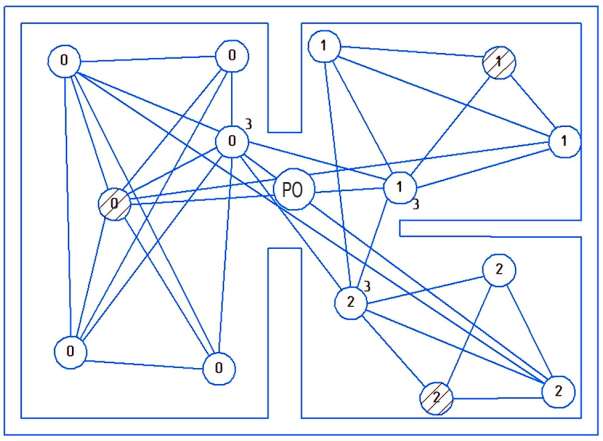

Fig. 3. Case of resolving ambiguity in line-of-sight determination with stations

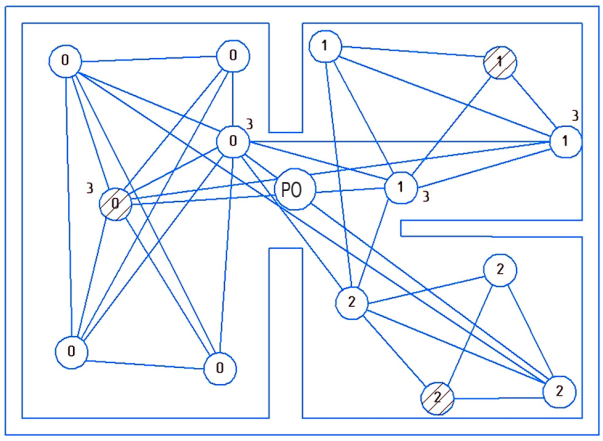

Fig. 4. Group 3 is a case of a possible overextended group

maximum distance of the stations included in the groups from each other is included in the algorithm, then, by varying this restriction, it is possible to find its optimal value. This value will correspond to the conditions for the autogrouping of stations with the creation of overlapping groups. Such a constraint will ensure that there are no conditions for the formation of excessively long groups, for example, as in Fig. 4. Group 3 in this case has a large extent, increasing the risk of incorrectly determining the range of stations in line of sight from the positioning object.

Thus, we can distinguish three principles, which should be incorporated into the algorithm of automatic station grouping:

1) mutual direct visibility of all stations belonging to the group;
2) the group cannot contain less than three stations;
3) stations in a group shall not be located at a distance from each other exceeding the specified maximum range.

ALGORITHM OF STATION AUTOGROUPING ACCORDING TO THE PROPOSED PRINCIPLES

Based on the proposed principles, an algorithm for autogrouping base stations of the indoor positioning system into overlapping groups was developed. The algorithm thus developed forms a set of groups of stations and allocates a reference station in each group. It should be separately noted that this algorithm assumes the availability of cartographic information about the location of obstacles in the potential working area of positioning.

The algorithm of station autogrouping is divided into the following steps:

1. Calculation of the table of presence and absence of line of sight between stations;
2. Formation of a two-dimensional array, each row of which is a list ranked by distance from the stations with the identifier corresponding to the column number to the station whose identifier corresponds to the row number of the two-dimensional array;
3. Exclusion from each line of the two-dimensional array of stations with no line of sight to the station whose identifier is equal to the line number;
4. Exclusion from each row of the two-dimensional array of stations with a distance exceeding the developer's distance limit to the station, and the identifier of which is equal to the row number;
5. Exclusion of lines containing less than three stations;
6. Exclusion of repeated lines;
7. Determining the matches between lines, deleting lines with station sets present in the line-ups of other lines and forming groups.

In order to illustrate the algorithm, a map of a 5 m × 5 m room with two additional room-dividing partitions was taken. The map with arranged stations and marked station identifiers is shown in Fig. 5.

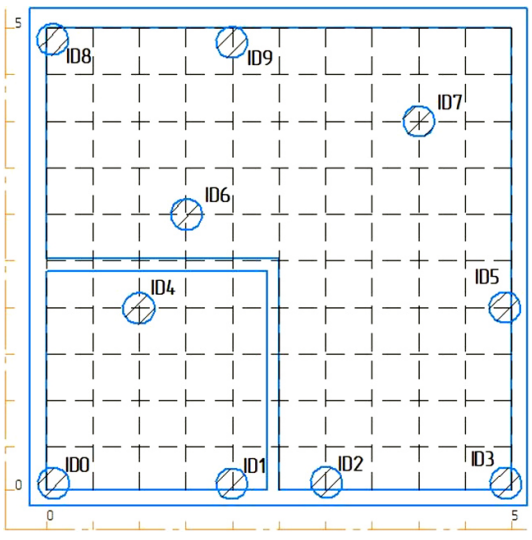

Fig. 5. Map of the working area for illustrating the principles of the program operation

Automatic grouping was provided by a program which implements the proposed algorithm. Figure 6 shows the map of the working area. The marks on the stations show which group they belong to, as a result of the algorithm. In addition, a reference station was identified in each group (in Fig. 6, such stations are marked with a black dot).

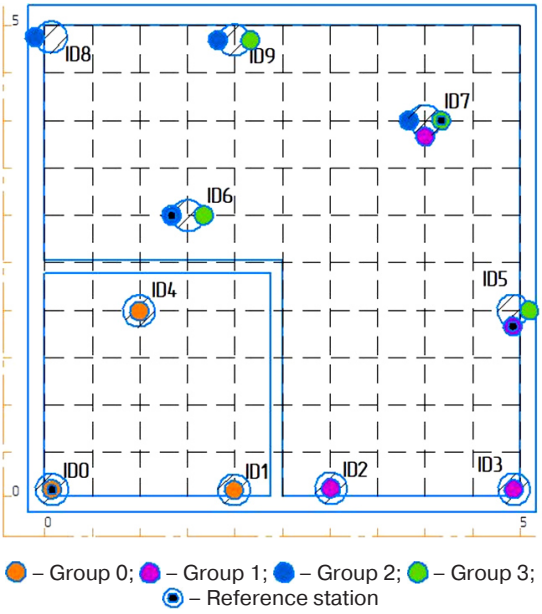

Fig. 6. Map of the working area with the results of the grouping performed

As can be seen, in Fig. 6, the possibility of ambiguity of line-of-sight station identification at the boundary of groups 1 and 2 is eliminated due to the intersection of groups, as well as due to the creation of an intermediate group 3.

Thus, the algorithm of automatic station grouping in the conditions of the working area with obstacles, logically complements and improves the algorithm given in [19].

CONCLUSIONS

The article proposes the principles of station autogrouping, and a universal algorithm for partitioning stations into groups. As a result, it is possible to prepare in automated mode the minimum necessary initial data for the operation of the program given in the article, in order to implement the positioning algorithm in the zone of inhomogeneous radio transparency. During the development of the autogrouping program, the method of mutual overlapping of groups by stations was introduced, in order to supplement the previously proposed algorithm. This enabled us to resolve the problem of ambiguous determination of line of sight between stations at the boundaries of groups. In further works, it is planned to supplement this set of software solutions with an intelligent algorithm for the optimal arrangement of stations of the indoor positioning system in premises. This will allow a complete program complex to be created, which will enable us to perform the preliminary arrangement and grouping of stations in the designed indoor positioning system.

Authors' contribution
All the authors have equally contributed to the research.

REFERENCES

1. Ninh D.B., He J., Trung V.T., Huy D.P. An effective random statistical method for Indoor Positioning System using WiFi fingerprinting. *Future Gener. Comput. Syst*. 2020;109:238–248. https://doi.org/10.1016/j.future.2020.03.043
2. Qin F., Zuo T., Wang X. Ccpos: Wifi fingerprint indoor positioning system based on CDAE-CNN. *Sensors*. 2021;21(4):1114. https://doi.org/10.3390/s21041114
3. Bellavista-Parent V., Torres-Sospedra J., Perez-Navarro A. New trends in indoor positioning based on WiFi and machine learning: A systematic review. In: *2021 International Conference on Indoor Positioning and Indoor Navigation* (*IPIN*). IEEE; 2021. https://doi.org/10.1109/IPIN51156.2021.9662521
4. Bai L., Ciravegna F., Bond R., Mulvenna M. A low cost indoor positioning system using bluetooth low energy. *IEEE Access*. 2020;8:136858–136871. http://dx.doi.org/10.1109/ACCESS.2020.3012342
5. Essa E., Abdullah B.A., Wahba A. Improve performance of indoor positioning system using BLE. In: *2019 14th International Conference on Computer Engineering and Systems* (*ICCES*). IEEE; 2019. P. 234–237. https://doi.org/10.1109/ICCES48960.2019.9068142
6. Spachos P., Plataniotis K.N. BLE beacons for indoor positioning at an interactive IoT-based smart museum. *IEEE Syst. J*. 2020;14(3):3483–3493. https://doi.org/10.1109/JSYST.2020.2969088
7. Dong Z.Y., Xu W.M., Zhuang H. Research on ZigBee indoor technology positioning based on RSSI. *Procedia Comput. Sci*. 2019;154:424–429. https://doi.org/10.1016/j.procs.2019.06.060
8. Ainul R.D. An enhanced trilateration algorithm for indoor RSSI based positioning system using ZigBee protocol. *J. INFOTEL* (*Informatics, Telecommunication, and Electronics*). 2022;14(4):301–306. https://doi.org/10.20895/infotel.v14i4.822
9. Cheng C.H., Syu S.J. Improving area positioning in ZigBee sensor networks using neural network algorithm. *Microsyst. Technol*. 2021;27(1):1419–1428. https://doi.org/10.1007/s00542-019-04309-2

10. Tian D., Xiang Q. Research on indoor positioning system based on UWB technology. In: *2020 IEEE 5th Information Technology and Mechatronics Engineering Conference* (*ITOEC*). IEEE; 2020. P. 662–665. https://doi.org/10.1109/ITOEC49072.2020.9141707
11. Li B., Zhao K., Sandoval E.B. A UWB-based indoor positioning system employing neural networks. *J. Geovis. Spat. Anal.* 2020;4(2):18. https://doi.org/10.1007/s41651-020-00059-2
12. Che F., Ahmed Q.Z., Fontaine J., et al. Feature-based generalized Gaussian distribution method for NLoS detection in ultra-wideband (UWB) indoor positioning system. *IEEE Sensors J*. 2022;22(19):18726–18739. https://doi.org/10.1109/JSEN.2022.3198680
13. Lopes S.I., Vieira J.M.N., Reis J., Albuquerque D., Carvalho N.B. Accurate smartphone indoor positioning using a WSN infrastructure and non-invasive audio for TDoA estimation. *Pervasive and Mobile Computing*. 2015;20:29–46. https://doi.org/10.1016/j.pmcj.2014.09.003
14. Zourmand A., Sheng N.W., Hing A.L.K., AbdulRehman M. Human Counting and Indoor Positioning System Using WiFi Technology. In: *2018 IEEE International Conference on Automatic Control and Intelligent Systems* (*I2CACIS*). IEEE: 2018. https://doi.org/10.1109/I2CACIS.2018.8603690
15. Zhao M., Chang T., Arun A., Ayyalasomayajula R., Zhang C., Bharadia D. ULoc: Low-Power, Scalable and cm-Accurate UWB-Tag Localization and Tracking for Indoor Applications. *Proceedings of the ACM on Interactive, Mobile, Wearable and Ubiquitous Technologies*. 2021;5(3):1–31. https://doi.org/10.1145/3478124
16. Renault S., Akbar Sheikh-Akbari, Ofoegbu E. Low Cost and Energy Efficient Hybrid Wireless Positioning System Using Wi-Fi and Bluetooth Technologies for Wearable Devices. *Preprints*. 2023. 2023092061. http://doi.org/10.20944/preprints202309.2061.v1
17. Astafiev A.V., Titov D.V., Zhiznyakov A.L., Demidov A.A. A method for mobile device positioning using a sensor network of BLE beacons, approximation of the RSSI value and artificial neural networks. *Komp'yuternaya optika = Computer Optics*. 2021;45(2):277–285 (in Russ.). https://doi.org/10.18287/2412-6179-CO-826
18. Subedi S., Pyun J.-Y. Practical fingerprinting localization for indoor positioning system by using beacons. *J. Sensors*. 2017;2017:9742170. https://doi.org/10.1155/2017/9742170
19. Krizhanovskiy M. Modeling of the algorithm for taking into account obstacles in the calculation of location in short-range positioning systems. *Voprosy elektromekhaniki. Trudy VNIIEM = Electromechanical Matters. VNIIEM Studies*. 2023;192(1):14–20 (in Russ.). https://www.elibrary.ru/evdpoc, Available from URL: https://jurnal.vniiem.ru/text/192/14-20.pdf
20. Obeidat H.A., Khan R., Obeidat O.A., et al. An indoor path loss prediction model using wall correction factors for WLAN and 5G indoor networks. *Radio Science J*. 2018;53(4):544–564. https://doi.org/10.1002/2018RS006536

About the authors

Mikhail N. Krizhanovsky, Assistant, Department of Radio Electronic Systems and Complexes, Institute of Radio Electronics and Informatics, MIREA – Russian Technological University (78, Vernadskogo pr., Moscow, 119454 Russia). E-mail: krizhanovskij@mirea.ru. RSCI SPIN-code 3063-6513, https://orcid.org/0009-0009-2710-0128

Olga V. Tikhonova, Dr. Sci. (Eng.), Senior Researcher, Professor, Department of Radio Electronic Systems and Complexes, Institute of Radio Electronics and Informatics, MIREA – Russian Technological University (78, Vernadskogo pr., Moscow, 119454 Russia). E-mail: o_tikhonova@inbox.ru. Scopus Author ID 57208923772, RSCI SPIN-code 3362-9924, https://orcid.org/0009-0009-4013-9182

Об авторах

Крижановский Михаил Николаевич, ассистент, кафедра радиоэлектронных систем и комплексов, Институт радиоэлектроники и информатики, ФГБОУ ВО «МИРЭА – Российский технологический университет» (119454, Россия, Москва, пр-т Вернадского, д. 78). E-mail: krizhanovskij@mirea.ru. SPIN-код РИНЦ 3063-6513, https://orcid.org/0009-0009-2710-0128

Тихонова Ольга Вадимовна, д.т.н., старший научный сотрудник, профессор, кафедра радиоэлектронных систем и комплексов, Институт радиоэлектроники и информатики, ФГБОУ ВО «МИРЭА – Российский технологический университет» (119454, Россия, Москва, пр-т Вернадского, д. 78). E-mail: o_tikhonova@inbox.ru. Scopus Author ID 57208923772, SPIN-код РИНЦ 3362-9924, https://orcid.org/0009-0009-4013-9182

Translated from Russian into English by Lyudmila O. Bychkova
Edited for English language and spelling by Dr. David Mossop

Modern radio engineering and telecommunication systems

Современные радиотехнические и телекоммуникационные системы

UDC 621.391.072
https://doi.org/10.32362/2500-316X-2025-13-1-76-88
EDN OQHKMM

RESEARCH ARTICLE

Optimization of signal constellations with amplitude-phase shift keying in communication channels with non-fluctuating interference

Gennady V. Kulikov [1, @], Dang Xuan Khang [1], Andrey A. Lelyukh [2]

[1] *MIREA – Russian Technological University, Moscow, 119454 Russia*
[2] *Moscow Scientific Research Institute of Radio Communications, Moscow, 109029 Russia*
[@] *Corresponding author, e-mail: kulikov@mirea.ru*

Abstract

Objectives. Multi-position amplitude-phase shift keying (APSK) with a ring-shaped signal constellation is one of the most effective ways for transmitting discrete information in satellite systems. The use of APSK is regulated by several standards. The main are DVB-S2 and VSAT which define both the modulation parameters, and the parameters of the signal constellations. The aim of the paper is to determine the best constellations of 16-APSK and 32-APSK, and provide a minimum BER for cases when the communication channel, along with noise, contains non-fluctuating interference.

Methods. Methods of statistical radio engineering, the theory of optimal signal reception, and computer modeling were used.

Results. The optimization of ring-shaped constellations of 16-APSK and 32-APSK signals is attained by changing the distribution of points along the radius and phase for a case in which the communication channel, along with noise, contains non-fluctuating interference: frequency-shift keyed, retransmitted, phase-shift keyed, and harmonic ones. The best constellations of 16-APSK and 32-APSK are determined, and a minimum bit error rate is provided.

Conclusions. In order to improve the quality of communication in information transmission systems in the presence of non-fluctuating interference, the existing constellations 16-APSK (4, 12) and 32-APSK (4, 12, 16) can be used by changing the ratios between the radii of circles 2.5 for 16-APSK and 2.5/3.9 for 32-APSK. Due to the more efficient use of signal power, the use of constellations with a zero-amplitude point for 16-APSK allows reception noise immunity to be increased. For example, when using constellation (1, 5, 10), the energy gain compared to the standard constellation (4, 12) can reach 1 dB.

Keywords: amplitude-phase shift keying, signal constellation, non-fluctuation interference, noise immunity, bit error rate

• **Submitted:** 25.12.2023 • **Revised:** 11.07.2024 • **Accepted:** 11.11.2024

For citation: Kulikov G.V., Dang X.Kh., Lelyukh A.A. Optimization of signal constellations with amplitude-phase shift keying in communication channels with non-fluctuating interference. *Russian Technological Journal*. 2025;13(1):76–88. https://doi.org/10.32362/2500-316X-2025-13-1-76-88, https://elibrary.ru/OQHKMM

Financial disclosure: The authors have no financial or proprietary interest in any material or method mentioned.

The authors declare no conflicts of interest.

НАУЧНАЯ СТАТЬЯ

Оптимизация созвездий сигналов с амплитудно-фазовой манипуляцией в каналах связи с нефлуктуационными помехами

Г.В. Куликов [1, @], Данг Суан Ханг [1], А.А. Лелюх [2]

[1] *МИРЭА – Российский технологический университет, Москва, 119454 Россия*
[2] *АО «Московский научно-исследовательский институт радиосвязи», Москва, 109029 Россия*
[@] *Автор для переписки, e-mail: kulikov@mirea.ru*

Резюме

Цели. Многопозиционная амплитудно-фазовая манипуляция (АФМ) с кольцевой формой сигнальных созвездий является одним из наиболее эффективных способов передачи дискретной информации в спутниковых системах. Применение АФМ регламентируется несколькими стандартами, основными из которых являются DVB-S2 и VSAT. Они определяют параметры модуляции, а также параметры сигнальных созвездий. Цель статьи – определение наилучших созвездий 16-АФМ и 32-АФМ, обеспечивающих минимум вероятности битовой ошибки для случаев, когда в канале связи наряду с шумовой присутствуют помехи нефлуктуационного вида.

Методы. Использованы методы статистической радиотехники, теории оптимального приема сигналов и компьютерного моделирования.

Результаты. Рассмотрены способы и проведена оптимизация созвездий кольцевой формы сигналов 16-АФМ и 32-АФМ изменением распределения точек по радиусу и фазе для случая, когда в канале связи наряду с шумовой присутствуют помехи нефлуктуационного вида: частотно-манипулированная, ретранслированная, фазоманипулированная, гармоническая. Определены наилучшие созвездия 16-АФМ и 32-АФМ, обеспечивающие минимум вероятности битовой ошибки.

Выводы. Для улучшения качества связи в системах передачи информации при наличии нефлуктуационных помех можно использовать существующие созвездия 16-АФМ (4, 12) и 32-АФМ (4, 12, 16) с изменением соотношений между радиусами окружностей 2.5 для 16-АФМ и 2.5/3.9 для 32-АФМ. За счет более эффективного использования мощности сигнала применение созвездий с точкой с нулевой амплитудой для 16-АФМ позволяет добиться увеличения помехоустойчивости приема. Например, в случае применения созвездия (1, 5, 10) энергетический выигрыш по сравнению со стандартным созвездием (4, 12) может достигать 1 дБ.

Ключевые слова: амплитудно-фазовая манипуляция, сигнальное созвездие, нефлуктуационные помехи, помехоустойчивость, вероятность битовой ошибки

• **Поступила:** 25.12.2023 • **Доработана:** 11.07.2024 • **Принята к опубликованию:** 11.11.2024

Для цитирования: Куликов Г.В., Данг С.Х., Лелюх А.А. Оптимизация созвездий сигналов с амплитудно-фазовой манипуляцией в каналах связи с нефлуктуационными помехами. *Russian Technological Journal*. 2025;13(1):76–88. https://doi.org/10.32362/2500-316X-2025-13-1-76-88, https://elibrary.ru/OQHKMM

Прозрачность финансовой деятельности: Авторы не имеют финансовой заинтересованности в представленных материалах или методах.

Авторы заявляют об отсутствии конфликта интересов.

INTRODUCTION

Multi-position amplitude and phase-shift keying (APSK) is one of the most effective methods for data transmission in satellite systems with limited and expensive access to the communication channel [1–3]. It allows the capacity of the radio channel to be increased when compared to the binary manipulation. It also provides good noise immunity and thus high efficiency of using the frequency resource.

There are several standards which use APSK modulation for satellite communications including DVB-S2[1] (the second generation of digital satellite television broadcasting) [3, 4] and VSAT (a very-small-aperture terminal) [3, 5]. These standards specify modulation parameters such as the type of signal constellations, signal-to-noise ratio (SNR), data rate, inter alia.

In the light of the growing needs for high-speed data transmission and increased noise immunity of communication systems, optimizing APSK signal constellation formats is quite important since this optimal format allows the radio spectrum efficiency to be increased and data transmission quality to be enhanced. This is particularly important in satellite communications and in communication systems which operate over long distances.

Numerous studies on noise immunity of communication systems with APSK consider signal reception against various noises [6–11] and in channels with non-linearity [12–15].

This paper discusses methods for optimizing 16-APSK and 32-APSK ring-shaped signal constellations by changing the distribution of points over radius and phase for the scenario with non-fluctuating interference present in the communication channel along with noise. The paper aims to determine the best 16-APSK and 32-APSK constellations which ensure minimum bit error rate (BER).

CALCULATION METHODS

The model for APSK signal has the following form:

$$s_i(t) = Ar_i \cos(\omega_0 t + \varphi_i), t \in \left(0, T_s\right], i = \overline{0, M-1}, \quad (1)$$

wherein $A = \sqrt{2E_s / T_s}$ is the average amplitude of the signal; $E_s = E_b \log_2 M$ is the average energy of channel symbol; E_b is the average energy per bit of information; ω_0 is carrier frequency; r_i and φ_i are values specifying the amplitude and phase of the signaling element; T_s is the symbol duration time; M is the signal positionality; and t is time.

[1] DVB. https://www.dvb.org/standards/dvb-s2x. Accessed November 11, 2023.

The constellation format may be optimized by estimating the probability of incorrect signal reception, i.e., by searching for the minimum of the function describing the dependence of the BER P_{eb} on constellation parameters. The methodology required for calculating BER is given in [16], while [16–19] offer details of the calculations of statistical characteristics of random process distributions in the optimal receiver solver, such as mathematical expectations, m_{mi}, and variances, D_{mi}, for different combinations of symbols in the presence of different types of non-fluctuating interference and noise interference at power spectral density N_0. These characteristics depend on various parameters of signals and interference. In particular, these include:

- exposure to phase-shift keyed interference [17]:

$$s_{int}(t) = \mu A a_j \cos[(\omega_0 t + \Delta\omega_{int})t + \varphi_{int}],$$
$$t \in ((j-1)T_{int}, jT_{int}], \; j = \overline{1, N_{int}},$$

wherein μ is relative (in amplitude) interference intensity, $a_j = \pm 1$ is random symbol of interference, φ_{int} is its random initial phase, N_{int} is relative channel velocity of interference, and $T_{int} = T_s/N_{int}$, $\Delta\omega_{int}$ is interference detuning,

$$m_{mi} = \frac{E_s}{N_0}\left\{2r_m[r_m - r_i\cos(\varphi_m - \varphi_i)] + \frac{\mu}{N_{int}} \times \right.$$
$$\times 2S(y)[r_m \sum_{j=0}^{N_{int}-1} a_j \cos(y(2j+1) + \varphi_{int} - \varphi_m)] -$$
$$\left. - r_i \sum_{j=0}^{N_{int}-1} a_j \cos(y(2j+1) + \varphi_{int} - \varphi_i)\right\}, \quad (2)$$
$$y = \frac{\Delta\omega_{int} T_s}{N_{int}}, \; S(y) = \frac{\sin y}{y};$$

- exposure to the frequency-shift keyed interference [18]:

$$s_{int}(t) = \mu A \cos[(\omega_0 + a_j \Delta\omega_d + \Delta\omega_{int})t + \varphi_{int}],$$
$$t \in ((j-1)T_{int}, jT_{int}], \; j = \overline{1, N_{int}},$$

wherein $\Delta\omega_d$ is interference deviation,

$$m_{mi} = \frac{E_s}{N_0}(r_m^2 + r_i^2 - 2r_m r_i \cos(\varphi_m - \varphi_i)) + \frac{2E_s}{N_0} \times$$
$$\times \frac{\mu}{N_{int}} \sum_{j=1}^{N_{int}} \frac{\sin y}{y}[r_m \cos(x(2j-1) + \varphi_{int} - \varphi_m)] -$$
$$- r_i \cos(x(2j-1) + \varphi_{int} - \varphi_i)], \quad (3)$$
$$y = \frac{(a_j \Delta\omega_d + \Delta\omega_{int})T_s}{2N_{int}};$$

- exposure to the retransmitted interference [19]:

$$s_{\text{int}}(t)=\begin{cases}\mu A r_\tau \cos(\omega_0(t-\tau)+\varphi_\tau+\varphi_{\text{int}}),\ 0<t\le\tau,\\ \mu A r_i \cos(\omega_0(t-\tau)+\varphi_i+\varphi_{\text{int}}),\ \tau<t\le T_s,\end{cases}$$

wherein τ is the interference delay,

$$m_{mi}=\frac{E_s}{N_0}[(r_m^2+r_i^2-2r_m r_i\cos(\varphi_m-\varphi_i)]+\frac{2E_s}{N_0}\mu r_\tau\times$$
$$\times\frac{\tau}{T_s}[r_m\cos(\varphi_{\text{int}}+\varphi_\tau-\varphi_m)-r_i\cos(\varphi_{\text{int}}+\varphi_\tau-\varphi_i)]+ \quad (4)$$
$$+\frac{2E_s}{N_0}\mu r_m\cdot\left(1-\frac{\tau}{T_s}\right)[r_m\cos\varphi_{\text{int}}-r_i\cos(\varphi_{\text{int}}+\varphi_\tau-\varphi_i)];$$

- exposure to harmonic interference [16]:

$$s_{\text{int}}(t)=\mu A\cos[(\omega_0+\Delta\omega_{\text{int}})t+\varphi_{\text{int}}],$$
$$m_{mi}=\frac{E_s}{N_0}[0.5(r_m^2+r_i^2-2r_m r_i\cos(\varphi_m-\varphi_i))+$$
$$+\mu\frac{\sin(\Delta\omega_{\text{int}}T_s/2)}{\Delta\omega_{\text{int}}T_s/2}(\cos\eta(r_m\cos\varphi_m-r_i\cos\varphi_i)- \quad (5)$$
$$-\sin\eta(r_m\sin\varphi_m-r_i\sin\varphi_i))],$$
$$\eta=\Delta\omega_{\text{int}}T_s/2+\varphi_{\text{int}}.$$

For all interference types, the variances of all random processes being studied herein are determined by the following equation:

$$D_{mi}=\frac{2E_s}{N_0}[r_m^2+r_i^2-2r_m r_i\cos(\varphi_m-\varphi_i)]. \quad (6)$$

The following parameters are assumed for the example calculations: SNR is E_b/N_0 = 13 dB, relative (in amplitude) interference intensity is $0.1\le\mu\le0.3$, interference detuning is $\Delta\omega_{\text{int}}=0$, while phase-shift keyed and frequency-shift keyed interferences have a relative channel velocity $N_{\text{int}}=2$; for frequency-shift keyed interference, the reduced deviation is $\Delta\omega_d T_s=6$ and relative delay of retransmitted interference is $\tau/T_s=0.5$.

OPTIMIZING THE CONSTELLATION FORMAT FOR 16-APSK

The 16-APSK signal constellation (4, 12). The 16-APSK signal constellation (4, 12) has two levels of signaling element amplitudes (Fig. 1): $A_1=r_1A$, and $A_2=r_2A$. The relation is expressed through coefficient k: $A_1=kA_2$, and two energy levels E_1 and E_2, respectively. Since constellation symbols have on average the same frequency of occurrence when transmitting information, the average symbol energy can be determined by averaging over the signaling constellation, as follows:

$$E_s=\frac{A^2}{2}T_s=\frac{1}{16}(4E_1+12E_2)=$$
$$=\frac{1}{16}\cdot\frac{A_1^2}{2}T_s(4+12k^2)=\frac{1}{8}A_1^2T_s(1+3k^2).$$

Hence,

$$A_1=\frac{2}{\sqrt{1+3k^2}}A,\ A_2=\frac{2k}{\sqrt{1+3k^2}}A. \quad (7)$$

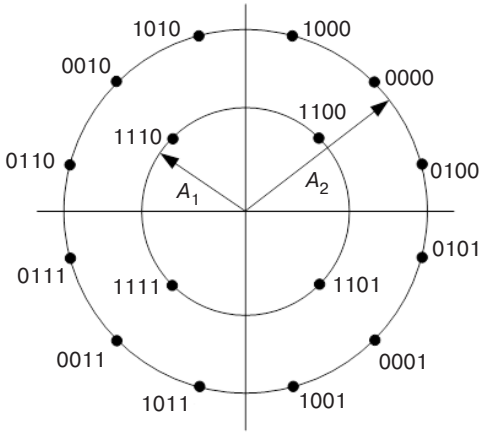

M = 16 (4, 12)

Fig. 1. 16-APSK signal constellation (4, 12)

Substituting (7) into (2)–(6) with allowance for (1) and methodology [16], BER dependencies on coefficient k can be obtained (Fig. 2).

The graphs show that in the presence of noise interference alone, BER minimum for the constellation format (4, 12) can be observed at k = 2.5. It shifts to a higher k value in the presence of non-fluctuating interference with high intensity in the radio channel.

Conventional 16-APSK constellations, such as (4, 12) in DVB-S2 and VSAT systems or (8, 8) in some other systems, have non-uniform energy distribution between points of different levels. The use of a zero-amplitude point in the center of the constellation can reduce this energy difference. The more uniform the energy distribution among points, the more efficiently the bandwidth can be utilized. In this case, the number of transmitted points in the constellation is reduced rather than the number of symbols, i.e., the information transmission rate is not reduced.

16-APSK signal constellations (1, 4, 11) and (1, 5, 10). We consider two types of 16-APSK constellation format: (1, 4, 11) and (1, 5, 10). In the

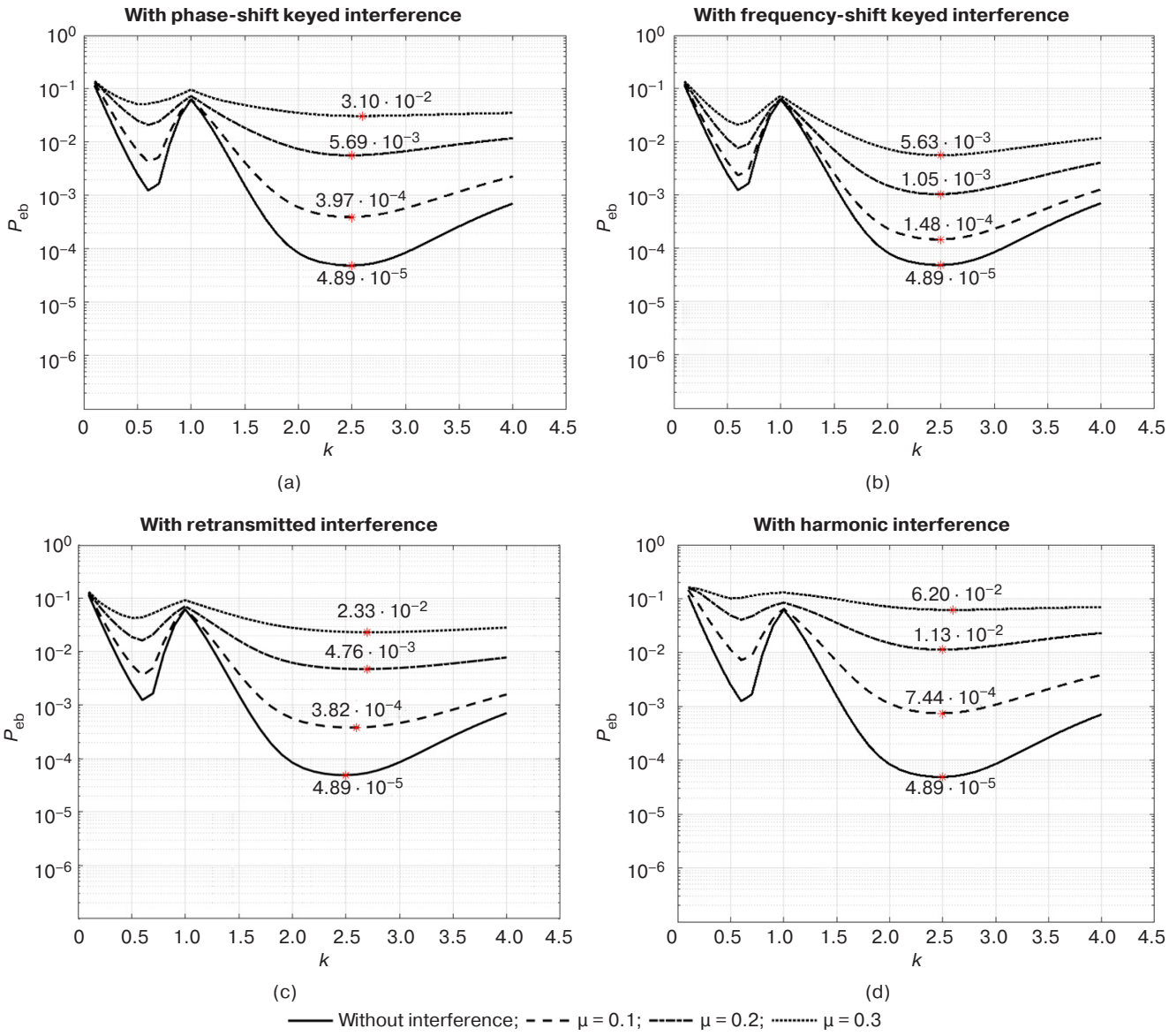

Fig. 2. Dependencies of BER on coefficient *k* for the 16-APSK constellation format (4, 12) at different types of interference

(1, 4, 11) configuration, there is 1 point with zero amplitude $A_1 = 0$ in the center of the constellation, 4 points with amplitude A_2 in the first (small) circle, and 11 points with amplitude $A_3 = kA_2$ in the large circle (Fig. 3a). Similar to (7), we determine the relations for A_2 and A_3:

$$E_s = \frac{A^2}{2}T_s = \frac{1}{16}(E_1 + 4E_2 + 11E_3) =$$
$$= 0 + \frac{1}{16}\cdot\frac{A_2^2}{2}T_s(4 + 11k^2) = \frac{A_2^2}{32}T_s(4 + 11k^2).$$

Hence,

$$A_1 = 0, A_2 = \frac{4A}{\sqrt{4 + 11k^2}}, A_3 = \frac{4kA}{\sqrt{4 + 11k^2}}.$$

Thus, for configuration (1, 5, 10) (Fig. 3b), the following may be obtained:

$$E_s = \frac{A^2}{2}T_s = \frac{1}{16}(E_1 + 5E_2 + 10E_3) =$$
$$= 0 + \frac{1}{16}\cdot\frac{A_2^2}{2}T_s(5 + 10k^2) = \frac{A_2^2}{32}T_s(5 + 10k^2),$$

$$A_1 = 0, A_2 = \frac{4A}{\sqrt{5 + 10k^2}}, A_3 = \frac{4kA}{\sqrt{5 + 10k^2}}.$$

Figure 4 shows dependencies of BER on coefficient *k* while receiving 16-APSK signals when applying the constellation format (1, 4, 11) for different types of interference.

Figure 5 shows similar results for the 16-APSK format (1, 5, 10).

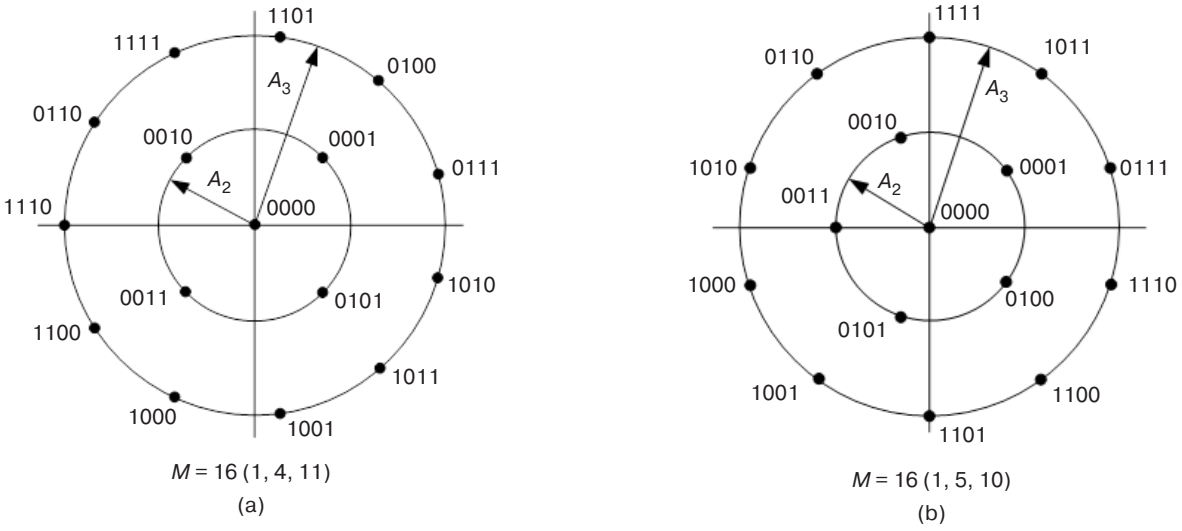

Fig. 3. 16-APSK signal constellations (1, 4, 11) and (1, 5, 10)

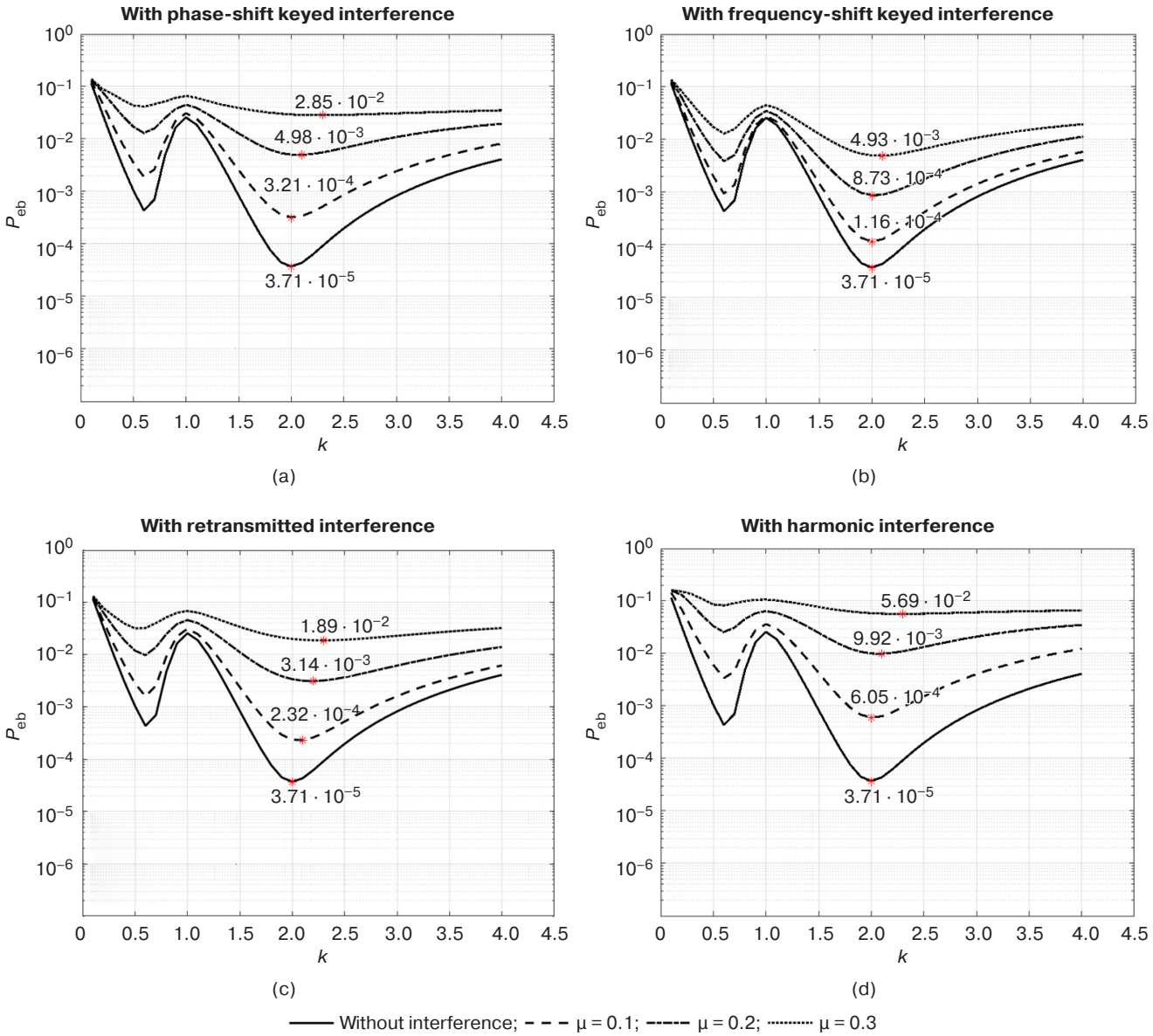

Fig. 4. Dependencies of BER on coefficient *k* for the 16-APSK constellation format (1, 4, 11) at different types of interference

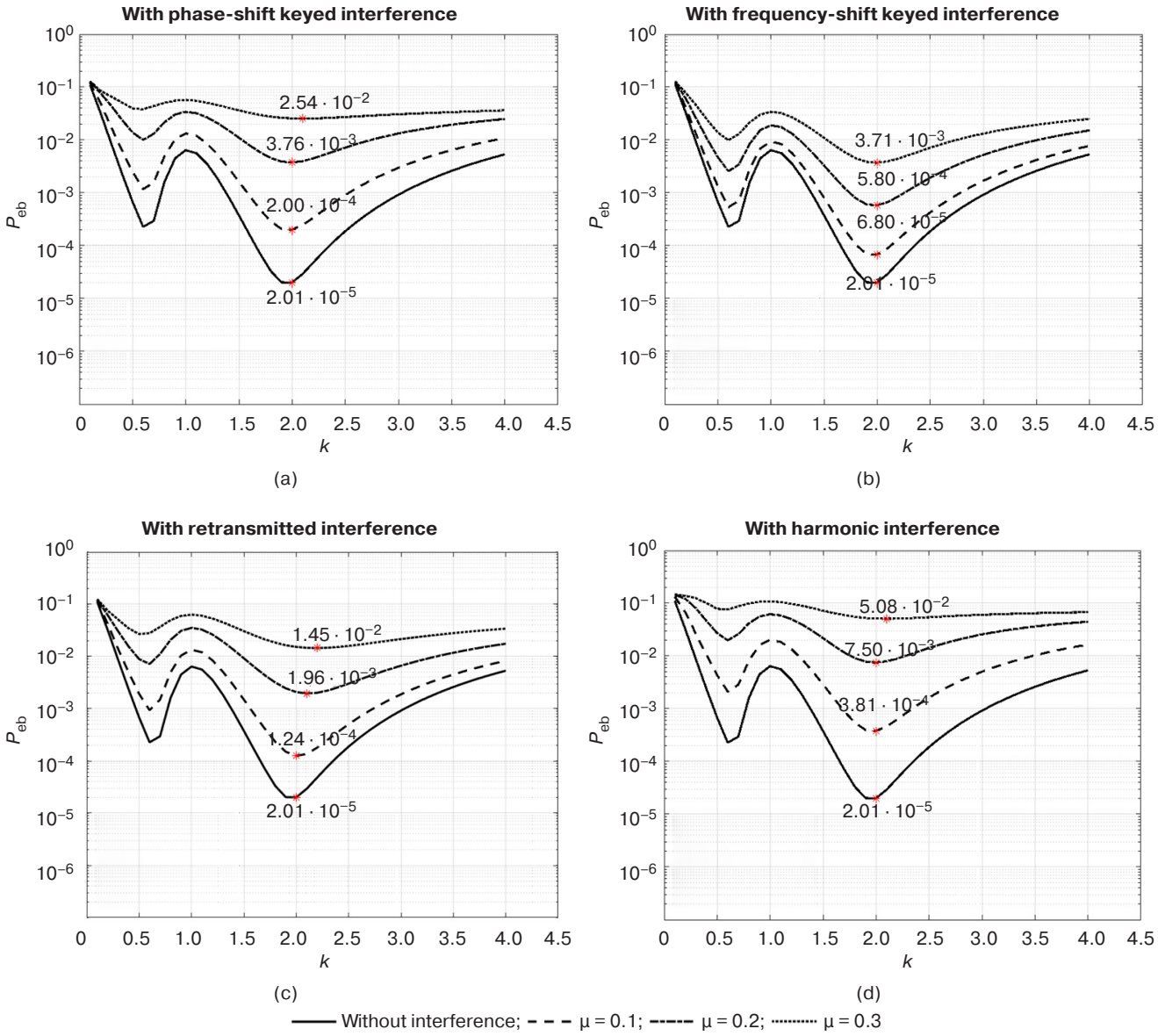

Fig. 5. Dependencies of BER on coefficient *k* for the 16-APSK constellation format (1, 5, 10) at different types of interference

The graphs show that the use of 16-APSK formats (1, 4, 11) and (1, 5, 10) yields some increase in noise immunity at the optimal value of coefficient *k* compared to format (4, 12). It can also be noted that with increasing relative interference intensity μ, the optimal value of *k* shifts to a higher value.

For comparison, Table 1 summarizes the optimal values of coefficients *k* for different formats, at which the BER is minimized.

Figure 6 shows the calculation results for the reception noise immunity of 16-APSK signals with formats (1, 4, 11) and (1, 5, 10). It also shows the optimized constellation (4, 12) (at $A_2 = 2.5A_1$) compared to the standard version (4, 12) (at $A_2 = 2.7A_1$) used in the DVB-S2 standard, when received against different types of interference with relative intensity μ = 0.16. The average energies for all formats are assumed to be similar.

The advantage of format (1, 5, 10) over other types of constellations is evident. The energy gain in this case reaches 1 dB. When using format (1, 4, 11), some increase in noise immunity is also observed when compared to the optimal constellation (4, 12). However, it is small.

Table 1. Optimal values of coefficients *k*

Format	$M = 16$					
	μ		0	0.1	0.2	0.3
1, 4, 11	*k*	Frequency-shift keyed	2	2	2	2.1
		Retransmitted	2	2	2.1	2.2
		Phase-shift keyed	2	2	2.1	2.3
		Harmonic	2	2	2.1	2.3
1, 5, 10	*k*	Frequency-shift keyed	2	2	2	2
		Retransmitted	2	2	2	2.1
		Phase-shift keyed	2	2	2	2.1
		Harmonic	2	2	2	2.1
4, 12	*k*	Frequency-shift keyed	2.5	2.5	2.5	2.5
		Retransmitted	2.5	2.6	2.7	2.9
		Phase-shift keyed	2.5	2.5	2.5	2.6
		Harmonic	2.5	2.5	2.5	2.6

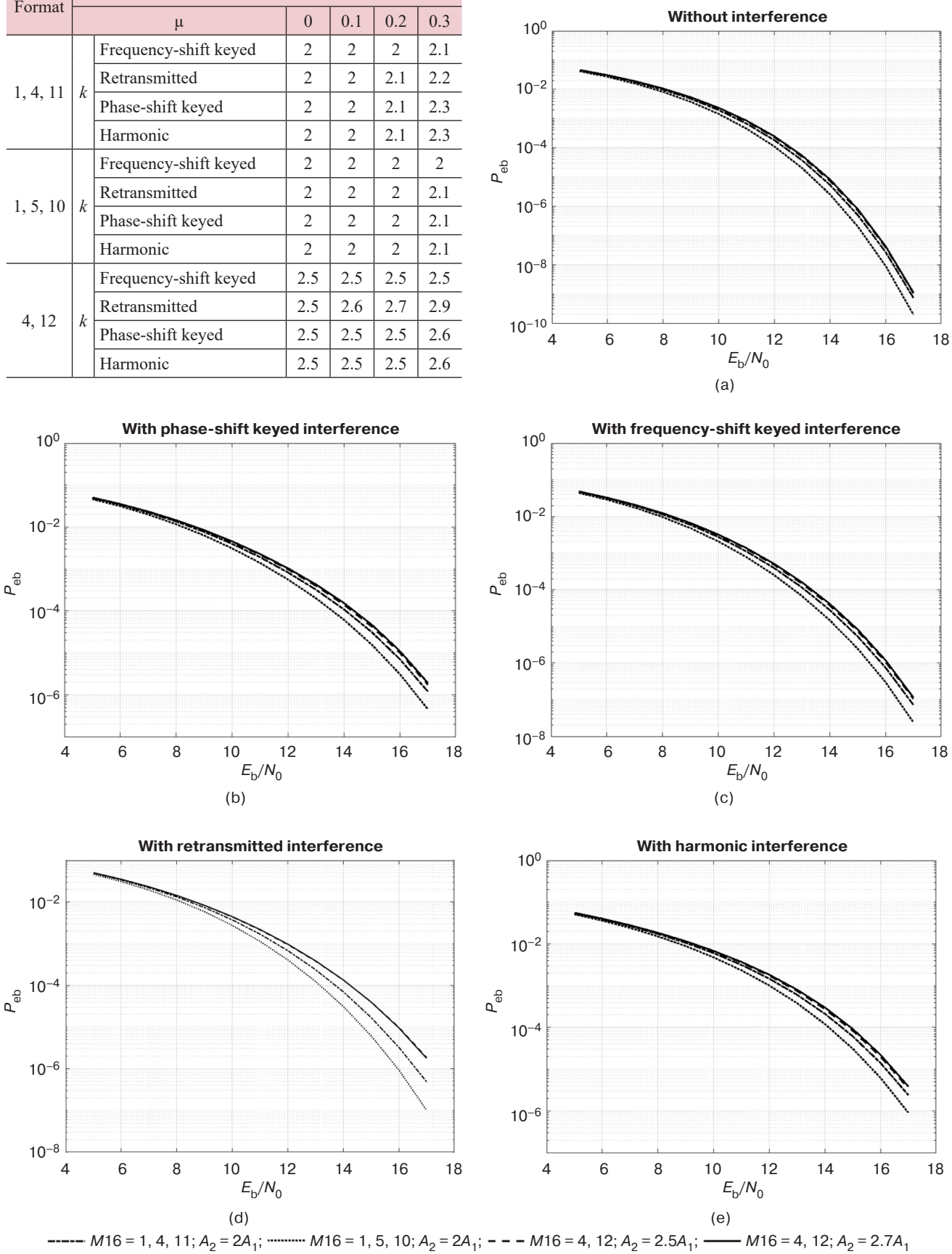

Fig. 6. Dependencies of BER on SNR for different constellation formats under different types of interference

OPTIMIZING THE CONSTELLATION FORMAT FOR 32-APSK

The 32-APSK (4, 12, 16) signal constellation (Fig. 7) has 3 circles with amplitude ratios $A_2 = k_2 A_1$ and $A_3 = k_3 A_1$ and three energy levels E_1, E_2, and E_3, respectively. The amplitude ratios can be calculated in a similar way to that of $M = 16$. The average symbol energy may be written, as follows:

$$E_s = \frac{A^2}{2} T_s = \frac{1}{32}(4E_1 + 12E_2 + 16E_3) = \\ = \frac{A_1^2}{16} T_s (1 + 3k_2^2 + 4k_3^2).$$

Hence,

$$A_1 = \frac{2\sqrt{2}A}{\sqrt{1 + 3k_2^2 + 4k_3^2}}, \quad A_2 = \frac{2\sqrt{2}k_2 A}{\sqrt{1 + 3k_2^2 + 4k_3^2}}, \\ A_3 = \frac{2\sqrt{2}k_3 A}{\sqrt{1 + 3k_2^2 + 4k_3^2}}.$$

The dependence of BER on coefficients k_2 and k_3 appears as a surface in the three-dimensional coordinate system. Figure 8 shows an example at SNR E_b/N_0 = 13 dB and the absence of interference. In this case, minimum P_{eb} value is achieved for $k_2 = 2.5$ and $k_3 = 3.9$.

The optimal values of coefficients k_2 and k_3 at which the BER is minimal in the presence of different types of interference are given in Table 2.

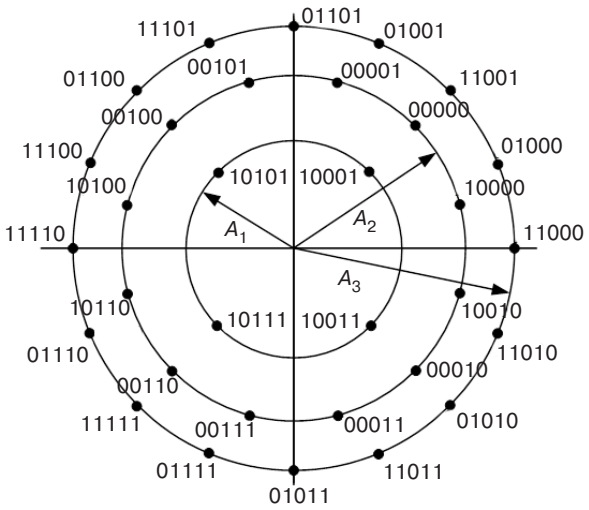

$M = 32$ (4, 12, 16)

Fig. 7. 32-APSK signal constellation (4, 12, 16)

It follows from Table 2 that the optimal values of these ratios increase with increasing interference intensity. Thus, if in the presence of noise interference only ($\mu = 0$), the optimal ratios are $A_2 = 2.5A_1$ and $A_3 = 3.9A_1$, then for $\mu = 0.3$, average ratios $A_2 = 2.65A_1$ and $A_3 = 5.2A_1$ are recommended.

Figure 9 shows the results of noise immunity calculation for 32-APSK format ($A_2 = 2.5A_1$ and $A_3 = 3.9A_1$) when compared to the format used in DVB-S2 standard ($A_2 = 2.64A_1$ and $A_3 = 4.64A_1$) under different types of interference. The average energies for both formats are assumed to be similar. It can be observed that BER is slightly reduced in all cases, and the energy gain at $10^{-5} \le P_{eb} \le 10^{-4}$ is about 1 dB.

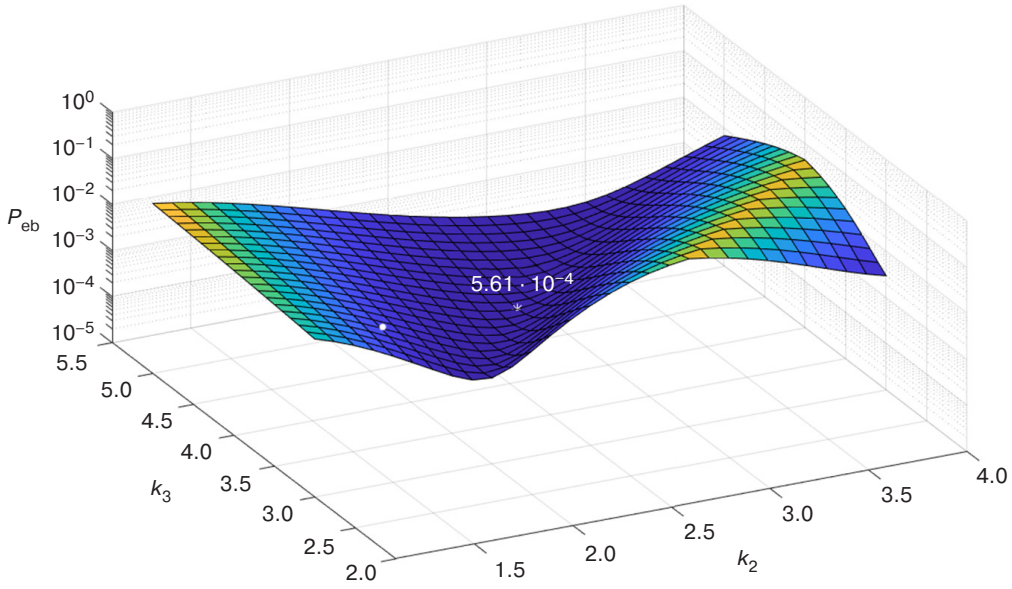

Fig. 8. Dependence of BER on k_2 and k_3 coefficients

Table 2. Optimal values of coefficients k_2 and k_3

Format	$M = 32$					
	μ		0	0.1	0.2	0.3
4, 12, 16	k_2/k_3	Frequency-shift keyed	2.5/3.9	2.5/3.9	2.5/4.0	2.6/4.4
		Retransmitted	2.5/3.9	2.5/3.9	2.6/4.5	2.6/4.8
		Phase-shift keyed	2.5/3.9	2.5/3.9	2.6/4.4	2.5/6.0
		Harmonic	2.5/3.9	2.5/4.0	2.6/4.4	3/6.0

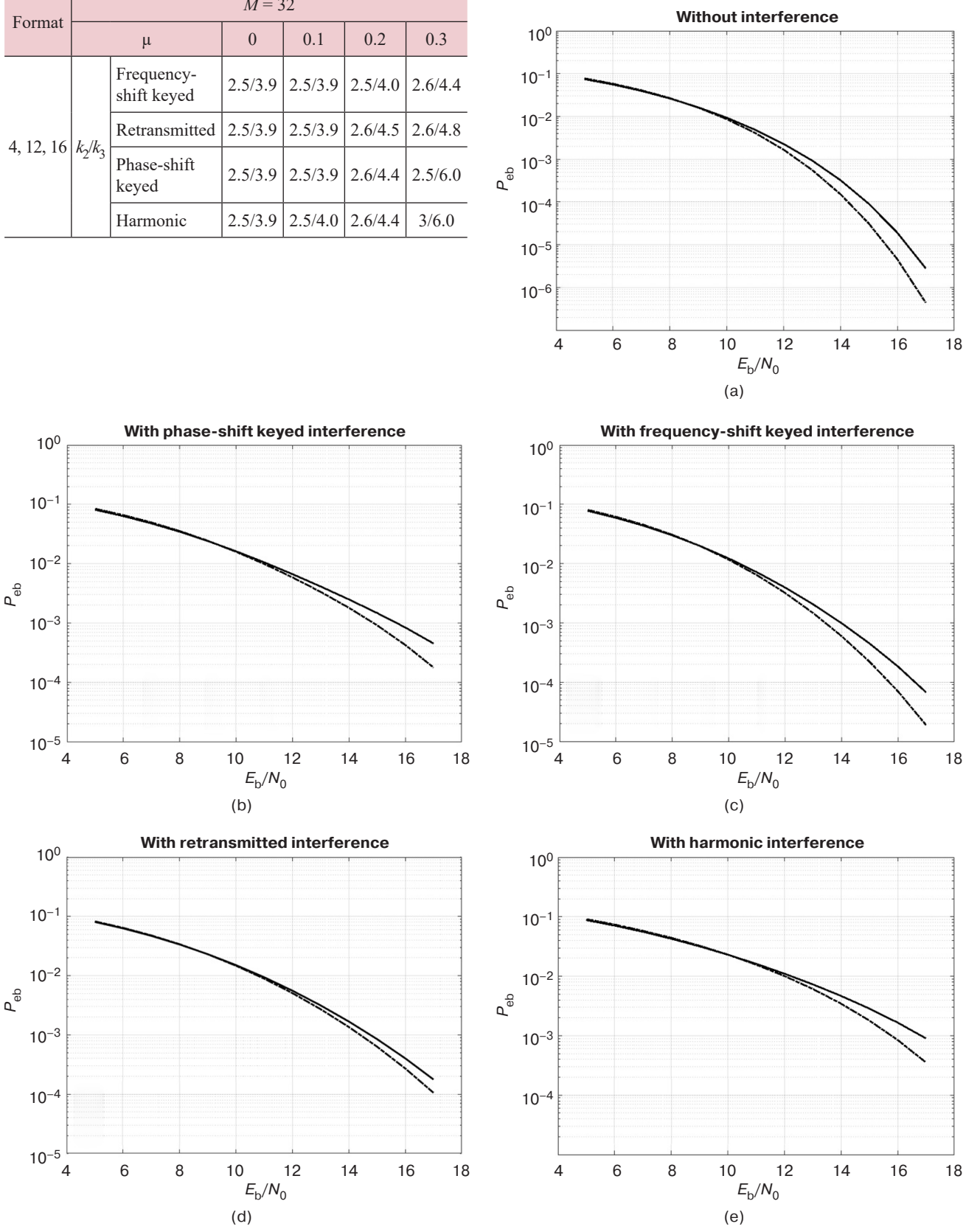

Fig. 9. Dependencies of BER on SNR for suggested amplitude ratios and standard ratios of DVB-S2 standard at different interference types

CONCLUSIONS

The following conclusions can be drawn as a result of this study:

1. The quality of communication in information transmission systems in the presence of non-fluctuating interference of low intensity can be improved by using the existing constellations of 16-APSK (4, 12) and 32-APSK (4, 12, 16), with a change in amplitude ratios ($A_2 = 2.5A_1$) for 16-APSK and ($A_2 = 2.5A_1$ and $A_3 = 3.9A_1$) for 32-APSK.
2. Due to the more efficient use of the signal power, applying constellations with a zero-amplitude point to 16-APSK allows reception noise immunity to be increased. For example, using constellation (1, 5, 10) with a ratio of $A_2 = 2A_1$, the power gain over standard constellation (4, 12) can be up to 1 dB.

Authors' contributions

G.V. Kulikov—the research idea, consultations on the issues of conducting all stages of the study.

X.Kh. Dang—conducting computer calculations.

A.A. Lelyukh—processing the results.

REFERENCES

1. Proakis J.G. *Digital Communications*. 4th ed. NY: McGraw-Hill; 2001. 1002 p.
2. Fuqin X. *Digital Modulation Techniques*. 2nd ed. Artech House Telecommunications Library. Artech House Publishers; 2006. 1039 p.
3. Somov A.M., Kornev S.F. *Sputnikovye sistemy svyazi* (*Satellite Communication Systems*). Moscow: Goryachaya liniya – Telekom; 2012. 244 p. (in Russ.). ISBN 978-5-9912-0225-1
4. Minoli D. *Innovations in Satellite Communications and Satellite Technology: The Industry Implications of DVB-S2X, High Throughput Satellites, Ultra HD, M2M, and IP*. NY: John Wiley & Sons Ltd; 2015. 441 p.
5. Shelukhin O.I., et al. *Seti sputnikovoi svyazi VSAT* (*VSAT Satellite Communication Networks*). Moscow: MGUL; 2004. 281 p. (in Russ.). ISBN 5-8135-0248-3
6. Savvateev Yu.I., Nazarov O.V. (Eds.). *Pomekhozashchishchennost' priema diskretnykh sig*nalov (*Noise Immunity of Reception of Discrete Signals*). Moscow: Radiotekhnika; 2015. 584 p. (in Russ.). ISBN 978-5-93108-094-9
7. Savishchenko N.V., Afrikantov I.N., Kapralov D.D., Kirillov V.S., Ostroumov O.A. Calculation of the probability of bit and symbolic errors for the communication channel when receiving signal structures of the DVB-S2 standard. *Informatsiya i kosmos = Information and Space*. 2015;1:9–15 (in Russ.).
8. Parshutkin A.V., Maslakov P.A. Noise stability of sattelite communication channels with amplitude-phase modulation to exposure to urged unsteady interference. *Voprosy oboronnoi tekhniki. Seriya 16. Tekhnicheskie sredstva protivodeistviya terrorizmu = Military Enginery. Counter-Terrorism Technical Divices. Issue 16.* 2019;11–12:96–101 (in Russ.).
9. Vyboldin Yu.K. Error probabilities for receiving multipositions APM signals in communication channels with fading. In: *GUAP Scientific Session:* collection of reports in 3 v. St. Petersburg: GUAP; 2018. V. 2. P. 32–37 (in Russ.). https://elibrary.ru/ypbhcx
10. Gorobtsov I.A., Kirik D.I. Estimation of noise immunity of signal reception with APSK. In: *Actual Problems of Infotelecommunications in Science and Education* (*APINO 2019*): Collection of scientific articles of the 8th International Scientific-Technical and Scientific-Methodical Conference in 4 v. 2019. V. 3. P. 111–116 (in Russ.). https://elibrary.ru/vmilnb
11. Dovbnya V.G., Koptev D.S., Babanin I.G. Assessment of potential interference of receiving digital signals used in modern and perspective radio-relay and satellite communication systems. *Proceedings of the Southwestern State University. Series: IT Management, Computer Science, Computer Engineering. Medical Equipment Engineering.* 2020;10(1):21–35 (in Russ.). https://elibrary.ru/xeofpi
12. Nosov V.I., Degtyarev S.S. Noise immunity analysis for M-APSK signaling over satellite link with nonlinear distortions. *Modern Science: Actual Problems of Theory & Practice. Series: Natural and Technical Sciences*. 2017;6:14–22 (in Russ.). https://elibrary.ru/yzlemn
13. Nosov V.I., Degtyarev S.S. *Issledovanie vliyaniya nelineinosti usilitelya moshchnosti retranslyatora na pomekhoustoichivost' sputnikovykh sistem svyazi* (*Investigation of the Influence of the Nonlinearity of the Repeater Power Amplifier on the Noise Immunity of Satellite Communication Systems*). Novosibirsk: SibGUTI; 2019. 171 p. (in Russ.). https://elibrary.ru/pgyqxr
14. Strukov A.P. Method of analytical calculation of SER and BER for APSK modulation in the nonlinear channel with AWGN. *Raketno-kosmicheskoe priborostroenie i informatsionnye sistemy = Rocket-Space Device Engineering and Information Systems*. 2017;4(4):83–88 (in Russ.). https://doi.org/10.17238/issn2409-0239.2017.4.83
15. Elkin P.E. Determination of the optimal operating mode of the amplifier when transmitting 16-APSK signals in a nonlinear channel with AFC. In: *Modern Problems of Telecommunications*: *Materials of the Russian Scientific and Technical Conference.* Novosibirsk: SibGUTI; 2017. P. 287–290 (in Russ.). https://elibrary.ru/zfmmlj
16. Kulikov G.V., Usmanov R.R., Trofimov D.S. Noise immunity analysis of amplitude and phase-shift keying signals reception in presence of harmonic interference. *Naukoemkie tekhnologii = Science Intensive Technologies*. 2020;21(1):22–29 (in Russ.). Available from URL: http://radiotec.ru/ru/journal/Science_Intensive_Technologies/number/2020-1/article/19749

17. Kulikov G.V., Dang X.Kh. Noise immunity of receiving signals with amplitude and phase-shift keying in the presence of phase-shift keying interference. *Zhurnal radioelektroniki = J. Radio Electronics*. 2021;11 (in Russ.). https://doi.org/10.30898/1684-1719.2021.11.7
18. Kulikov G.V., Khang D.X, Starikovskiy A.I. Noise immunity of signal reception with amplitude-phase shift keying in the background of frequency shift keying interference. *Voprosy radioelektroniki. Seriya: Tekhnika televideniya = Questions of Radio Electronics. Series: TV Technique*. 2022;4:44–51 (in Russ.). https://elibrary.ru/uvasse
19. Kulikov G.V., Dang X.Kh. Noise immunity of reception of signal with amplitude-phase shift keying in a two-path communication channel. *Voprosy radioelektroniki. Seriya: Tekhnika televideniya = Questions of Radio Electronics. Series: TV Technique*. 2022;2:43–49 (in Russ.).

СПИСОК ЛИТЕРАТУРЫ

1. Proakis J.G. *Digital Communications*. 4th ed. NY: McGraw-Hill; 2001. 1002 p.
2. Fuqin X. *Digital Modulation Techniques*. 2nd ed. Artech House Telecommunications Library. Artech House Publishers; 2006. 1039 p.
3. Сомов А.М., Корнев С.Ф. *Спутниковые системы связи*. М.: Горячая линия – Телеком; 2012. 244 с. ISBN 978-5-9912-0225-1
4. Minoli D. *Innovations in Satellite Communications and Satellite Technology: The Industry Implications of DVB-S2X, High Throughput Satellites, Ultra HD, M2M, and IP*. NY: John Wiley & Sons Ltd; 2015. 441 p.
5. Шелухин О.И. и др. *Сети спутниковой связи VSAT*. М.: Изд-во МГУЛ; 2004. 281 с. ISBN 5-8135-0248-3
6. Савватеев Ю.И., Назаров О.В. (ред.). *Помехозащищенность приема дискретных сигналов.* М.: Радиотехника; 2015. 584 с. ISBN 978-5-93108-094-9
7. Савищенко Н.В., Африкантов И.Н., Капралов Д.Д., Кириллов В.С., Остроумов О.А. Расчет вероятности битовой и символьной ошибок для канала связи при приеме сигнальных конструкций стандарта DVB-S2. *Информация и космос*. 2015;1:9–15.
8. Паршуткин А.В., Маслаков П.А. Помехоустойчивость каналов связи с амплитудно-фазовой модуляцией к воздействию непреднамеренных нестационарных помех. *Вопросы оборонной техники. Серия 16. Технические средства противодействия терроризму*. 2019;11–12:96–101.
9. Выболдин Ю.К. Помехоустойчивость приема многопозиционных АФМ сигналов в каналах связи с замираниями. В сб.: *Научная сессия ГУАП:* сборник докладов в 3-х ч. СПб.: ГУАП; 2018. Ч. 2. С. 32–37. https://elibrary.ru/ypbhcx
10. Горобцов И.А., Кирик Д.И. Оценка помехоустойчивости приема сигналов с амплитудно-фазовой модуляцией. В сб.: *Актуальные проблемы инфотелекоммуникаций в науке и образовании* (*АПИНО 2019*): сборник научных статей VIII Международной научно-технической и научно-методической конференции в 4 т. 2019. Т. 3. С. 111–116. https://elibrary.ru/vmilnb
11. Довбня В.Г., Коптев Д.С., Бабанин И.Г. Оценка потенциальной помехоустойчивости приема цифровых сигналов, используемых в современных и перспективных системах радиорелейной и спутниковой связи. *Известия Юго-Западного государственного университета. Серия: Управление, вычислительная техника, информатика. Медицинское приборостроение*. 2020;10(1):21–35. https://elibrary.ru/xeofpi
12. Носов В.И., Дегтярев С.С. Анализ помехоустойчивости спутниковой линии связи с модуляцией M-APSK при учете нелинейных искажений. *Современная наука: актуальные проблемы теории и практики. Серия: Естественные и технические науки.* 2017;6:14–22. https://elibrary.ru/yzlemn
13. Носов В.И., Дегтярев С.С. *Исследование влияния нелинейности усилителя мощности ретранслятора на помехоустойчивость спутниковых систем связи.* Новосибирск: СибГУТИ; 2019. 171 с. https://elibrary.ru/pgyqxr
14. Струков А.П. Метод аналитического расчета вероятности символьной и битовой ошибок сигнала с амплитудно-фазовой манипуляцией в нелинейном канале. *Ракетно-космическое приборостроение и информационные системы*. 2017;4(4):83–88. https://doi.org/10.17238/issn2409-0239.2017.4.83
15. Елкин П.Е. Определение оптимального режима работы усилителя при передаче сигналов 16-APSK в нелинейном канале с АФК. В: *Современные проблемы телекоммуникаций*: *материалы Российской научно-технической конференции.* Новосибирск: СибГУТИ; 2017. С. 287–290. https://elibrary.ru/zfmmlj
16. Куликов Г.В., Усманов Р.Р., Трофимов Д.С. Анализ помехоустойчивости приема сигналов с многопозиционной амплитудно-фазовой манипуляцией в присутствии гармонической помехи. *Наукоемкие технологии*. 2020;21(1):22–29. URL: http://radiotec.ru/ru/journal/Science_Intensive_Technologies/number/2020-1/article/19749
17. Куликов Г.В., Данг С.Х. Помехоустойчивость приема сигналов с амплитудно-фазовой манипуляцией в присутствии фазоманипулированной помехи. *Журнал радиоэлектроники*. 2021;11. https://doi.org/10.30898/1684-1719.2021.11.7
18. Куликов Г.В., Ханг Д.С., Стариковский А.И. Помехоустойчивость приема сигналов с амплитудно-фазовой манипуляцией на фоне частотно-манипулированной помехи. *Вопросы радиоэлектроники. Серия: Техника телевидения.* 2022;4:44–51. https://elibrary.ru/uvasse
19. Куликов Г.В., Данг С.Х. Помехоустойчивость приема сигналов с амплитудно-фазовой манипуляцией в двухлучевом канале связи. *Вопросы радиоэлектроники. Серия: Техника телевидения*. 2022;2:43–49.

About the authors

Gennady V. Kulikov, Dr. Sci. (Eng.), Professor, Department of Radio Electronic Systems and Complexes, Institute of Radio Electronics and Informatics, MIREA – Russian Technological University (78, Vernadskogo pr., Moscow, 119454 Russia). E-mail: kulikov@mirea.ru. Scopus Author ID 36930533000, RSCI SPIN-code 2844-8073, http://orcid.org/0000-0001-7964-6653

Dang Xuan Khang, Postgraduate Student, Department of Radio Electronic Systems and Complexes, Institute of Radio Electronics and Informatics, MIREA – Russian Technological University (78, Vernadskogo pr., Moscow, 119454 Russia). E-mail: dangxuankhang147@gmail.com. https://orcid.org/0000-0002-3372-7172

Andrey A. Lelyukh, Cand. Sci. (Eng.), Deputy Head of the Technical Center of Special Equipment, Moscow Research Institute of Radio Communications (32, Nizhegorodskaya ul., Moscow, 109029 Russia). E-mail: a.lel@mail.ru. Scopus Author ID 57218678005, RSCI SPIN-code 1021-5094

Об авторах

Куликов Геннадий Валентинович, д.т.н., профессор, профессор кафедры радиоэлектронных систем и комплексов, Институт радиоэлектроники и информатики, ФГБОУ ВО «МИРЭА – Российский технологический университет» (119454, Россия, Москва, пр-т Вернадского, д. 78). E-mail: kulikov@mirea.ru. Scopus Author ID 36930533000, SPIN-код РИНЦ 2844-8073, http://orcid.org/0000-0001-7964-6653

Данг Суан Ханг, аспирант, кафедра радиоэлектронных систем и комплексов, Институт радиоэлектроники и информатики, ФГБОУ ВО «МИРЭА – Российский технологический университет» (119454, Россия, Москва, пр-т Вернадского, д. 78). E-mail: dangxuankhang147@gmail.com. https://orcid.org/0000-0002-3372-7172

Лелюх Андрей Александрович, к.т.н., заместитель начальника технического центра специальной аппаратуры, АО «Московский научно-исследовательский институт радиосвязи» (109029, Россия, Москва, Нижегородская ул., д. 32). E-mail: a.lel@mail.ru. Scopus Author ID 57218678005, SPIN-код РИНЦ 1021-5094

Translated from Russian into English by K. Nazarov
Edited for English language and spelling by Dr. David Mossop

Modern radio engineering and telecommunication systems

Современные радиотехнические и телекоммуникационные системы

UDC 621.396.946
https://doi.org/10.32362/2500-316X-2025-13-1-89-102
EDN OVSTWY

RESEARCH ARTICLE

Modeling of digital spatial processing under conditions of troposphere propagation of centimeter radio waves for wireless telecommunication

Ilia W. Peshkov [1, @], Dmitry N. Borisov [2]

[1] *Bunin Yelets State University, Yelets, 399770 Russia*
[2] *Voronezh State University, Voronezh, 394018 Russia*
[@] *Corresponding author, e-mail: ilvpeshkov@gmail.com*

Abstract

Objectives. A radio beam traveling through the layers of the atmosphere depends on the refractive index and its vertical variation. In this regard, attenuation may occur when radio rays propagate in a waveguide manner at low altitudes. A multipath fading effect may also occur when several rays reflected from different layers of the troposphere and having different spatial coordinates in elevation arrive at the receiver. The aim of the study is to simulate the operational algorithms of digital antenna arrays (DAA) in order to increase the range and reliability of radio communication using a tropospheric waveguide. The main advantage of the DAA consists in the high gain and controllability of the pattern shape. In order to evaluate algorithms for direction-of-arrival estimation with super-resolution and beamforming, it is necessary to select an appropriate method for modeling beam propagation in the layers of the troposphere. It is proposed to use DAA to increase the range and reliability of radio communications using a tropospheric waveguide. The performance of algorithms for direction-of-arrival estimation and beamforming in the troposphere can be evaluated using ray tracing simulation.

Methods. Parabolic equations are used to estimate the path losses of radio waves in the centimeter range. A ray tracing algorithm referring to a tropospheric waveguide is used to estimate the phases in the aperture of the receiving array. A spatial correlation matrix is reliably generated to form the basis for calculating coordinates using a super-resolution multiple signal classification (MUSIC) method and the weighting factor vector (algorithm for maximizing the signal-to-noise + noise ratio).

Results. Typical cases of a tropospheric waveguide based on a modified refractive index were considered. The bit error rate curves are obtained as a function of the geometry of the antenna arrays after the signal has passed through the tropospheric waveguide. Circular and spherical antenna arrays composed of directional antenna elements are considered.

Conclusions. Numerical studies suggest that the range of communication links using digital antenna arrays increases in the centimeter band. The best geometry for this purpose is circular, since providing the lowest bit error rate for binary phase-shift keyed signals.

Keywords: digital antenna array, direction-of-arrival estimation, MUSIC method, beamforming, tropospheric waveguide, simulation

• **Submitted:** 09.10.2023 • **Revised:** 22.07.2024 • **Accepted:** 10.12.2024

For citation: Peshkov I.W., Borisov D.N. Modeling of digital spatial processing under conditions of troposphere propagation of centimeter radio waves for wireless telecommunication. *Russian Technological Journal*. 2025;13(1):89–102. https://doi.org/10.32362/2500-316X-2025-13-1-89-102, https://elibrary.ru/OVSTWY

Financial disclosure: The authors have no financial or proprietary interest in any material or method mentioned.

The authors declare no conflicts of interest.

НАУЧНАЯ СТАТЬЯ

Моделирование цифровой пространственной обработки в условиях тропосферного распространения сантиметровых радиоволн для задач телекоммуникации

И.В. Пешков [1, @], **Д.Н. Борисов** [2]

[1] *Елецкий государственный университет им. И.А. Бунина, Елец, 399770 Россия*
[2] *Воронежский государственный университет, Воронеж, 394018 Россия*
[@] *Автор для переписки, e-mail: ilvpeshkov@gmail.com*

Резюме

Цели. Прохождение радиолуча в слоях атмосферы зависит от показателя преломления и характера его вертикального изменения. В связи с этим могут возникнуть условия, когда радиолучи на малых высотах будут распространяться волноводным образом. При этом происходит затухание сигнала с отличающимися угловыми координатами по углу места. Целью работы является исследование на основе моделирования алгоритмов работы цифровых антенных решеток (ЦАР) для повышения дальности и надежности радиосвязи в условиях тропосферного волновода. Основными преимуществами ЦАР являются высокий коэффициент усиления и управляемость формы диаграммы направленности. При этом необходимо воспользоваться методами моделирования распространения луча в слоях тропосферы для оценки работы алгоритмов оценки угловых координат со сверхразрешением с последующим диаграммообразованием.

Методы. В работе используется аппарат параболических уравнений для оценки коэффициента затуханий радиоволн сантиметрового диапазона, а также алгоритм трассировки лучей через тропосферный волновод для оценки фаз в раскрыве антенн ЦАР. В этом случае будет достоверно сформирована пространственная корреляционная матрица, являющаяся основой для вычисления координат со сверхразрешением (метод MUSIC) и вектора весовых коэффициентов (алгоритм максимизации отношения сигнал/помеха + шум).

Результаты. Рассмотрены типичные случаи возникновения тропосферного волновода на основе модифицированного показателя преломления. Получены графики вероятности битовых ошибок после прохождения сигнала по тропосферному волноводу при разной геометрии антенных решеток. Рассмотрены кольцевые и сферические решетки из направленных антенных элементов.

Выводы. Проведенные численные исследования позволяют сделать вывод, что дальность связи в диапазоне сантиметровых волн увеличивается с помощью ЦАР. Кроме того, установлено, что кольцевая антенная решетка позволяет получить самые низкие значения вероятности битовой ошибки при приеме дискретных радиосигналов в тропосферном волноводе.

Ключевые слова: цифровые антенные решетки, пеленгация, MUSIC, диаграммообразование, тропосферная связь, моделирование

• **Поступила:** 09.10.2023 • **Доработана:** 22.07.2024 • **Принята к опубликованию:** 10.12.2024

Для цитирования: Пешков И.В., Борисов Д.Н. Моделирование цифровой пространственной обработки в условиях тропосферного распространения сантиметровых радиоволн для задач телекоммуникации. *Russian Technological Journal*. 2025;13(1):89–102. https://doi.org/10.32362/2500-316X-2025-13-1-89-102, https://elibrary.ru/OVSTWY

Прозрачность финансовой деятельности: Авторы не имеют финансовой заинтересованности в представленных материалах или методах.

Авторы заявляют об отсутствии конфликта интересов.

INTRODUCTION

The propagation of ultrashort radio waves in the atmosphere is not typically rectilinear, but curved in such a way that the radio wave can undergo refraction in the lower layers and/or multiple reflections from the Earth's surface [1]. In this case, signals of centimeter wavelengths can reach receivers several hundred kilometers away from the transmitter [2–4]. This effect is due to temperature, humidity, and pressure differences in the layers of the troposphere, for which reason it has been named *tropospheric waveguide* [5–7]. This type of long-distance communication can be promising as it does not require expensive means such as satellites [8]. However, communication reliability and stability depends on factors such as the degree of attenuation, the accuracy of determining the height of the tropospheric waveguide in relation to the distance to the receiver, etc. [9]. In this regard, it is necessary to study the application of a digital beam-steering antenna array in tropospheric waveguide conditions as a means of overcoming the associated communication problems. Such devices allow digital shaping of the array pattern peaks and zeros in the desired directions.

The present work proposes a combined simulation method based on the stepwise determination of the loss value and phases of the centimeter range rays propagating in atmospheric layers as a function of the refractive index at different altitudes. The possibility of using digital antenna arrays (DAAs) for such communication is additionally investigated. The first step of the simulation consists in estimating the attenuation of the radio signal. Next, the propagation path from the transmitter to the receiving DAA is calculated using the ray tracing algorithm. Finally, the beamforming algorithms (estimation of the angular coordinates of all beams and digital formation of the array pattern) are modeled to calculate of the bit error rate (BER).

BEAM PROPAGATION IN THE TROPOSPHERE

It is known that the propagation path of a single ray is governed by the well-known Snell's law for a continuous spherically layered medium, as follows[1]:

$$n(h)(R_E + h)\cos e = \text{const}, \quad (1)$$

where n is the refractive index of the medium, h is the height above the Earth's surface, and R_E is the Earth's radius. For a more detailed consideration of the formation mechanism for tropospheric propagation, e represents the angle of the beam location.

The real part of the refractive index can be expressed as a function of atmospheric pressure, humidity, and air temperature. The formula for the index is semi-empirical and can be expressed as follows[2]:

$$n = 1 + 77.6 \cdot 10^{-6} \frac{P}{T} + 0.373 \frac{p}{T^2}, \quad (2)$$

where P is the atmospheric pressure in millibars; T is the temperature in degrees Kelvin; p is the water vapor pressure in millibars.

Equation (2) is known as the Debye formula. It has been shown to have an error of ±0.5% [10]. The refractive index n rarely exceeds 1.0004 at the surface. This introduces the so-called radio wave refraction N, which is defined as follows[3]:

$$N = (n-1) \cdot 10^6. \quad (3)$$

The propagation of radio waves depends more on refraction gradients than on N itself [10]. Typically, noticeable refraction gradients in the horizontal direction occur on much larger scales (tens of meters to tens of kilometers) than in the vertical direction (tens of meters to hundreds of meters). Therefore, the atmosphere is often assumed to be horizontally stratified, and only the height dependence of the refraction is considered, neglecting any horizontal variations.

[1] Recommendation ITU-R P.834-6. *Effects of tropospheric refraction on radiowave propagation* (in Russ.).
[2] The Handbook on Radiometeorology. ITU, 2014. https://www.itu.int/dms_pub/itu-r/opb/hdb/R-HDB-26-2013-OAS-PDF-R.pdf. Accessed October 09, 2023.
[3] Recommendation ITU-R P.453-12(09/2016). *Radio wave refraction index: its formula and refraction data* (in Russ.).

Similarly, the modified or changed refraction M is determined from the modified or changed index of refraction m to include the curvature of the Earth [11]:

$$M = (m-1)\cdot 10^6 = 10^6 \times \left(n - 1 + \frac{h}{R_E}\right) = \\ = N + 10^6 \cdot \frac{h}{R_E}. \quad (4)$$

Figure 1 depicts a simulation of the surface and elevated waveguides using a three-line curve referred to as a profile. The case shown in Fig. 1a illustrates the structure of a simple surface channel. Here, the waveguide extends from a certain boundary height to the Earth's surface, while the trapping layer, where the condition $dM/dh < 0$ favors wave refraction, extends along the entire wave propagation path. The *S*-shaped channel at the surface is shown in Fig. 1b. The trapping layer does not reach the surface since the condition $dM/dh > 0$ applies near the surface. In both cases, the depth of the channel is the height difference between the surface and the top of the channel where the minimum of the modified refraction profile is reached[4]. The general conditions for an elevated channel are summarized in Fig 1c, where the value of M at the Earth's surface is less than at the top of the channel, for which reason the channel cannot reach the surface.

As mentioned above, the appearance of the waveguide is the result of strong vertical changes in atmospheric refractive index between air masses of different temperature and humidity, especially at lower atmospheric levels. In this way, the tropospheric waveguide allows electromagnetic energy to propagate over long distances, enabling long-range radio communications over the horizon.

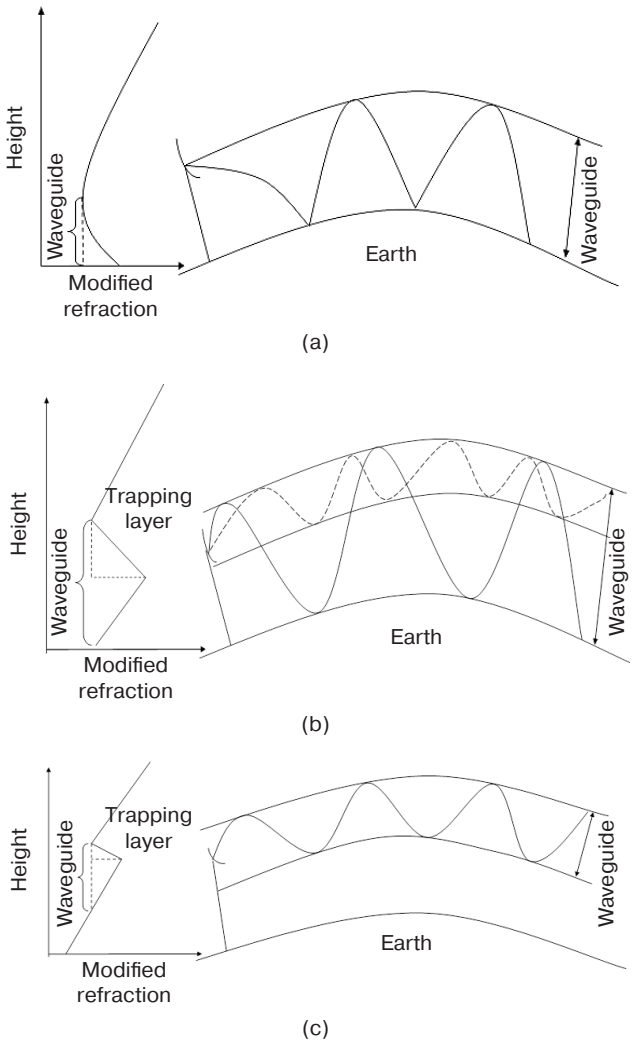

Fig. 1. *M*-profile for different conduction types: (a) simple surface (ground) waveguide, (b) surface waveguide, and (c) elevated waveguide

CALCULATION OF RADIO SIGNAL ATTENUATION USING THE PARABOLIC EQUATION METHOD

This section describes the parabolic equation (PE) apparatus for tropospheric radio propagation problems to estimate the degree of attenuation. Since its original introduction by Leontovich and Fock in 1946 [12], its design has been gradually improved.

According to the Helmholtz equation, the component φ of the electric or magnetic field satisfies the condition [13]:

$$\frac{\partial^2 \varphi}{\partial x^2} + \frac{\partial^2 \varphi}{\partial z^2} + k^2 n^2 \varphi = 0, \quad (5)$$

where k is the free space wave number and φ is the electromagnetic field component, either *Ey* or *Hy* for horizontal and vertical polarization, respectively.

We introduce the so-called reduced field function $u(x, z)$ as a function of the coordinates x and z:

$$\dot{u}(x,z) = e^{-ikx}\varphi(x,z). \quad (6)$$

The point of making this substitution and solving for $\dot{u}(x,z)$ instead of $\varphi(x, z)$ is that $\dot{u}(x,z)$ changes slowly depending on the propagation direction. Following this substitution, the scalar wave Eq. (5) takes the following form:

$$\left\{\frac{\partial^2}{\partial x^2} + \frac{\partial^2}{\partial z^2} + 2ik\frac{\partial}{\partial x} + k^2\left[n^2 - 1\right]\right\}\dot{u}(x,z) = 0. \quad (7)$$

[4] Lindquist T. *Wave Propagation Models in the Troposphere for Long-Range UHF/SHF Radio Connections.* PhD Thesis. 2020. https://urn.kb.se/resolve?urn=urn:nbn:se:kau:diva-80679. Accessed October 09, 2023.

Since this equation is still classified as elliptic rather than parabolic, it is acceptable to introduce a pseudo-differential operator $Q = \sqrt{\frac{1}{k^2}\frac{\partial^2}{\partial z^2} + n^2} = \sqrt{1+q}$, $q = \frac{1}{k^2}\frac{\partial^2}{\partial z^2} + (n(x,z)-1)$ and to factorize Eq. (7). This substitution makes the derivation more general [14]:

$$\left\{\frac{\partial}{\partial x} + ik\left(1-Q\right)\right\}\left\{\frac{\partial}{\partial x} + ik\left(1+Q\right)\right\}u = 0. \quad (8)$$

Equation (9) is simply repeated in steps of Δx until a target point with coordinates x, z is reached, provided that the initial reduced field $u(0, z)$ is known [12, 13]:

$$u\left(x+\Delta x, z\right) = \mathrm{e}^{ik\Delta x(Q-1)}u\left(x,z\right). \quad (9)$$

There are several methods for solving Eq. (9) [14]. The most widely referred to in the existing literature are the split-step Fourier PU, finite element, and finite difference methods[5].

After the field strength has been calculated in accordance with (9), it is necessary to estimate the degree of attenuation along the path by means of propagation and loss factors. The propagation factor *PF* (dB) is defined as the square of the ratio of the electric field amplitude at a given point under specified conditions to that of the same point under free propagation. Equation (10), which expresses the *PF* through the field relative to free space, also shows the relationship with the value of the propagation loss *PL* (dB) [15–17]:

$$PF = 20\lg\left|\dot{u}(x,z)\right| + 10\lg(r) + 10\lg(\lambda), \quad (10)$$

$$PL = 20\lg\left(\frac{4\pi r}{\lambda}\right) - PF, \quad (11)$$

where λ is the wavelength and r is the range of the radio wave propagation.

RAY TRACING METHOD BASED ON THE ORDINARY DIFFERENTIAL EQUATION OF THE 2ND ORDER

This section describes an algorithm for ray tracing in tropospheric layers. It calculates the number of beams and their azimuthal and angular coordinates in the antenna array opening with subsequent digital processing. We write Snell's law (1) by rewriting h as a function of r, that is:

$$n\left[h(r)\right]\left[R_\mathrm{E} + h(r)\right]\cos e = \mathrm{const}. \quad (12)$$

For infinitesimal dh and dr, the geometric representation of the quantities (Fig. 2) gives the following [18]:

$$\sin e = \frac{dh}{dr}, \quad (13)$$

$$\cos e = \sqrt{1-\left(\frac{dh}{dr}\right)^2}\left(\geq 0, \text{ т.е. } e \in \left[-\frac{\pi}{2}, \frac{\pi}{2}\right]\right). \quad (14)$$

Then,

$$nh(r)\left[R_\mathrm{E} + h(r)\right]\sqrt{1-\left(\frac{dh}{dr}\right)^2} = \mathrm{const}. \quad (15)$$

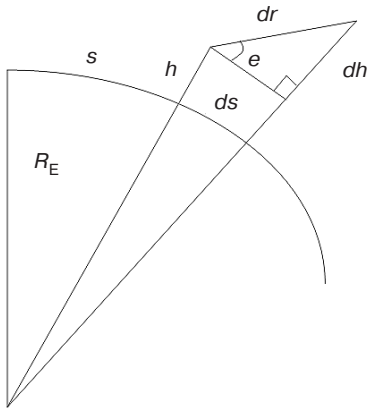

Fig. 2. Geometric representation of R_E, h, and s and their differentials

Assuming h is a function of r, refractive index n implicitly depends on r. Differentiating Eq. (15) with respect to r gives the following:

$$\frac{dn}{dh}\frac{dh}{dr}\left(R_\mathrm{E}+h\right)\sqrt{1-\left(\frac{dh}{dr}\right)^2} + n\frac{dh}{dr}\sqrt{1-\left(\frac{dh}{dr}\right)^2} + n\left(R_\mathrm{E}+1\right)\frac{-2\frac{dh}{dr}\frac{d^2h}{dr^2}}{2\sqrt{1-\left(\frac{dh}{dr}\right)^2}} = 0. \quad (16)$$

The equivalent system of two coupled equations of the first order is obtained after simple transformations and the introduction of the substitution $\frac{dh}{dr} = u$, as follows [18]:

$$\frac{dh}{dr} = u, \quad (17)$$

[5] Ehn J. *Propagation of Radio Waves in a Realistic Environment using a Parabolic Equation Approach*. PhD Thesis. 2019. https://urn.kb.se/resolve?urn=urn:nbn:se:liu:diva-157610. Accessed October 09, 2023.

$$\frac{du}{dr} = -u^2\left(\frac{1}{n}\frac{dn}{dh} + \frac{1}{R_E + h}\right) + \left(\frac{1}{n}\frac{dn}{dh} + \frac{1}{R_E + h}\right). \quad (18)$$

Equations (17) and (18) can be considered as an initial value problem:

$$u(r=0) = \left.\frac{dh}{dr}\right|_{r=0} = \sin e_0, \quad (19)$$

$$h(r=0) = h_0. \quad (20)$$

This ordinary differential equation uniquely solves the ray tracing problem.

Equations (17) and (18) are discretized and solved in iteration steps of Δr. The value of the iteration step from $(l-1)$ to l is determined as follows [18].

Step 1: Estimate the values $\frac{1}{n_{l-1}}$ and $\left.\frac{dn}{dh}\right|_{l-1}$ at height h_{l-1} using experimental data or approximations.

Step 2. Solve Eqs. (17) and (18) with the initial values u_{l-1} and h_{l-1} to obtain the values u_l and h_l.

Step 3. Calculate s_l, which is the propagation distance of the beam at the step l, as follows:

$$s_l = s_{l-1} + R_E \arcsin\left(\frac{\cos e_{l-1}\Delta r}{R_E + h_l}\right), \quad (21)$$

and the angle

$$e_l = \arcsin(u_{l-1}). \quad (22)$$

Steps 1–3 are repeated from $l = 1$ to $l = L$, which corresponds to the endpoint of the calculation of the beam propagation paths. The numerical differentiation in step 2 is carried out using the 4th order Runge–Kutta method. For the first iteration, $l = 1$, the initial values in step 2 are given by Eqs. (19) and (20). The refractive index and its derivative should be evaluated at the height h_0 where the transmitting antenna is located, giving the values $\frac{1}{n_0}$ and $\left.\frac{dn}{dh}\right|_0$, respectively. The distance from the transmitting point to the DAA is thus divided into L points. At each point of l iterations, s_l, e_l, n_l, and h_l are calculated for each beam.

SIMULATION

In the theoretical part of the paper, the methods for calculating the propagation of electromagnetic beams in the stratified atmosphere have been presented. The radio signals obtained in this way are combined in the opening of the DAA for subsequent spatial filtering, the scheme of which is shown in Fig. 3 [19].

Consider an antenna array consisting of K directional antenna elements (AEs). It receives D independent signals from different directions with azimuth θ_D and location angle ϕ_D as shown in Fig. 3. Here, $q_D(t)$ is the incident signal, while $v_K(t)$ is the received signal from the Kth AE at a discrete time t. In the following, the index "1" denotes the useful signal. Consequently, the DAA output signal matrix has the following form:

$$\vec{\mathbf{v}} = \mathbf{A}\vec{\mathbf{q}} + \vec{\mathbf{n}}, \quad (23)$$

where $\vec{\mathbf{n}}$ is the noise vector; $\mathbf{A}$ is the matrix of scan vectors $\vec{\mathbf{a}}(\theta, \phi)$ determining the array field amplitude-phase distribution.

Thus,

$$\mathbf{A} = \left[\vec{\mathbf{a}}(\theta_1, \phi_1)\ \ \vec{\mathbf{a}}(\theta_2, \phi_2) \cdots \vec{\mathbf{a}}(\theta_D, \phi_D)\right], \quad (24)$$

$$\vec{\mathbf{a}}(\theta, \phi) = \left[g_1(\theta, \phi)e^{j\mathbf{k}\mathbf{r}_1^T} \quad g_2(\theta, \phi)e^{j\mathbf{k}\mathbf{r}_2^T} \quad \ldots \quad g_K(\theta, \phi)e^{j\mathbf{k}\mathbf{r}_K^T}\right], \quad (25)$$

where $\mathbf{k} = \frac{2\pi}{\lambda}(k_x, k_y, k_z) = \frac{2\pi}{\lambda}(\sin\phi\cos\theta, \sin\phi\sin\theta, \cos\phi)$ is the wave vector; $\mathbf{r}_n^T = (x_n, y_n, z_n)^T$ is the radius

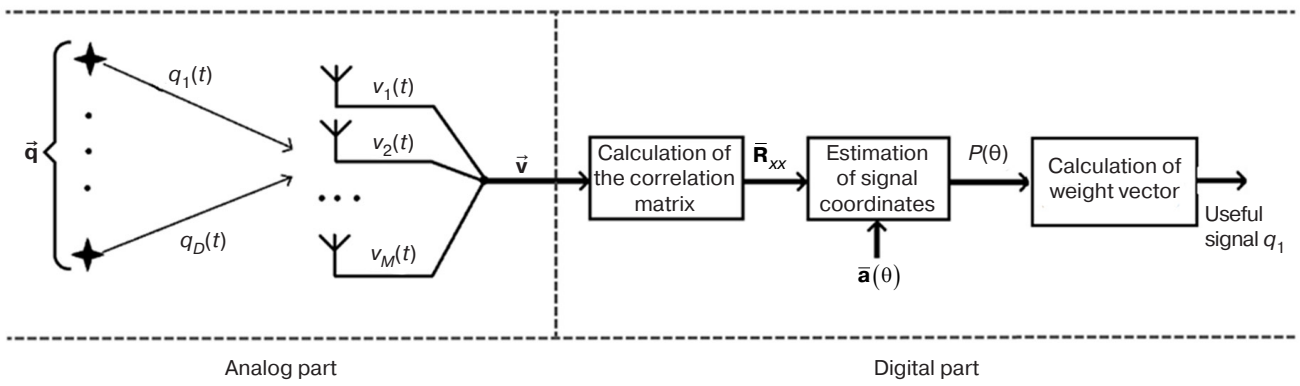

Fig. 3. Scheme of signal processing in DAA

vector to the nth AE; $g_n(\theta, \phi)$ is the array pattern of the nth AE.

The following equation determines the spatial correlation matrix of the signals:

$$\hat{\mathbf{R}} = \frac{1}{T}\sum_{t=1}^{T}\vec{\mathbf{v}}(t)^{\mathrm{H}}\vec{\mathbf{v}}(t), \quad (26)$$

where T is the number of samples of the digital signal, while the index H indicates the Hermite transpose of the vector $\vec{\mathbf{v}}(t)$.

The angular coordinates of the signals are then determined using the multiple signal classification (MUSIC) method[6], which is essentially structural and overcomes the Rayleigh criterion resolution. This means that its resolution is less than the main lobe width of the array pattern [20]:

$$P_{\mathrm{MU}}(\theta) = \frac{1}{\left|\vec{\mathbf{a}}^{\mathrm{H}}(\theta)\mathbf{E}_{\mathrm{noise}}\mathbf{E}_{\mathrm{noise}}^{\mathrm{H}}\vec{\mathbf{a}}(\theta)\right|}, \quad (27)$$

where $\mathbf{E}_{\mathrm{noise}}$ is the noise eigenvector.

The weighting factor vector for the formation of the DAA array pattern is calculated as follows [21]:

$$\vec{\mathbf{w}} = \frac{\mathbf{R}^{-1}\vec{\mathbf{a}}(\theta_1, \phi_1)}{\vec{\mathbf{a}}(\theta_1, \phi_1)^{\mathrm{H}}\mathbf{R}^{-1}\vec{\mathbf{a}}(\theta_1, \phi_1)}. \quad (28)$$

Thus, the DAA determines the spatial coordinates of the signal in accordance with Eqs. (26) and (27) to form the array pattern in the digital domain on the basis of the obtained vector $\vec{\mathbf{w}}$. Then the signal at the output is as follows:

$$q_1 = \vec{\mathbf{w}}\vec{\mathbf{v}}. \quad (29)$$

On the basis of simulation, a study was carried out to estimate the propagation range of telecommunication signals in the tropospheric layers. In all cases, the maximum range is chosen to be equal to 150 km with a resolution Δr equal to 500 m. Obviously, the tracking of all the rays from a transmitter arriving at the receiving DAA would require ray tracing over the full range of declination angles. However, the expression giving the limits of the declination angle within which radio wave propagation occurs in an airborne tropospheric waveguide is well known [22]:

$$\varphi_{\min,\max} = \pm\sqrt{2\left(\frac{1}{n(0)}\frac{dn}{dh} - \frac{1}{R_0}\right)(h_t - \delta)}, \quad (30)$$

[6] Multiple signal classification is an algorithm for estimating sinusoidal sum frequencies against noise from a series of measurements and for determining angular coordinates of multiple signal sources in digital antenna arrays.

where δ is the trapping layer thickness and h_t is the transmitting antenna height.

The generalized scheme of the simulation is shown in Fig. 4. In the experiments, the transmitter antenna is mounted at a height of 200 m under noise and multipath conditions. The signal used is a 1 Mbit/s binary phase-shift keyed signal. The transmitter power is 10 W, while the noise power in the ultrashort wavelength range is $1.7 \cdot 10^{-13}$ W [23]. The bit error rate is estimated as the ratio of the number of bits received in error to the total number of bits.

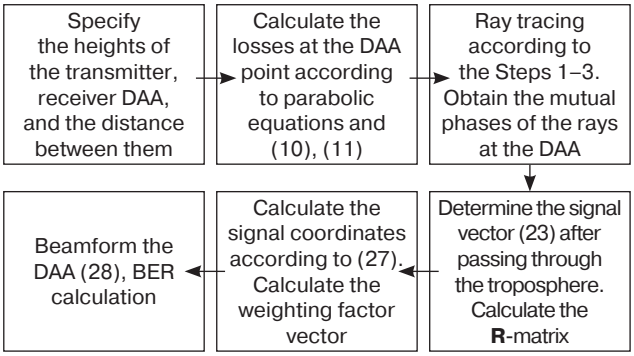

Fig. 4. Generalized scheme of simulation

Experiment 1: Idealized surface tropospheric waveguide

In this experiment, a surface waveguide is simulated. The modified refractive profile is shown in Fig. 5. It has a negative slope of −100 M-units km^{-1} in the height range from 0 to 350 m and a slope of 117 M-units km^{-1}.

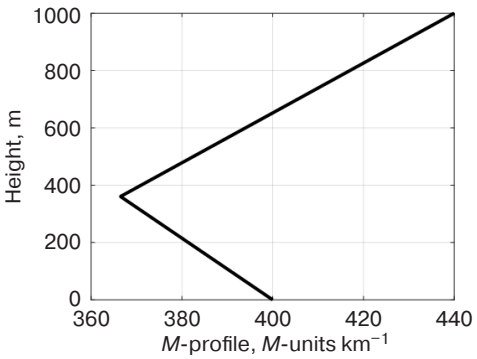

Fig. 5. Modified M-profile of the surface waveguide

The electromagnetic field distribution as a function of the distance from the transmitter and height above the Earth's surface is shown in Fig. 6. The calculation is made using the PU apparatus and the numerical Fourier splitting algorithm. The carrier frequency is 5 GHz, while the transmitter antenna is a half-wave dipole.

Figure 6 shows that the field distribution is not uniform.

The rays for the refractive profile considered are shown in Fig. 7.

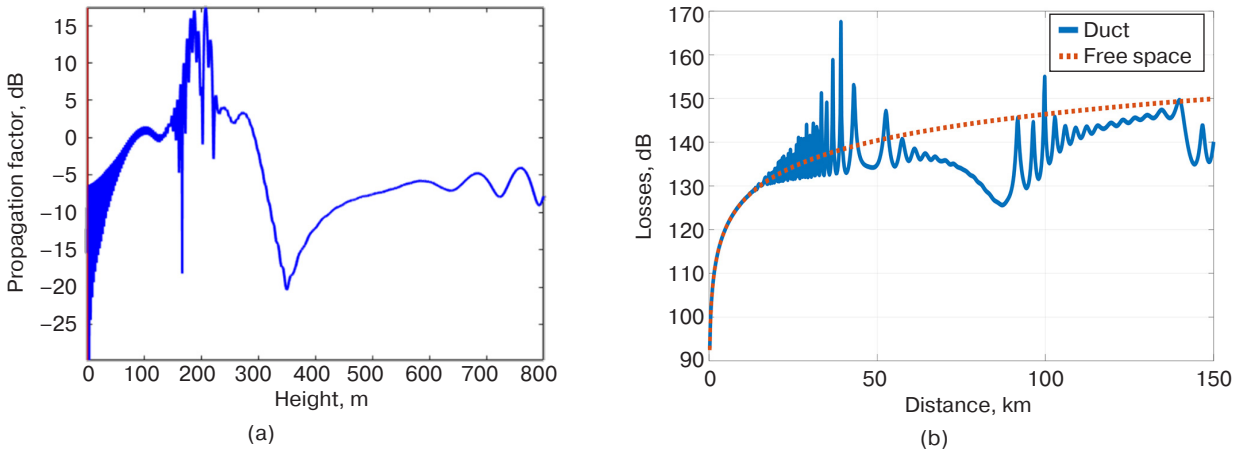

Fig. 6. Field distribution parameters:
(a) propagation factor for a vertical slice at a height of 25 km,
(b) losses in a horizontal slice at a height of 200 m (the solid blue line is in the atmosphere presented in Fig. 5; the dotted red line is in free space)

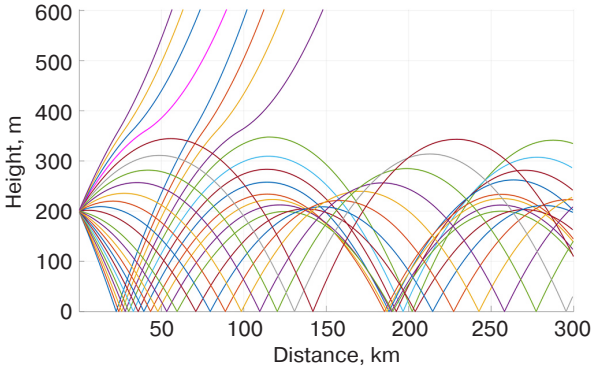

Fig. 7. Rays propagating in the lower layers of the tropospheric waveguide

It can be seen that the rays are reflected from the upper boundary of the trapping layer. They then reach the Earth's surface where they are reflected again. This process continues up to the receiver DAA, which is attenuated as shown in Fig. 6. One of these rays crossing the receiving DAA is shown in Fig. 8.

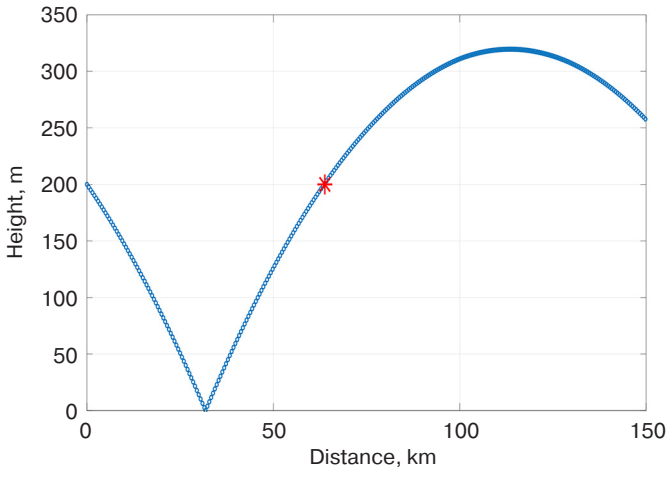

Fig. 8. Example of ray crossing (blue line) and DAA (red asterisk)

The graph showing the BER depending on the type of antenna array used and the distance over which reception could be achieved (50 to 100 km from the transmitter) is shown in Fig. 9. The radio signal attenuation is approximately −135 dB in this case. The circular and the hemispherical geometry of the receiving DAAs with directional AEs are used [23].

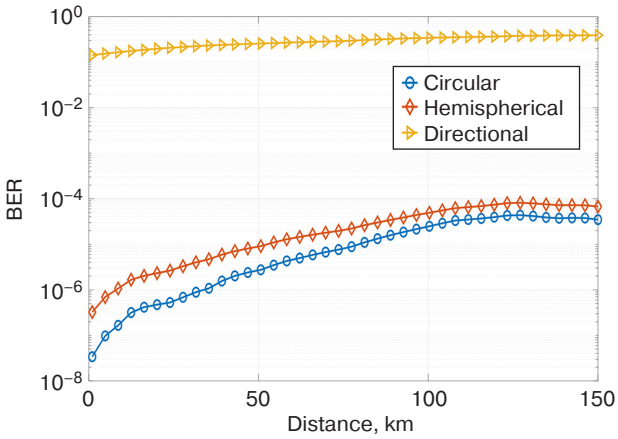

Fig. 9. BER vs distance

The graphs in Fig. 9 show that the circular DAA provides the lowest BER (up to 10^{-6}) at distances up to 50 km. If a hemispherical shape of the receiving DAA is used with a directional antenna, the BER value at this distance is about 10^{-5} and 0.3, respectively. This is in agreement with previous results [19]. In this case, the attenuation of the signal after passing through the atmosphere is about 135 dB as shown in Fig. 6; then, the ratio of the signal power to the noise power at the output of each receiving AE is 10 dB. Simultaneously, there is no obvious dependence of bit error on distance in Fig. 9 and beyond, especially from 15 km. This can be explained by the fact that, as can be seen from Eq. (11), the value of the power loss is linearly dependent on the

distance travelled by the radio wave, whereas the field strength is inversely proportional to $\sqrt{r}$.

Experiment 2: Idealized S-shaped tropospheric waveguide

Consider an idealized S-shaped channel surface characterized by the M and N profiles as shown in Fig. 10. The M profile starts with a slope of 117 M-units km^{-1} for the lowest 100 m and then changes to a slope of −100 M-units km^{-1} up to a height of 400 m, after which it returns to the value of 117 M-units km^{-1}.

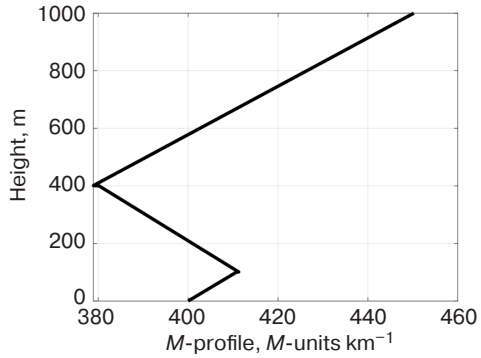

Fig. 10. Modified M-profile of atmospheric layers

The characteristics of the electromagnetic field distribution according to the profile of the modified refractive index shown in Fig. 10 are shown in Fig. 11.

It can be seen from Fig. 11a that the PF at the transmitter height of 200 m is 15 dB higher than that of the wave in free space. Loss values as a function of the distance between the transmitter and the receiving DAA are plotted in Fig. 11b. From this it can be concluded that the electromagnetic wave inside the tropospheric waveguide loses 15–20 dB less power than the radio signal in free space or outside the trapping layer.

The ray trajectories for the type of refractive index under consideration are shown in Fig. 12.

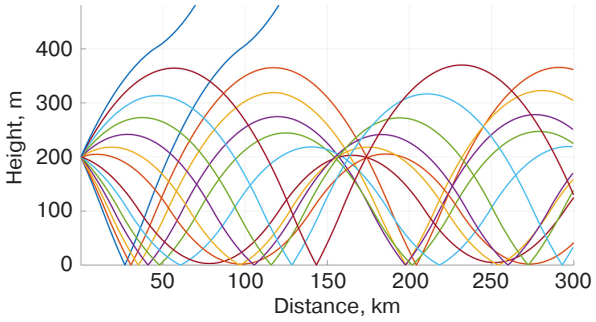

Fig. 12. Rays propagating in the lower layers of the tropospheric waveguide

It can be seen that the rays can be both reflected back from the Earth's surface and refracted at the lower and upper boundaries of the tropospheric layers.

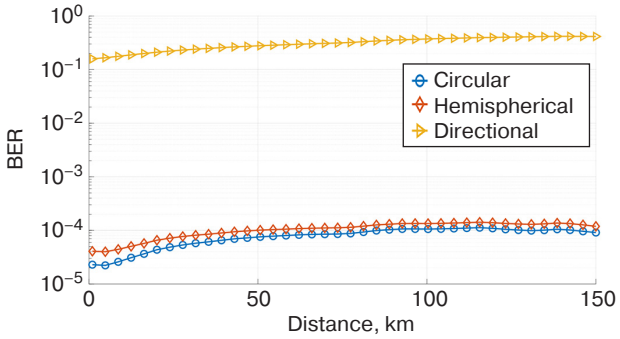

Fig. 13. BER vs distance

The circular DAA gives the lowest BER as shown in Fig. 13. From the analysis of Fig. 11–13, it can be concluded that radio signals at a frequency of 5 GHz can reach a receiver located more than 100 km from the transmitter with BER within 10^{-5}, which is acceptable for the majority of modern wireless telecommunications systems.

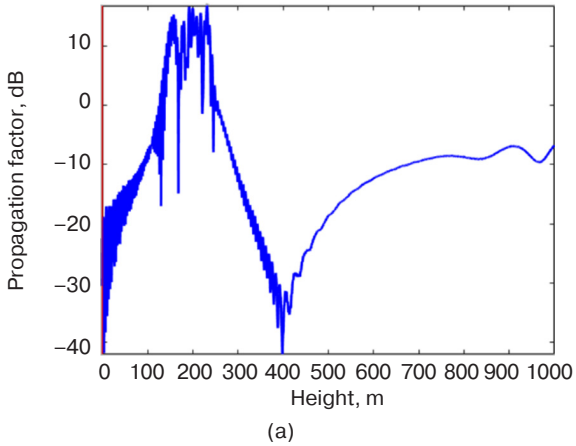

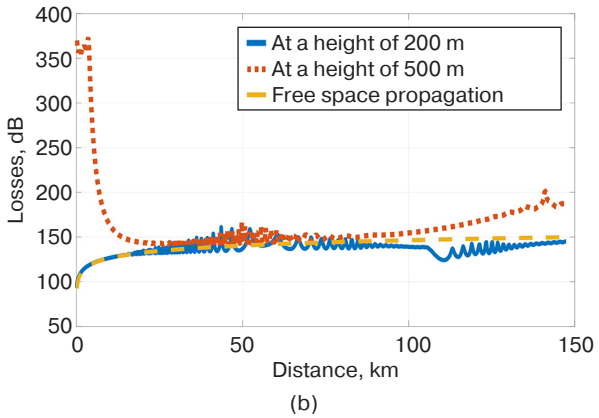

Fig. 11. Field distribution characteristics:
(a) propagation factor for the vertical slice at 110 km,
(b) losses for the horizontal slice

Experiment 3. Ideal elevated waveguide

Consider an ideal elevated waveguide, whose corresponding *M*-profile is shown in Fig. 14. The modified *M*-profile starts with a slope of 117 *M*-units km^{-1} for the first 250 m of height. It then changes to −100 *M*-units km^{-1} up to 400 m before returning to 117 *M*-units km^{-1}. Within the trapping layer, the antenna height is 300 m.

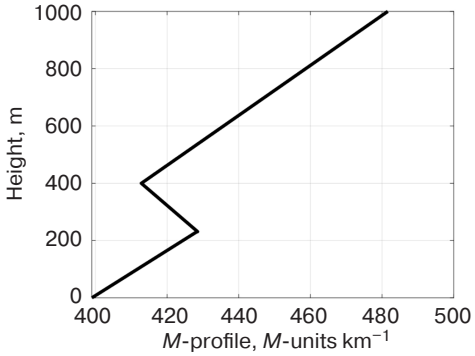

Fig. 14. Modified *M*-profile typical of an elevated waveguide

It can be seen from Fig. 14 that the waveguide in this case is elevated and does not touch the Earth's surface. Figure 15 depicts the distribution of the electromagnetic field as a function of the distance from the transmitter and the height above the Earth's surface.

As shown in Fig. 15a, the 5 GHz electromagnetic wave at a transmitting height of 300 m has a higher power compared to free rectilinear propagation. It is also clear from Fig. 15b that the advantage of propagation inside the tropospheric waveguide becomes apparent at distances above 100 km, where the loss is 20 dB less than in free space.

Typical ray trajectories for an elevated waveguide are shown in Fig. 16.

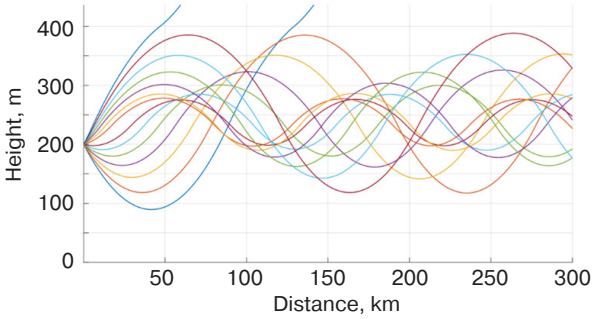

Fig. 16. Rays propagating in the lower layers of a tropospheric waveguide

In this case, it is clear that the rays, which are only refracted at the upper and lower limits of the refractive index variation, do not reach the Earth's surface.

The graphs of BER versus distance between transmitter and DAA inside the waveguide, also at 300 m height, are shown in Fig. 17.

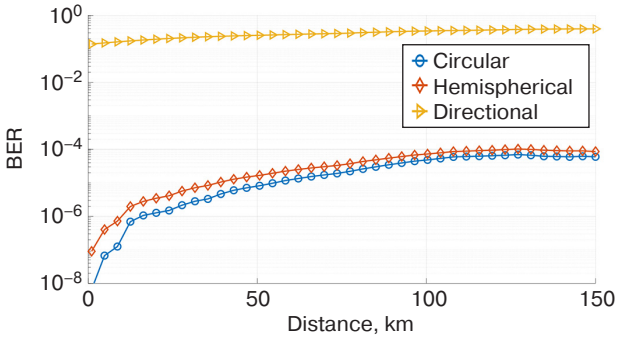

Fig. 17. BER vs distance

The graphs in Fig. 17 show that the circular DAA gives the lowest BER (10^{-6}) compared to the hemispherical geometry and simple directional antenna up to 50 km, where the BER is 10^{-5} and 0.3, respectively. This geometry offers the advantage that

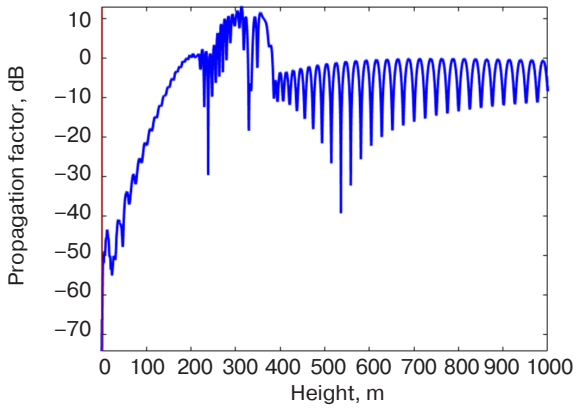

(a)

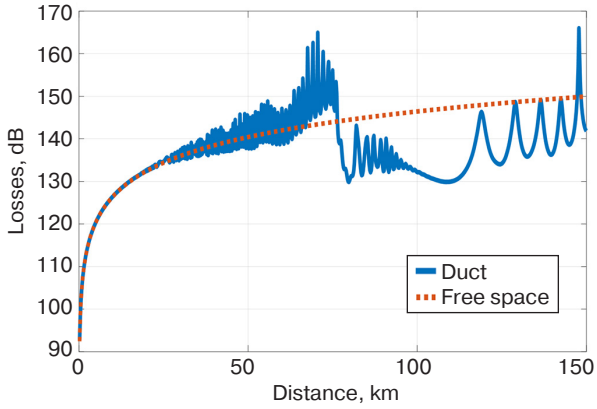

(b)

Fig. 15. Field distribution parameters:
(a) propagation factor for a vertical slice at 80 km,
(b) losses in a horizontal slice at a height of 50 m (the solid blue line is in the atmosphere shown in Fig. 2; the dotted red line is in free space)

the electromagnetic rays reaching the array inside the tropospheric waveguide have negligible declination angles, most of them being $\varphi \approx 90°$.

CONCLUSIONS

When a modified refractive index changes from a maximum near the Earth's surface to a minimum at a certain altitude, a tropospheric waveguide manifests in the lower atmosphere. In this case, the electromagnetic radiation in the ultrashort centimeter-wave range (5 GHz) from the transmitter does not propagate in a straight line, but instead propagates by reflection from the Earth (or the lower trapping layer) and refraction from the upper trapping layer. Stable receiving distances are limited to several hundred kilometers, resulting in significant attenuation. In addition, a number of rays with different amplitudes and phases may be present at the receiving point, resulting in multipath propagation. In order to overcome such difficulties, the use of antenna arrays with digital formation of the array pattern on the receiver side is proposed.

The presented approaches for correctly modelling signal propagation in the tropospheric waveguide and DAA include the calculation of propagation paths and losses taking into account distance, refractive index, antenna height, and carrier frequency. The rays appearing in the opening of the DAA antenna are obtained. In the final stage, the BER is estimated by evaluating the angular coordinates of the rays and the digital beamforming procedure.

When combined with digital spatial processing, a circular antenna array shape is shown to be optimal.

ACKNOWLEDGMENTS

The study was supported by the Russian Science Foundation, project No. 23-21-00125, https://rscf.ru/project/23-21-00125/.

Authors' contributions

I.W. Peshkov—setting the goals and objectives of the study, development of processing methods, conducting research.

D.N. Borisov—research planning, scientific editing of the article, interpretation and generalization of the results.

REFERENCES

1. Schelleng J.C., Burrows C.R., Ferell E.B. Ultra-shortwave propagation. In: *Proceedings of the Institute of Radio Engineers* (*Proc. I.R.E.*). 1933;21(3):427–463. https://doi.org/10.1109/JRPROC.1933.227639
2. Anderson K. Radar measurements at 16.5 GHz in the oceanic evaporation duct. *IEEE Trans. Antennas Propag.* 1989;37(1):100–106. https://doi.org/10.1109/8.192171
3. Ivanov V.K., Shalyapin V.N., Levadny Y.V. Microwave scattering by tropospheric fluctuations in an evaporation duct. *Radiophys. Quantum. El.* 2009;52(4):277–286. https://doi.org/10.1007/s11141-009-9133-z
[Original Russian Text: Ivanov V.K., Shalyapin V.N., Levadny Y.V. Microwave scattering by tropospheric fluctuations in an evaporation duct. *Izvestiya Vysshikh Uchebnykh Zavedenii. Radiofizika.* 2009;52(4):307–317 (in Russ.).]
4. Dinc E., Akan O.B. Beyond-line-of-sight communications with ducting layer. *IEEE Commun. Mag*. 2014;52(10):37–43. https://doi.org/10.1109/MCOM.2014.6917399
5. Ma J., Wang J., Yang C. Long-Range Microwave Links Guided by Evaporation Ducts. *IEEE Commun. Mag.* 2022;60(5):68–72. https://doi.org/10.1109/MCOM.002.00508
6. Woods G.S., Ruxton A., Huddlestone-Holmes C., Gigan G. High-Capacity, Long-Range, Over Ocean Microwave Link Using the Evaporation Duct. *IEEE J. Oceanic Eng*. 2009;34(3):323–330. https://doi.org/10.1109/JOE.2009.2020851
7. Mentes Ş., Kaymaz Z. Investigation of Surface Duct Conditions over Istanbul, Turkey. *J. Appl. Meteor. Climatol*. 2007;46(3):318–337. https://doi.org/10.1175/JAM2452.1
8. Pishchin O.N., Kalambatskaya O.V. Characteristics of UHF waves distribution in land and water surface tropospheric waveguide. *Vestnik Astrakhanskogo gosudarstvennogo tekhnicheskogo universiteta. Seriya: Upravlenie, vychislitel'naya tekhnika i informatika = Vestnik of Astrakhan State Technical University. Series: Management, Computer Science and Informatics.* 2019;4:115–121 (in Russ.). https://doi.org/10.24143/2072-9502-2019-4-115-121
9. Pishchin O.N. The analysis and experimental researches of attenuation of a radio signal of systems of a cellular mobile radio communication above a water smooth surface. *Izvestiya Yuzhnogo federal'nogo universiteta. Seriya: Tekhnicheskie nauki* (*Izvestiya YuFU. Seriya: tekhnicheskie nauki*) = *Izvestiya SFedU. Engineering Sciences*. 2009;1:43–49 (in Russ.).
10. Hartree D.R., Michel J.G.L., Nicolson P. Practical methods for the solution of the equations of tropospheric refraction. In: *Meteorological Factors in Radio-Wave Propagation. Report of a Conference. The Physical Society and The Royal Meteorological Society*. 1947. P. 127–168.
11. Dedov N.M., Tolstykh V.D., Serebryakov M.A. The influence of tropospheric ducts on the radar operation over the sea surface. In: *Actual Problems of the Activities of Departments of the Penal System: Collection of Materials of the All-Russian Scientific and Practical Conference*: in 2 v. Voronezh; 2020. P. 128–132 (in Russ.). https://www.elibrary.ru/nptlot
12. Leontovich M.A., Fok V.A. Solution of propagation of electromagnetic waves along the Earth's surface by the method of parabolic equations. *J. Phys. USSR.* 1946;10(1):13–23.

13. Akhiyarov V.V. Attenuation factor calculation for backscattering from the terrain using the parabolic equation technique. *Zhurnal radioelektroniki = J. Radio Electronics*. 2019;11 (in Russ.). https://doi.org/10.30898/1684-1719.2019.11.1
14. Zhang P., Lu Bai, Wu Z., Guo L. Applying the parabolic equation to tropospheric groundwave propagation: A review of recent achievements and significant milestones. *IEEE Trans. Antennas Propag. Mag*. 2016;58(3):31–44. https://doi.org/10.1109/MAP.2016.2541620
15. Levy M. *Parabolic Equation Methods for Electromagnetic Wave Propagation*. London: IET; 2000. 336 p.
16. Ozlem O., Gokhan A., Mustafa K., Levent S. PETOOL: MATLAB-based one-way and two-way split-step parabolic equation tool for radiowave propagation over variable terrain. *Computer Phys. Commun*. 2011;182(12):2638–2654. https://doi.org/10.1016/j.cpc.2011.07.017
17. Sirkova I. Propagation Factor and Path Loss Simulation Results for Two Rough Surface Reflection Coefficients Applied to the Microwave Ducting Propagation Over the Sea. *Progress In Electromagnetics Research M.* (*PIERM*). 2011;17:151–166. http://doi.org/10.2528/PIERM11020602
18. Zeng Y., Blahak U., Neuper M., Jerger D. Radar Beam Tracing Methods Based on Atmospheric Refractive Index. *J. Atmos. Oceanic Technol*. 2014;31(12):2650–2670. https://doi.org/10.1175/JTECH-D-13-00152.1
19. Nechaev Y.B., Peshkov I.V. Study of digital diagram formation for optimum interference and noise reduction in antenna arrays of different shapes with directional radiators. *Fizika volnovykh protsessov i radiotekhnicheskie sistemy = Physics of Wave Processes and Radio Systems*. 2022;25(2):73–82 (in Russ.). https://doi.org/10.18469/1810-3189.2022.25.2.73-82
20. Schmidt R.O Multiple Emitter Location and Signal Parameter Estimation. *IEEE Trans. Antennas Propag*. 1986;AP-34(3):276–280. https://doi.org/10.1109/TAP.1986.1143830
21. Balanis C., Ioannides P. *Introduction to Smart Antennas*. San Rafael: Morgan & Claypool Publishers; 2007. 174 p.
22. Dinc E., Akan O.B. Channel Model for the Surface Ducts: Large-Scale Path-Loss, Delay Spread, and AOA. *IEEE Trans. Antennas and Propag.* 2015;63(6):2728–2738. http://doi.org/10.1109/TAP.2015.2418788
23. Nechaev Y.B., Peshkov I.W. Simulation of Digital and Analog Spatial Filtering of VHF Signals in Channel with Losses due to Multipple Diffraction. In: *2022 Systems of Signals Generating and Processing in the Field of on Board Communications*. 2022. https://doi.org/10.1109/IEEECONF53456.2022.9744371

СПИСОК ЛИТЕРАТУРЫ

1. Schelleng J.C., Burrows C.R., Ferell E.B. Ultra-shortwave propagation. In: *Proceedings of the Institute of Radio Engineers* (*Proc. I.R.E.*). 1933;21(3):427–463. https://doi.org/10.1109/JRPROC.1933.227639
2. Anderson K. Radar measurements at 16.5 GHz in the oceanic evaporation duct. *IEEE Trans. Antennas Propag.* 1989;37(1):100–106. https://doi.org/10.1109/8.192171
3. Иванов В.К., Шаляпин В.Н., Левадный Ю.В. Рассеяние ультракоротких радиоволн на тропосферных флуктуациях в приводном волноводе. *Известия вузов. Радиофизика.* 2009;52(4):307–317.
4. Dinc E., Akan O.B. Beyond-line-of-sight communications with ducting layer. *IEEE Commun. Mag*. 2014;52(10):37–43. https://doi.org/10.1109/MCOM.2014.6917399
5. Ma J., Wang J., Yang C. Long-Range Microwave Links Guided by Evaporation Ducts. *IEEE Commun. Mag.* 2022;60(5):68–72. https://doi.org/10.1109/MCOM.002.00508
6. Woods G.S., Ruxton A., Huddlestone-Holmes C., Gigan G. High-Capacity, Long-Range, Over Ocean Microwave Link Using the Evaporation Duct. *IEEE J. Oceanic Eng*. 2009;34(3):323–330. https://doi.org/10.1109/JOE.2009.2020851
7. Mentes Ş., Kaymaz Z. Investigation of Surface Duct Conditions over Istanbul, Turkey. *J. Appl. Meteor. Climatol*. 2007;46(3):318–337. https://doi.org/10.1175/JAM2452.1
8. Пищин О.Н., Каламбацкая О.В. Особенности распространения радиоволн УВЧ диапазона в приземном и приводном тропосферном волноводе. *Вестник Астраханского государственного технического университета. Серия: Управление, вычислительная техника и информатика*. 2019;4:115–121. https://doi.org/10.24143/2072-9502-2019-4-115-121
9. Пищин О.Н. Анализ и экспериментальные исследования затухания радиосигнала систем сотовой подвижной радиосвязи над водной гладью. *Известия ЮФУ. Серия: Технические науки*. 2009;1:43–49.
10. Hartree D.R., Michel J.G.L., Nicolson P. Practical methods for the solution of the equations of tropospheric refraction. In: *Meteorological Factors in Radio-Wave Propagation. Report of a Conference. The Physical Society and The Royal Meteorological Society*. 1947. P. 127–168.
11. Дедов Н.М., Толстых В.Д., Серебряков М.А. Влияние тропосферных волноводов на работу радиолокатора над морской поверхностью. В сб.: *Актуальные проблемы деятельности подразделений уголовно-исполнительной системы:* Сборник материалов Всероссийской научно-практической конференции в 2-х т. Воронеж; 2020. Т. 1. С. 128–132. https://www.elibrary.ru/nptlot
12. Leontovich M.A., Fok V.A. Solution of propagation of electromagnetic waves along the Earth's surface by the method of parabolic equations. *J. Phys. USSR.* 1946;10(1):13–23.
13. Ахияров В.В. Вычисление множителя ослабления при обратном рассеянии от земной поверхности методом параболического уравнения. *Журнал радиоэлектроники*. 2019;11. https://doi.org/10.30898/1684-1719.2019.11.1
14. Zhang P., Lu Bai, Wu Z., Guo L. Applying the parabolic equation to tropospheric groundwave propagation: A review of recent achievements and significant milestones. *IEEE Trans. Antennas Propag. Mag*. 2016;58(3):31–44. https://doi.org/10.1109/MAP.2016.2541620

15. Levy M. *Parabolic Equation Methods for Electromagnetic Wave Propagation*. London: IET; 2000. 336 p.
16. Ozlem O., Gokhan A., Mustafa K., Levent S. PETOOL: MATLAB-based one-way and two-way split-step parabolic equation tool for radiowave propagation over variable terrain. *Computer Phys. Commun*. 2011;182(12):2638–2654. https://doi.org/10.1016/j.cpc.2011.07.017
17. Sirkova I. Propagation Factor and Path Loss Simulation Results for Two Rough Surface Reflection Coefficients Applied to the Microwave Ducting Propagation Over the Sea. *Progress In Electromagnetics Research M.* (*PIERM*). 2011;17:151–166. http://doi.org/10.2528/PIERM11020602
18. Zeng Y., Blahak U., Neuper M., Jerger D. Radar Beam Tracing Methods Based on Atmospheric Refractive Index. *J. Atmos. Oceanic Technol*. 2014;31(12):2650–2670. https://doi.org/10.1175/JTECH-D-13-00152.1
19. Нечаев Ю.Б., Пешков И.В. Исследование цифрового диаграммообразования для оптимального помехо- и шумоподавления в антенных решетках различной формы с направленными излучателями. *Физика волновых процессов и радиотехнические системы*. 2022;25(2):73–82. https://doi.org/10.18469/1810-3189.2022.25.2.73-82
20. Schmidt R.O Multiple Emitter Location and Signal Parameter Estimation. *IEEE Trans. Antennas Propag*. 1986;AP-34(3): 276–280. https://doi.org/10.1109/TAP.1986.1143830
21. Balanis C., Ioannides P. *Introduction to Smart Antennas*. San Rafael: Morgan & Claypool Publishers; 2007. 174 p.
22. Dinc E., Akan O.B. Channel Model for the Surface Ducts: Large-Scale Path-Loss, Delay Spread, and AOA. *IEEE Trans. Antennas and Propag.* 2015;63(6):2728–2738. http://doi.org/10.1109/TAP.2015.2418788
23. Nechaev Y.B., Peshkov I.W. Simulation of Digital and Analog Spatial Filtering of VHF Signals in Channel with Losses due to Multipple Diffraction. In: *2022 Systems of Signals Generating and Processing in the Field of on Board Communications*. 2022. https://doi.org/10.1109/IEEECONF53456.2022.9744371

About the authors

Ilia W. Peshkov, Cand. Sci. (Phys.–Math.), Associate Professor, Department of Physics, Radio Engineering and Electronics, Bunin Yelets State University (28, Kommunarov ul., Yelets, 399770 Russia). E-mail: ilvpeshkov@gmail.com. Scopus Author ID 7003332128, ResearcherID L-6734-2013, RSCI SPIN-code 8009-4805, https://orcid.org/0000-0001-8370-6954

Dmitry N. Borisov, Cand. Sci. (Eng.), Associate Professor, Head of the Department of Information systems, Voronezh State University (1, Universitetskaya pl., Voronezh, 394018 Russia). E-mail: borisov@sc.vsu.ru. Scopus Author ID 54901090900, ResearcherID J-5289-2014, RSCI SPIN-code 6556-0285, https://orcid.org/0000-0002-1265-7195

Об авторах

Пешков Илья Владимирович, к.ф.-м.н., доцент, кафедра физики, радиотехники и электроники, ФГБОУ ВО «Елецкий государственный университет им. И.А. Бунина» (399770, Россия, Елец, ул. Коммунаров, д. 28). E-mail: ilvpeshkov@gmail.com. Scopus Author ID 7003332128, ResearcherID L-6734-2013, SPIN-код РИНЦ 8009-4805, https://orcid.org/0000-0001-8370-6954

Борисов Дмитрий Николаевич, к.т.н. доцент, заведующий кафедрой информационных систем, ФГБОУ ВО «Воронежский государственный университет» (394018, Россия, Воронеж, Университетская пл., д. 1). E-mail: borisov@sc.vsu.ru. Scopus Author ID 54901090900, ResearcherID J-5289-2014, SPIN-код РИНЦ 6556-0285, https://orcid.org/0000-0002-1265-7195

Translated from Russian into English by K. Nazarov
Edited for English language and spelling by Thomas A. Beavitt

Modern radio engineering and telecommunication systems

Современные радиотехнические и телекоммуникационные системы

UDC 621.314.6; 621.373.5
https://doi.org/10.32362/2500-316X-2025-13-1-103-114
EDN UORVPM

RESEARCH ARTICLE

Resonant power supply for high-power microwave devices

Damir R. Hafizov [1, 2, @], Ilya N. Lobov [1], Leonid Y. Fetisov [2]

[1] *NPO "Almaz", Moscow, 125190 Russia*
[2] *MIREA – Russian Technological University, Moscow, 119454 Russia*
[@] *Corresponding author, e-mail: hafizov98@yandex.ru*

Abstract

Objectives. The ever-increasing demands on the technical parameters of microwave radio transmission devices necessitate a search for ways of improving their efficiency and reliability, as well as means for reducing their weight and size parameters. Since such requirements largely relate to secondary power supplies, the present work set out to develop secondary power supplies for the cathode heating and bias circuits of a floating-drift multibeam klystron capable of operating at a high potential of the klystron cathode and providing stable voltage in all operating modes.

Methods. In order to calculate the parameters of the resonant circuit, the first harmonic approximation method is used.

Results. Approaches for designing secondary supplies are described along with the method for developing the cathode heating and bias supplies for a floating-drift multipath klystron. The calculation method used for testing the design of the transformer windings is presented. The design avoids the use of chokes as separate elements by integrating them inside a magnetic system and providing isolation by high potential of the secondary winding. The results of testing the power supply using complex test bench waveforms are given along with the main obtained parameters. The operation of the power supply is demonstrated in switching mode at zero voltage for the minimum, nominal, and maximum input voltages in the range of the inductive resistance of the circuit when the voltage phase precedes the current phase.

Conclusions. The calculated efficiencies of the presented cathode heating and bias supplies are 85% and 92%, respectively. The developed supplies, which have smaller dimensions than their transformer analogues, allow a stable output voltage to be maintained when the input voltage varies, while the use of the soft start method allows the life of the klystron to be extended.

Keywords: voltage converter, resonant converter, power supply of microwave devices, pulse transformer, klystron

• **Submitted:** 11.02.2024 • **Revised:** 14.06.2024 • **Accepted:** 11.12.2024

For citation: Hafizov D.R., Lobov I.N., Fetisov L.Y. Resonant power supply for high-power microwave devices. *Russian Technological Journal.* 2025;13(1):103–114. https://doi.org/10.32362/2500-316X-2025-13-1-103-114, https://elibrary.ru/UORVPM

Financial disclosure: The authors have no financial or proprietary interest in any material or method mentioned.

The authors declare no conflicts of interest.

НАУЧНАЯ СТАТЬЯ

Резонансный источник электропитания для мощных сверхвысокочастотных устройств

Д.Р. Хафизов [1, 2, @],
И.Н. Лобов [1],
Л.Ю. Фетисов [2]

[1] *НПО «Алмаз», Москва, 125190 Россия*
[2] *МИРЭА – Российский технологический университет, Москва, 119454 Россия*
[@] *Автор для переписки, e-mail: hafizov98@yandex.ru*

Резюме

Цели. Постоянно растущие требования к техническим параметрам радиопередающих сверхвысокочастотных (СВЧ) устройств вызывают необходимость искать способы повышения их эффективности и надежности, а также уменьшения массогабаритных показателей. Эти требования в значительной мере касаются источников вторичного электропитания. Целью данной работы является разработка источников вторичного электропитания цепей накала и смещения для пролетного многолучевого клистрона, способных работать под высоким потенциалом катода клистрона и обеспечивать стабильное напряжение во всех рабочих режимах.

Методы. Для расчета параметров резонансного контура использован метод аппроксимации первой гармоники.

Результаты. Описан метод разработки источников вторичного электропитания, разработаны источники питания накала и смещения для пролетного многолучевого клистрона. Представлен метод расчета и апробирована конструкция обмоток трансформатора, позволяющие отказаться от использования дросселей как отдельных элементов путем их интеграции внутри одной магнитной системы и обеспечить развязку по высокому потенциалу вторичной обмотки. Проведены испытания источника питания в составе комплексного испытательного моделирующего стенда, получены осциллограммы основных параметров. Показана работа источника питания в режиме переключения при нулевом напряжении для минимального, номинального и максимального входного напряжения в области с индуктивным сопротивлением контура, когда фаза напряжения опережает фазу тока.

Выводы. Коэффициенты полезного действия источников накала и смещения составили 85% и 92% соответственно. Разработанные источники имеют меньшие габариты по сравнению с трансформаторными аналогами и позволяют поддерживать стабильное выходное напряжение при изменении входного напряжения, а использование метода плавного пуска позволит продлить срок службы клистрона.

Ключевые слова: преобразователь напряжения, резонансный преобразователь, электропитание СВЧ-устройств, импульсный трансформатор, клистрон

• **Поступила:** 11.02.2024 • **Доработана:** 14.06.2024 • **Принята к опубликованию:** 11.12.2024

Для цитирования: Хафизов Д.Р., Лобов И.Н., Фетисов Л.Ю. Резонансный источник электропитания для мощных сверхвысокочастотных устройств. *Russian Technological Journal.* 2025;13(1):103–114. https://doi.org/10.32362/2500-316X-2025-13-1-103-114, https://elibrary.ru/UORVPM

Прозрачность финансовой деятельности: Авторы не имеют финансовой заинтересованности в представленных материалах или методах.

Авторы заявляют об отсутствии конфликта интересов.

INTRODUCTION

Klystrons and travelling wave tubes are powerful amplifying microwave radio transmission devices that convert electron flux into microwave oscillation energy [1]. These devices are used as output power amplifiers in radio transmitting equipment [2–4]. The ever-increasing requirements for the specifications of microwave radio transmission devices necessitate the search for ways to improve their efficiency and reliability, as well as to reduce their weight and size parameters. These requirements are largely related to the secondary power supplies.

Today, power supplies for microwave equipment use network transformers operating at frequencies of 50 and 400 Hz. The major disadvantage of such power supplies is their large overall size, as determined by the size and weight of the power transformer, filter, and voltage stabilizer components. Voltage stabilizers are used to maintain high stability of the output voltage in the secondary circuit with some reduction in the efficiency of the source.

The most commonly used devices are pulsed power supplies in which voltage stabilization is provided by the control circuit to regulate the power transfer to the transformer on the primary side. The use of high frequency pulse transformers, which can operate at frequencies above 10^5 Hz, allows the overall size of the device to be reduced; as compared to a mains transformer having the same total transformer core power, the weight and size of a pulse transformer is significantly less.

Pulse-width modulation (PWM) converters are used as the basis for switching power supplies that convert the rectified mains voltage into a square-wave pulse voltage allowing the output voltage to be regulated by changing the duration of the pulses. PWM converters are characterized by abrupt changes in current and voltage, which cause high switching losses and limit the upper operating frequency of the converter. On the other hand, large rates of change in current and voltage cause electromagnetic interference in a wide range of the spectrum, thus precluding the use of pulse power supplies for high power microwave devices [5].

The aim of the present work is to develop secondary power supplies for the cathode heating and bias circuits of a floating-drift multibeam klystron capable of operating at high klystron cathode potentials of about 25 kV.

RESONANT POWER SUPPLIES

A resonant converter power supply, whose output voltage is almost sinusoidal due to the use of an LC circuit in the converter, avoids the disadvantages described above by reducing the noise level in comparison with PWM converters [5, 6]. At the same time, the use of resonant circuits makes it possible to implement the zero-voltage method for switching transistors when the in-phase circuit current lags behind the voltage to significantly reduce switching losses [7]. While resonant converters have various topologies, they are all based on a similar operating principle [8].

A series-parallel LLC converter is described in [9]. The series-parallel resonant converter is a preferred topology in the design of high voltage power supplies due to its ability to smoothly switch over a wide range of operating frequencies [10]. The circuit diagram of a half-bridge resonant LLC converter is shown in Fig. 1.

The circuit contains the input voltage source V_{in}, transistors VT1 and VT2 connected by a half-bridge circuit, resonant capacitor C_r, series inductor L_r, transformer T with ratio n and shunt parallel inductor L_{sh}. In practice, the parallel inductance can be eliminated from the circuit as a separate physical element. This can be achieved by using the intrinsic magnetizing inductance L_m of the transformer, whose value is achieved by introducing an air gap in the transformer core as discussed later. The secondary voltage is rectified by diodes VD1 and VD2 and then fed to a capacitive smoothing filter formed by capacitor C1 and resistor R1 as an equivalent output load. For high secondary current values, synchronous rectifiers with field MOSFETs[1] are used as voltage rectifiers. Due to the low resistance of the drain-to-source channel, these rectifiers are more efficient than diodes [11]. The soft-start method is used to limit the inrush current at switch-on [12, 13].

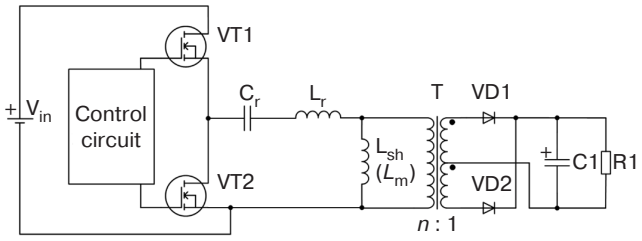

Fig. 1. Circuit diagram of a resonant half-bridge LLC converter. Here and in the following figures, the designations of the circuit elements correspond to those adopted in GOST 2.710-81[2]

In the resonant circuit, the current lags behind the voltage. This allows transistors to switch at zero voltage while current flows through the antiparallel diode of the transistor [14]. The sinusoidal voltage is applied to the load via the transformer. The output voltage is adjusted by changing the operating frequency of the transistors,

[1] Metal–oxide–semiconductor.

[2] GOST 2.710-81. Interstate Standard. *Unified system for design documentation. Alpha-numerical designations in electrical diagrams*. Moscow: Izd. Standartov; 1985 (in Russ.).

thus changing the operating mode of the converter. Due to the presence of both series and parallel components, the converter has a lower and an upper resonant frequency [15]. The lower frequency is determined by the elements L_r and C_r together with the value L_m, while the upper frequency is due to the elements L_r and C_r.

RESONANT CIRCUIT CALCULATION

The cathode heating power supply parameters are calculated using the first harmonic approximation method [16]. The power supply is fed from the 220 V ± 10% mains at a frequency of 400 Hz. The output voltage of the source is (13 ± 0.5) V, while the nominal current is 12 A, and the maximum current does not exceed 15 A. The transformation ratio n at the nominal input voltage is determined when the transfer coefficient M of the circuit is equal to one.

$$n = M\frac{V_{in}/2}{V_{out}} = 12, \quad (1)$$

where nominal input voltage V_{in} = 311 V and output voltage V_{out} = 13 V.

The equivalent alternating current resistance R_{ac} is defined in the following way:

$$R_{ac} = \frac{8n^2V_{out}}{\pi^2 I_{out}} = 126 \text{ Ohm}. \quad (2)$$

The following expressions are used to determine the maximum and minimum values of the transmission coefficients:

$$M_{min} = \frac{nV_{out\_min}}{V_{in\_max}/2} = 0.87, \quad (3)$$

$$M_{max} = \frac{nV_{out\_max}}{V_{in\_min}/2} = 1.15, \quad (4)$$

where V_{out_min} = 12.5 V, V_{out_max} = 13.5 V, V_{in_min} = 279 V, V_{in_max} = 341 V.

The resonant frequency of the circuit is determined by the following equation:

$$f_r = \frac{1}{2\pi\sqrt{L_rC_r}}. \quad (5)$$

The operating frequency of the power supply which is chosen on the basis of the specifications for the design of the source for the radar station, must not exceed 100 kHz.

The resonance frequency value is chosen such that the resonance capacitor capacitance is equal to or a multiple of the standard value, e.g., E24 series. The resonance frequency chosen is f_r = 80 kHz.

The following equation determines the capacitance value of capacitor C_r:

$$C_r = \frac{1}{2\pi QfR_{ac}} = 22 \text{ nF}, \quad (6)$$

where the quality factor (Q factor) of the circuit is Q = 0.7, while the switching frequency is f = 80 kHz.

The Q value is selected on the basis of the maximum and minimum transmission coefficient. This is done by plotting several transmission characteristics with different Q values on the same graph. On this graph, horizontal lines are drawn corresponding to the maximum M_{max} and minimum M_{min} transmission coefficients. The transmission coefficient curve is selected from those plotted that intersects both horizontal lines in the selected frequency range is selected.

High Q values reduce the peak transmission coefficient. However, a reserve of approximately 15% of the peak transmission coefficient is required to ensure zero voltage switching over the entire operating frequency range. The optimum value is therefore Q = 0.7.

The inductance L_r is calculated using the following equation:

$$L_r = \frac{1}{(2\pi f)^2 C_r} = 181 \text{ μH}. \quad (7)$$

To simplify inductance calculations, L_m and L_r are combined into a total inductance parameter. Total inductance is defined as follows:

$$L_n = \frac{L_m}{L_r}. \quad (8)$$

The L_n value is selected by plotting the circuit transfer coefficient curves for different L_n values. As L_n decreases, the peak transfer coefficient increases along with a decrease in the magnetizing inductance and increase in the magnetizing current; therefore, the optimum value of L_n = 3...7. In the calculations, the value L_n = 3 and the value of the magnetizing inductance L_m = 543 μH are used.

The following expression can be used to analyze changes in the transfer characteristic when the resonant circuit parameters are changed:

$$M = \left| \frac{L_n f_n^2}{[(L_n + 1) f_n^2 - 1] + j[(f_n^2 - 1) f_n Q L_n]} \right|, \quad (9)$$

where f_n is the ratio of switching frequency f to the circuit resonant frequency f_r,

$$f_n = \frac{f}{f_r}. \quad (10)$$

With known values L_r, C_r, and R_{ac}, the circuit Q factor is defined as follows:

$$Q = \frac{\sqrt{L_r / C_r}}{R_{ac}}. \quad (11)$$

The transfer characteristics of the converter are plotted for different circuit Q factors using the above equations (Fig. 2).

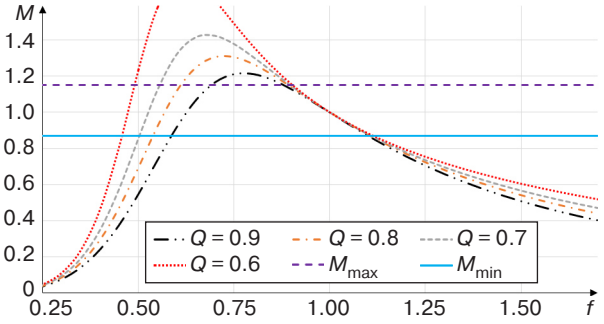

Fig. 2. Circuit transmission coefficient as a function of the circuit Q factor (current frequency normalized to the resonant frequency)

Depending on the region of the transfer characteristic in which the converter operates, different switching modes can be implemented: at zero current and at zero voltage [17]. If the operating frequency of the converter is to the left of the peak factor M, the converter operates in the region where the capacitance of the converter is primary. However, when operating with a capacitive load, the current in the circuit is ahead of the voltage and the zero-current switching mode is implemented. Operating in this region results in high losses due to the transistors switching under harsh conditions. If the operating frequency of the converter is to the right of the peak factor M, the inductive impedance is dominant. However, when operating in the inductive region, the voltage in the circuit is higher than the current. Therefore, it is in this operating region that the zero-voltage switching mode is implemented, allowing the transistors to switch with minimum loss. Consequently, the optimum operating region of the converter is to the right of the peak factor M.

INTEGRATED MAGNETIC SYSTEM

The resonant circuit consists of three electromagnetic components comprising a transformer T, parallel inductor L_{sh} (L_m), and series inductor L_r. Although each of these components is manufactured on a separate core (magnetic core), it would be more rational to integrate them in a magnetic system based on a transformer. The possibility of integrating the components within a magnetic system is justified by the equivalent circuit of a two-winding transformer in which the output load is reduced to the primary winding [18]. The inductance L_r can be replaced by the scattering inductance L_{S1} of the primary winding while the parallel inductance L_{sh} can be replaced by the transformer magnetizing inductance L_m [19].

For correct operation of the circuit while preserving the possibility of implementing switching at zero voltage, the magnetizing inductance should be within $(3...8)L_r$. This can be achieved by introducing a nonmagnetic gap in the transformer. The core used in the calculation is the Epcos core N87 (size ER 42/22/15, magnetic permeability $\mu = 2200$, and saturation induction $B_s = 0.49$ T).

The magnetizing inductance for gap transformers is defined as follows [20]:

$$L_m = \frac{\mu_{eff} \mu_0 N_1^2 S_c}{l_{av}}, \quad (12)$$

where μ_{eff} is the effective magnetic permeability; μ_0 is the magnetic constant; N_1 is the number of turns of the primary winding; S_c is the cross-sectional area of the magnetic core; l_{av} is the length of the central line of the magnetic core.

The effective magnetic permeability is the magnetic permeability of the core material with a gap, which is defined as follows:

$$\mu_{eff} = \frac{1}{\frac{1}{\mu} + \frac{l_g}{l_{av}}}, \quad (13)$$

where μ is the magnetic permeability of the material; l_g is the length of the nonmagnetic gap.

The number of turns of the primary winding is determined by the following equation:

$$N_1 = \frac{n(V_{out} + V_f)}{2 f_{min} M_{min} B S_c} = 20, \quad (14)$$

where the direct voltage drop across the rectifier diode $V_f = 0.6$ V, the minimum operating frequency $f_{min} = 72$ kHz, and the value of maximum induction $B = 0.4$ T.

The minimum operating frequency f_{min} is determined from the graph (Fig. 2).

The value of the maximum induction is determined from the value of the core saturation induction using the following equation:

$$B = 0.8B_s = 0.4 \text{ T}. \quad (15)$$

Taking into account the transformation ratio, the number of secondary winding turns $N_2 = 2$.

Substituting (13) into (12), the value of the nonmagnetic gap is calculated to obtain the required magnetizing inductance, as follows:

$$l_g = \frac{\mu\mu_0 N_1^2 S_c - l_{av} L_m}{\mu L_m} = 0.11 \text{ mm}, \quad (16)$$

where the cross-sectional area of the magnetic core S_c = 170 mm^2, and the length of the center line of the magnetic core l_{av} = 99 mm.

The scattering inductance of the primary winding is that part of the inductance which is not connected by the common magnetic flux to the secondary winding and the magnetic core, while the magnetic flux is short-circuited through the air. For *W*- and *U*-shaped magnetic circuits, the scattering inductance can be calculated using the following equation for an inductor without a magnetic core:

$$L_{S1} = \frac{\mu_0 N_1^2 S_{i.s.}}{h_w}, \quad (17)$$

where the area of inductive system $S_{i.s.}$ is the effective area covered by the current, excluding the magnetic core area; h_w is the winding height.

The effective area is determined by the following equation:

$$S_{i.s.} = l_{w1\_av}\delta_{w1}, \quad (18)$$

where l_{w1_av} is the average primary winding turn length; δ_{w1} is the distance from the average primary winding turn to the magnetic core.

Equations (17) and (18) show that in order to increase the scattering inductance, it is necessary to separate the primary and secondary windings on the transformer frame by increasing the number of turns of the winding and its thickness, as well as reducing the length of the winding on the magnetic core.

The scattering inductance close to the calculated value can be obtained by using the sectional winding method shown in Fig. 3. Unlike the winding method, where the primary and secondary windings are layered along the entire length of the frame, the sectional method gives the highest value of scattering inductance.

Once the transformer has been wound, it is necessary to check that the inductance of the primary winding is equal to the value of the total inductance $L_m + L_r$. If it differs from the calculated value, the difference can be compensated by adjusting the core gap. The next step is to check that the value obtained for the scattering inductance is within 10% of the calculated value. This is done by short-circuiting all the output windings and measuring the inductance of the primary winding. If the measured value differs from the calculated value by more than 10%, the transformer should be remanufactured. If all parameters match the calculated values, the transformer is suitable for use.

While the primary and secondary sectional winding method is suitable for achieving relatively low output voltage levels, it is not suitable for achieving the high voltages required by bias sources where output voltages can range from units to tens of kilovolts and ensuring electrical robustness is of paramount importance.

For high voltage levels, a *U*-shaped core is used with the primary and secondary windings separated by a certain distance. The primary and secondary windings are fixed on opposite core bars, while the secondary winding is divided into separate sections. After winding, the transformer windings are filled with insulating compound (Fig. 4).

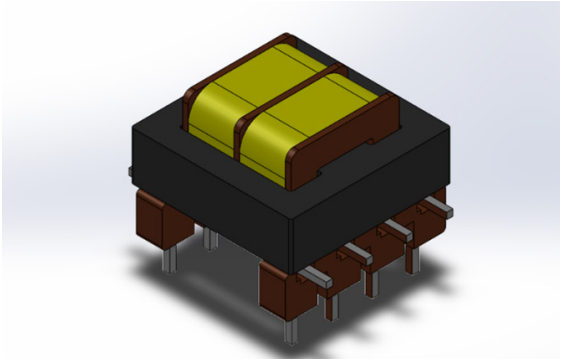

Fig. 3. Winding arrangement of the cathode heating transformer

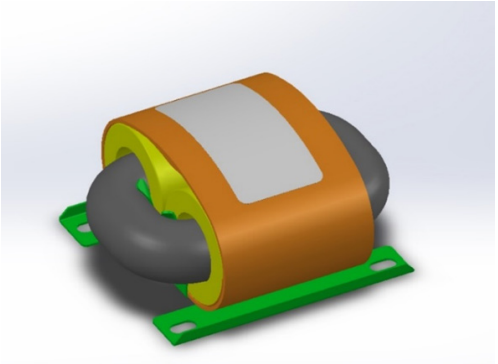

Fig. 4. Example of high voltage transformer layout for powering the klystron bias circuit

TESTING THE DEVELOPED SOURCE

The cathode heating and bias power supplies for the floating-drift multibeam klystron are designed according to the described method.

The source of the cathode heating circuit has the following parameters: cathode heating voltage $U_{cath.heat.} = 13$ V; nominal cathode heating current $I_{cath.heat.} = 12$ A; resonance capacitor capacity $C_r = 22$ nF; resonance inductance $L_r = 182$ μH; and resonance frequency $f_r = 80$ kHz. The soft start method is implemented in the source to extend the life of the klystron.

The klystron bias source provides voltage $U_{bias} = 6$ kV at a current not exceeding than $I_{bias} = 100$ mA, resonant frequency $f_r = 80$ kHz, resonant capacitor capacitance $C_r = 68$ nF, and resonant inductance $L_r = 58$ μH.

The development of such a source is complicated by the electrical robustness of the transformer at the high potential of the secondary winding, which is below the cathode potential of about 25 kV. This is achieved by filling the transformer with a compound. For the cathode heating transformer, the secondary winding is made of high-voltage conductive wire with combined insulation to increase the electrical strength. The electrical strength of the insulation between the primary and secondary windings is tested at 30 kV on an electrical breakdown system. The source parameters are measured. Waveforms showing the klystron cathode heater operation are presented in Figs. 5 and 6. Waveforms of the converter operating at the nominal input mains voltage are shown in Fig. 5; here, the yellow line (*1*) represents the voltage at the current sensor with a resistance of 0.51 Ohms (the vertical line is the voltage on a scale of 1 V/div), the green line (*2*) represents the voltage at the resonance capacitor (the vertical line is the voltage on a scale of 150 V/div), while the red line (*3*) represents the drain-to-source voltage of the upper transistor VT1. The horizontal line shows the time on a scale of 5 μs/div. It is clear from the waveforms shown that the voltage phase is ahead of the current phase and that the circuit is operating in the inductive region. Since the mains input voltage is stable, the converter operates close to the resonance frequency $f \approx 80$ kHz, which corresponds to the calculated values. In this mode, there is no need to change the operating frequency since the inverter parameters do not depend on the power consumption.

The transistor switching waveforms and the current sensor voltage at the input mains voltage of 198 V are shown in Fig. 6. The red (*1*) and yellow (*2*) lines represent the drain-to-source voltages of the upper VT1 and lower VT2 transistors, respectively (vertically, the voltage is on a scale of 200 V/div). The green line (*3*) shows the voltage at the current sensor (vertical is the voltage on a scale of 2 V/div). The horizontal line shows the time on a scale of 5 μs/div.

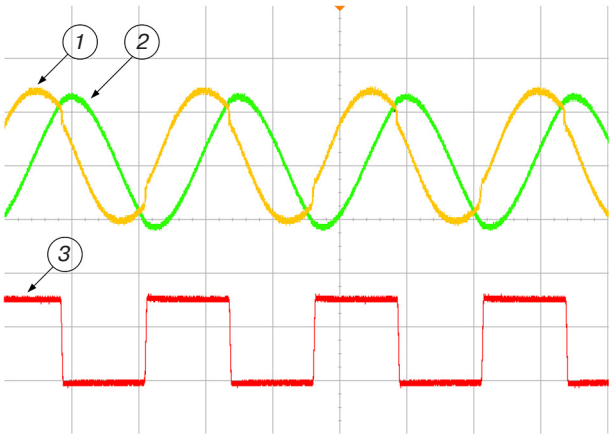

Fig. 5. Waveforms of the converter operating at rated input voltage

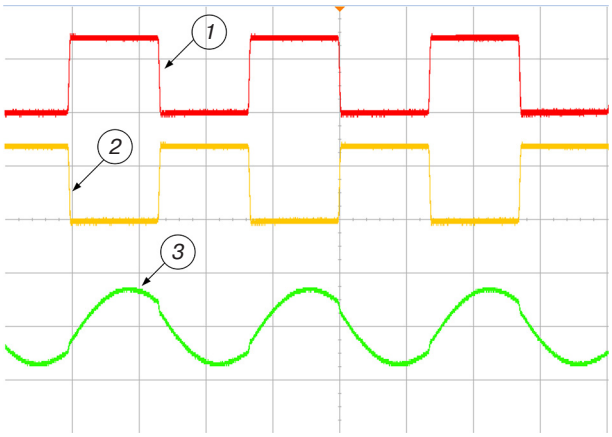

Fig. 6. Transistor switching waveforms at minimum input voltage

Similar to Fig. 6, Fig. 7 shows the inverter operating at maximum input voltage, which is 242 V.

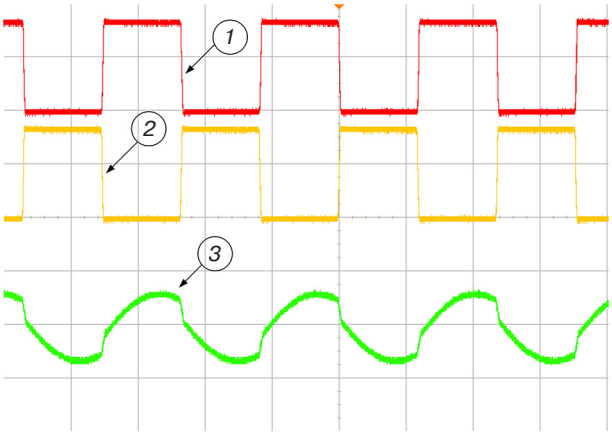

Fig. 7. Waveforms of the inverter operating at maximum input voltage

The zero-voltage switching mode is always implemented; the output voltage is maintained at the set level when the inverter is operated with different input voltages.

The operation of the converter can be divided into the following four stages:

1. Transistor VT1 is opened, the transformer primary current I_1 flows through the resonant circuit, and resonance occurs. When the resonance ceases, the current drops to the magnetizing current I_m.
2. Transistor VT1 is closed. The magnetizing current I_m continues to flow through the body diode of transistor VT2.
3. Transistor VT2 is opened, the energy stored in capacitor C_r generates current I_1 in the reverse direction, and the magnetizing current I_m crosses the zero point and increases in the reverse direction. Resonance occurs. When the resonance ceases, the current drops to the magnetizing current I_m.
4. Transistor VT2 is closed, and the magnetizing current I_m continues to flow through the body diode of transistor VT1. Transistor VT1 opens and the process is repeated.

In step 2, current flows through the body diode of transistor VT2, then the transistor opens when its drain-to-source voltage is close to zero (zero voltage switching). Similarly, transistor VT1 switches at zero voltage in step 4.

The measured efficiencies of the cathode heating and bias sources are 85% and 92%, respectively.

The prototype model of the resonant power supply is tested in the laboratory as part of the complex test simulation test bench for the radio transmitter of the multifunctional radar station. The functional scheme of the test bench is shown in Fig. 8.

In the initial state, a bias voltage of −6 kV is applied to the CE klystron via the R2 resistor assembly, and the klystron is locked. The voltage at the CE with respect to the collector −30 kV is the sum of the voltages of the cathode and bias supplies connected in series. After the control pulse in the modulator opens the start-up channel, the klystron opens and amplifies the input microwave signal. The voltage at the CE with respect to the collector is −24 kV. At the end of the control pulse, the start channel closes, the breakdown channel opens, a voltage of −30 kV is applied to the CE with respect to the collector, and the klystron closes. This process is shown in the waveform in Fig. 9.

The red (bottom) line shows the voltage at the CE relative to the klystron collector (vertically, the voltage is on a scale of 5 kV/div). The violet (top) line shows the envelope of the microwave output signal (vertical is the voltage on a scale of 5 V/div). The horizontal line shows the time on a scale of 2 μs/div.

From the depicted waveforms, it can be seen that, when the klystron is locked, the voltage at the CE is −29.75 kV and stable at the specified level. The microwave output power of the klystron, which is also stable, meets the specified nominal power. It can therefore be concluded that the developed sources are suitable for use in prototype radio transmitters.

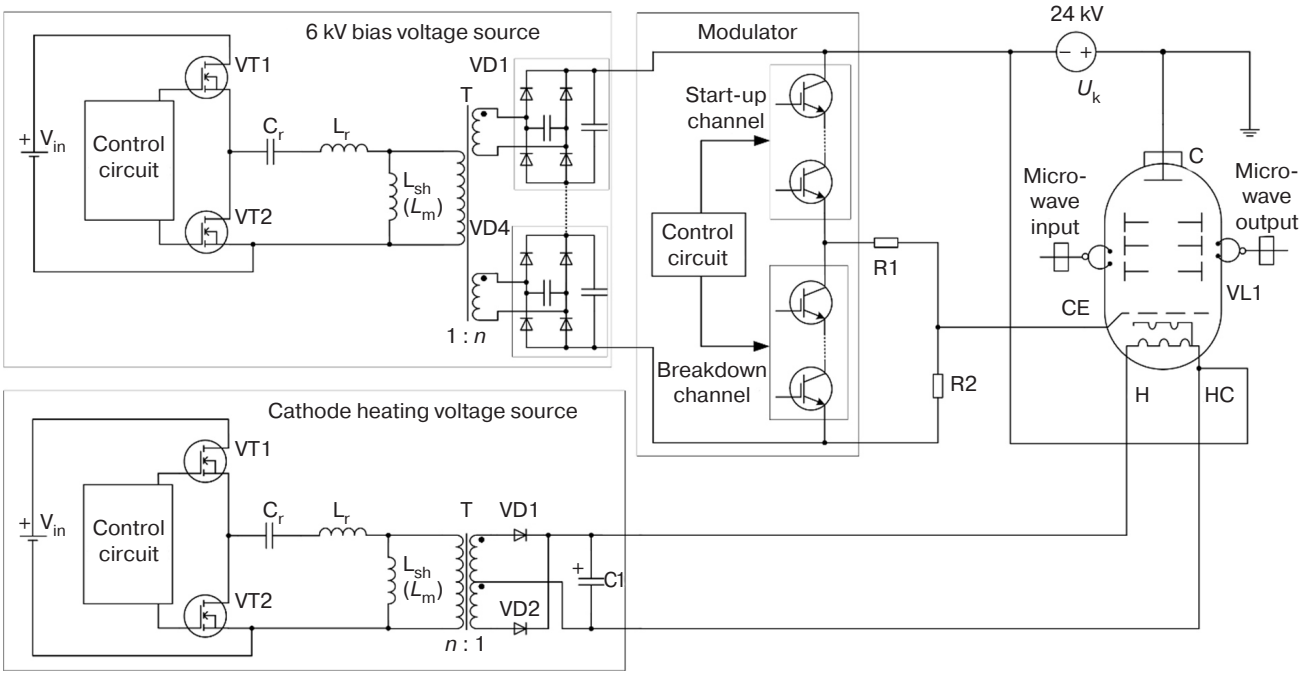

Fig. 8. Functional scheme of the test bench.
CE is the control electrode; H is the heater; HC is the heater-cathode; C is the collector; VL1 is the klystron; R1 is the current limiting resistor assembly; R2 is the bias pull-up resistor assembly; U_k is the power supply voltage of the klystron cathode

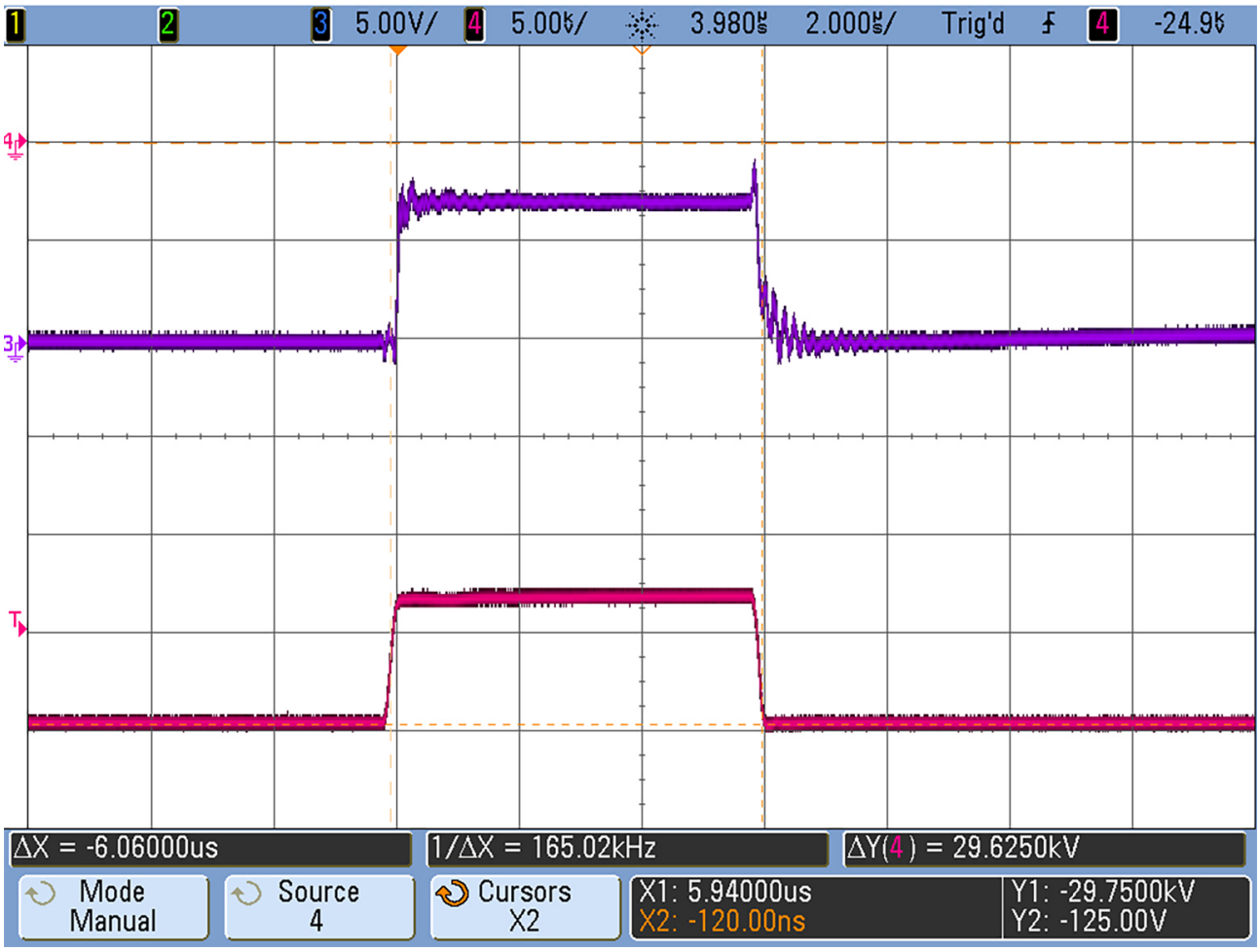

Fig. 9. Klystron operation

CONCLUSIONS

In the present work, a method for designing secondary power supplies for a vacuum microwave amplifier is proposed. The theory and calculation method of the resonant LLC source is presented. A method for calculating and carrying out transformer winding is discussed and tested. This method avoids the use of inductors as separate elements by integrating them into a magnetic system and providing decoupling by the high potential of the secondary winding.

The power supply is tested as part of a radio transmitter test bench complex. Waveforms of the cathode heater converter at minimum, nominal, and maximum input mains voltage are obtained. It is shown that the source operates in switching mode at zero voltage in the inductive region. The efficiencies of the cathode heating and bias sources are 85% and 92% respectively.

The developed power sources are smaller than transformer analogues and can maintain a stable output voltage when the input voltage changes, while the use of a soft start-up can help to extend the life of the klystron.

Authors' contribution

All authors have equally contributed to the research work.

REFERENCES

1. Sukhodolets L.G. *Moshchnye vakuumnye SVCh pribory* (*Powerful Vacuum Microwave Devices*). Textbook on the Study of Microwave Vacuum Devices. Moscow: IKAR; 2014. 272 p. (in Russ.).
2. Zabolotnaya S.V., Emelyanov E.V., Tsytsarev A.Yu., Albutov A.N. Automatic control, monitoring and protection system of multifunctional radar transmitter output amplifier. *Vestnik vozdushno-kosmicheskoi oborony = Aerospace Defense Herald*. 2017;2(14):70–76 (in Russ.). https://elibrary.ru/ysdqqr
3. Lobov I.N., Berezin O.K. A High-voltage pulse modulator for the MFR transmitter. *Vestnik vozdushno-kosmicheskoi oborony = Aerospace Defense Herald*. 2020;3(27):22–30 (in Russ.). https://www.elibrary.ru/atttkk
4. Baranov V.V., Lobov I.N., Khafizov D.R. High-voltage pulse modulator for a traveling wave lamp of radio transmitting equipment MRL. *Vestnik vozdushno-kosmicheskoi oborony = Aerospace Defense Herald*. 2023;2(38):55–62 (in Russ.). https://www.elibrary.ru/cqkgfd
5. Zinov'ev G.S. *Osnovy silovoi elektroniki* (*Fundamentals of Power Electronics*). Part 2. Novosibirsk: NGTU; 2000. 197 p. (in Russ.).
6. Polishchuk A. Highly efficient sources of secondary high-voltage power supply for microwave radio transmitters. *Silovaya Elektronika*. 2004;2:66–70 (in Russ.). https://elibrary.ru/mvrpnb
7. Lee S.-S., Moon G.-W. Full ZVS-Range Transient Current Buildup Half-Bridge Converter with Different ZVS Operations to Load Variation. *IEEE Trans. Ind. Electron*. 2008;55(6):2557–2559. https://doi.org/10.1109/TIE.2008.921239
8. Steigerwald R.L. A Comparison of Half-Bridge Resonant Converter Topologies. *IEEE Trans. Power Electron*. 1988;3(2): 174–182. http://doi.org/10.1109/63.4347
9. Zhang B., Zhao M., Huang P., Wang Q. Optimal design of GaN HEMT based high efficiency LLC converter. *Energy Rep*. 2022;8(5):1181–1190. https://doi.org/10.1016/j.egyr.2022.02.276
10. Zhang S., Li L., Zhao Z., Fan S., Wang C. Optimal trajectory based start-up control of LCC resonant converter for X-ray generator applications. *Energy Rep*. 2022;8(5):957–965. https://doi.org/10.1016/j.egyr.2022.02.266
11. Wei Y., Luo Q., Mantooth H.A. Synchronous Rectification for LLC Resonant Converter: An Overview. *IEEE Trans. Power Electron*. 2021;36(6):7264–7280. https://doi.org/10.1109/TPEL.2020.3040603
12. Li N., Cao Y., Zhang Y., Li Z., Jiang L., Zhang X.P. Parameter optimization strategy of LLC converter soft start-up process based on a simplified numerical calculation model. *Energy Rep*. 2023;9(10):909–919 https://doi.org/10.1016/j.egyr.2023.05.118
13. Kucka J., Dujic D. Equal Loss Distribution in Duty-Cycle Controlled H-Bridge LLC Resonant Converters. *IEEE Trans. Power Electron*. 2021;36(5):4937–4941. https://doi.org/10.1109/TPEL.2020.3028879
14. Smirnova V. A highly efficient, compact resonant ZVS bridge converter based on a 1200 V SiC MOSFET. *Silovaya Elektronika*. 2016;6(63):54–60 (in Russ.). https://elibrary.ru/xrngcd
15. Novikov Yu., Solomatin M. Development of a half-bridge resonant converter based on IRS2795. *Elektronnye komponenty*. 2011;3:103–111 (in Russ.).
16. Duerbaum T. First harmonic approximation including design constraints. In: *INTELEC – Twentieth International Telecommunications Energy Conference* (*Cat. No.98CH36263*). 1998. P. 321–328. https://doi.org/10.1109/INTLEC.1998.793519
17. Skuto A., Gaito A. The choice of a half-bridge resonant LLC converter and a MOSFET of the primary side. *Silovaya Elektronika*. 2016;2(59):30–32 (in Russ.). https://elibrary.ru/waoxqt
18. Semenov B.Yu. *Silovaya elektronika ot prostogo k slozhnomu* (*Power Electronics from Simple to Complex*). Moscow: SOLON-Press; 2005. 416 p. (in Russ.).
19. Chen Q., Long X., Chen Y., Xu S., Chen W. The Structure and Its Leakage Inductance Model of Integrated LLC Transformer With Wide Range Value Variation. *CPSS Trans. Power Electron. Appl*. 2022;7(4):409–420. https://doi.org/10.24295/CPSSTPEA.2022.00037
20. Khnykov A.V. *Teoriya i raschet transformatorov istochnikov vtorichnogo elektropitaniya* (*Theory and Calculation of Transformers of Secondary Power Supply Sources*). Moscow: SOLON-Press; 2004. 128 p. (in Russ.).

СПИСОК ЛИТЕРАТУРЫ

1. Суходолец Л.Г. *Мощные вакуумные СВЧ приборы.* Учебное пособие по изучению ЭВП СВЧ. М.: ИКАР; 2014. 272 с.
2. Заболотная С.В., Емельянов Е.В., Цыцарев А.Ю., Албутов А.Н. Система автоматизированного управления, защиты и контроля выходного усилителя передающего устройства многофункционального радиолокатора. *Вестник воздушно-космической обороны*. 2017;2(14):70–76. https://elibrary.ru/ysdqqr
3. Лобов И.Н., Березин О.К. Высоковольтный импульсный модулятор для аппаратуры передающего устройства МФР. *Вестник воздушно-космической обороны*. 2020;3(27):22–30. https://www.elibrary.ru/atttkk
4. Баранов В.В., Лобов И.Н., Хафизов Д.Р. Высоковольтный импульсный модулятор для лампы бегущей волны радиопередающей аппаратуры МРЛС. *Вестник воздушно-космической обороны*. 2023;2(38):55–62. https://www.elibrary.ru/cqkgfd
5. Зиновьев Г.С. *Основы силовой электроники. Часть 2*. Новосибирск: НГТУ; 2000. 197 с.

6. Полищук А. Высокоэффективные источники вторичного электропитания высокого напряжения для радиопередающих устройств СВЧ. *Силовая электроника*. 2004;2:66–70. https://elibrary.ru/mvrpnb
7. Lee S.-S., Moon G.-W. Full ZVS-Range Transient Current Buildup Half-Bridge Converter with Different ZVS Operations to Load Variation. *IEEE Trans. Ind. Electron*. 2008;55(6):2557–2559. https://doi.org/10.1109/TIE.2008.921239
8. Steigerwald R.L. A Comparison of Half-Bridge Resonant Converter Topologies. *IEEE Trans. Power Electron*. 1988;3(2): 174–182. http://doi.org/10.1109/63.4347
9. Zhang B., Zhao M., Huang P., Wang Q. Optimal design of GaN HEMT based high efficiency LLC converter. *Energy Rep*. 2022;8(5):1181–1190. https://doi.org/10.1016/j.egyr.2022.02.276
10. Zhang S., Li L., Zhao Z., Fan S., Wang C. Optimal trajectory based start-up control of LCC resonant converter for X-ray generator applications. *Energy Rep*. 2022;8(5):957–965. https://doi.org/10.1016/j.egyr.2022.02.266
11. Wei Y., Luo Q., Mantooth H.A. Synchronous Rectification for LLC Resonant Converter: An Overview. *IEEE Trans. Power Electron*. 2021;36(6):7264–7280. https://doi.org/10.1109/TPEL.2020.3040603
12. Li N., Cao Y., Zhang Y., Li Z., Jiang L., Zhang X.P. Parameter optimization strategy of LLC converter soft start-up process based on a simplified numerical calculation model. *Energy Rep*. 2023;9(10):909–919. https://doi.org/10.1016/j.egyr.2023.05.118
13. Kucka J., Dujic D. Equal Loss Distribution in Duty-Cycle Controlled H-Bridge LLC Resonant Converters. *IEEE Trans. Power Electron*. 2021;36(5):4937–4941. https://doi.org/10.1109/TPEL.2020.3028879
14. Смирнова В. Высокоэффективный, компактный резонансный ZVS мостовой конвертер на основе 1200 В SiC-MOSFET. *Силовая электроника*. 2016;6(63):54–60. https://www.elibrary.ru/xrngcd
15. Новиков Ю., Соломатин М. Разработка полумостового резонансного преобразователя на основе IRS2795. *Электронные компоненты*. 2011;3:103–111.
16. Duerbaum T. First harmonic approximation including design constraints. In: *INTELEC – Twentieth International Telecommunications Energy Conference* (*Cat. No. 98CH36263*). 1998. P. 321–328. https://doi.org/10.1109/INTLEC.1998.793519
17. Скуто А., Гайто А. Выбор полумостового резонансного LLC-преобразователя и MOSFET первичной стороны. *Силовая электроника*. 2016;2(59):30–32. https://elibrary.ru/waoxqt
18. Семенов Б.Ю. *Силовая электроника от простого к сложному*. М.: СОЛОН-Пресс; 2005. 416 с.
19. Chen Q., Long X., Chen Y., Xu S., Chen W. The Structure and Its Leakage Inductance Model of Integrated LLC Transformer With Wide Range Value Variation. *CPSS Trans. Power Electron. Appl*. 2022;7(4):409–420. https://doi.org/10.24295/CPSSTPEA.2022.00037
20. Хныков А.В. *Теория и расчет трансформаторов источников вторичного электропитания*. М.: СОЛОН-Пресс; 2004. 128 с.

About the authors

Damir R. Hafizov, Engineer, A.A. Raspletin NPO Almaz (80/16, Leningradskii pr., Moscow, 125190 Russia); Postgraduate Student, Department of Nanoelectronics, Institute for Advanced Technologies and Industrial Programming, MIREA – Russian Technological University (78, Vernadskogo pr., Moscow, 119454 Russia). E-mail: hafizov98@yandex.ru. RSCI SPIN-code 3037-0537, https://orcid.org/0009-0004-2662-0299

Ilya N. Lobov, Head of the Department, A.A. Raspletin NPO Almaz (80/16, Leningradskii pr., Moscow, 125190 Russia). E-mail: lobov.en@mail.ru. https://orcid.org/0009-0003-6741-825X

Leonid Y. Fetisov, Dr. Sci. (Phys.-Math.), Professor, Department of Nanoelectronics, Institute for Advanced Technologies and Industrial Programming, MIREA – Russian Technological University (78, Vernadskogo pr., Moscow, 119454 Russia). E-mail: fetisovl@yandex.ru. Scopus Author ID 26431336600, ResearcherID D-1163-2013, RSCI SPIN-code 9788-0680, https://orcid.org/0000-0002-3699-4321

Об авторах

Хафизов Дамир Ринатович, инженер, ПАО «НПО «Алмаз» имени академика А.А. Расплетина (125190, Россия, Москва, Ленинградский пр-т, д. 80, корп. 16); аспирант, кафедра наноэлектроники, Институт перспективных технологий и индустриального программирования, ФГБОУ ВО «МИРЭА – Российский технологический университет» (119454, Россия, Москва, пр-т Вернадского, д. 78). E-mail: hafizov98@yandex.ru. SPIN-код РИНЦ 3037-0537, https://orcid.org/0009-0004-2662-0299

Лобов Илья Николаевич, начальник отдела, ПАО «НПО «Алмаз» имени академика А.А. Расплетина (125190, Россия, Москва, Ленинградский пр-т, д. 80, корп. 16). E-mail: lobov.en@mail.ru. https://orcid.org/0009-0003-6741-825X

Фетисов Леонид Юрьевич, д.ф.-м.н., доцент, профессор кафедры наноэлектроники, Институт перспективных технологий и индустриального программирования, ФГБОУ ВО «МИРЭА – Российский технологический университет» (119454, Россия, Москва, пр-т Вернадского, д. 78). E-mail: fetisovl@yandex.ru. Scopus Author ID 26431336600, ResearcherID D-1163-2013, SPIN-код РИНЦ 9788-0680, https://orcid.org/0000-0002-3699-4321

Translated from Russian into English by K. Nazarov
Edited for English language and spelling by Thomas A. Beavitt

Micro- and nanoelectronics. Condensed matter physics

Микро- и наноэлектроника. Физика конденсированного состояния

UDC 537.632
https://doi.org/10.32362/2500-316X-2025-13-1-115-121
EDN OABAYG

RESEARCH ARTICLE

Magneto-optical transverse Kerr effect in $Co_x(CoO)_{1-x}$ nanocomposites

Maxim M. Yashin @,
Vitaly E. Ryabukhin,
Alexey N. Yurasov

MIREA – Russian Technological University, Moscow, 119454 Russia
@ *Corresponding author, e-mail: yashin@mirea.ru*

Abstract

Objectives. The aim of this paper is to attain and investigate the spectra of the magneto-optical transverse Kerr effect (TKE) in $Co_x(CoO)_{1-x}$ nanocomposites, to compare the obtained results with experimental data, and identify their specific features. Magneto-optical spectroscopy is a method for non-destructive testing and research of a wide class of nanostructures with promising and interesting properties, and such studies are essential in terms of both fundamental and practical aspects.

Methods. Computer modeling is used as part of the promising effective medium method. This is in the form of the Bruggeman approximation, according to which the structure under study is replaced by a medium with effective properties.

Results. TKE experimental spectra were studied and Kerr effect spectra in the range of 1.5–3.0 eV were obtained by computer modeling. In this case, the modeling is performed by means of two methods, ignoring and considering the quasiclassical size effect. The final result is the comparison of the model and experimental Kerr effect spectra, in which the influence of size effects on the appearance of the TKE spectra is shown. The reliability of methods is well confirmed by comparing the results obtained with empirical data. The value of the results obtained stems from the fact that all the calculated parameters of the nanocomposite under study and the shape of TKE spectral dependencies are in good agreement with the observation results.

Conclusions. The optimal parameters of the sample under study are established as part of computer modeling: form factor, average granule size, and the anomalous Hall effect coefficient. The described approach allows the magneto-optical properties of promising nanomaterials to be studied in a non-contact and non-destructive manner. These results are useful for creating new types of devices as well as electronics and nanoelectronics elements.

Keywords: nanocomposites, effective medium approach, transverse Kerr effect, cobalt oxide, size effects

• **Submitted:** 26.04.2024 • **Revised:** 17.05.2024 • **Accepted:** 28.11.2024

For citation: Yashin M.M., Ryabukhin V.E., Yurasov A.N. Magneto-optical transverse Kerr effect in $Co_x(CoO)_{1-x}$ nanocomposites. *Russian Technological Journal.* 2025;13(1):115–121. https://doi.org/10.32362/2500-316X-2025-13-1-115-121, https://elibrary.ru/OABAYG

Financial disclosure: The authors have no financial or proprietary interest in any material or method mentioned.

The authors declare no conflicts of interest.

НАУЧНАЯ СТАТЬЯ

Магнитооптический экваториальный эффект Керра в нанокомпозитах $Co_x(CoO)_{1-x}$

М.М. Яшин [@], **В.Е. Рябухин**, **А.Н. Юрасов**

МИРЭА – Российский технологический университет, Москва, 119454 Россия
[@] *Автор для переписки, e-mail: yashin@mirea.ru*

Резюме

Цели. Целью работы является получение и исследование спектров магнитооптического экваториального эффекта Керра (ЭЭК) в нанокомпозитах $Co_x(CoO)_{1-x}$, сравнение полученных результатов с экспериментальными данными, выявление их особенностей. Подобные исследования являются, безусловно, важными, как с фундаментальной точки зрения, так и с практической, т.к. магнитооптическая спектроскопия – метод неразрушающего контроля и исследования широкого класса наноструктур с перспективными и интересными свойствами.

Методы. Для достижения поставленной цели применялось компьютерное моделирование в рамках перспективного метода эффективной среды – приближения Бруггемана, согласно которому исследуемая структура заменяется средой с эффективными свойствами.

Результаты. Изучены экспериментальные спектры ЭЭК и в рамках компьютерного моделирования получены спектры эффекта Керра в диапазоне 1.5–3.0 эВ. При этом моделирование проводилось двумя способами: без учета и с учетом квазиклассического размерного эффекта. Конечным результатом стало сопоставление модельных и экспериментальных спектров эффекта Керра, где было показано влияние размерных эффектов на вид спектров ЭЭК. Достоверность методик хорошо подтверждается сравнением полученных результатов с эмпирическими данными, а ценность полученных результатов обусловлена тем, что все рассчитанные параметры обсуждаемого нанокомпозита и форма спектральных зависимостей ЭЭК хорошо согласуются с результатами наблюдений.

Выводы. В рамках компьютерного моделирования установлены оптимальные параметры исследуемого образца: форм-фактор, средний размер гранул, коэффициент аномального эффекта Холла. Описанный подход позволяет бесконтактным и неразрушимым способом изучать магнитооптические свойства перспективных наноматериалов, а полученные результаты являются важными при создании новых типов устройств, а также элементов электроники и наноэлектроники.

Ключевые слова: нанокомпозиты, теория эффективной среды, экваториальный эффект Керра, оксид кобальта, размерные эффекты

• **Поступила:** 26.04.2024 • **Доработана:** 17.05.2024 • **Принята к опубликованию:** 28.11.2024

Для цитирования: Яшин М.М., Рябухин В.Е., Юрасов А.Н. Магнитооптический экваториальный эффект Керра в нанокомпозитах $Co_x(CoO)_{1-x}$. *Russian Technological Journal.* 2025;13(1):115–121. https://doi.org/10.32362/2500-316X-2025-13-1-115-121, https://elibrary.ru/OABAYG

Прозрачность финансовой деятельности: Авторы не имеют финансовой заинтересованности в представленных материалах или методах.

Авторы заявляют об отсутствии конфликта интересов.

INTRODUCTION

Achievements in magneto-optics are being actively applied today in the modern electronic industry. Magneto-optics is a branch of physics which studies the phenomena resulting from interactions of electromagnetic radiation (of the optical range in the infrared (IR), visible, and near-ultraviolet regions of the spectrum) with magnetized matter. The transverse Kerr effect (TKE) described in Fig. 1 is one of the magneto-optical effects.

TKE is actively used in studying nanostructures, magnetic reading, and recording data from magnetic disks. Current trends in the development of information storage devices are driving the search for new materials in the field of magnetic granular alloys and nanocomposites.

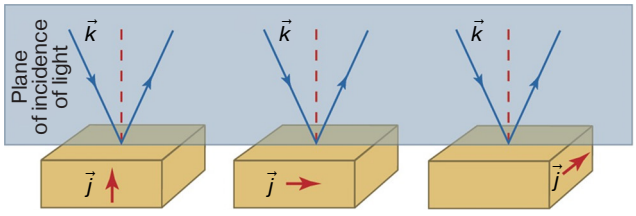

Fig. 1. Kerr effect in polar (a), meridional (b), and equatorial (c) geometries.
$\vec{k}$ is wave vector; $\vec{j}$ is magnetization

Thus research into the properties of promising nanostructures represent an important research task. This is particularly relevant to the possibility of significantly enhancing important practical effects such as magnetoresistance, quantum Hall effects, magnetorefractive effect, and many others [1–3]. Co–CoO-based nanocomposite is an interesting example of a nanostructure, while modeling the observed optical and magneto-optical effects enables various characteristic parameters of the investigated samples to be assessed in a non-contact manner [4–7].

The experiment described in [8, 9] established the spectral dependencies of the TKE parameter (δ) in the equatorial geometry of $Co_x(CoO)_{1-x}$ nanocomposite at different values of the cobalt volume fraction X (Fig. 2).

MATHEMATICAL MODEL AND CALCULATION METHODOLOGY

The phenomenological theory of magneto-optical effects requires Maxwell's equations to be resolved with allowance for the dielectric permittivity in matrix (tensor) form; $\hat{\varepsilon}$ is the dielectric permittivity tensor (DPT):

$$\hat{\varepsilon} = \begin{pmatrix} \varepsilon & i\gamma & 0 \\ -i\gamma & \varepsilon & 0 \\ 0 & 0 & \varepsilon \end{pmatrix}. \quad (1)$$

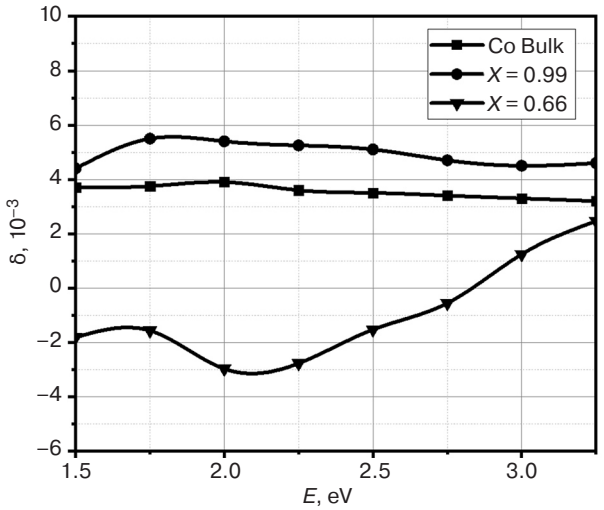

Fig. 2. Experimental TKE spectra of $Co_x(CoO)_{1-x}$ nanocomposite. E is the electromagnetic wave energy [8, 9]

The magnetic induction vector is directed along the z-axis while the ε and γ components of DPT have the following form:

$$\gamma = \gamma_1 - i\gamma_2, \quad \varepsilon = \varepsilon_1 - i\varepsilon_2, \quad (2)$$

wherein ε and γ are complex quantities. In this case, ε_1 and γ_1 are the real part of diagonal and nondiagonal DTP components, while ε_2 and γ_2 are the imaginary part of DTP components, respectively.

Any magneto-optical effect can be unambiguously expressed through DTP components. Magneto-optical effects enable the contribution of left and right spin subzones to be separated, whereas studying frequency dependencies of imaginary parts of diagonal and nondiagonal DTP components provides comprehensive information on the zone structure of the investigated medium.

Furthermore, magneto-optical effects allow the domain structure to be visualized. It is thus one of the most important tools in studying magnetic nano- and micro-objects, including the working zone of magnetic heads and domain boundaries [1–6].

The global advantage of magneto-optical Kerr spectroscopy is the ability to determine non-diagonal components of tensors using TKE, and, in practical terms, to "screen out" noise and interference in the experimental setup. At the same time, the Kerr effect parameter δ can be measured experimentally on the p-component only. This is due to the fact that the δ_s-effect on the s-component in metallic ferromagnets is 2–3 times smaller than δ [9]:

$$\delta = (A\gamma_1 + B\gamma_2) + \frac{2\sin 2\varphi}{A^2 + B^2}, \quad (3)$$

wherein $A = \varepsilon_2(2\varepsilon_1 \cos^2\varphi - 1)$, $B = \cos^2\varphi(\varepsilon_2^2 - \varepsilon_1^2 + 1) + \varepsilon_1 - 1$, φ is the light incidence angle.

The effective medium theory is optimal in describing spectral dependencies of nanostructures and nanocomposites in particular [10]. In the IR spectral region, the significant influence of the quasi-classical size effect due to intraband transitions should be taken into account when using this theory [11]. The size effects are accounted for by varying the form factors of particles L and by adding the ferromagnetic component of the nanocomposite to the diagonal and nondiagonal DTP components, due to the electron scattering on granule surfaces. Finally, when allowing for the contribution of dimensional effects to the permittivity tensor, according to the Drude–Lorentz model, DTP components are represented in the following form [11]:

$$\varepsilon_{mod} = \varepsilon_{Co} + \frac{\omega_p^2}{\omega(\omega + i/\tau_{bulk})} - \frac{\omega_p^2}{\omega(\omega + i/\tau_{part})},$$
$$\gamma_{mod} = \gamma_{Co} - \frac{4\pi\sigma_{xy}^{bulk}/\tau_{bulk}^2}{\omega(\omega + i/\tau_{bulk})^2} + \frac{4\pi\sigma_{xy}^{gr}/\tau_{part}^2}{\omega(\omega + i/\tau_{part})^2}, \quad (4)$$

wherein ε_{Co} and γ_{Co} are the diagonal and non-diagonal DTP components of the ferromagnet (cobalt in this case); ω is the frequency of the incident electromagnetic wave; ω_p is the plasma frequency; τ_{bulk} and τ_{part} are the average electron path times in bulk samples and granules, respectively; $\sigma_{xy}^{bulk} = 4\pi M_s R_{bulk}/\rho_{bulk}^2$; $\sigma_{xy}^{gr} = 4\pi M_s R_{gr}/\rho_{gr}^2$; M_s is the saturation magnetization of the ferromagnet; R_{gr} and R_{bulk} are coefficients of the anomalous Hall effect (AHE) for granules and bulk sample, respectively; ρ_{bulk} is the bulk sample resistivity; and ρ_{gr} is the granule resistivity. The size effect is evident both in the AHE parameter and in the resistivity, as follows:

$$R_{gr} = R_{bulk} + 0.2R\frac{l}{r_0}\left(1 + \frac{l}{r_0}\right), \quad (5)$$

$$\rho_{gr} = \rho_{bulk}\left(1 + \frac{l}{r_0}\right), \quad (6)$$

wherein R is the AHE parameter value of the granule surface material, r_0 is the nanocomposite particle size, and l is the free path length.

Further expressions (4), (5) are substituted into effective medium formulas (e.g., see [6]) and finally into (3).

MODELING RESULTS

The values of the TKE parameter are obtained using formulas (1)–(3) within the framework of the Bruggeman approximation [12] as a promising effective medium method. Differences in the form of particles L (form factor) are allowed for while ignoring the size effect. They are compared with the experimental data obtained by the research laboratory at the Department of Magnetism, Faculty of Physics, Lomonosov Moscow State University [12] (Fig. 3). The nanocomposite with the cobalt volume fraction $X = 0.66$ is chosen as a comparative sample.

It can be seen in Fig. 3 that the best agreement is observed at $L = 0.3$. For more precise TKE description, we consider the influence of the quasiclassical size effect (formulas (4) and (5)) (Fig. 4).

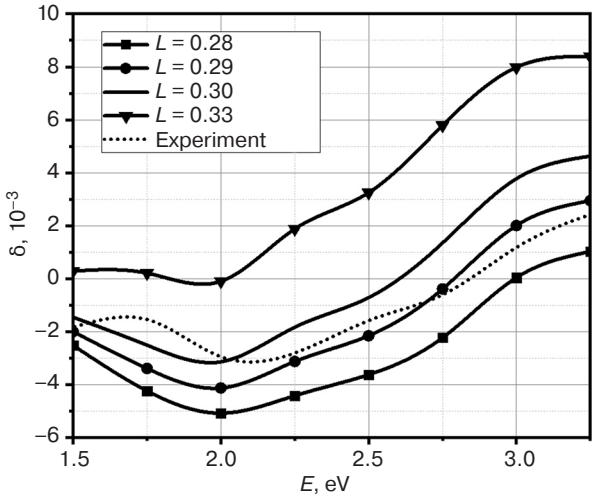

Fig. 3. Model TKE spectra of the $Co_x(CoO)_{1-x}$ nanocomposite ignoring the size effect at different values of the particle form factor

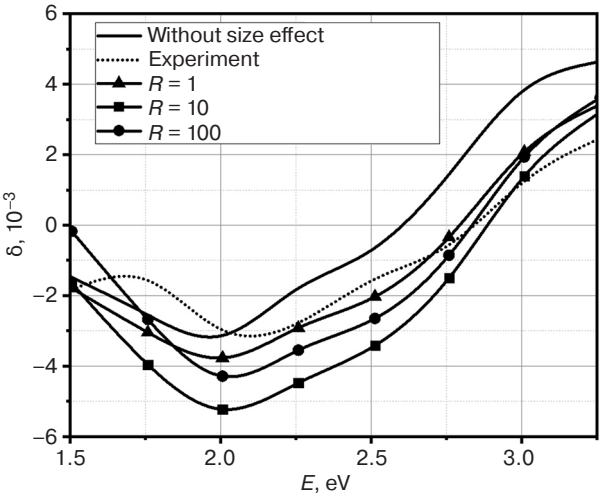

Fig. 4. Model TKE spectra of the $Co_x(CoO)_{1-x}$ nanocomposite ignoring and considering the size effect at different values of AHE parameter R

Figure 4 shows that considering the quasiclassical size effect allows the TKE change in the near-IR region of the spectrum to be described in a better way. The best coincidence of the model and experimental curves is observed at $R = 1$. The average size of the Co_xCoO_{1-x} nanocomposite granules is found to be $r_0 = 2.5$ nm. These results are useful in creating new types of devices, as well as elements of electronics and nanoelectronics [13–15].

CONCLUSIONS

As a result of the study, TKE model spectra in the $Co_x(CoO)_{1-x}$ nanocomposite were obtained and compared with experimental data.

The study also showed the significance of considering the contribution of the particle form factor, as well as the quasi-classical size effect on the TKE spectral dependencies. By means of computer modeling, the optimal parameters of the sample investigated, such as form-factor, average granule size, and AEC coefficient were established.

Thus, the above approach enables the magneto-optical properties of promising nanomaterials to be studied in a noncontact and nondestructive manner.

ACKNOWLEDGEMENTS

The study was supported by the program "Accelerator 4.0 RTU MIREA second wave" and the Ministry of Science and Higher Education of the Russian Federation (State Assignment for Universities No. FGFZ-2023-0005).

Authors' contributions

M.M. Yashin—computer simulation, discussion of results, and writing and editing the text of the article.

V.E. Ryabukhin—processing of literary sources, computer simulation, discussion of results, and writing the text of the article.

A.N. Yurasov—model development, computer simulation, discussion of results, and writing the text of the article.

REFERENCES

1. Gan'shina E.A., Golik L.L., Kun'kova Z.E., Zykov G.S., Rukovishnikov A.I., Markin Yu.V. Magnetic inhomogeneity manifestations in the magneto-optical spectra of (In-Mn)As layers. *IEEE Magn. Lett.* 2020;11:2502105. https://doi.org/10.1109/LMAG.2020.2982849
2. Gan'shina E.A., Pripechenkov I.M., Perova N.N., et al. Magneto-Optical Spectroscopy of GaSb–MnSb Composites. *Bull. Russ. Acad. Sci. Phys.* 2023;87(3):282–286. https://doi.org/10.3103/s1062873822701088
[Original Russian Text: Gan'shina E.A., Pripechenkov I.M., Perova N.N., Kanazakova E.S., Oveshnikov L.N., Dzhaloliddinzoda M., Ril' A.I., Granovskii A.B., Aronzon B.A. Magneto-optical spectroscopy of composites GaSb–MnSb. *Izvestiya Rossiiskoi akademii nauk. Seriya fizicheskaya.* 2023;87(3):328–332 (in Russ.). https://doi.org/10.31857/S0367676522700570]
3. Granovsky A.B., Khanikaev A.B., Kioussis N., Kalitsov A.V. Influence of grain size on the extraordinary Hall effect in magnetic granular alloys. *J. Magn. Magn. Mater.* 2003;258–259:87–89. https://doi.org/10.1016/S0304-8853(02)01119-8
4. Zvezdin A.K., Kotov V.A. *Magnitooptika tonkikh plenok* (*Magneto-Optics of Thin Films*). Moscow: Nauka; 1988. 192 p. (in Russ.).
5. Ganshina E.A., Garshin V.V., Pripechenkov I.M., Ivkov S.A., Domashevskaya E.P., Sitnikov A.V. Effect of phase transformations of a metal component on the magneto-optical properties of thin-films nanocomposites $(CoFeZr)_x(MgF2)_{100-x}$. *Nanomaterials*. 2021;11(7):1666. https://doi.org/10.3390/nano11071666
6. Yurasov A.N., Yashin M.M., Gladyshev I.V., Ganshina E.A., Kanazakova E.S., Saifulina D.A., Simdyanova M.A. Granule size distribution influence on the nanocomposite magneto-optical properties. *Vestnik MGTU im. N.E. Baumana. Seriya Estestvennye nauki = Herald of the Bauman Moscow State Technical University. Series Natural Sciences*. 2023;110(5):63–72 (in Russ.). Available from URL: https://vestniken.bmstu.ru/catalog/phys/cryst/1111.html
7. Blinov M.I., Chernenko V., Prudnikov V.N., Aseguinolaza I.R., Barandiaran J.M., Lahderanta E., Granovsky A.B. Anomalous hall effect in $Ni_{47.3}Mn_{30.6}Ga_{22.1}$/Mg O(001) thin films. *Phys. Rev. B*. 2020;102(6):064413. https://doi.org/10.1103/PhysRevB.102.064413
8. Domashevskaya E.P., Ivkov S.A., Sitnikov A.V., et al. Influence of the relative content of the metal component in the dielectric matrix on the formation and size of cobalt nanocrystals in $Co_x(MgF_2)_{100-x}$ film composites. *Phys. Solid State*. 2019;61(2):71–79. https://doi.org/10.1134/S1063783419020112
9. Gan'shina A., Garshin V.V., Perova N.N., et al. Magnetooptical Kerr Spectroscopy of Nanocomposites. *J. Exp. Theor. Phys.* 2023;137(4):572–581. https://doi.org/10.1134/S1063776123100151
[Original Russian Text: Gan'shina A., Garshin V.V., Perova N.N., Pripechenko I.M., Yurasov A.N., Yahin M.M., Rylkov V.V., Granovskii A.B. Magnetooptical Kerr Spectroscopy of Nanocomposites. *Zhurnal eksperimental'noi i teoreticheskoi fiziki*. 2023;164(4):662–772 (in Russ.). https://doi.org/10.31857/S0044451023100188]
10. Yurasov A.N., Yashin M.M. Methods of effective media as optimal methods for modeling the physical properties of nanostructures. *Rossiiskii tekhnologicheskii zhurnal.* 2020;8(5):68–77 (in Russ.). https://doi.org/10.32362/2500-316X-2020-8-5-68-77
11. Aleshnikov A.A., Kalinin Yu.E., Sitnikov A.V., Fedosov A.G. Magnetic properties of multilayer structures based on $(Co_{45}Fe_{45}Zr_{10})_x(Al_2O_3)_{100-x}$ nanocomposites. *Perspektivnye Materialy.* 2012;5:68–75 (in Russ.).
12. Sitnikov A.V., Makagonov V.A., Kalinin Y.E., Kushchev S.B., Foshin V.A., Perova N.N., Ganshina E.A., Granovsky A.B. Magnetic, magnetoresistive and structural properties of $Co_x(CoO)_{100-x}$ thin film composites. *J. Magn. Magn. Mater.* 2023;587(39):171154. https://doi.org/10.1016/j.jmmm.2023.171154

13. Fadeev E.A., Blinov M.I., Garshin V.V., et al. Magnetic properties of $(Co_{40}Fe_{40}B_{20})_x(SiO_2)_{100-x}$ nanocomposites near the percolation threshold. *Bull. Russ. Acad. Sci. Phys.* 2019;83(7):835–837. https://doi.org/10.3103/S1062873819070153
[Original Russian Text: Sitnikov A.V., Makagonov V.A., Kalinin Y.E., Kushchev S.B., Foshin V.A., Perova N.N., Ganshina E.A., Granovsky A.B. Magnetic properties of $(Co_{40}Fe_{40}B_{20})_x(SiO_2)_{100-x}$ nanocomposites near the percolation threshold. *Izvestiya Rossiiskoi akademii nauk. Seriya fizicheskaya.* 2019;83(7):917–920 (in Russ.). https://doi.org/10.1134/S0367676519070159]
14. Mikhailovsky Yu.O., Mettus D.E., Kazakov A.P., et al. Anomalous Hall effect in $(Co_{41}Fe_{39}B_{20})_x(Al–O)_{100-x}$ nanocomposites. *JETP Lett*. 2013;97(8):473–477 https://doi.org/10.1134/S0021364013080110
[Original Russian Text: Mikhailovsky Yu.O., Mettus D.E., Kazakov A.P., Prudnikov V.N., Kalinin Yu.E., Sitnikov A.S., Gerber A., Bartov D., Granovsky A.B. Anomalous Hall effect in $(Co_{41}Fe_{39}B_{20})_x(Al–O)_{100-x}$ nanocomposites. *Pis'ma v Zhurnal eksperimental'noi i teoreticheskoi fiziki*. 2013;97(7–8):544–548 (in Russ.).]
16. Manoharan S.S., Elefant D., Reiss G., Goodenough J.B. Extrinsic giant magne-toresistance in chromium (IV) oxide, CrO_2. *Appl. Phys. Lett*. 1998;72(8):984–986. https://doi.org/10.1063/1.120616

СПИСОК ЛИТЕРАТУРЫ

1. Gan'shina E.A., Golik L.L., Kun'kova Z.E., Zykov G.S., Rukovishnikov A.I., Markin Yu.V. Magnetic inhomogeneity manifestations in the magneto-optical spectra of (In-Mn)As layers. *IEEE Magn. Lett.* 2020;11:2502105. https://doi.org/10.1109/LMAG.2020.2982849
2. Ганьшина Е.А., Припеченков И.М., Перова Н.Н., Каназакова Е.С., Овешников Л.Н., Джалолиддинзода М., Риль А.И., Грановский А.Б., Аронзон Б.А. Магнитооптическая спектроскопия композитов GaSb–MnSb. *Известия Российской академии наук. Серия физическая.* 2023;87(3):328–332. https://doi.org/10.31857/S0367676522700570
3. Granovsky A.B., Khanikaev A.B., Kioussis N., Kalitsov A.V. Influence of grain size on the extraordinary Hall effect in magnetic granular alloys. *J. Magn. Magn. Mater.* 2003;258–259:87–89. https://doi.org/10.1016/S0304-8853(02)01119-8
4. Звездин А.К., Котов В.А. *Магнитооптика тонких пленок*. М.: Наука; 1988. 192 с.
5. Ganshina E.A., Garshin V.V., Pripechenkov I.M., Ivkov S.A., Domashevskaya E.P., Sitnikov A.V. Effect of phase transformations of a metal component on the magneto-optical properties of thin-films nanocomposites $(CoFeZr)_x(MgF2)_{100-x}$. *Nanomaterials*. 2021;11(7):1666. https://doi.org/10.3390/nano11071666
6. Юрасов А.Н., Яшин М.М., Гладышев И.В., Ганьшина Е.А., Каназакова Е.С., Сайфулина Д.А., Симдянова М.А. Влияние распределения гранул по размерам на магнитооптические свойства нанокомпозитов. *Вестник МГТУ им. Н.Э. Баумана. Сер. Естественные науки.* 2023;110(5):63–72. URL: https://vestniken.bmstu.ru/catalog/phys/cryst/1111.html
7. Blinov M.I., Chernenko V., Prudnikov V.N., Aseguinolaza I.R., Barandiaran J.M., Lahderanta E., Granovsky A.B. Anomalous hall effect in $Ni_{47.3}Mn_{30.6}Ga_{22.1}$/Mg O(001) thin films. *Phys. Rev. B*. 2020;102(6):064413. https://doi.org/10.1103/PhysRevB.102.064413
8. Domashevskaya E.P., Ivkov S.A., Sitnikov A.V., et al. Influence of the relative content of the metal component in the dielectric matrix on the formation and size of cobalt nanocrystals in $Co_x(MgF_2)_{100-x}$ film composites. *Phys. Solid State*. 2019;61(2):71–79. https://doi.org/10.1134/S1063783419020112
9. Ганьшина Е.А., Гаршин В.В., Перова Н.Н., Припеченков И.М., Юрасов А.Н., Яшин М.М., Рыльков В.В., Грановский А.Б. Магнитооптическая керр-спектроскопия нанокомпозитов. *Журнал экспериментальной и теоретической физики*. 2023;164(4):662–672. https://doi.org/10.31857/S0044451023100188
10. Юрасов А.Н., Яшин М.М. Методы эффективной среды как оптимальные методы моделирования физических свойств наноструктур. *Российский технологический журнал*. 2020;8(5):68–77. https://doi.org/10.32362/2500-316X-2020-8-5-68-77
11. Алешников А.А., Калинин Ю.Е., Ситников А.В., Федосов А.Г. Магнитные свойства многослойных структур на основе нанокомпозитов $(Co_{45}Fe_{45}Zr_{10})_x(Al_2O_3)_{100-x}$. *Перспективные материалы*. 2012;5:68–75.
12. Sitnikov A.V., Makagonov V.A., Kalinin Y.E., Kushchev S.B., Foshin V.A., Perova N.N., Ganshina E.A., Granovsky A.B. Magnetic, magnetoresistive and structural properties of $Co_x(CoO)_{100-x}$ thin film composites. *J. Magn. Magn. Mater.* 2023;587(39):171154. https://doi.org/10.1016/j.jmmm.2023.171154
13. Фадеев Е.А., Блинов М.И., Гаршин В.В., Тарасова О.С., Ганьшина Е.А., Прудникова М.В., Прудников В.Н., Ляхдеранта Э., Рыльков В.В., Грановский А.Б. Магнитные свойства нанокомпозитов $(Co_{40}Fe_{40}B_{20})_x(SiO_2)_{100-x}$ вблизи порога перколяции. *Известия Российской академии наук. Серия физическая.* 2019;83(7):917–920. https://doi.org/10.1134/S0367676519070159
14. Михайловский Ю.О., Меттус Д.Е., Казаков А.П., Прудников В.Н., Калинин Ю.Е., Ситников А.С., Гербер А., Бартов Д., Грановский А.Б. Аномальный эффект холла в нанокомпозитах $(Co_{41}Fe_{39}B_{20})_x(Al–O)_{100-x}$. *Письма в Журнал экспериментальной и теоретической физики.* 2013;97(7–8):544–548.
15. Manoharan S.S., Elefant D., Reiss G., Goodenough J.B. Extrinsic giant magne-toresistance in chromium (IV) oxide, CrO_2. *Appl. Phys. Lett*. 1998;72(8):984–986. https://doi.org/10.1063/1.120616

About the authors

Maxim M. Yashin, Cand. Sci. (Phys.–Math.), Associate Professor, Department of Nanoelectronics, Institute for Advanced Technologies and Industrial Programming, MIREA – Russian Technological University (78, Vernadskogo pr., Moscow, 119454 Russia). E-mail: yashin@mirea.ru. ResearcherID G-6809-2017, Scopus Author ID 57210607470, RSCI SPIN-code 2438-6135, https://orcid.org/0000-0001-8022-9355

Vitaly E. Ryabukhin, Student, Institute for Advanced Technologies and Industrial Programming, MIREA – Russian Technological University (78, Vernadskogo pr., Moscow, 119454 Russia). E-mail: vitas900@gmail.com. https://orcid.org/0009-0001-0421-4845

Alexey N. Yurasov, Dr. Sci. (Phys.-Math.), Professor, Department of Nanoelectronics, Institute for Advanced Technologies and Industrial Programming, MIREA – Russian Technological University (78, Vernadskogo pr., Moscow, 119454 Russia). E-mail: alexey_yurasov@mail.ru, ResearcherID M-3113-2016, Scopus Author ID 6602974416, RSCI SPIN-code 4259-8885, https://orcid.org/0000-0002-9104-3529

Об авторах

Яшин Максим Михайлович, к.ф.-м.н., доцент, кафедра наноэлектроники, Институт перспективных технологий и индустриального программирования, ФГБОУ ВО «МИРЭА – Российский технологический университет» (119454, Россия, Москва, пр-т Вернадского, д. 78). E-mail: yashin@mirea.ru. ResearcherID G-6809-2017, Scopus Author ID 57210607470, SPIN-код РИНЦ 2438-6135, https://orcid.org/0000-0001-8022-9355

Рябухин Виталий Евгеньевич, магистрант, Институт перспективных технологий и индустриального программирования, ФГБОУ ВО «МИРЭА – Российский технологический университет» (119454, Россия, Москва, пр-т Вернадского, д. 78). E-mail: vitas900@gmail.com. https://orcid.org/0009-0001-0421-4845

Юрасов Алексей Николаевич, д.ф.-м.н., профессор, профессор кафедры наноэлектроники, Институт перспективных технологий и индустриального программирования, ФГБОУ ВО «МИРЭА – Российский технологический университет» (119454, Россия, Москва, пр-т Вернадского, д. 78). E-mail: alexey_yurasov@mail.ru. ResearcherID M-3113-2016, Scopus Author ID 6602974416, SPIN-код РИНЦ 4259-8885, https://orcid.org/0000-0002-9104-3529

Translated from Russian into English by K. Nazarov
Edited for English language and spelling by Dr. David Mossop

Analytical instrument engineering and technology

Аналитическое приборостроение и технологии

UDC 53.082.52+621.391.822
https://doi.org/10.32362/2500-316X-2025-13-1-122-135
EDN OABDBH

RESEARCH ARTICLE

Noise properties of preamplifier to be used with LN_2-cooled HgCdTe photodetector

Dmitry V. Kazantsev [1, 2, @], Elena A. Kazantseva [3]

[1] *P.N. Lebedev Physical Institute, Russian Academy of Sciences, Moscow, 119991 Russia*
[2] *HSE – Higher School of Economy, Moscow, 101000 Russia*
[3] *MIREA – Russian Technological University, Moscow, 119454 Russia*
[@] *Corresponding author, e-mail: kaza@itep.ru*

Abstract

Objectives. Photoresistors based on a solid solution of mercury–cadmium–tellurium (MCT) have been used in infrared (IR) technology for over 60 years. They can have a sensitivity range in the wavelength region from 1 μm to 15 μm, depending on $Hg_{1-x}Cd_xTe$ composition. The resistance of photosensitive MCT elements is (depending on their area) tens of Ohms, and for such a resistor the thermodynamically expected Nyquist noise is less than $1\ nV/\sqrt{Hz}$. Modern semiconductor technologies ensure a high level of quality of both photodetectors and input stages of integrated circuits for amplifying the signal from them. The aim of this work is to study the noise properties of the electronic unit developed for joint operation with a liquid nitrogen cooled MCT-photodetector.

Methods. An analog input-output digital signal processor card P25M (Innovative, Inc., USA) was used to measure and accumulate the noise spectra of the signal in the frequency range 0–1 MHz. The card has four 16-bit ADCs of sampling rate up to 25MSpS, a Spartan-3 field-programmable gate array controlling them, a TMS320C6713 processor, and RAM, in order to transmit the collected digital data to the motherboard through a common PCI-X slot. The spectra of the received data were calculated using the fast Fourier transform algorithm with subsequent averaging of the square of the amplitude for all spectral components.

Results. The noise properties of comparatively modern integrated circuits currently used for this task were considered. The noise density spectra of the first stage (ADA4898-2), the second stage (AD8034), and bias current sources (AD8397 and LT3009) were measured. It was found that the spectral density of the input noise of the operational amplifier ADA4898-2 is comparable to the Nyquist (thermodynamically expected) noise of a 20–100-Ohm resistor corresponding to the resistance of the photosensitive element. This means that the selected operational amplifier is ideal for resolving the technical problem discussed herein. Meanwhile, it was also established that the noise spectrum of the LT3009, ADR510 voltage and current stabilizer integrated circuits contains a noticeable drift component with a spectral density of "pink noise" $1/f^{\alpha}$ (f – frequency, $\alpha \approx 1$).

Conclusions. It was shown that the spectral noise density of the electronic components, reduced to the input of the device, is several times lower than the noise density of the photodetector used.

Keywords: IR-photodetector, MCT-photodetector, low-noise electronics, input stages, analog electronics

• **Submitted:** 19.02.2024 • **Revised:** 09.09.2024 • **Accepted:** 28.11.2024

For citation: Kazantsev D.V., Kazantseva E.A. Noise properties of preamplifier to be used with LN_2-cooled HgCdTe photodetector. *Russian Technological Journal.* 2025;13(1):122–135. https://doi.org/10.32362/2500-316X-2025-13-1-122-135, https://elibrary.ru/OABDBH

Financial disclosure: The authors have no financial or proprietary interest in any material or method mentioned.

The authors declare no conflicts of interest.

НАУЧНАЯ СТАТЬЯ

Шумовые свойства предварительного усилителя для инфракрасного фотоприемника на основе HgCdTe

Д.В. Казанцев [1, 2, @], Е.А. Казанцева [3]

[1] *ФИАН – Физический институт им. П.Н. Лебедева РАН, Москва, 119991 Россия*
[2] *НИУ ВШЭ – Высшая школа экономики, Москва, 101000 Россия*
[3] *МИРЭА – Российский технологический университет, Москва, 119454 Россия*
[@] *Автор для переписки, e-mail: kaza@itep.ru*

Резюме

Цели. Фоторезисторы на основе твердого раствора кадмий-ртуть-теллур (КРТ) применяются в инфракрасной (ИК) технике более 60 лет и в зависимости от композиции $Hg_{1-x}Cd_xTe$ имеют диапазон чувствительности в области длин волн от 1 до 15 мкм. Сопротивление светочувствительных КРТ-элементов составляет (в зависимости от площади) десятки Ом, и термодинамически ожидаемый шум Найквиста составляет менее $1\,нВ/\sqrt{Гц}$ для такого резистора. Современные полупроводниковые технологии обеспечивают высокое качество как фотоприемных устройств, так и входных каскадов микросхем для усиления сигнала с них. Целью работы является исследование шумовых свойств разработанного электронного блока, предназначенного для совместной работы с КРТ-фотоприемником, охлаждаемым жидким азотом.

Методы. Для измерения и накопления шумовых спектров сигнала в диапазоне частот 0–1 МГц использована микропроцессорная плата аналогового ввода-вывода P25M производства Innovative, Inc. (США). Плата, на которой имеются четыре 16-битовых аналого-цифровых преобразователя с частотой до 25 МГц, управляющая ими программируемая логическая интегральная схема Spartan-3, процессор TMS320C6713 и оперативная память, передает собранные цифровые данные в материнскую плату через общий для них слот PCI-X. Спектры принятых данных вычислялись с помощью алгоритма быстрого преобразования Фурье с последующим усреднением квадрата амплитуды для всех спектральных составляющих.

Результаты. Измерены спектры плотности шума первого каскада (ADA4898-2), второго каскада (AD8034) и источников тока смещения (AD8397 и LT3009). Обнаружено, что спектральная плотность шумов входа операционного усилителя ADA4898-2 сравнима с найквистовым (термодинамически ожидаемым) шумом резистора 20–100 Ом, соответствующего сопротивлению светочувствительного элемента. Это означает, что выбранный операционный усилитель идеально подходит для решения обсуждаемой технической задачи. Обнаружено также, что спектр шумов микросхем стабилизаторов напряжения и тока LT3009, ADR510 содержит заметную дрейфовую составляющую со спектральной плотностью вида $1/f^{\alpha}$ (f – частота, $\alpha \approx 1$).

Выводы. Показано, что спектральная плотность шумов электронных компонентов, приведенная ко входу устройства, в несколько раз ниже плотности шумов использованного фотоприемника.

Ключевые слова: ИК-фотоприемник, КРТ-приемник, малошумящая аппаратура, входные каскады, аналоговая электроника

• **Поступила:** 19.02.2024 • **Доработана:** 09.09.2024 • **Принята к опубликованию:** 28.11.2024

Для цитирования: Казанцев Д.В., Казанцева Е.А. Шумовые свойства предварительного усилителя для инфракрасного фотоприемника на основе HgCdTe. *Russian Technological Journal.* 2025;13(1):122–135. https://doi.org/10.32362/2500-316X-2025-13-1-122-135, https://elibrary.ru/OABDBH

Прозрачность финансовой деятельности: Авторы не имеют финансовой заинтересованности в представленных материалах или методах.

Авторы заявляют об отсутствии конфликта интересов.

INTRODUCTION

The aim of this paper is to investigate noise properties of an electronic unit designed and manufactured with the intent for joint operation with a liquid nitrogen (LN_2) cooled infrared (IR) photodetector based on mercury–cadmium–tellurium (MCT) solid solution, as well as noise properties of such photodetector on the whole.

$Hg_{1-x}Cd_xTe$-based photodetectors [1–5] are widely used for receiving optical signals in the mid-IR range. The bandgap in this semiconductor depends on the cadmium fraction [6]. The first study [7] stated a bandgap to be 95 mV (13 μm), although it could be less, depending on the proportions of cadmium and tellurium in the crystal. Optical measurements of the absorption band edge [8, 9] along with magnetoresistance measurements [10, 11] determine that with increasing cadmium fraction x in the $Hg_{1-x}Cd_xTe$ solid solution, the curve of the bandgap dependence crosses zero. This is due to the valence zone and conduction zone swapping their positions in the energy diagram.

Industry is currently pursuing the development of IR photodetectors based on new principles. Success has been achieved in the formation of heterostructures of wide-bandgap semiconductors in which the small energy of the working optical transition corresponding to the value of the received light quantum is determined by the difference in the subband position of neighboring layers [12, 13]. Success has been reported in the use of graphene [14] and superconducting [15] structures to receive long-wavelength (low-energy) light quanta. Nevertheless, photoresistive IR detectors (especially for using in single-channel photodetectors) are still in demand due to their simplicity, manufacturability, and decades of proven functionality.

Although the theoretical detectivity D^* of an ideal photodiode should be two times greater than that of the ideal photoresistor [16], photodetectors with photoresistive detection of the IR light falling on them are much more widespread. The occupation of energy levels in a semiconductor obeys the Fermi distribution, as follows:

$$N(E) = N_0(E)\frac{1}{e^{\frac{E-E_F}{kT}}+1}, \quad (1)$$

wherein E stands for the electron level energy; $N(E)$ is the number of actually populated states with such energy; $N_0(E)$ is the number of states with energy E that are suitable in principle as wave functions in a semiconductor crystal; and E_F is the Fermi level position in the distribution. The scale blurring the population step corresponds to temperature potential φ_T:

$$\varphi_T = \frac{kT}{e^-}. \quad (2)$$

Here, T is the temperature in Kelvins, k is Boltzmann constant, and e^- is the electron charge. This temperature potential is 26 mV at room temperature (20°C). This means that the number of thermodynamically excited electrons and holes at room temperature would be approximately $e^{-\frac{50\text{ mV}}{26\text{ mV}}} = 2.71^{-2} = 0.13$ of the total number of states (approximately 10^{23} pcs/cm^3), and the contribution of optically excited electron–hole pairs would be negligible compared to that. To reduce such a thermal generation of the electron-hole pairs, narrow-bandgap semiconductor photodetectors should be cooled. Satisfactory results are obtained at the liquid nitrogen temperature T = 77 K; the argument of the exponent then increases 300 K / 77 K = 3.89 times while the exponent itself increases 1795 times.

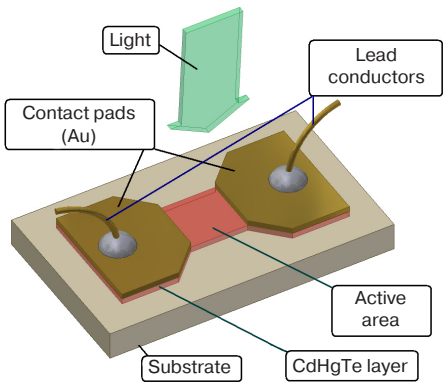

Fig. 1. $Hg_{1-x}Cd_xTe$-based photodetectors photodetector placed on a substrate[1]

[1] The idea for the composition of a drawing is taken from the booklet "Mercury Cadmium Telluride Detectors." Teledyne Judson Technologies. http://www.judsontechnologies.com/mercadm_pc.html. Accessed January 31, 2022.

When $Hg_{1-x}Cd_xTe$ is used in the photoconductive mode, the current is applied to the semiconductor crystal from the sides (Fig. 1). The semiconductor material is deposited on a non-conductive substrate. The active photosensitive area is located between conductive (e.g., gold) contacts sputtered on the surface of the semiconductor layer and its size is typically 50–1000 μm. The object of measurement is the voltage drop across such a photoresistor. It is natural to expect that the variations of the bias current ΔI_{bias} multiplied by resistance R_{det} of the photoresistor (see Fig. 2) turn into voltage variations $\Delta U_{det} = \Delta I_{bias} R_{det}$ at the output of the circuit.

A circuit in which a certain voltage is applied to the photoresistor (Fig. 2a) and in which the object of measurement is the resulting photoconductive current, is practically not used. In many cases the semiconductor photosensitive strip is placed in a nitrogen cryostat on a cold finger with one end of this strip grounded, in such a way that this scheme is not applicable from the engineering point of view. The connection scheme (Fig. 2b) in which a stabilized current is applied to the MCT-photoresistor and the object of measurement is the resulting voltage at the ends of the photosensitive strip is quite feasible. It provides a high linearity of response. However, supplying a well stabilized current is quite complex from the engineering point of view and requires some additional radio components. The most commonly used application circuit is shown in Fig. 2c, where the bias current source for the photoresistor is a fairly large resistor connected to a stable voltage source at the other end. At the midpoint of the voltage divider formed by photoresistor R_{det} and resistor R_{bias}, a voltage is formed which depends on photoresistor illumination.

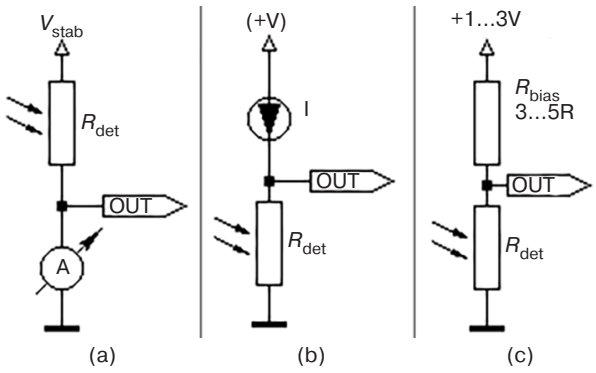

Fig. 2. Current-measuring photoresistor connection circuit (a), bias supply circuit from current generator (b), and conventional connection circuit[2] of the $Hg_{1-x}Cd_xTe$-based photoresistor (c)

These methods of obtaining an electrical signal (response to optical radiation) have been available for more than 60 years. A number of studies have been devoted to investigating the noise of the photodetector itself. In particular, it was stated that the component of the $1/f^{\alpha}$ type (f is frequency, $\alpha \approx 1$) is noticeable in the noise spectrum [17].

Noises with a spectral density of the $1/f^{\alpha}$ type must also be considered. As a radiophysical phenomenon, this noise was apparently first discovered by Johnson [18] when studying the noise spectrum of a tube triode. Schottky named it 'flicker noise' providing the radiophysical explanation [19] that the emissivity of different parts of a glowing cathode undergoes constant chaotic changes, which then persist for a long time. However, it was discovered during the 20th century that a huge number of processes, such as the coordinate of a particle in Brownian motion [20], heartbeat parameters, the radio broadcast signal of music or news [21], the annual flow of the Nile, the sea level, etc., have a noise spectrum of the $1/f^{\alpha}$ type. Many reviews [22, 23] and textbooks [24], have been written on this subject. Radiophysicists [25] also still address this topic. In all cases, the dependence of spectral-noise density $\langle U_N^2 \rangle$ on frequency is of the $\langle U_N^2 \rangle \sim 1/f^{\alpha}$ -type, where the index of power $\alpha \sim 0.5 \ldots 1.5$ is approximately 1.

Meanwhile, the quality of photosensitive semiconductors, as well as technological capabilities of the electronic components used, have been growing over recent years. The noise level (depending on the value of the band gap in the MCT crystal used) has already approached the fundamental limit set in statistical physics by the Nyquist formula:

$$\langle U_N^2 \rangle = 4kTR_{det}\Delta f \text{ (in the frequency band } \Delta f), \quad (3)$$

based on the value of the ohmic resistance of the photoresistor. Substituting the values of Boltzmann constant, $k = 1.38 \cdot 10^{-23}$ J/K, resistance, $R_{det} = 50$ Ohm, and temperature, $T = 77$ K, spectral-noise density $0.46\ \text{nV}/\sqrt{\text{Hz}}$ is expected. The noise level of modern operational amplifiers (OpAmps) is of the same order of magnitude as that of a 50-Ohm resistor. For example, $0.9\ \text{nV}/\sqrt{\text{Hz}}$ for the ADA4898-2 chip[3].

The time constant for J15Dxx photodetectors manufactured by Teledyne Judson Technologies (USA) ranges from 0.1 to 0.5 μs, depending on the area and size of the photosensitive element. It is reasonable to assume a gain bandwidth of 5–10 MHz from the preamplifier, in order to fully utilize frequency capabilities of the

[2] PB212. J15D Series. Operating Instructions. Teledyne Judson Technologies. https://www.teledynejudson.com/prods/Documents/PB212.pdf. Accessed January 31, 2022.

[3] https://www.analog.com/ADA4898-2/datasheet. Accessed January 31, 2022.

photoresistor. This requires searching for models with a unit gain frequency ($G = 1$) $f_{G=1}$ greater than 50 MHz in the OpAmp list. Modern manufacturers have such models. For example, the lowest noise model ADA4898-2 from the spreadsheet offered to developers by Analog Devices[4] has a cutoff frequency of $f_{G=1}$ = 65 MHz.

METHODS

Connection circuit for photodetector and amplifying electronics

In this paper, the J15D12-M204-100u MCT-photodetector (Teledyne Judson Technologies) mounted in a liquid nitrogen-filled M204 Dewar vessel is used as a photodetector. This photodetector is mainly designed for CO_2-laser operation and is used to detect the weak optical wave scattered by the probing tip in the ASNOM scanning microscope [26–28] manufactured by NT-MDT-SI (Zelenograd, Russia). The electrical signal is fed from the photodetector to the input of an electronic circuit (Fig. 3), described in basic terms in [29]. The first stage is implemented on a low-noise ADA4898-2 OpAmp. Feedback resistors set a gain of 40 to the stage. The second stage is mounted on the board in two versions: based on DA3A OpAmp with a gain of 50 (approximately equal values allow achieving the width of the flat amplitude-frequency response (AFR) of two consecutive stages with unity gain frequency $f_{G=1}$ = 65 MHz of each stage OpAmp), and based on DA3B OpAmp with a gain of 5 which can be sometimes used for a large value of the optical signal. The bias current required for the photoresistor operation (see Fig. 2c) is supplied through resistor R_{bias} from the output of the regulated voltage source DA1.

The board also provides another source of a stabilized current for measuring the temperature of a cold finger in a cryostat carrying a photoresistor. A semiconductor diode is installed on the cold finger in the Dewar vessel next to the photoresistor, and the voltage drop across it is determined by the Shockley formula [30]:

$$I_D(U_D) = I_0\left(\exp\left(\frac{U_D e^-}{kT}\right) - 1\right) \approx I_0 \exp\left(\frac{U_D e^-}{kT}\right).$$

Thus, the voltage across diode U_D at the given current I_D is proportional to the temperature. The measurement (by the voltage drop across resistor R39) and stabilization of the bias current is carried out using the DA4B OpAmp, while the "ideal" voltage for it is formed by the DA5 ADR510 "Zener diode" (integrated circuit[5]).

In order to measure the bias current supplied to the photoresistor when setting the electronics, the board provides sockets into which resistor R_{meas} can be inserted instead of the cable disconnected from the photodetector at that time.

The analog input measuring microprocessor board

In order to record the noise spectra of the photodetector and signal preamplifier, an analog I/O microprocessor board P25M manufactured by Innovative, Inc., USA, is used [31]. The board contains 4 channels of analog-to-digital converter (ADC), 4 channels of digital-to-analog converter (16 bits, digitization frequency of both is up to 25 MHz), Spartan-3 field-programmable gate array integrated circuit (FPGA) controlling them, a TMS320C6713 processor, and RAM. The FPGA logic provides a very precise setting of the input voltage digitization frequency (digital frequency divider followed by phase lock loop circuitry for a precise sampling frequency setting and control for an ADC). Before starting the measurement, the ADC sampling frequency, the length of the ADC sampling frame, acquisition frame triggering mode, and some other parameters should be loaded into the FPGA logic. After the frame acquisition is started, no additional intervention from the TMS320C6713 processor of the P25M board is required. Several thousand ADC sampling values as an array of 16-bit integers are first received in a direct memory access mode into a RAM of P25M board in its address space. After data array is received by P25M board from its FPGA logic driving ADC, the board's CPU transfers this data through a common PCI-X slot to the motherboard of a *Windows*-based computer. Such way of an ADC operation ensures that all ADC sampling events are perfectly spaced on the time scale. In this respect, the input signal spectrum calculated from such data can be considered as reliable.

Processing the spectrum data thus obtained

The ADC data frame received from the measurement board is processed in a computer using C++ language. The basis for the spectrum calculation is the Fast Fourier Transform algorithm [32, 33]. The direct Fourier transform is calculated from the data array received from the I/O board. The data is converted from the original short (int16) format into the floating-point *double* format, where these actual values correspond to the input voltage

[4] https://www.analog.com. Accessed January 31, 2022.

[5] https://www.analog.com/ADR510/datasheet. Accessed January 31, 2022.

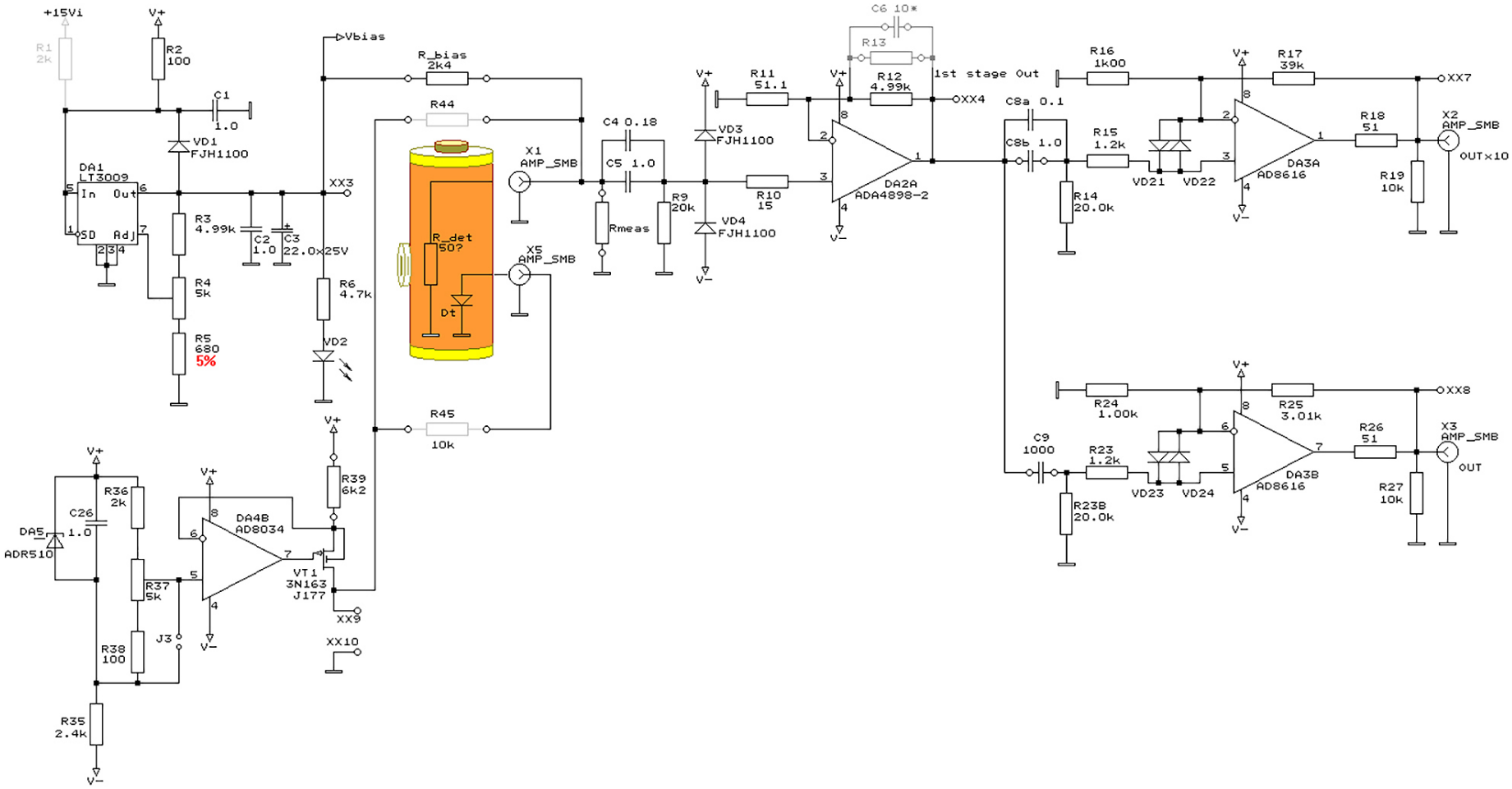

Fig. 3. Circuit diagram of the preamplifier board intended for joint operation with HgCdTe photodetector operating in the mid-infrared range. Designations are partially given in accordance with GOST 2.710-81[6]

[6] GOST 2.710-81. Interstate standard. *Unified system for design documentation. Alpha-numerical designations in electrical diagrams*. Moscow: Standardinform; 2008 (in Russ.).

in volts. The ADC sampling frequency and the duration of the data frame are known to the program. They are stored into the class data fields, whereas the calculations on the 'time axis' are performed in dimensionless form. This ensures the accuracy of transformations, after verifying for different lengths of the data array that the amplitudes of spectral components remain unchanged, that Parseval's theorem is always fulfilled (the sum of squares of harmonics "on the frequency scale" must be equal to the sum of squares of samples "on the time scale"), and that the magnitude of spectral components is independent of the sampling frequency. Additionally, in order to meet these requirements, the obtained harmonic values should be normalized by the square root of the data array working length.

After the spectral components have been calculated, the square of their complex magnitude is averaged. The mean value of the amplitude of any harmonic (probably, except zero) tends to zero when averaging a chaotic signal, while the mean square naturally tends to the mean noise level in this spectrum region. The invariability of the limit to which the mean squares of spectral component amplitudes tend with increasing number of acquisition attempts to average the spectra, as well as the independence of the result from the number of partition points and from the ADC response frequency, are convincing proof that the method for accumulating and averaging data has been chosen correctly.

At the user's command, the accumulated data displayed on the virtual display during measurement can be exported to hard disk drive as ASCII-text. In this spreadsheet, the first column contains the number of the spectral point, the second column contains the frequency of the spectral component, and the third column contains its RMS amplitude. When exported, the data is normalized by the square root of the spectrum width taken from the known sampling frequency of the acquired data.

RESULTS

ADC input noise spectrum

Before measuring the parameters of the amplifier considered herein, it is necessary to ensure that the P25M analog I/O board as a measuring device introduces little noise and distortion into the measured signal itself. The noise spectra obtained from an empty (unconnected) ADC input are shown in Fig. 4. According to the figure, the spectral density of the noise introduced by the measuring device does not depend on the frequency. The level of spectral density of the input noise of the measurement board (about $1.4\,\mathrm{nV}/\sqrt{\mathrm{Hz}}$) matches the predictions of expression (3) quite well at its input impedance of $50\ \mathrm{Ohm}$. It should be noted that the preamplifier at the ADC input allows software gain setting (variants {GND, ±200 mV, ±1 V, ±2.5 V} for acceptable signal ranges) before starting measurements. The noise level at wide input signal range (the range of measured input signal values is ±2.5 V), i.e., at moderate gain to the ADC input, is noticeably higher (Fig. 4) than the noise in the high gain mode at the measuring board input (the input signal range is ±200 mV).

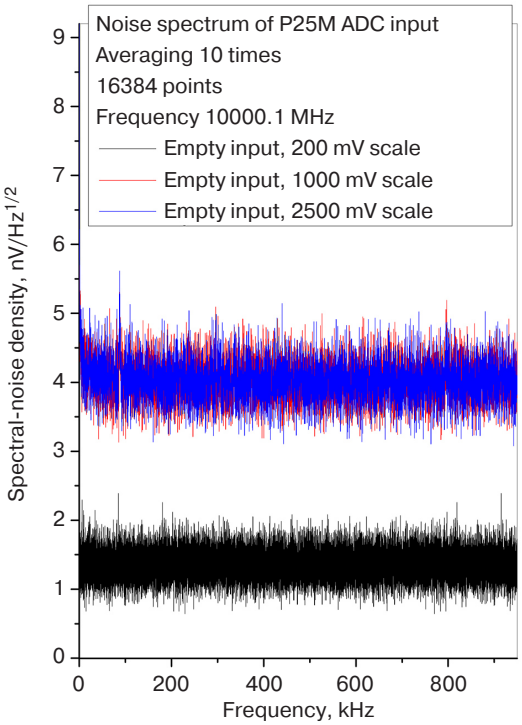

Fig. 4. Noise spectra recorded from the unconnected ADC0 input of the measuring ADC, obtained at different scales of its input scale

The dependencies of the spectral-noise density on frequency recorded for the output signal of the investigated board are shown in Fig. 5. The spectral density curves are recalculated to the circuit input by dividing by gain, $G_{\mathrm{OUT}\times 1} = 200$, for the data obtained from the output of the low gain channel, OUT × 1, and by gain, $G_{\mathrm{OUT}\times 10} = 2000$, for the data obtained from the output of the high gain channel, OUT × 10. The magnitude of the spectral-noise density is also some $\mathrm{nV}/\sqrt{\mathrm{Hz}}$ for this case. The role of the second stage is noticeably reduced at high gain of $G_{\mathrm{OUT}\times 10} = 2000$. The spectral-noise density curve for the noise introduced by the measurement board (Fig. 4) is placed next to the noise curves of the preamplifier board shown in Fig. 5. For visual compatibility of the curves in a single figure, this data (Fig. 4) is divided by gain, $G_{\mathrm{OUT}\times 1} = 200$, corresponding to the lower of the two possible values used to convert the noise density measured at the output to the input of the considered amplifier. Fig. 5 clearly shows that, taking into account the high gain of the investigated circuit, the role of noise of the input stages of the P25M measuring board is negligible, even if the

measured root mean square (RMS) value of the noise signal at the unconnected ADC input is divided by a relatively small number of $G_{OUT \times 1} = 200$.

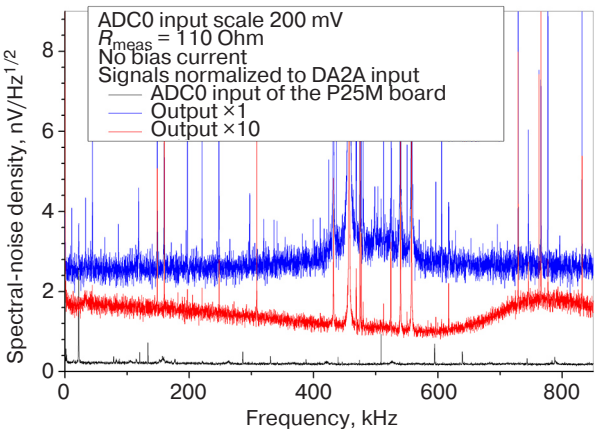

Fig. 5. Spectral-noise density curves recorded from the board output ×1 (total gain 200), output ×10 (total gain 2000), and unconnected ADC0 input of the measuring ADC

Dependence of input noise on the input resistor value

In order to check whether the recorded spectra of the amplifier input noise are a physical phenomenon or an artefact of the software algorithm, the dependence of the spectral-noise density reduced to the input on resistance value R_{meas} of resistor connecting the input to the board ground is measured (Fig. 6).

The spectral density of the signal collected using ADC is divided by the gain of two stages: $G_{OUT \times 10} = 40 \times 50 = 2000$, for the gain channel with output to connector OUT × 10. In general, the noise level scale of $(0.8...5)\,\mathrm{nV}/\sqrt{\mathrm{Hz}}$ is consistent with the value given in the ADA4898-2 datasheet[7] $(0.9\,\mathrm{nV}/\sqrt{\mathrm{Hz}})$. The graph shows that the spectral-noise density is far from the imaginary ideal. There are many sharp lines in the laboratory ether spectrum corresponding, apparently, to the operation of numerous switching power supplies. In addition, the noise spectral density is not a flat curve on average, since the noise level is somewhat higher at low frequencies. This is most likely due to chaotic shifts of the average bias level of the input radio components (flicker noise) with its characteristic spectrum of $1/f^{\alpha}$.

Nevertheless, the measured noise level corresponds well to the dependence of the noise density on the signal source resistance (resistor R_{meas}) as expected from the Nyquist formula (3), shown in Fig. 6b. The recorded noise density at frequencies above 700–1000 kHz is even slightly lower for resistors with resistance greater than 1 kOhm compared to predictions of statistical physics. However, this noise density is obtained by dividing the output signal by the gain of two consecutive stages (by 2000), whereas the amplifier's AFC starts decreasing at 800–1000 kHz. The gain of each stage is set by feedback resistors is about 50. For OpAmps with a unity gain frequency of $f_T \approx 50$–60 MHz used in the paper, this value is quite a challenge in the frequency range of 1 MHz or higher. This means that the graphs for the noise density below the Nyquist level shown in Fig. 6 are just an illusion in the frequency region of 1500 kHz.

[7] https://www.analog.com/ADA4898-2/datasheet. Accessed January 31, 2022.

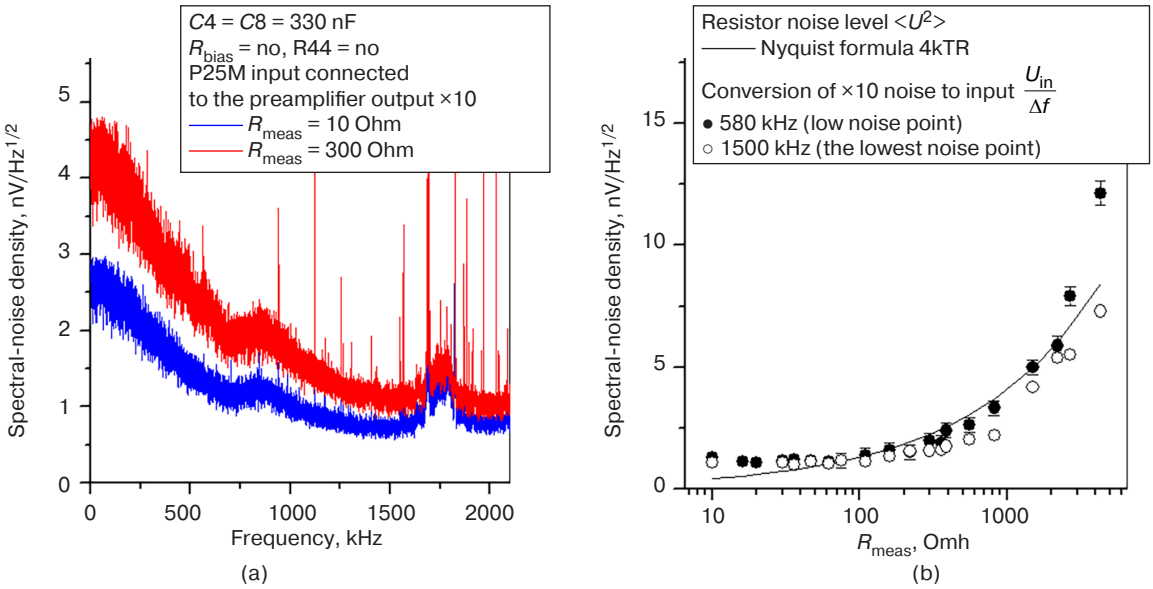

Fig. 6. (a) Spectral-noise density measured at a sampling frequency of 4 MHz when the input is connected to ground through resistor R_{meas} = 10 Ohm; (b) dependence of noise density in "quiet" areas on the resistor resistance R_{meas}. For comparison, the curve is plotted using the Nyquist formula

Input noise level when operating from the bias resistor

Figure 7 shows the noise signal spectrum measured when bias current is applied through resistor R_{bias} = 820 Ohm from the adjustable reference voltage source DA1 LT3009. As a load for the bias current, resistor R_{bias} = 110 Ohm (component designations are given in Fig. 3) is used instead of a photodetector. At such connection, the $1/f^{\alpha}$-type noise introduced by the LT3009 bias voltage generator, V_{bias}, starts dominating in the spectrum at frequencies up to 200 kHz.

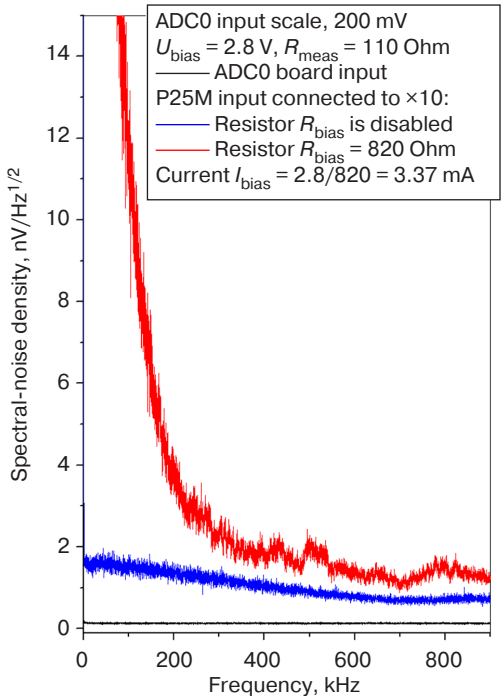

Fig. 7. Noise spectra recorded when bias current is applied through resistor R_{bias} = 820 Ohm from stabilized voltage V_{bias} = 2.8 V

It is not surprising that the noise level with a spectrum of the $1/f^{\alpha}$ type in the voltage stabilized by the LT3009 chip is noticeably higher when compared to the white Nyquist noise of the input resistor R_{meas} and the first stage of the selected (in terms of noise) ADA4898-2 OpAmp model. The datasheet[8] for the LT3009 regulated stabilizer chip states that the typical RMS output noise voltage for this model is 150 μV at filter capacitance of $C3$ = 1.0 μF. Integrating the noise level observed in the experiment within the 0–200 kHz range gives approximately this value. The capacitance of the filter capacitor insignificantly assists the stage output voltage to be stabilized at desired low frequencies.

[8] https://www.analog.com/media/en/technical-documentation/data-sheets/3009fd.pdf. Accessed January 31, 2022.

Input noise level when operating from the stabilized current source

The presence of a significant component of the $1/f^{\alpha}$ type in the signal spectrum when using a bias resistor operating from the LT3009 voltage stabilizer prompts the bias current to be supplied from a stable current generator (Fig. 8). The design of the printed circuit board provides this possibility, namely, sockets for installing resistor R44. In such a connection, stabilization of the current flowing through the MCT-photoresistor is carried out by the DA4B chip (Fig. 3), which compares the voltage drop on the current measuring resistor R39 with the voltage on the DA5 "Zener diode" (ADR510 chip). For this measurement, the R39 value is reduced to 620 Ohms.

The noise spectra of the input signal collected with this electronic circuitry configuration (Fig. 8) show that this method of supplying bias current to the photosensitive element of the photodetector provides no gain in the RMS noise level of the hardware recalculated to the input of the device.

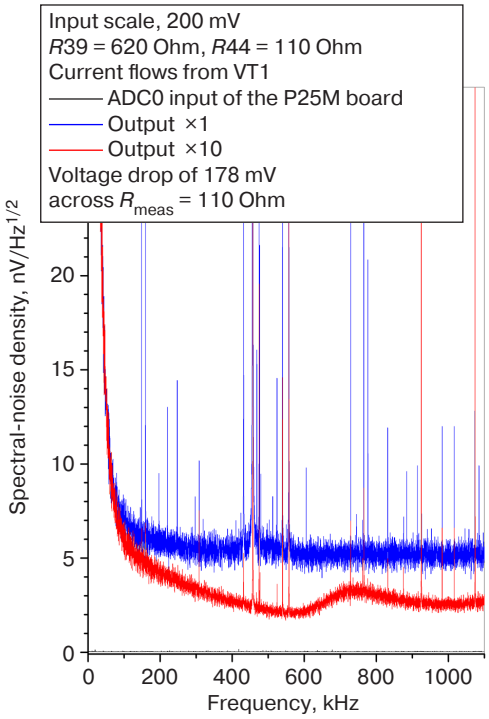

Fig. 8. Noise spectra recorded when bias current is applied through resistor R44

In this case, the noise is determined by noise levels of the AD8034 integrated circuit itself, the ADR510 reference voltage generator, and (last but not least) by leakage through the VT1 gate. Expectations that installing the selected low-noise OpAmp as DA4B should ensure low noise levels are not fulfilled. The main contribution to the appearance of noise comes from the ADR510 "Zener diode" chip; the RMS-average of its

noise is 4 μV in the 0–10 Hz range against a stabilization voltage of 1 V.

Noise spectrum of preamplifier connected to photodetector

Figure 9 shows the noise spectra recorded when the photodetector is connected to the input of the preamplifier being investigated. It should be noted that in our case, the optical sensitivity of the photodetector should be reduced rather than enhanced. In the operating mode, when the 17 mW laser beam at line ν = 934.93 cm^{-1} is fed to the input of the Michelson circuit used to detect the signal scattered by the ASNOM probing tip, the electrical signal should be reduced in such a way that the output stage of the preamplifier and the ADC scale used cannot enter the voltage cut-off mode. Fig. 9 also shows the spectrum of the collected electrical signal over the surface of the crystalline sample at the amplitude of the probe oscillations of 70 nm being normal to the surface. When obtaining this data, the bias current of the MCT-sensor is set to 1.5 mA, instead of 2.5 mA as recommended by the manufacturer for achieving the maximum signal-to-noise ratio (in this case, the photosensitive element had an area of 100 × 100 $μm^2$). For this, the bias is applied to the MCT-sensor from the output of the regulated voltage source DA1 LT3009, V_{bias} = 2.8 V, through resistor R_{bias} = 1.8 kOhm. When measuring the noise spectrum of the real photocurrent (Fig. 9), a photodetector Dewar vessel was filled with liquid nitrogen, in order to ensure the operating temperature. The electrical signal is taken from output ×1 of the preamplifier rather than from output ×10, which (see Fig. 4) corresponds to slightly worse noise properties of the photodetector with the preamplifier compared to using output ×10 of the electronics converted to the circuit input.

According to Fig. 9 (middle curve), the intrinsic noise level of the photodetector recalculated to the preamplifier input exceeds the measured noise levels of the investigated circuit input by 3–5 times (for comparison, the lower curve in Fig. 9 contains the spectrum of input noise of the preamplifier for the case when the photodetector is replaced by the 11-Ohm resistor). In practical terms, this means that further attempts to reduce the noise level are meaningless. The spectrum of the optical signal collected in the ASNOM operating mode (amplitude of normal tip oscillations is 70 nm, frequency is 55 kHz, and sample is SiC) is presented in the upper graph (Fig. 9). As can be seen, the region of the increased noise of the $1/f^{\alpha}$ type introduced by the voltage sources used in the circuit design ends already by the frequency of the second (110 kHz) and the higher harmonics of the "tip–surface distance" modulation frequency (165 kHz, 220 kHz...). These appear to be useful for the experimenter within the

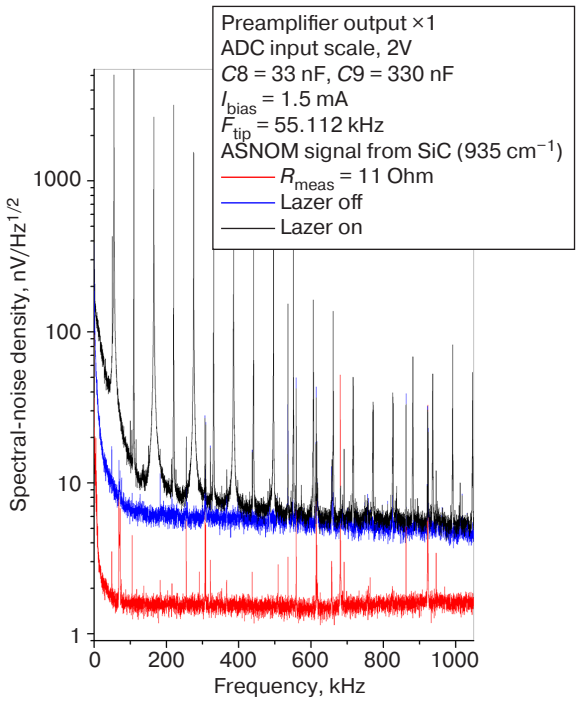

Fig. 9. Noise spectra recorded when the nitrogen-cooled MCT-photodetector is connected to the investigated amplifier. F_{tip} is the cantilever oscillation frequency

ASNOM technique. At the same time, it can be stated that the noise with the $1/f^{\alpha}$-type spectrum introduced by the MCT-photodetector itself considerably exceeds the noise level of chips used in the experiment in the frequency range up to 100 kHz.

CONCLUSIONS

Using low-noise ADA4898-2 OpAmps in the first stage of a preamplifier circuit designed for operation with the MCT-photodetector with an active element area of 100 × 100 $μm^2$ allows a spectral-noise density lower than $1\,nV/\sqrt{Hz}$ to be obtained, and recalculated to its input within the frequency range of 0–1 MHz. However, it was found that when forming the bias current through the resistor according to the scheme conventional for MCT-photodetectors, the LT3009 chip used as a source of the regulated reference voltage introduces the $1/f^{\alpha}$-type noise, noticeable at frequencies up to 100 kHz. The source of the current on a MOS-transistor[9] using the ADR510 "Zener diode" as an "ideal" voltage and not very low-noise AD8034 as a current regulator also introduces the $1/f^{\alpha}$-type noise, noticeable within the range up to 150–200 kHz. Furthermore, the measured noise spectrum of the photodetector itself in the operating mode (at liquid nitrogen temperature) has a typical amplitude of $5\,nV/\sqrt{Hz}$. The operating frequencies, at which the

[9] MOS—metal-oxide semiconductor.

measurements should be carried out in further experiments, are harmonics of the frequency of the ASNOM cantilever mechanical oscillations. For the FMG01/Pt cantilever model used in the paper, this frequency amounts to 60–80 kHz, in such a way that the higher harmonic frequencies start at 120 kHz. In practical terms, this means that the observed drift noise of the bias current sources is not crucial. However, the noise properties of the stabilized voltage sources should be considered seriously when designing electronic circuits for joint operation with MCT-photodetectors.

Authors' contribution
All authors equally contributed to the research work.

REFERENCES

1. Norton P. HgCdTe infrared detectors. *Opto-Electron. Rev*. 2002;10(3):159–174.
2. Kopytko M., Rogalski A. New insights into the ultimate performance of HgCdTe photodiodes. *Sensors and Actuators A: Physical.* 2022;339:113511. https://www.doi.org/10.1016/j.sna.2022.113511
3. Józwikowska A., Józwikowski K., Rogalski A. Performance of mercury cadmium telluride photoconductive detectors. *Infrared Phys*. 1991;31(6):543–554. https://www.doi.org/10.1016/0020-0891(91)90141-2
4. Rogalski A. Commentary on the Record-Breaking Performance of Low-Dimensional Solid Photodetectors. *ACS Photonics*. 2023;10(3):647–653. https://www.doi.org/10.1021/acsphotonics.2c01672
5. Kulchitsky N.A., Naumov A.B., Startsev V.V. Cooled IR photodetectors based on cadmium-mercury-tellurium: current status and development prospects. *Elektronika: nauka, tekhnologiya, biznes = Electronics: Science, Technology, Business*. 2020;6(197):114–121 (in Russ.). https://doi.org/10.22184/1992-4178.2020.197.6.114.121
6. Hansen G.L., Schmit J.L., Casselman T.N. Energy gap versus alloy composition and temperature in $Hg_{1-x}Cd_xTe$. *J. App. Phys*. 1982;53(10):7099–7101. https://www.doi.org/10.1063/1.330018
7. Lawson W., Nielsen S., Putley E., Young A. Preparation and properties of HgTe and mixed crystals of HgTe–CdTe. *J. Phys. Chem. Solids*. 1959;9(3–4):325–329. https://www.doi.org/10.1016/0022-3697(59)90110-6
8. Schmit J.L., Stelzer E.L. Temperature and Alloy Compositional Dependences of the Energy Gap of $Hg_{1-x}Cd_xTe$. *J. Appl. Phys*. 1969;40(12):4865–4869. https://www.doi.org/10.1063/1.1657304
9. Scott M.W. Energy Gap in $Hg_{1-x}Cd_xTe$ by Optical Absorption. *J. Appl. Phys*. 1969;40(10):4077–4081. https://www.doi.org/10.1063/1.1657147
10. Elliott C., Melngailis J., Harman T., Kafalas J., Kernan W. Pressure Dependence of the Carrier Concentrations in *p*-Type Alloys of $Hg_{1-x}Cd_xTe$ at 4.2 and 77°K. *Phys. Rev. B*. 1972;5(8):2985. https://www.doi.org/10.1103/PhysRevB.5.2985
11. McCombe B.D., Wagner R.J., Prinz G.A. Far-Infrared Observation of Electric-Dipole-Excited Electron-Spin Resonance in $Hg_{1-x}Cd_xTe$. *Phys. Rev. Lett.* 1970;25(2):87–90. https://www.doi.org/10.1103/PhysRevLett.25.87
12. Xin W., Zhong W., Shi Y., Shi Y., Jing J., Xu T., Guo J., Liu W., Li Y., Liang Z., Xin X., Cheng J., Hu W., Xu H., Liu Y. Low-Dimensional-Materials-Based Photodetectors for Next-Generation Polarized Detection and Imaging. *Adv. Mater*. 2024;36(7):2306772. https://doi.org/10.1002/adma.202306772
13. Xue X., Chen M., Luo Y., Qin T., Tang X., Hao Q. High-operating-temperature mid-infrared photodetectors via quantum dot gradient homojunction. *Light: Sci. Appl*. 2023;12(1):2. https://doi.org/10.1038/s41377-022-01014-0
14. Agarwal H., Nowakowski K., Forrer A., Principi A., Bertini R., Batlle-Porro S., Reserbat-Plantey A., Prasad P., Vistoli L., Watanabe K., Taniguchi T., Bachtold A., Scalari G., Krishna Kumar R., Koppens F.H.L. Ultra-broadband photoconductivity in twisted graphene heterostructures with large responsivity. *Nat. Photon*. 2023;17(12):1047–1053. https://doi.org/10.1038/s41566-023-01291-0
15. Lau J.A., Verma V.B., Schwarzer D., Wodtke A.M. Superconducting single-photon detectors in the mid-infrared for physical chemistry and spectroscopy. *Chem. Soc. Rev*. 2023;52:921–941. https://doi.org/10.1039/d1cs00434d
16. Rogalski A. HgCdTe infrared detector material: history, status and outlook. *Rep. Prog. Phys*. 2005;68(10):2267. http://doi.org/10.1088/0034-4885/68/10/R01
17. Kimchi J., Frederick J.R., Wong T.T.S. Low-frequency noise in photoconductive HgCdTe detectors. *Proc. SPIE*. 1996;2812. 12 p. https://doi.org/10.1117/12.254098
18. Johnson J.B. The Schottky Effect in Low Frequency Circuits. *Phys. Rev*. 1925;26(1):71–85. https://doi.org/10.1103/PhysRev.26.71
19. Schottky W. Small-Shot Effect and Flicker Effect. *Phys. Rev.* 1926;28(1):74–103. https://doi.org/10.1103/PhysRev.28.74
20. Dutta P., Horn P.M. Low-frequency fluctuations in solids: 1/f noise. *Rev. Mod. Phys.* 1981;53(3):497–516. https://doi.org/10.1103/RevModPhys.53.497
21. Voss R.F., Clarke J. 1/f noise in music and speech. *Nature*. 1975;258(5533):317. https://doi.org/10.1038/258317a0
22. Press W.H. Flicker noises in astronomy and elsewhere. *Comments Astrophys*. 1978;7(4):103–119.
23. Milotti E. 1/f noise: a pedagogical review. 2002; *ArXiV_0204033v1.* https://arxiv.org/pdf/physics/0204033
24. Rytov S.M. *Vvedenie v statisticheskuyu radiofiziku. Chast' 1. Sluchainye protsessy* (*Introduction to Statistical Radiophysics. Part 1. Random Processes*). Moscow: Nauka; 1976. 496 p. (in Russ.).
25. Morikawa M., Nakamichi A. A simple model for pink noise from amplitude modulations. *Sci. Rep*. 2023;13(1):8364. https://doi.org/10.1038/s41598-023-34816-2

26. Zenhausern F., O'Boyle M.P., Wickramasinghe H.K. Apertureless near-field optical microscope. *Appl. Phys. Lett*. 1994;65(13):1623–1625. http://doi.org/10.1063/1.112931
27. Zenhausern F., Martin Y., Wickramasinghe H.K. Scanning Interferometric Apertureless Microscopy: Optical Imaging at 10 Angstrom Resolution. *Science*. 1995;269(5227):1083–1085. https://doi.org/10.1126/science.269.5227.1083
28. Keilmann F., Hillenbrand R. Near-Field Microscopy by Elastic Light Scattering from a Tip. *Philos. Trans.: Math., Phys. Eng. Sci.* 2004;362(1817):787–805. https://doi.org/10.1098/rsta.2003.1347
29. Kazantsev D.V., Kazantseva E.A. A Preamplifier for a CdHgTe Photodetector. *Instrum. Exp. Tech.* 2020;63(1):133–138. https://doi.org/10.1134/S0020441220010194
[Original Russian Text: Kazantsev D.V., Kazantseva E.A. A Preamplifier for a CdHgTe Photodetector. *Pribory i tekhnika eksperimenta.* 2020;1:144–150 (in Russ.). https://doi.org/10.31857/S0032816220010218]
30. Shockley W. The Theory of p-n Junctions in Semiconductors and p-n Junction Transistors. *Bell System Tech. J.* 1949;28(3): 435–489. https://doi.org/10.1002/j.1538-7305.1949.tb03645.x
31. Kazantsev D.V., Kazantseva E.A. Digital Detection of Optical Signals in a Near-Optical-Field Microscope. *Instrum. Exp. Tech.* 2022;65(2):273–291. https://doi.org/10.1134/S0020441222020130
[Original Russian Text: Kazantsev D.V., Kazantseva E.A. Digital Detection of Optical Signals in a Near-Optical-Field Microscope. *Pribory i tekhnika eksperimenta.* 2022;2:79–98 (in Russ.). Available from URL: https://sciencejournals.ru/view-article/?j=pribory&y=2022&v=0&n=2&a=Pribory2202014Kazantsev]
32. Cooley J.W., Tukey J.W. An algorithm for the machine calculation of complex Fourier series. *Math. Comp*. 1965;19(90): 297–301. https://doi.org/10.1090/S0025-5718-1965-0178586-1
33. Stephens D.R., Diggins C., Turkanis J., Cogswell J. *C++ Cookbook*. O'Reilly Media, Inc.; 2005. 592 p. ISBN 978-059-600-761-4

СПИСОК ЛИТЕРАТУРЫ

1. Norton P. HgCdTe infrared detectors. *Opto-Electron. Rev*. 2002;10(3):159–174.
2. Kopytko M., Rogalski A. New insights into the ultimate performance of HgCdTe photodiodes. *Sensors and Actuators A: Physical.* 2022;339:113511. https://www.doi.org/10.1016/j.sna.2022.113511
3. Józwikowska A., Józwikowski K., Rogalski A. Performance of mercury cadmium telluride photoconductive detectors. *Infrared Phys*. 1991;31(6):543–554. https://www.doi.org/10.1016/0020-0891(91)90141-2
4. Rogalski A. Commentary on the Record-Breaking Performance of Low-Dimensional Solid Photodetectors. *ACS Photonics*. 2023;10(3):647–653. https://www.doi.org/10.1021/acsphotonics.2c01672
5. Кульчицкий Н.А., Наумов А.Б., Старцев В.В. Охлаждаемые фотоприемные устройства ИК-диапазона на кадмий-ртуть-теллуре: состояние и перспективы развития. *Электроника: наука, технология, бизнес*. 2020;6(197): 114–121. https://doi.org/10.22184/1992-4178.2020.197.6.114.121
6. Hansen G.L., Schmit J.L., Casselman T.N. Energy gap versus alloy composition and temperature in $Hg_{1-x}Cd_xTe$. *J. App. Phys*. 1982;53(10):7099–7101. https://www.doi.org/10.1063/1.330018
7. Lawson W., Nielsen S., Putley E., Young A. Preparation and properties of HgTe and mixed crystals of HgTe–CdTe. *J. Phys. Chem. Solids*. 1959;9(3–4):325–329. https://www.doi.org/10.1016/0022-3697(59)90110-6
8. Schmit J.L., Stelzer E.L. Temperature and Alloy Compositional Dependences of the Energy Gap of $Hg_{1-x}Cd_xTe$. *J. Appl. Phys*. 1969;40(12):4865–4869. https://www.doi.org/10.1063/1.1657304
9. Scott M.W. Energy Gap in $Hg_{1-x}Cd_xTe$ by Optical Absorption. *J. Appl. Phys*. 1969;40(10):4077–4081. https://www.doi.org/10.1063/1.1657147
10. Elliott C., Melngailis J., Harman T., Kafalas J., Kernan W. Pressure Dependence of the Carrier Concentrations in *p*-Type Alloys of $Hg_{1-x}Cd_xTe$ at 4.2 and 77°K. *Phys. Rev. B*. 1972;5(8):2985. https://www.doi.org/10.1103/PhysRevB.5.2985
11. McCombe B.D., Wagner R.J., Prinz G.A. Far-Infrared Observation of Electric-Dipole-Excited Electron-Spin Resonance in $Hg_{1-x}Cd_xTe$. *Phys. Rev. Lett.* 1970;25(2):87–90. https://www.doi.org/10.1103/PhysRevLett.25.87
12. Xin W., Zhong W., Shi Y., Shi Y., Jing J., Xu T., Guo J., Liu W., Li Y., Liang Z., Xin X., Cheng J., Hu W., Xu H., Liu Y. Low-Dimensional-Materials-Based Photodetectors for Next-Generation Polarized Detection and Imaging. *Adv. Mater*. 2024;36(7):2306772. https://doi.org/10.1002/adma.202306772
13. Xue X., Chen M., Luo Y., Qin T., Tang X., Hao Q. High-operating-temperature mid-infrared photodetectors via quantum dot gradient homojunction. *Light: Sci. Appl*. 2023;12(1):2. https://doi.org/10.1038/s41377-022-01014-0
14. Agarwal H., Nowakowski K., Forrer A., Principi A., Bertini R., Batlle-Porro S., Reserbat-Plantey A., Prasad P., Vistoli L., Watanabe K., Taniguchi T., Bachtold A., Scalari G., Krishna Kumar R., Koppens F.H.L. Ultra-broadband photoconductivity in twisted graphene heterostructures with large responsivity. *Nat. Photon*. 2023;17(12):1047–1053. https://doi.org/10.1038/s41566-023-01291-0
15. Lau J.A., Verma V.B., Schwarzer D., Wodtke A.M. Superconducting single-photon detectors in the mid-infrared for physical chemistry and spectroscopy. *Chem. Soc. Rev*. 2023;52:921–941. https://doi.org/10.1039/d1cs00434d
16. Rogalski A. HgCdTe infrared detector material: history, status and outlook. *Rep. Prog. Phys*. 2005;68(10):2267. http://doi.org/10.1088/0034-4885/68/10/R01
17. Kimchi J., Frederick J.R., Wong T.T.S. Low-frequency noise in photoconductive HgCdTe detectors. *Proc. SPIE*. 1996;2812. 12 p. https://doi.org/10.1117/12.254098

18. Johnson J.B. The Schottky Effect in Low Frequency Circuits. *Phys. Rev*. 1925;26(1):71–85. https://doi.org/10.1103/PhysRev.26.71
19. Schottky W. Small-Shot Effect and Flicker Effect. *Phys. Rev.* 1926;28(1):74–103. https://doi.org/10.1103/PhysRev.28.74
20. Dutta P., Horn P.M. Low-frequency fluctuations in solids: 1/f noise. *Rev. Mod. Phys.* 1981;53(3):497–516. https://doi.org/10.1103/RevModPhys.53.497
21. Voss R.F., Clarke J. 1/f noise in music and speech. *Nature*. 1975;258(5533):317. https://doi.org/10.1038/258317a0
22. Press W.H. Flicker noises in astronomy and elsewhere. *Comments Astrophys*. 1978;7(4):103–119.
23. Milotti E. 1/f noise: a pedagogical review. 2002; *ArXiV_0204033v1.* https://arxiv.org/pdf/physics/0204033
24. Рытов С.М. *Введение в статистическую радиофизику. Часть 1. Случайные процессы.* М.: Наука; 1976. 496 с.
25. Morikawa M., Nakamichi A. A simple model for pink noise from amplitude modulations. *Sci. Rep*. 2023;13(1):8364. https://doi.org/10.1038/s41598-023-34816-2
26. Zenhausern F., O'Boyle M.P., Wickramasinghe H.K. Apertureless near-field optical microscope. *Appl. Phys. Lett*. 1994;65(13):1623–1625. http://doi.org/10.1063/1.112931
27. Zenhausern F., Martin Y., Wickramasinghe H.K. Scanning Interferometric Apertureless Microscopy: Optical Imaging at 10 Angstrom Resolution. *Science*. 1995;269(5227):1083–1085. https://doi.org/10.1126/science.269.5227.1083
28. Keilmann F., Hillenbrand R. Near-Field Microscopy by Elastic Light Scattering from a Tip. *Philos. Trans.: Math., Phys. Eng. Sci.* 2004;362(1817):787–805. https://doi.org/10.1098/rsta.2003.1347
29. Казанцев Д.В., Казанцева Е.А. Предусилитель для CdHgTe-фотодетектора. *Приборы и техника эксперимента*. 2020;1:144–150. https://doi.org/10.31857/S0032816220010218
30. Shockley W. The Theory of p-n Junctions in Semiconductors and p-n Junction Transistors. *Bell System Tech. J.* 1949;28(3):435–489. https://doi.org/10.1002/j.1538-7305.1949.tb03645.x
31. Казанцев Д.В., Казанцева Е.А. Цифровое детектирование оптического сигнала в микроскопе ближнего оптического поля. *Приборы и техника эксперимента*. 2022;2:79–98. URL: https://sciencejournals.ru/view-article/?j=pribory&y=2022&v=0&n=2&a=Pribory2202014Kazantsev
32. Cooley J.W., Tukey J.W. An algorithm for the machine calculation of complex Fourier series. *Math. Comp*. 1965;19(90):297–301. https://doi.org/10.1090/S0025-5718-1965-0178586-1
33. Stephens D.R., Diggins C., Turkanis J., Cogswell J. *C++ Cookbook*. O'Reilly Media, Inc.; 2005. 592 p. ISBN 978-059-600-761-4

About the authors

Dmitry V. Kazantsev, Dr. Sci. (Phys.-Math.), Senior Research, P.N. Lebedev Physical Institute of the Russian Academy of Sciences (53, Leninskii pr., Moscow, 119991 Russia); Professor, Faculty of Physics, HSE University (21/5, Staraya Basmannaya ul., Moscow, 101000 Russia). E-mail: kaza@itep.ru. Scopus Author ID 6603178750, https://orcid.org/0000-0002-0547-3785

Elena A. Kazantseva, Senior Lecturer, Higher Mathematics Department, Institute of Cybersecurity and Digital Technologies, MIREA – Russian Technological University (78, Vernadskogo pr., Moscow, 119454 Russia). E-mail: kanele19@gmail.com. Scopus Author ID 57219932826, https://orcid.org/0009-0004-2019-3310

Об авторах

Казанцев Дмитрий Всеволодович, д.ф.-м.н., старший научный сотрудник, ФГБУН «Физический институт имени П.Н. Лебедева Российской академии наук» (ФИАН) (119991, Россия, Москва, Ленинский пр-т, д. 53); профессор, факультет физики, Национальный исследовательский университет «Высшая школа экономики» (101000, Россия, Москва, Старая Басманная ул., д. 21/5). E-mail: kaza@itep.ru. Scopus Author ID 6603178750, https://orcid.org/0000-0002-0547-3785

Казанцева Елена Адольфовна, старший преподаватель, кафедра высшей математики, Институт кибербезопасности и цифровых технологий, ФГБОУ ВО «МИРЭА – Российский технологический университет (119454, Россия, Москва, пр-т Вернадского, д. 78). E-mail: kanele19@gmail.com. Scopus Author ID 57219932826, https://orcid.org/0009-0004-2019-3310

Translated from Russian into English by K. Nazarov
Edited for English language and spelling by Dr. David Mossop

Mathematical modeling

Математическое моделирование

UDC 536.2
https://doi.org/10.32362/2500-316X-2025-13-1-136-143
EDN XIFHYB

RESEARCH ARTICLE

A smoothed particle hydrodynamics approach for numerical simulation of tube heat exchangers

Anna E. Korenchenko [@], Anton V. Sukhov

MIREA – Russian Technological University, Moscow, 119454 Russia
[@] Corresponding author, e-mail: korenchenko@mirea.ru

Abstract

Objectives. In the confined space of heat exchangers, heat transfer rate plays a key role. The cross-sectional shape of the tubes can affect the heat transfer characteristics. Although circular tubes are easier and less expensive to manufacture, heat transfer in heat exchangers with tubes of other cross-sections can take place at higher rates, thus providing economic advantages. This makes the mathematical modeling of hydrodynamics and heat exchange in a tube apparatus relevant and interesting both from the theoretical and applied point of view. The aim of this study is to determine the influence of the shape of the tube cross-section on the heat transfer intensity.

Methods. Numerical investigations were carried out using smoothed particle hydrodynamics. The possibilities of the smoothed particle method for resolving industrial heat transfer problems were demonstrated.

Results. Heat transfer intensity was analyzed for tubes of circular and rectangular cross-sections. In cases where the cross sections of tubes in the heat exchanger are elongated in a given direction, the influence of the tube position in relation to the oncoming flow was studied. This was performed either with the long side along the flow or across it. The influence of tube surface protrusions on heat exchange was investigated. The flow around tubes with different cross-sectional shapes was also analyzed. The features of the flow around the tubes were established, and the velocity and temperature fields in the heat exchanger volume were defined. The values of the dimensionless heat flux (Nusselt number) for each case were also found.

Conclusions. The influence of finned tubes in the laminar flow regime of heated fluid through the bundle of heat transfer tubes is insignificant. The highest value of the heat flux was observed for tubes of rectangular cross section with the long side transverse to the flow, and the difference with the data obtained for standard round tubes was found to be more than 15%.

Keywords: heat transfer, heat exchanger, numerical modeling, smoothed particle hydrodynamics, incompressible fluid, periodic boundary conditions

• **Submitted:** 06.03.2024 • **Revised:** 02.09.2024 • **Accepted:** 19.11.2024

For citation: Korenchenko A.E., Sukhov A.V. A smoothed particle hydrodynamics approach for numerical simulation of tube heat exchangers. *Russian Technological Journal.* 2025;13(1):136–143. https://doi.org/10.32362/2500-316X-2025-13-1-136-143, https://elibrary.ru/XIFHYB

Financial disclosure: The authors have no financial or proprietary interest in any material or method mentioned.

The authors declare no conflicts of interest.

НАУЧНАЯ СТАТЬЯ

Моделирование работы трубчатых теплообменников методом сглаженных частиц

А.Е. Коренченко [@], А.В. Сухов

МИРЭА – Российский технологический университет, Москва, 119454 Россия
[@] Автор для переписки, e-mail: korenchenko@mirea.ru

Резюме

Цели. В работе теплообменных аппаратов ключевую роль играет скорость теплопередачи в условиях ограниченного пространства. Форма сечения труб может повлиять на характеристики теплообмена. Хотя производство труб кругового сечения проще и обходится дешевле, теплообмен в аппаратах с трубами других поперечных сечений может происходить с большей скоростью, так, чтобы это давало экономические преимущества. Поэтому проведение математического моделирования гидродинамики и теплообмена в трубчатом теплообменном аппарате актуально и интересно как теоретически, так и с прикладной точки зрения. Цель исследования – определение влияния формы сечения труб на интенсивность теплопередачи.

Методы. Численные исследования выполнены методом гидродинамики сглаженных частиц. Продемонстрированы возможности метода сглаженных частиц для решения задач промышленного теплообмена.

Результаты. Анализ интенсивности теплопередачи проведен для труб круглых и прямоугольных сечений. В случаях, когда поперечные сечения труб в теплообменнике являются вытянутыми вдоль некоторого направления, исследовано влияние расположения труб по отношению к набегающему потоку: длинной стороной вдоль потока или поперек его. Исследовано влияние на теплообмен выступов на поверхности труб. Проведен анализ обтекания труб с различными формами поперечных сечений. Выявлены особенности обтекания, найдены поля скоростей и температуры в объеме теплообменника. Найдены значения безразмерного теплового потока (числа Нуссельта) для каждого случая.

Выводы. Сделан вывод о малом влиянии оребрения труб при ламинарном режиме протекания нагреваемой жидкости через пучок труб-теплоносителей. Наибольшее значение теплового потока наблюдалось для труб прямоугольного сечения, расположенных длинной стороной поперек потока, причем различие с данными, полученными для стандартных круглых труб, составило более 15%.

Ключевые слова: теплопередача, теплообменные аппараты, численное моделирование, гидродинамика сглаженных частиц, несжимаемая жидкость, периодические граничные условия

• **Поступила:** 06.03.2024 • **Доработана:** 02.09.2024 • **Принята к опубликованию:** 19.11.2024

Для цитирования: Коренченко А.Е., Сухов А.В. Моделирование работы трубчатых теплообменников методом сглаженных частиц. *Russian Technological Journal.* 2025;13(1):136–143. https://doi.org/10.32362/2500-316X-2025-13-1-136-143, https://elibrary.ru/XIFHYB

Прозрачность финансовой деятельности: Авторы не имеют финансовой заинтересованности в представленных материалах или методах.

Авторы заявляют об отсутствии конфликта интересов.

INTRODUCTION

In the modern technological society, there is an extremely great need for heat exchangers. Heat exchangers are used at enterprises in the petrochemical, metallurgical, and food industries, as well as in shipbuilding and in housing and communal services. In particular, communal heating, hot water supply, and air conditioning systems are built on the basis of heat exchangers. The majority of such heat-exchange equipment involves water-water and steam-water tube heat exchangers. The heat exchanger consists of a block of tubes immersed in the fluid flow. A fluid or gas is passed through the tubes, wherein the fluid media in the tubes and flow possesses differing initial temperatures. The heat exchanger characteristics are of considerable practical interest and have therefore been the subject of numerous experimental and theoretical studies [1–5]. Methods have been developed for heat transfer intensification involving complicating the shape of heat exchanger tubes by finning the surface [6, 7], installing turbulators [8], and rotating the heat exchanger tubes [8]. In [9], the melting characteristics of gallium in a shell-and-tube type heat exchanger with tubes of circular, rectangular, or elliptical cross-section are numerically considered. Here, the solid-liquid transition rate of gallium depends on the heat transfer intensity from tubes. The findings show that the shortest melting time was achieved when using a heat exchanger with tubes of rectangular cross-section, while using tubes of circular cross-section yielded the lowest heat transfer intensity. In [10], the energy feasibility of using elliptical cross-section tubes in thermal energy storage systems is shown.

However, the literature review shows that the possibility of increasing heat transfer by changing the cross-section shape of tubes with heat-transfer medium has not been considered sufficiently and should be investigated additionally.

Smoothed particles hydrodynamics (SPH) is a meshless Lagrangian method for resolving hydrodynamic and aerodynamic problems. The method consists of approximating the fields of physical quantities by a discrete system of particles [11–13]. The method properly describes heat transfer processes in liquid and gas media. It shows good performance and can be used for resolving heat transfer problems in industrial production.

The paper aims to model heat transfer in a tubular heat exchanger and to analyze the heat transfer intensity depending on the cross-section shape of tubes with heat-transfer medium.

1. MATHEMATICAL MODEL

This paper models a scheme (Fig. 1) in which a flow of cold water (T_0 = 283 K), bounded at the top and bottom by flat surfaces, runs into a block of heated parallel tubes the temperature of which is kept equal (T_H = 363 K). The direction of velocity in the flow is perpendicular to the tubes. The fluid in the flow is assumed to be incompressible and Newtonian. The gravity effect is neglected. We consider the problem in a two-dimensional formulation acceptable under the condition that the tube length is much greater than the distance between the bounding planes.

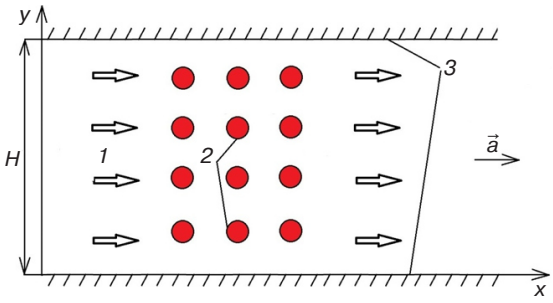

Fig. 1. Schematic diagram of the experiment. *H* is the heat exchanger gap; *1* is the fluid flow; *2* is the tubes; *3* is the bounding planes

Conservation equations for the fluid in the flow are written as follows:

$$\frac{\partial \vec{V}}{\partial t} + \left(\vec{V}\vec{\nabla}\right)\vec{V} = -\frac{1}{\rho}\vec{\nabla}P + \nu\vec{\nabla}^2\vec{V} + \vec{a}, \quad (1)$$

$$\frac{\partial \rho}{\partial t} + \vec{\nabla}\left(\rho\vec{V}\right) = 0, \quad (2)$$

$$\frac{\partial T}{\partial t} + \vec{\nabla}\left(T\vec{V}\right) = \frac{\kappa}{\rho c}\vec{\nabla}^2 T. \quad (3)$$

Wherein, (1) is the momentum conservation law, (2) is the continuity equation and (3) is the heat balance equation in neglecting viscous dissipation, where P is pressure in the fluid; $\vec{V} = \{V_x, V_y\}$ and T are velocity and temperature, respectively; $\vec{a}$ is acceleration due to an external force. The thermophysical characteristics of the fluid (water) are denoted as follows: ρ is density, ν is kinematic viscosity coefficient, κ is heat conduction coefficient, and c is specific heat capacity. Their values are given in Table 1. The following boundary conditions were chosen: the flat surfaces and tubes are isothermal; while the conditions of non-slip and impermeability for flow particles are fulfilled on solid walls.

Table 1. Physical and chemical properties of water

ρ	1000 kg/m^3
κ	0.55 W/(m · K)
ν	10^{-6} m^2/s
c	4200 J/(kg · K)

2. SMOOTHED PARTICLE HYDRODYNAMICS

To calculate system (1)–(3) the smoothed particle hydrodynamics (SPH) is used [11–13]. This method replaces the value for physical variable $f(r)$ at a point in space by the sum of weighted values of this variable for particles located in the neighborhood. The weight is determined by the kernel function, as follows

$$f(\vec{r}) \approx \sum_{j=1}^{N} \frac{m_j}{\rho_j} f_j W(\vec{r} - \vec{r}_j, h). \quad (4)$$

Wherein, m_j, ρ_j are mass and density of the jth particle, $W(\vec{r} - \vec{r}_j, h)$ is kernel function, and h is smoothing radius. The summation is performed on the particles trapped inside the sphere of radius h. The approximations for the gradient, divergence, and Laplace operator are defined as [11, 12]:

$$\begin{aligned} \vec{\nabla} f(\vec{r}) &\approx \sum_{j=1}^{N} \frac{m_j}{\rho_j} f_j \vec{\nabla} W(\vec{r} - \vec{r}_j, h), \\ \vec{\nabla} \vec{F}(\vec{r}) &\approx \sum_{j=1}^{N} \frac{m_j}{\rho_j} \vec{F}_j \vec{\nabla} W(\vec{r} - \vec{r}_j, h), \\ \Delta f(\vec{r}) &\approx \sum_{j=1}^{N} \frac{m_j}{\rho_j} f_j \Delta W(\vec{r} - \vec{r}_j, h). \end{aligned} \quad (5)$$

Equations (1–3) written for the ith Lagrangian particle have the following form:

$$\begin{cases} \dfrac{d\vec{V}_i}{dt} = -\dfrac{1}{\rho_i} \displaystyle\sum_{j=1}^{N} \frac{m_j}{\rho_j} P_j \vec{\nabla} W(\vec{r} - \vec{r}_j, h)\Big|_{\vec{r}=\vec{r}_i} + \\ \qquad + \nu \displaystyle\sum_{j=1}^{N} \frac{m_j}{\rho_j} \vec{V}_j \Delta W(\vec{r} - \vec{r}_j, h)\Big|_{\vec{r}=\vec{r}_i} + \vec{a}, \\ \dfrac{d\rho_i}{dt} = -\displaystyle\sum_{j=1}^{N} m_j \vec{V}_j \vec{\nabla} W(\vec{r} - \vec{r}_j, h)\Big|_{\vec{r}=\vec{r}_i}, \\ \dfrac{dT_i}{dt} = \dfrac{\kappa}{\rho_i c} \displaystyle\sum_{j=1}^{N} \frac{m_j}{\rho_j} T_j \Delta W(\vec{r} - \vec{r}_j, h)\Big|_{\vec{r}=\vec{r}_i}. \end{cases} \quad (6)$$

The kernel function $W(\vec{r} - \vec{r}_j, h)$ is chosen in the following form [14]:

$$W(\vec{r} - \vec{r}_j, h) = \frac{7}{4\pi h^2} \left(1 - \frac{q}{2}\right)^4 (2q + 1),$$
$$q = |\vec{r} - \vec{r}_j|, \quad 0 \le q \le 2.$$

System (6) is supplemented by the equation of state of water [11], as follows:

$$P = \frac{\rho_0 c_{snd}^2}{7} \left(\left(\frac{\rho}{\rho_0} \right)^7 - 1 \right), \quad (7)$$

wherein c_{snd} = 1500 m/s is the speed of sound propagation in the fluid, and ρ_0 is the density of the undisturbed medium. It is stated in [11] that equation (7) provides a compressibility value not exceeding real water compressibility of about 0.1%.

The mirror particle method proposed in [13] was used to provide slip and impermeability conditions at solid boundaries. The system of ordinary differential equations (6) was resolved using the Runge–Kutta method for the 3rd order of accuracy.

3. RESULTS AND DISCUSSION

3.1. Poiseuille flow between two parallel planes

In order to verify calculation accuracy, a test problem of viscous fluid flow through a gap between two solid planar surfaces was conducted. Figure 1 shows the schematic diagram of the experiment with correction for the absence of tubes in the computational domain.

At the initial moment of time, the fluid is at rest and fills the gap. The force field with a strength $\vec{a}$ starts affecting it at moment $t = 0$. The fluid and the bounding planes have the same temperature and are assumed to be isothermal. In order to model the flow, a system of equations (6) needs to be resolved, with the exclusion of the heat balance equation. In the flow direction, periodic boundary conditions are set [14, 15]. In two-dimensional formulation and in the absence of gravity, the problem has an analytical solution. Based on this solution, the dependence of fluid velocity components on distance y from the bottom plane is expressed by the following formula:

$$V_x(y) = \frac{a}{2\nu}\left(Hy - y^2\right), \quad V_y = 0. \quad (8)$$

Thus, the velocity of motion in the flow is parallel to bounding planes and is described by the parabolic dependence on transverse coordinate y, with the highest value reached at $y = H/2$ and expressed by the following formula:

$$V_{x\max} = aH^2/(8\nu). \quad (9)$$

The solution is performed for $a = 0.1$ m/s^2, $H = 2.5$ mm. The Reynolds number $Re = V_{x\max} H/\nu$ in this case does not

exceed 1500 corresponding to the laminar flow regime. The calculation results are shown in Figs. 2 and 3. The velocity profiles in the gap at different moments of time are shown in Fig. 2. During the transient time interval of ~10 s, the velocity distribution is established in the gap which differs from the analytical solution (8) by less than 0.1%. The dependence of the highest velocity in the flow on the gap width is shown in Fig. 3. This figure shows that the numerical and analytical results are close to each other, thus demonstrating SPH capabilities for solving hydrodynamics problems.

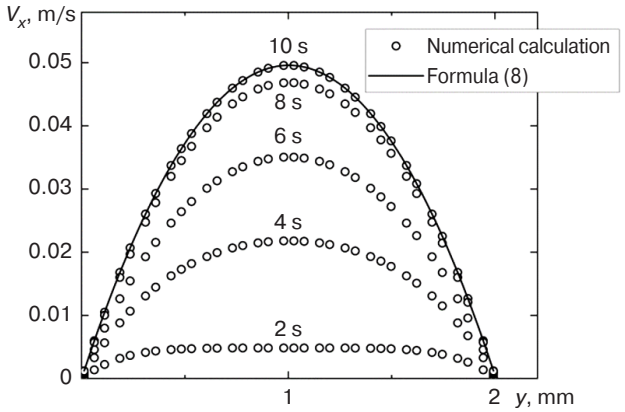

Fig. 2. Calculation results for the velocity in the exit section of the gap at different moments of time and analytical calculation of the steady-state velocity profile: $H = 2$ mm, $a = 0.1$ m/s^2

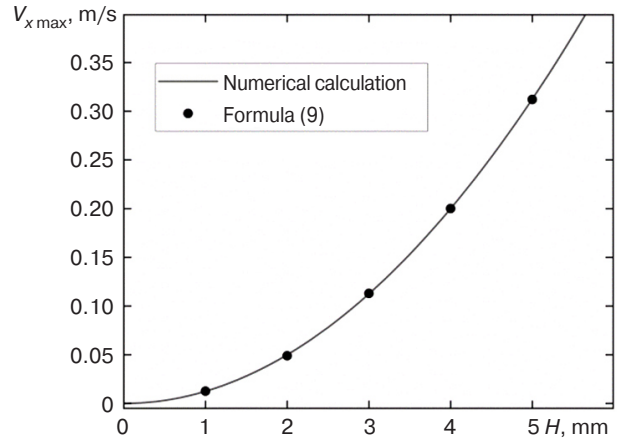

Fig. 3. Numerical and analytical dependencies of the highest velocity in the gap on the gap width

3.2. Heating water in a tube heat exchanger

Figure 1 shows a schematic representation of a cross-flow heat exchanger. The fluid flows into the heat exchanger from left to right under the influence of a force field and meets a bundle of tubes arranged at right angles to the flow (cross sections are shown in the figure). The distance between centers of the tubes is 4 cm in both vertical and horizontal rows. Numerical calculations were performed for $H = 0.2$ m, and the heat exchanger length is $L_H = 1$ m. The force field strength is chosen to be equal This gives the maximum velocity value estimated "from above" by formula (9), $V_{x\,max} \approx 2$ m/s and allows it to be stated that the flow will occur in the laminar regime ($Re < 2000$). Tubes with the following different cross sections were considered (Fig. 4): a) circular; b) rectangular with vertical location of the long side (across the flow); c) rectangular with location of the long side along the flow; and d) finned surface model, where rectangular protrusions of 1 mm × 2 mm are located along the pipe surface. At the beginning of calculation, the fluid was filled in the heat exchanger and was at rest at temperature $T_0 = 283$ K. At moment $t = 0$, the force field is switched on with an intensity level $\vec{a}$. The tube temperature is $T_H = 363$ K and is not changed during heat exchange. The problem is resolved in a two-dimensional formulation, and the perimeter of the tube cross-section serves as the measure of the heat source area S_H in this case.

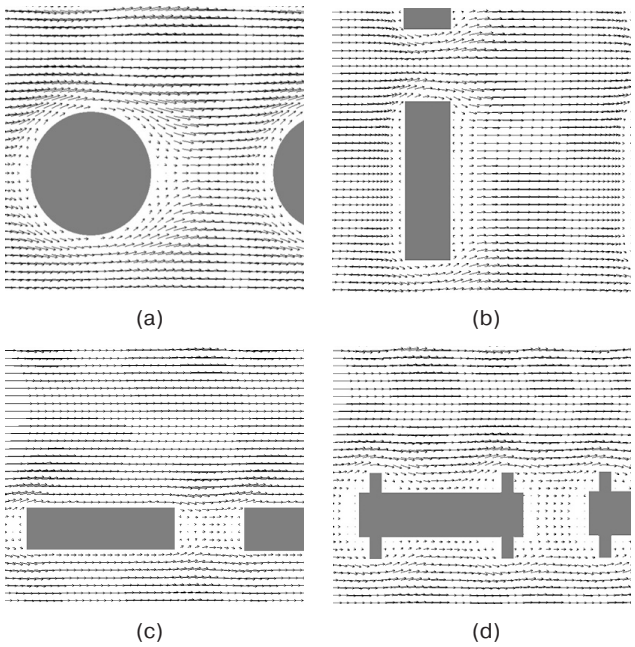

Fig. 4. Velocity distribution in the flow when flowing around tubes with different cross sections

Figure 4 shows the fields of velocity distributions during flow around tubes. The length of the velocity vector is proportional to its magnitude, and all figures are drawn to the same scale. The cross-section perimeters for tubes in Figs. 4 (a)–(c) are 6.28 cm. The flow around occurs in the laminar regime, with no vortices or breakaway currents formed. Thus, the flow regime, once established, is no longer disturbed. The figures show that in cases (c) and (d), there is practically no fluid motion in gaps between tubes, and velocities in the volume are strictly horizontal, i.e., there is no convective heat propagation in the transverse flow direction.

Figure 5 shows the dependencies of the dimensionless heat flux that is Nusselt number $Nu = \int_{S_H} \frac{\partial T}{\partial \vec{n}} d\sigma \cdot \frac{L_H}{S_H (T_1 - T_0)}$ on the cross-section perimeter for different tube shapes (Fig. 4). Changes in the perimeter of tubes of circular cross-section result from changes in the radius. For tubes of rectangular cross-section, the length of the short side was fixed at 0.5 cm. The perimeter was changed by modifying the length of the other side or by finning the tube.

The graphs in Fig. 5 allow the following patterns to be established.

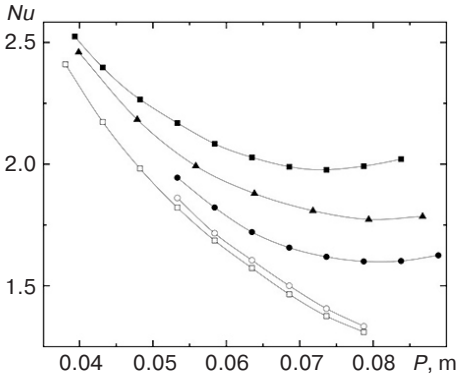

Fig. 5. Dependence of dimensionless heat flux on the cross-section perimeter for tubes with different cross-sectional shapes: ▲ is circular cross-section (a); ■ is vertical rectangle without protrusions (b); ● is vertical rectangle with 4 protrusions of 1 mm × 2 mm; □ is horizontal rectangle without protrusions (c); ○ is horizontal rectangle with 4 protrusions of 1 mm × 2 mm (d)

As the tube surface area increases, the Nusselt number decreases. The exception is the flux calculated for round tubes (a) and tubes with a cross-section in the form of a vertical rectangle (b). The figure shows that in these cases, the flow begins to increase for some perimeter value as the perimeter increases. This is apparently due to an increase in the size of tubes in the direction perpendicular to the flow resulting in overlapping of gaps between them, so that the entire flow is directed along the walls of the apparatus, thus intensifying heat transfer insignificantly.

The dependencies of heat flux on tube perimeter converge with decreasing perimeter. This is due to the fact that when reducing the tube size, the cross-section shape becomes an insignificant factor.

Under the considered conditions, finning tubes cannot intensify heat exchange. Protrusions on tubes of horizontally elongated rectangular cross-section (d) result in an insignificant increase of heat flow (~2%) compared to tubes without protrusions. However, for cross-section (b), protrusions result in a noticeable heat flux decrease (~25%), which is apparently due to fluid inhibition and stagnation. In the turbulent regime of flows, the protrusions cause the appearance of breakaway vortex currents, which result in an increase in the heat transfer intensity [16]. However, calculations show that in the laminar regime, this can reduce the heat flux from the heat transfer medium.

The graphs of *Nu* dependence on cross-sectional shape and heat transfer medium size show that in case (c), the molecular thermal conductivity mechanism prevails, while the Nusselt number has the lowest value. The highest Nusselt number value can be observed for tubes with a vertical rectangular cross-section, with the difference between the heat flux and values obtained for tubes with a circular cross-section is ~15%.

CONCLUSIONS

In this paper, mathematical modeling of heat transfer in a tubular heat exchanger under cross-sectional flow around tubes is performed. Numerical studies were carried out for laminar flow regime and for tubes with different shapes and cross-section perimeters, which allow the following conclusions to be drawn.

1. Finning the outer surface of tubes would not cause a significant increase in the heat flux. In turbulent flow regime, the protrusions generate vortices and breakaway flows resulting in heat transfer intensification. However, this can reduce the heat flux in the laminar regime due to the fluid braking near the pipe when flowing around protrusions.
2. Given equal perimeters, the highest heating intensity occurs in tubes with cross-section stretched across the flow, with an increase in heat flux of ~15% compared to the values obtained for standard-type tubes.
3. Phenomena leading to fluid braking or stagnation cause a decrease in heat transfer intensity.

Authors' contribution

All the authors have equally contributed to the scientific work.

REFERENCES

1. Zolotonosov Ya.D., Bagoutdinova A.G., Zolotonosov A.Ya. *Trubchatye teploobmenniki. Modelirovanie, raschet* (*Tubular Heat Exchangers. Modeling, Calculation*). Moscow: Lan; 2021. 2272 p. (in Russ.). Available from URL: https://lanbook.com/catalog/energetika/trubchatye-teploobmenniki-modelirovanie-raschet/.
2. Golovin V.A., Tyurina S.A., Shchelkov V.A. Contemporary approaches to reducing scale formation in heat-exchange equipment. *Russian Technological Journal*. 2022;10(3):93–102. https://doi.org/10.32362/2500-316X-2022-10-3-93-102
3. Cui P., Yang W., Zhang W., Zhu K., Spitler J.D., Yu M. Advances in ground heat exchangers for space heating and cooling: Review and perspectives. *Energy and Built Environment*. 2024;5(2):255–269. https://doi.org/10.1016/j.enbenv.2022.10.002
4. Luo J., Lu P., Chen K., Luo X., Chen J., Liang Y., Yang Z., Chen Y. Experimental and simulation investigation on the heat exchangers in an ORC under various heat source/sink conditions. *Energy.* 2023;264:126189. https://doi.org/10.1016/j.energy.2022.126189
5. Safronova E.V., Spiridonov A.V., Molotok E.V., Trus V.A. Computer simulation and optimization of heat transfer processes in ANSYS software using the example of a heat exchanger installation AVT-2 JSC "NAFTAN". *Vestnik Polotskogo gosudarstvennogo universiteta. Seriya B. Promyshlennost'. Prikladnye nauki = Vestnik of Polotsk State University. Series B.* 2024;49(1):95–100 (in Russ.). https://doi.org/10.52928/2070-1616-2024-49-1-95-100
6. Artemyev D.V., Zaitsev A.V., Sanavbarov R.I. Simulation of heat transfer process in shell-and-tube heat exchanger. *Vestnik Mezhdunarodnoi Akademii Kholoda = Bulletin of the International Academy of Refrigeration*. 2021;3:5–14 (in Russ.). https://doi.org/10.17586/1606-4313-2021-20-3-5-14
7. Romanova E.V., Koliukh A.N., Lebedev E.A. Application of ANSYS package in research of hydraulic resistance of finned heat exchanger. *Vestnik Tambovskogo gosudarstvennogo tehnicheskogo universiteta = Transactions of Tambov State Technical University*. 2017;23(3):420–427 (in Russ.). https://doi.org/10.17277/vestnik.2017.03.pp.420-427
8. Kustov B.O., Balchugov A.V., Badenikov A.V., Gerasimchuk M.V., Zakharov K.D. Experimental studies of promising methods of heat transfer intensification in a tubular heat exchanger. *Izvestiya Tomskogo politekhnicheskogo universiteta* (*Izvestiya TPU*). *Inzhiniring georesursov = Bulletin of the Tomsk Polytechnic University. Geo Assets Engineering*. 2020;331(3):174–183 (in Russ.). https://doi.org/10.18799/24131830/2020/3/2560
9. Rana S., Zunaid M., Kumar R. CFD analysis for heat transfer comparison in circular, rectangular and elliptical tube heat exchangers filled with PCM. *Mater. Today Proc.* 2022;56(2):637–644. https://doi.org/10.1016/j.matpr.2021.12.412
10. Khuda M.A., Sarunac N. A comparative study of latent heat thermal energy storage (LTES) system using cylindrical and elliptical tubes in a staggered tube arrangement. *J. Energy Storage*. 2024;87:111333. https://doi.org/10.1016/j.est.2024.111333
11. Monaghan J.J. Smoothed Particle Hydrodynamics. *Reports on Progress in Physics*. 2005;68(8):1703. https://doi.org/10.1088/0034-4885/68/8/R01
12. Lucy L.B. A numerical approach to the testing of the fission hypothesis. *Astron. J.* 1977;82:1013–1024. https://doi.org/10.1086/112164
13. Morris J.P., Fox P.J., Zhu Y. Modeling Low Reynolds Number Incompressible Flows Using SPH. *J. Comput. Phys*. 1997;136(1):214–226. https://doi.org/10.1006/jcph.1997.5776
14. Hosain M.L., Dominguez J.M., Bel Fdhila R., Kyprianidis K. Smoothed particle hydrodynamics modeling of industrial processes involving heat transfer. *Appl. Energy*. 2019;252:113441. https://doi.org/10.1016/j.apenergy.2019.113441
15. Jonsson P., Andreasson P., Hellström J.G.I., Jonsén P., Lundström T.S. Smoothed Particle Hydrodynamic simulation of hydraulic jump using periodic open boundaries. *Appl. Math. Model*. 2016;40(19–20):8391–8405. https://doi.org/10.1016/j.apm.2016.04.028
16. Afanasiev V.N., Kon Dehai, Egorov K.S. Verification of models for turbulent heat fluxes in the flow over rectangular rib on a plate. *Izvestiya vysshikh uchebnykh zavedenii. Mashinostroenie = BMSTU J. Mechan. Eng*. 2019;1(706):58–71 (in Russ.). http://doi.org/10.18698/0536-1044-2019-1-58-71

СПИСОК ЛИТЕРАТУРЫ

1. Золотоносов Я.Д., Багоутдинова А.Г., Золотоносов А.Я. *Трубчатые теплообменники. Моделирование, расчет.* М.: Лань; 2021. 272 с. URL: https://lanbook.com/catalog/energetika/trubchatye-teploobmenniki-modelirovanie-raschet/
2. Головин В.А., Тюрина С.А., Щелков В.А. Современные подходы к снижению накипеобразования в теплообменном оборудовании. *Russian Technological Journal*. 2022;10(3):93–102. https://doi.org/10.32362/2500-316X-2022-10-3-93-102
3. Cui P., Yang W., Zhang W., Zhu K., Spitler J.D., Yu M. Advances in ground heat exchangers for space heating and cooling: Review and perspectives. *Energy and Built Environment*. 2024;5(2):255–269. https://doi.org/10.1016/j.enbenv.2022.10.002
4. Luo J., Lu P., Chen K., Luo X., Chen J., Liang Y., Yang Z., Chen Y. Experimental and simulation investigation on the heat exchangers in an ORC under various heat source/sink conditions. *Energy.* 2023;264:126189. https://doi.org/10.1016/j.energy.2022.126189
5. Сафронова Е.В., Спиридонов А.В., Молоток Е.В., Трус В.А. Компьютерное моделирование и оптимизация процессов теплообмена в программе ANSYS на примере теплообменного аппарата установки «НАФТАН». *Вестник Полоцкого государственного университета. Серия В. Промышленность. Прикладные науки*. 2024;49(1):95–100. https://doi.org/10.52928/2070-1616-2024-49-1-95-100

6. Артемьев Д.В., Зайцев А.В., Санавбаров Р.И. Моделирование процесса теплопередачи в кожухотрубном теплообменном аппарате. *Вестник Международной Академии Холода*. 2021;3:5–14. https://doi.org/10.17586/1606-4313-2021-20-3-5-14
7. Романова Е.В., Колиух А.Н., Лебедев Е.А. Применение пакета ANSYS при исследовании гидравлического сопротивления оребреного рекуператора. *Вестник ТГТУ*. 2017;23(3):420–427. https://doi.org/10.17277/vestnik.2017.03.pp.420-427
8. Кустов Б.О., Бальчугов А.В., Бадеников А.В., Герасимчук М.В., Захаров К.Д. Экспериментальные исследования перспективных способов интенсификации теплопередачи в трубчатом теплообменнике. *Известия ТПУ. Инжиниринг георесурсов*. 2020;331(3):174–183. https://doi.org/10.18799/24131830/2020/3/2560
9. Rana S., Zunaid M., Kumar R. CFD analysis for heat transfer comparison in circular, rectangular and elliptical tube heat exchangers filled with PCM. *Mater. Today Proc.* 2022;56(2):637–644. https://doi.org/10.1016/j.matpr.2021.12.412
10. Khuda M.A., Sarunac N. A comparative study of latent heat thermal energy storage (LTES) system using cylindrical and elliptical tubes in a staggered tube arrangement. *J. Energy Storage*. 2024;87:111333. https://doi.org/10.1016/j.est.2024.111333
11. Monaghan J.J. Smoothed Particle Hydrodynamics. *Reports on Progress in Physics*. 2005;68(8):1703. https://doi.org/10.1088/0034-4885/68/8/R01
12. Lucy L.B. A numerical approach to the testing of the fission hypothesis. *Astron. J.* 1977;82:1013–1024. https://doi.org/10.1086/112164
13. Morris J.P., Fox P.J., Zhu Y. Modeling Low Reynolds Number Incompressible Flows Using SPH. *J. Comput. Phys*. 1997;136(1):214–226. https://doi.org/10.1006/jcph.1997.5776
14. Hosain M.L., Dominguez J.M., Bel Fdhila R., Kyprianidis K. Smoothed particle hydrodynamics modeling of industrial processes involving heat transfer. *Appl. Energy*. 2019;252:113441. https://doi.org/10.1016/j.apenergy.2019.113441
15. Jonsson P., Andreasson P., Hellström J.G.I., Jonsén P., Lundström T.S. Smoothed Particle Hydrodynamic simulation of hydraulic jump using periodic open boundaries. *Appl. Math. Model*. 2016;40(19–20):8391–8405. https://doi.org/10.1016/j.apm.2016.04.028
16. Афанасьев В.Н., Кон Дехай, Егоров К.С. Верификация моделей для турбулентных тепловых потоков при обтекании прямоугольного выступа на пластине. *Известия вузов. Машиностроение.* 2019;1(706):58–71. http://doi.org/10.18698/0536-1044-2019-1-58-71

About the authors

Anna E. Korenchenko, Dr. Sci. (Phys.-Math.), Professor, Higher Mathematics Department, Institute of Cybersecurity and Digital Technologies, MIREA – Russian Technological University (78, Vernadskogo pr., Moscow, 119454 Russia). E-mail: korenchenko@mirea.ru. Scopus Author ID 10043443100, RSCI SPIN-code 9908-9198, https://orcid.org/0000-0002-3413-8855

Anton V. Sukhov, Student, Institute of Cybersecurity and Digital Technologies, MIREA – Russian Technological University (78, Vernadskogo pr., Moscow, 119454 Russia). E-mail: tosha.sukhov@inbox.ru. https://orcid.org/0009-0006-0812-6099

Об авторах

Коренченко Анна Евгеньевна, д.ф.-м.н., профессор, кафедра высшей математики, Институт кибербезопасности и цифровых технологий, ФГБОУ ВО «МИРЭА – Российский технологический университет (119454, Россия, Москва, пр-т Вернадского, д. 78). E-mail: korenchenko@mirea.ru. Scopus Author ID 10043443100, SPIN-код РИНЦ 9908-9198, https://orcid.org/0000-0002-3413-8855

Сухов Антон Владимирович, студент, Институт кибербезопасности и цифровых технологий, ФГБОУ ВО «МИРЭА – Российский технологический университет (119454, Россия, Москва, пр-т Вернадского, д. 78). E-mail: tosha.sukhov@inbox.ru. https://orcid.org/0009-0006-0812-6099

Translated from Russian into English by K. Nazarov
Edited for English language and spelling by Dr. David Mossop

Mathematical modeling

Математическое моделирование

UDC 51.7
https://doi.org/10.32362/2500-316X-2025-13-1-144-156
EDN WPRKRW

RESEARCH ARTICLE

Multivariate discriminant analysis of the electrocardiogram

Polina A. Sakharova [@], **Vyacheslav A. Balandin**

MIREA – Russian Technological University, Moscow, 119454 Russia
[@] *Corresponding author, e-mail: polinka6777@gmail.com*

Abstract

Objectives. The article presents a study of heart rate variability using multivariate discriminant analysis. Representing an effective statistical method of classification, discriminant analysis can be used to divide objects into groups based on differences in the parameters characterizing these objects. The effectiveness of multivariate discriminant analysis, which is actively used in medicine to diagnose cardiovascular pathologies, is due to the wide range of analyzed parameters: statistical, spectral, and autocorrelation. The aim of the work is to identify the parameters of variational pulsometry, which provide the best distinction between healthy patients and patients with arrhythmia, by means of discriminant analysis.

Methods. The durations of cardiac intervals of patients aged 63–72 years, which had been placed in the open database of biomedical signals PhysioNet.org, were used as initial data. When selecting the arguments of the discriminant function, priority was given to parameters that were weakly correlated with each other, had a normal distribution, and differed between healthy and ill patients. The statistical significance of differences between the parameters of the two groups was tested using Student's *t*-test and Mann–Whitney *U* test.

Results. Two discriminant functions were obtained: the first depended on three time-domain parameters, while the second included one spectral and one autocorrelation parameter in addition to time-domain parameters. In both cases, the average values of the discriminant function for healthy and sick patients were calculated. The statistical significance of differences in the average values of the discriminant function in the two groups was investigated using Student's *t*-test.

Conclusions. The values of the first discriminant function are shown to differ insignificantly between healthy and sick patients, while the inclusion of autocorrelation and spectral parameters in the number of arguments of the discriminant function provides pronounced and statistically significant differences between patients of the two groups. Thus, the high significance of spectral and autocorrelation parameters in arrhythmia diagnosis was demonstrated.

Keywords: heart rate variability, variational pulsometry, spectral analysis, autocorrelation analysis, RR-intervals, multivariate discriminant analysis, discriminant function

• **Submitted:** 26.03.2024 • **Revised:** 09.06.2024 • **Accepted:** 10.12.2024

For citation: Sakharova P.A., Balandin V.A. Multivariate discriminant analysis of the electrocardiogram. *Russian Technological Journal.* 2025;13(1):144–156. https://doi.org/10.32362/2500-316X-2025-13-1-144-156, https://elibrary.ru/WPRKRW

Financial disclosure: The authors have no financial or proprietary interest in any material or method mentioned.

The authors declare no conflicts of interest.

НАУЧНАЯ СТАТЬЯ

Многофакторный дискриминантный анализ электрокардиограммы

П.А. Сахарова [@], **В.А. Баландин**

МИРЭА – Российский технологический университет, Москва, 119454 Россия
[@] *Автор для переписки, e-mail: polinka6777@gmail.com*

Резюме

Цели. Статья посвящена исследованию вариабельности сердечного ритма с помощью многофакторного дискриминантного анализа. Дискриминантный анализ является эффективным статистическим методом классификации, позволяющим разбивать объекты на группы исходя из различий между характеризующими эти объекты параметрами. Эффективность многофакторного дискриминантного анализа, который активно используется в медицине для диагностики сердечно-сосудистых патологий, обусловлена широким набором анализируемых параметров: статистических, спектральных и автокорреляционных. Цель работы – выявление методом дискриминантного анализа параметров вариационной пульсометрии, которые обеспечивают наилучшее различение между здоровыми пациентами и пациентами с аритмией.

Методы. В качестве исходных данных использовались длительности кардиоинтервалов пациентов возраста 63–72 лет, размещенные в открытой базе биомедицинских сигналов PhysioNet.org. При выборе аргументов дискриминантной функции преимущество отдавалось слабо коррелирующим между собой параметрам, имеющим нормальное распределение и различающимся у здоровых и больных пациентов. Статистическая значимость различий между параметрами двух групп проверялась с помощью *t*-критерия Стьюдента и *U*-критерия Манна – Уитни.

Результаты. Получены две дискриминантные функции: первая зависела от трех временных параметров; вторая, помимо временных, включала один спектральный и один автокорреляционный. В обоих случаях были рассчитаны средние значения дискриминантной функции для здоровых и больных пациентов. Статистическая значимость различий средних значений дискриминантной функции в двух группах исследовалась с помощью *t*-критерия Стьюдента.

Выводы. Показано, что значения первой дискриминантной функции незначительно различаются у здоровых и больных пациентов, в то время как включение автокорреляционного и спектрального параметров в число аргументов дискриминантной функции обеспечивает выраженные и статистически значимые различия между пациентами двух групп. Тем самым продемонстрирована высокая значимость спектральных и автокорреляционных параметров в диагностике аритмии.

Ключевые слова: вариабельность сердечного ритма, вариационная пульсометрия, спектральный анализ, автокорреляционный анализ, RR-интервалы, многофакторный дискриминантный анализ, дискриминантная функция

• **Поступила:** 26.03.2024 • **Доработана:** 09.06.2024 • **Принята к опубликованию:** 10.12.2024

Для цитирования: Сахарова П.А., Баландин В.А. Многофакторный дискриминантный анализ электрокардиограммы. *Russian Technological Journal.* 2025;13(1):144–156. https://doi.org/10.32362/2500-316X-2025-13-1-144-156, https://elibrary.ru/WPRKRW

Прозрачность финансовой деятельности: Авторы не имеют финансовой заинтересованности в представленных материалах или методах.

Авторы заявляют об отсутствии конфликта интересов.

INTRODUCTION

Currently, cardiovascular diseases (CVDs) are the main cause of death worldwide [1]. Among them, a special place is occupied by diseases associated with heart rhythm disorders characterized by various arrhythmias [2]. According to statistics, about one third of people with CVDs suffer from arrhythmias [3]. In view of high mortality rates from CVDs, timely diagnosis of cardiovascular system disorders becomes especially important.

Along with traditional amplitude-time analysis, an important approach to diagnosing CVD involves the study of heart rate variability (HRV) [4]. Various methods are used for quantitative determination of HRV indices, among which the following can be emphasized [5]:

1. Methods based on statistical transformations. These include temporal analysis of HRV, whose numerical characteristics are average value of cardiac interval duration (RR normal-to-normal interval, RRNN), standard deviation (SD) of normal-to-normal intervals (SDNN) of the cardiac cycle (standard deviation of normal-to-normal intervals, SDNN), percentage of consecutive normal-to-normal intervals that differ by more than 50 ms (pNN50), square root of the mean sum of squares of the successive differences (root mean square of the successive differences, RMSSD);
2. Geometric methods, including scatterographic and histographic analysis, whose objects are mode (Mo)—the value of cardiointerval duration that occurs most frequently in the sample, mode amplitude (AMo)—the share of cardiointervals (in %) that fall within the modal interval, coefficient of variation (in %) $CV = \frac{SD}{RRNN}$, variation range (delta RR interval, dRR)—the difference between the maximum and minimum values of cardiointervals, as well as a set of indices, of which the Baevsky tension index (TI) of the regulatory systems is the most widespread $TI = \frac{AMo}{2Mo \cdot dRR}$;
3. Wave structure analysis methods, comprising:

- spectral method analyzing the power of the spectrum of RR-intervals in the region of very low frequencies (VLF) 0.004–0.03 Hz, low frequencies (LF) 0.04–0.15 Hz, high frequencies (HF) 0.15–0.40 Hz, normalized values of the last two parameters (LF_{norm}, HF_{norm}), centralization index CI = (HF + LF)/VLF, and vagosympathetic interaction index LF/HF;
- autocorrelation method that calculates the shift number at which the autocorrelation function first becomes negative (C0) and the value of the autocorrelation function at the first shift (C1).

The description of the parameters and their diagnostic significance are given in detail in [6].

These parameters are calculated from rhythmograms, which are obtained from the electrocardiograms (ECGs) as time differences between the occurrence of consecutive R beats. Figure 1 shows how the intervals between the occurrence of R beats on the ECG are plotted on the rhythmogram on the ordinate axis and numbered on the abscissa axis.

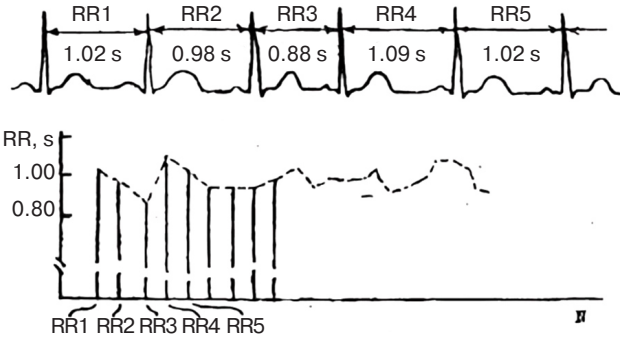

Fig. 1. Obtaining a rhythmogram from the original ECG[1]

The obtained values of the indicators are analyzed by a number of statistical methods to establish significant differences between healthy and sick patients. Among such methods, multivariate discriminant analysis (MDA), which consists in constructing a linear combination of the most informative features that would best ensure the difference between groups, assumes an important place. The effectiveness of MDA application in cardiology was demonstrated, in particular, in [7], which resulted in a model for the distribution of children and adolescents into groups with different cardiovascular system conditions, providing an accuracy of 98.1%.

In [8], it is shown that the significance of MDA based only on statistical parameters of variation pulsometry significantly depends on the type of cardiac pathology. In particular, in arrhythmia, the difference between the discriminant function (DF) values of healthy and sick patients is ~25%, which is significantly lower than that of chronic heart failure, for instance.

Thus, the present study set out to identify the most informative features among the above-mentioned features that would significantly increase the differences of DF in the presence or absence of arrhythmia.

MATERIALS AND METHODS

The initial materials for the work were fragments of ECG examination results, namely, RR interval durations. These records were obtained from the PhysioBank open

[1] Methodical development of practical training on pathophysiology for 3rd year students of general medicine and pediatrics departments. https://patfizo.narod.ru/read/heartprakt.htm (in Russ.). Accessed June 05, 2024.

Table 1. HRV indices of a healthy patient at different ECG recording durations

Parameter \ Duration	1 min	2 min	5 min	10 min	15 min	20 min	30 min	Norm [8]
Heart rate (HR), bpm	82	82	79	78	79	80	81	60–90
RRNN, ms	736	734	760	773	764	751	744	660–937
dRR, ms	125	172	250	250	289	312	312	310–450
SDNN, ms	26	32	46	42	49	52	54	40–80
Mo, ms	750	750	750	789	789	750	750	870–930
AMo, %	59	48	45	45	40	37	35	32–38
CV, %	3.5	4.4	6	5.5	6.4	6.9	7.2	3–12
pNN50, %	7.2	6.7	6.1	5.4	4.7	4.6	5.6	1–9
RMSSD, ms	27.7	26.1	26.5	25.6	24.7	24.7	25.7	20–50
TI, c.u.	315	186	120	115	87	78	75	80–150

database of biomedical signals made available via the PhysioNet portal[2]. Data on healthy patients were taken from the Normal Sinus Rhythm RR Interval Database. Records of sick patients diagnosed with arrhythmias were taken from the MIT-BIH Arrhythmia Database, which contains ECG records of various cardiac rhythm disturbances. It should be noted that in this database there is no differentiation of sick patients according to the type of arrhythmia. Therefore, in this study, the selection of patients was randomized according to the specific type of arrhythmia.

In the present work, the records of 10 healthy patients and 10 patients diagnosed with arrhythmia were selected from the given databases for the purposes of analysis. The age range of the patients is 63–72 years.

To estimate the effective duration of ECG recording, statistical HRV parameters of a healthy patient were preliminarily calculated using rhythmograms of 1, 2, 5, 10, 15, 20, and 30 min duration. The values of the most common temporal and histographic parameters are given in Table 1.

The Norm column of the Table 1 shows the ranges of values of HRV parameters that, according to the authors [5, 9], meet the clinical norm[3].

Within the framework of the task of this work, it is inappropriate to consider recordings of 1-and 2-min duration for which the values of some indices (SDNN, AMo, pNN50, dRR) and TI index differ significantly from the average values.

The advisability of using 5-min recording segments as base samples when analyzing data regardless of the duration of registration is noted in [10]. The consideration of two or three such consecutive segments confirms the conditions of physiological status stability. In the case of rhythm disturbances (arrhythmia), however, it is better to consider recordings having a duration of at least 10 min.

As can be seen from Table 1, SDNN, TI parameters stabilize only at a recording duration of 15 min. Thus, in the present work, recordings of 15 min duration were used to calculate statistical parameters. The choice of this duration is also argued by the fact that, as shown in [8], with 5-min recordings used for rapid diagnosis of CVD, the differences between healthy patients and patients with arrhythmia are not so significant.

It is recommended to estimate spectral and autocorrelation parameters during short ECG recordings (lasting about 5 min) due to their rather rapid stabilization [11]; moreover, at this interval, their changes can be considered as stationary processes.

RESULTS AND DISCUSSION

Table 2 shows HRV parameters for healthy patients; Table 3—for patients with arrhythmia. Confidence intervals were calculated according to the standard methodology for small samples using Student's *t*-test for 95% confidence probability.

[2] The Research Resource for Complex Physiologic Signals. https://physionet.org. Accessed March 24, 2024.

[3] Analysis of heart rate variability. http://protein.bio.msu.ru/~akula/varCI/VarCI.htm (in Russ.). Accessed March 24, 2024.

Table 2. Values of HRV parameters of healthy patients

Parameter \ Patient	1	2	3	4	5	6	7	8	9	10	Average	Norm [8]
HR, bpm	75	82	75	89	108	76	87	77	79	77	82.5 ± 7.3	60–90
RRNN, ms	795	728	805	674	553	789	689	784	762	779	735.8 ± 56.1	660–937
dRR, ms	282	305	398	343	227	375	368	391	422	329	344 ± 43	310–450
SDNN, ms	49	61	41	80	54	76	78	64	73	64	64 ± 9	40–80
Mo, ms	828	727	797	742	594	773	633	797	711	812	741.4 ± 55.5	870–930
AMo, %	41	34	54	27	45	25	41	42	26	40	37.5 ± 6.7	32–38
CV, %	6.1	8.4	5.1	11.8	10	9.6	11.6	8.1	9.6	8.2	8.9 ± 1.5	3–12
pNN50, %	3.9	1.6	2.1	0.7	0.2	13.6	3.1	3.2	8.1	0.5	3.7 ± 3.0	1–9
RMSSD, ms	24	19	20	15	10	41	21	24	31	16	22.1 ± 6.3	20–50
TI, c.u.	88	77	85	53	167	44	88	67	43	74	78.6 ± 25.3	80–150
VLF, %	51	61	74.3	69	53.5	49	72.5	60.4	49.8	40.4	58.1 ± 8.0	15–30
LF, %	35.8	34.5	19.8	23.8	37.9	32	23.1	30.6	34.1	54.6	32.6 ± 7.0	15–40
HF, %	13.2	4.6	5.9	7.2	8.6	19	4.4	9	16.1	5	9.3 ± 3.7	15–25
LF/HF	2.7	7.6	3.3	3.3	4.4	1.6	5.3	3.4	2.1	11	4.5 ± 2.1	1.5–2
LFnorm	73.1	88.3	77	76.9	81.6	62.2	84	77.2	67.9	91.7	78.0 ± 6.4	41.2–60
HFnorm	26.9	11.7	23	23.1	18.4	37.8	16	22.8	32.1	8.3	22.0 ± 6.4	40–58.8
C0	16	31	81	46	44	37	51	28	52	25	41.1 ± 13.1	–
C1	0.72	0.94	0.86	0.93	0.77	0.51	0.87	0.88	0.7	0.89	0.81 ± 0.10	–

Table 3. Values of HRV parameters of sick patients

Parameter \ Patient	1	2	3	4	5	6	7	8	9	10	Average	Norm [8]
HR, bpm	76	74	71	83	66	79	82	74	88	73	76.6 ± 4.6	60–90
RRNN, ms	789	808	841	720	905	759	735	811	680	820	786.8 ± 46.7	660–937
dRR, ms	500	403	342	405	281	711	673	775	997	575	566 ± 160	310–450
SDNN, ms	46	39	46	32	56	83	79	71	147	78	67.7 ± 23.8	40–80
Mo, ms	792	825	869	731	903	761	712	842	581	836	785.2 ± 66.9	870–930
AMo, %	50	50	47	58	32	69	39	37	17	43	44.2 ± 10.2	32–38
CV, %	5.8	4.8	5.4	4.4	6.2	11	10.8	8.8	21.6	9.6	8.8 ± 3.7	3–12
pNN50, %	7.1	26.2	13.2	7.2	26.4	15.7	33.9	14.7	80.4	34.5	25.9 ± 15.4	1–9
RMSSD, ms	54	55	56	45	47	141	126	101	258	110	99.3 ± 47.2	20–50
TI, c.u.	63	75	80	98	63	64	41	28	15	44	57 ± 18	80–150
VLF, %	4.8	4.5	2.1	3.7	9.7	4.1	19.7	14.2	12.3	11	8.6 ± 4.1	15–30
LF, %	6.5	9.6	25.3	3.6	8	8.6	12.3	10.2	15	17.4	11.7 ± 4.5	15–40
HF, %	88.7	85.9	72.6	92.7	82.2	87.3	68	75.6	72.7	71.7	79.7 ± 6.2	15–25
LF/HF	0.07	0.11	0.35	0.04	0.1	0.1	0.18	0.14	0.21	0.24	0.15 ± 0.07	1.5–2
LFnorm	6.8	10	25.8	3.7	8.9	9	15.3	11.9	17.1	19.6	12.8 ± 4.7	41.2–60
HFnorm	93.2	90	74.2	96.3	91.1	91	84.7	88.1	82.9	80.4	87.2 ± 4.7	40–58.8
C0	1	1	2	2	4	1	1	1	1	1	1.5 ± 0.7	–
C1	−0.04	−0.09	0.28	0.05	0.34	−0.5	−0.4	−0.3	−0.22	−0.06	−0.09 ± 0.20	–

The diagram in Fig. 2, which shows the *p*-values of Student's *t*-test (in cases of normal distribution of the trait in both groups) and Mann–Whitney *U* test (in cases where at least in one sample the distribution of the trait is different from normal), demonstrates the differences between the indicators in the groups more clearly. The dashed line corresponds to the selected confidence level of $p = 0.05$.

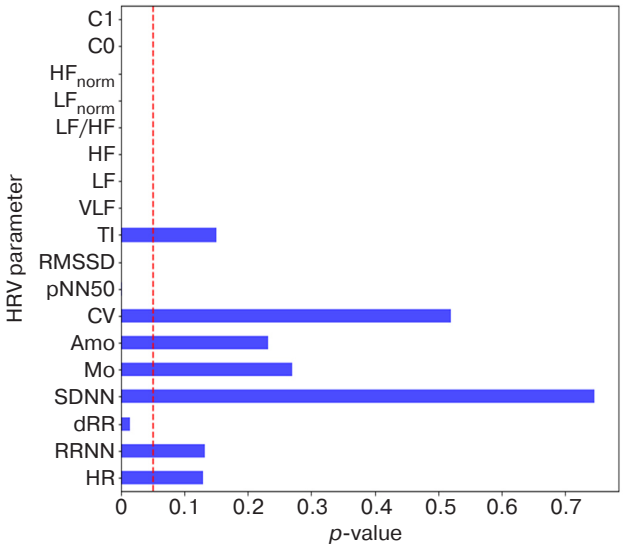

Fig. 2. Diagram of *p*-values for HRV parameters

From an analysis of the parameters of Tables 2 and 3 and the *p*-values of the diagram in Fig. 2, we can conclude that spectral and autocorrelation parameters have the greatest differentiating power for this pathology. Consequently, the inclusion of these parameters in the DF will increase the differentiation between sick and healthy patients. To confirm this assumption, two DFs are compared:

- dependent only on statistical parameters of HRV (stage 1);
- dependent on the complex of HRV parameters: statistical, autocorrelation and spectral (stage 2).

The decision as to which function most adequately separates patients into two clusters will be made based on the results of Student's *t*-test assessing the significance of differences in average values in the two samples.

Stage 1. Discriminant function of statistical indices

1.1. Parameter selection for discriminant analysis

Parameters of an effective DF that carry different information and do not repeat each other should meet the following requirements:

- it is desirable that they have a normal distribution;
- parameters should not be significantly correlated among themselves;
- parameters should be well differentiated in representatives of two groups (differences of average values in the group of healthy and the group of patients should be statistically significant).

An analysis of the data presented in Tables 2 and 3 shows that the values of dRR, RMSSD and pNN50 are very different in healthy and sick patients: the values of dRR are on average 65% higher in the sick group than in the healthy group; RMSSD is 349% higher in the sick group, while pNN50 is 600% higher in the sick group, respectively. Due to RMSSD and pNN50 being highly correlated [12], i.e., interchangeable, RMSSD was used for further analysis.

The AMo parameter usually has a good prognostic significance: exceeding the value of 50% by this parameter is considered as the presence of cardiovascular disease [5]. Therefore, despite the fact that the mode amplitude in patients is on average only 18% higher than in healthy individuals, the decision was taken to include the mode amplitude in the set of DF arguments.

All statistical tests were performed at a significance level of $\alpha = 0.05$.

The hypothesis of normality of parameter distribution was tested using the Shapiro–Wilk test suitable for small samples. The results are summarized in Table 4. The Shapiro–Wilk test statistic is denoted by the letter *W*. The null hypothesis H_0 represents the assumption that a given distribution does not contradict the normal distribution.

It should be noted that, due to irregular rhythmic disturbances in sick patients, the distribution of RR intervals does not tend to normal; thus, the law of distribution of HRV indices may also differ from normal.

Since $W > W_{crit}$, the null hypothesis is not rejected; therefore, there is no reason to believe that the distribution of parameters AMo, dRR, and RMSSD in the group of healthy patients differs from normal.

When applying Student's *t*-test to identify the significance of differences between the average values for each parameter in the group of patients and healthy individuals, it is necessary for the distribution in both samples to correspond to the normal distribution. Table 4 shows that the distribution of the RMSSD parameter in the group of patients with arrhythmia differs from normal. In this case, the *t*-test was replaced by a nonparametric analog comprising a calculation of the Mann–Whitney *U* test, which is less sensitive to distribution deviations from normal and allows us to compare the expression of the parameter in two samples.

The results of Student's *t*-test and the Mann–Whitney *U* test are shown in Table 5. The null hypothesis H_0 in case of the *t*-test rests in the assumption that the differences between the average values in the groups of healthy and sick people are insignificant (or the distribution of the trait in the two groups is the same in the case of the *U* test).

Table 4. Results of testing the hypothesis of normality of distribution of HRV parameters

Group	HRV parameter	Critical value W_{crit}	Calculated value W	Accepted hypothesis
Healthy	AMo	0.842	0.9224	H_0
	RMSSD	0.842	0.9194	H_0
	dRR	0.842	0.9576	H_0
	LF/HF	0.842	0.835	H_0
	C0	0.842	0.9249	H_0
Sick	AMo	0.842	0.9850	H_0
	RMSSD	0.842	0.7976	H_1
	dRR	0.842	0.9533	H_0
	LF/HF	0.842	0.9277	H_0
	C0	0.842	0.6033	H_1

Table 5. Results of Student's *t*-test and Mann–Whitney *U* test

HRV parameters with normal distribution	Critical value t_{crit}	Calculated value t	Accepted hypothesis
AMo	2.101	1.237	H_0
LF/HF	2.101	4.757	H_1
dRR	2.101	3.035	H_1
HRV parameters, the distribution of which differs from the normal distribution	Critical value U_{crit}	Calculated value U	Accepted hypothesis
RMSSD	23	0	H_1
C0	23	0	H_1

As shown in Table 5 the RMSSD and dRR parameters differ markedly between sick and healthy patients. This is because the *t*-statistics value for dRR exceeds the tabulated value, while the *U* value, which is interpreted differently, does not exceed the tabulated value for RMSSD; however, the mode amplitude in this case showed poor discriminatory power. This is most likely due to insufficient sample size, as well as the fact that extrasystoles in patients with arrhythmias strongly affect indices such as TI and AMo. As a result, their values differ little from normal. Nevertheless, in the present work, this indicator was left in place due to its typically high prognostic significance and weak correlation with other HRV parameters. The effectiveness of DF can be additionally evaluated by the value of the coefficient in front of the AMo parameter: it should not be greater than that of the most informative features.

The correlation coefficients were calculated using Pearson's rule and are contained in Table 6 (3 first rows and 3 first columns).

Table 6. Correlation between HRV statistical parameters

Parameter / Parameter	AMo	RMSSD	dRR	LF/HF	C0
AMo	1	−0.52	−0.22	0.22	0.28
RMSSD	−0.52	1	0.58	−0.53	−0.06
dRR	−0.22	0.58	1	−0.30	0.44
LF/HF	0.22	−0.53	−0.30	1	−0.29
C0	0.28	−0.06	0.44	−0.29	1

As Table 6 shows, the correlation between the parameters is weak to moderate (according to the Cheddock scale).

1.2. Standardization and normalization

In the literature on classification methods, standardization [13, 14] or minimax normalization [15, 16] is often used to eliminate differences between parameter units. Otherwise,

DF weights can be misleading regarding the importance of parameters.

Figure 3 shows a characteristic view of a 15-min rhythmogram section with a duration of 1 min, as well as values of HRV parameters calculated from the full (15-min) rhythmogram. Due to large differences in the values of parameters, normalization is necessary to obtain adequate results.

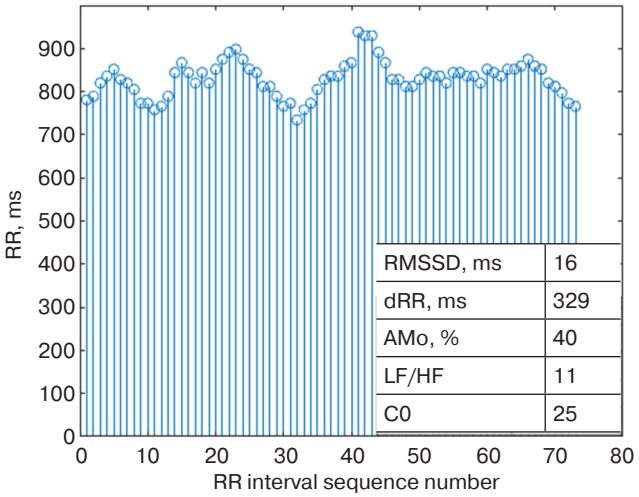

Fig. 3. Rhythmogram section of a healthy patient and HRV parameters

There is no consensus on which method of converting values to a single scale should be preferred. In order to study the differences between the two methods and to identify the most effective one for this study, it was decided to construct two DFs, the parameters of which:

1) have been preliminarily standardized;
2) have been preliminarily normalized.

Standardization was performed using the formula $\frac{x - x_{av}}{\sigma}$, where σ is the SDNN; x_{av} is the average value of the parameter.

Normalization was carried out according to the formula $\frac{x - x_{min}}{x_{max} - x_{min}}$, where x_{min} is the minimum value of the trait; x_{max} is the maximum value of the trait.

1.3. Discriminant analysis

Multivariate discriminant analysis was performed according to the methodology detailed in [17].

The raw data are presented in matrix form. A vector of average values is formed for each trait and each class. Then centered and covariance matrices are calculated. Based on the covariance matrices for two classes (healthy and sick), a general covariance matrix and its inverse matrix are calculated. In order to find the vector of DF coefficients, it is necessary to multiply the matrix inverse to the general covariance matrix by the difference of the two centered matrices.

In the case of standardization, the DF has the following form:

$$DF_s = 1.27 \cdot dRR - 1.73 \cdot AMo - 4.28 \cdot RMSSD. \quad (1)$$

In the case of normalization DF has the following form:

$$DF_n = 4.85 \cdot dRR - 7.217 \cdot AMo - 17.397 \cdot RMSSD. \quad (2)$$

Table 7 shows the results of checking whether the distribution of DF values conforms to the normal law.

According to the Shapiro–Wilk test, the distribution of values of the two DFs in both groups does not contradict the normal distribution. Consequently, to assess the significance of the differences between the averages, we apply Student's *t*-test.

In the case of classification by both DF_s and DF_n (1.44 and 1.94, respectively), the calculated values of Student's *t*-test were less than the critical value of t_{crit} equal to 2.26. Therefore, there is no reason to reject the hypothesis that the average values of DFs in healthy and sick people do not differ.

Figure 4 shows the point distribution of DF values for healthy and sick patients in the case of standardization (a) and normalization (b). The average values of DF are shown with a solid line, while the confidence intervals of DF values are shown with dashed lines. Here, a conclusion about the low efficiency of discrimination becomes obvious, since the confidence intervals of PF values for both groups overlap, and it is not possible to reliably separate the two clusters.

Table 7. Results of testing the hypothesis of normality of distribution of DF values

Group	DF	Critical value W_{crit}	Calculated value W	Accepted hypothesis
Healthy	DF_s	0.842	0.9170	H_0
	DF_n	0.842	0.9157	H_0
Sick	DF_s	0.842	0.8573	H_0
	DF_n	0.842	0.8745	H_0

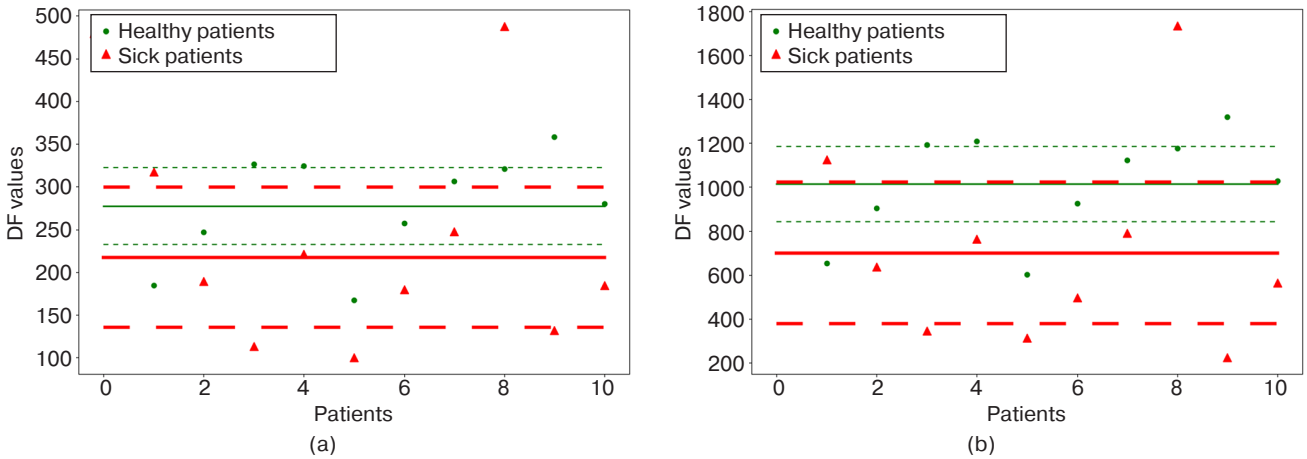

Fig. 4. DF values in case of standardization (a) and normalization (b) (3 parameters) (p = 0.95)

The low efficiency of DF_s and DF_n functions confirms the assumption that statistical parameters are insufficient for reliable arrhythmia detection. This conclusion is confirmed by the results of [8], in which the values of DFs depending on five statistical parameters differed by no more than 25% in healthy patients and patients with arrhythmia.

It is worth noting that both scaling methods assigned the same rank to the traits in terms of their level of contribution to the DF: RMSSD, AMo, dRR (in descending order of importance).

Stage 2. Discriminant function of time, spectral and autocorrelation indices

2.1. Selection of parameters for discriminant analysis

To the previously selected statistical parameters, we added two parameters among the most different in sick and healthy patients: C0 and LF/HF.

From Table 4 it can be seen that the value of W-statistics in the group of sick patients in the case of C0 does not exceed the critical tabular value; since the distribution of this parameter contradicts the normal distribution, while LF/HF statistics correspond to the tabular value within the margin of error, the distribution of this parameter can be considered as not contradicting the normal distribution.

The significance of the differences between the parameters in the two groups was tested using Student's t-test (LF/HF) and the Mann–Whitney U test (C0). Test results are given in Table 5. In both cases, the alternative hypothesis of a statistically significant difference in the values of the parameters in the two groups was confirmed.

The new parameters are weakly or moderately correlated with those introduced earlier. The correlation coefficients between all parameters are shown in Table 6.

2.2. Standardization and normalization of the new parameters

Standardization and normalization of LF/HF and C0 were performed using the calculation formulas given in Section 1.2.

2.3. Discriminant analysis

For standardized parameters, the DF is as follows:

$$DF_s = 0.804 \cdot dRR + 2.732 \cdot AMo + 2.381 \times \\ \times RMSSD - 8.242 \cdot C0 - 5.194 \cdot LF/HF. \quad (3)$$

For normalized parameters DF takes the form:

$$DF_n = 3.357 \cdot dRR + 11.418 \cdot AMo + 9.623 \times \\ \times RMSSD - 27.568 \cdot C0 - 19.162 \cdot LF/HF. \quad (4)$$

Since the hypothesis of normal distribution of DF values was confirmed (the calculated values of W-statistics are given in Table 8), we apply Student's t-test in order to determine the effectiveness of discrimination.

The Student's t-test confirmed the statistical significance of the differences between the averages in the two samples: the value of t-statistics in the case of discrimination by DF_s is equal to 6.67, by DF_n is equal to 6.27, i.e., in both cases it exceeds the critical value of 2.26.

Figure 5 shows the point distribution of DF values for healthy and sick patients in the case of standardization (a) and normalization (b). Average DF values are shown by a solid line, confidence intervals of DF values are shown by a solid range for healthy and sick patients.

It can be seen that the confidence intervals do not overlap, allowing the groups of healthy patients and patients with arrhythmia to be reliably distinguished.

Table 8. Results of testing the hypothesis of normality of distribution of DF values

Group	DF	Critical value W_{crit}	Calculated value W	Accepted hypothesis
Healthy	DF_s	0.842	0.9688	H_0
	DF_n	0.842	0.9682	H_0
Sick	DF_s	0.842	0.9393	H_0
	DF_n	0.842	0.9395	H_0

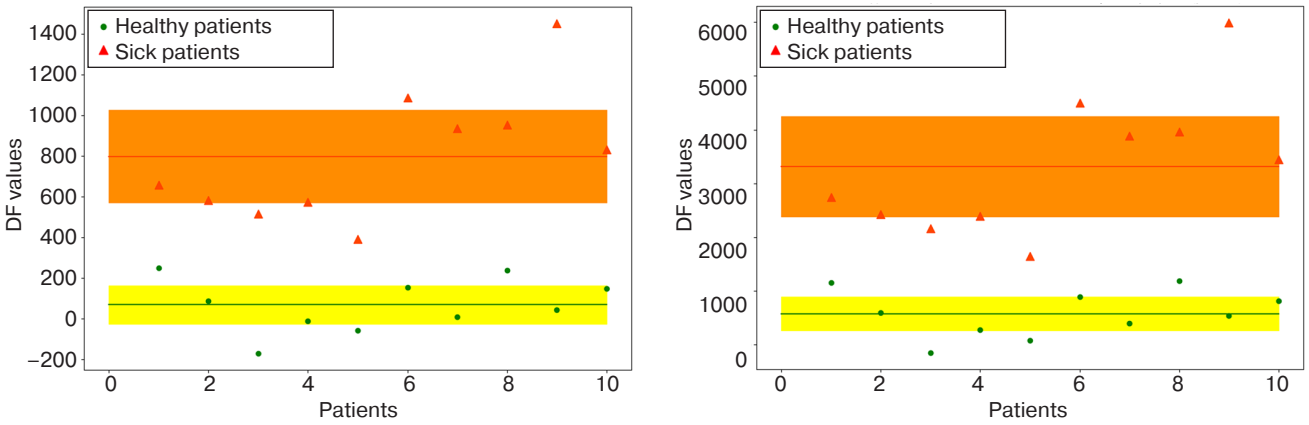

Fig. 5. DF values in case of standardization (a) and normalization (b) (5 parameters)

Both functions arranged the parameters in the same order in decreasing order of their significance: C0, LF/HF, AMo, RMSSD, dRR. Here it should also be noted that the scatter of DF values relative to the average value is identical for both types of scaling, indicating the consistency of the results obtained by standardization and normalization methods.

CONCLUSIONS

The values of variation pulsometry indices for 10 healthy patients and 10 patients with arrhythmia were calculated in this work.

When selecting informative features for MDA, priority was given to the features that have high prognostic significance and those that meet the following criteria: normal distribution, weak correlation, and significantly differing between sick and healthy patients. Two groups of features were formed: a group of statistical parameters (RMSSD, dRR, AMo) and a more representative group that additionally included one spectral and one autocorrelation parameter (RMSSD, dRR, AMo, LF/HF, C0).

DFs were constructed for both groups using different approaches to scaling the values of informative features. Standardization and normalization are shown to lead to the same results: coincidence of the distinguishing ability of the functions and the same estimation of parameter contributions to the DF.

Student's *t*-test clearly demonstrated high classification ability of DF in the case of adding LF/HF and C0 parameters to statistical parameters; DF values for sick and healthy patients overlap neither in the case of standardization nor that of normalization. Thus, it has been shown that MDA can be used to effectively identify differences between patients with arrhythmias and healthy patients. However, it should be noted that the study was conducted on small samples (10 healthy and 10 sick patients); for this reason, these preliminary conclusions are subject to refinement on larger samples.

Authors' contributions

P.A. Sakharova—processing initial data, calculation of parameters, and analysis of the results.

V.A. Balandin—problem statement, development of the research program, analysis of the results.

REFERENCES

1. Ermoshkin V.I. The proposed mechanism of arrhythmia human heart. *Obrazovatel'nyi vestnik "Soznanie" = Educational Bulletin "Consciousness"*. 2013;15(6):4–15 (in Russ.).
2. Getman S.I. Characteristics of Disturbances of Heart Rhythm and Conduction Among Patients Attending Consultation of a Cardiologist at Ambulatory Stage. *Kardiologiya.* 2018;58(6):20–28 (in Russ.). https://doi.org/10.18087/cardio.2018.6.10130
3. Arzykulov Zh.A., Omarov A.A., Kituev B.B., Tursunova F.A., Eshtai A.A., Pavlova N.G. Innovations in the treatment of cardiac arrhythmia. *Vestnik khirurgii Kazakhstana = Bulletin of Surgery in Kazakhstan*. 2012;4(32):4–5 (in Russ.).
4. Ziep B.M., Taratukhin E.O. Heart rate variability assessment and its potential. *Rossiiskii kardiologicheskii zhurnal = Russian Journal of Cardiology*. 2011;6:69–75 (in Russ.).
5. Babunts I.V., Miridzhanyan E.M., Mashaekh Yu.A. *Azbuka analiza variabel'nosti serdechnogo ritma* (*The ABC of Heart Rate Variability Analysis*). Stavropol: Print-Master; 2002. 112 p. (in Russ.).
6. Baevskii R.M., Ivanov G.G., Gavrilushkin A.P., et al. Analysis of heart rate variability using various electrocardiographic systems (Part 1). *Vestnik aritmologii = Journal of Arrhythmology.* 2002;24:65–86 (in Russ.).
7. Bykh A.I., Vysotskaya E.V., Porvan A.P., et al. Using of discriminant analysis for diagnosis chronic cardiac insufficiency on teenagers. *Vestnik Natsional'nogo tekhnicheskogo universiteta Khar'kovskii politekhnicheskii institut. Seriya: Informatika i modelirovanie = Bulletin of the National Technical University Kharkov Polytechnic Institute. Series: Informatics and Modeling*. 2010;31:16–22 (in Russ.).
8. Silkina U.I., Balandin V.A. Discriminant analysis of variational pulsometry parameters. *Rossiiskii tekhnologicheskii zhurnal.* 2020;8(3):81–91 (in Russ.). https://doi.org/10.32362/2500-316X-2020-8-3-81-91
9. Novikov A.A., Smolensky A.V., Mikhailova A.V. Approaches to assessing heart rate variability (literature review). *Vestnik novykh meditsinskikh tekhnologii. Elektronnoe izdanie = J. New Medical Technologies.* 2023;17(3):85–94 (in Russ.). https://doi.org/10.24412/2075-4094-2023-3-3-3
10. Baevsky R.M., Ivanov G.G. Cardiac Rhythm variability: theoretical aspects and opportunities of clinical application. *Ul'trazvukovaya i funktsional'naya diagnostika = Ultrasonnd & Functional Diagnostics*. 2001;3:108–127 (in Russ.).
11. Alejnikova T.V. Heart rate variability (literature review). *Problemy zdorov'ya i ekologii = Health and Ecology Issues*. 2012;1:17–23 (in Russ.). https://doi.org/10.51523/2708-6011.2012-9-1-3
12. Besedina S.A., Balandin V.A. Correlation of heart rhythm variability parameters. *Nauchnyi dialog: Molodoi uchenyi = Scientific Dialog: Young Scientist*. 2017. P. 33–37 (in Russ.). https://doi.org/10.18411/spc-22-11-2017-11
13. Kulikov A.L., Bezdushnii D.I., Osokin V.Yu. Application of linear discriminant analysis for classification of emergency grid emergency states. *Vestnik Ivanovskogo gosudarstvennogo energeticheskogo universiteta = Vestnik of Ivanovo State Power Engineering University*. 2020;5:38–47 (in Russ.). https://doi.org/10.17588/2072-2672.2020.5.038-047
14. Sukiasyan A.G., Markina V.S., Mitrofanov D.P., Shabalina U.M. Clustering departments of integrated groups of enterprises according to level of risk based on methods of multivariate statistical analysis. *Fundamental'nye issledovaniya = Fundamental Research*. 2019;5:115–125 (in Russ.).
15. Budko O.N., Senko E.V. Classification functions for express diagnostics of the degree of disease with arterial hypertension. In: *BIG DATA Advanced Analytics: Collection of Materials of the Fourth International Scientific and Practical Conference*. 2018. P. 360–365 (in Russ.). Available from URL: https://elib.grsu.by/doc/48339
16. Pavlenkov M.N., Smirnova N.A. Development of technology for the assessment of stability of an enterprise of the chemical complex. *Statistika i Ekonomika = Statistics and Economics*. 2013;3:66–69 (in Russ.).
17. Sizykh D.S., Sizykh N.V. Features of teaching methods of discriminant analysis for training specialists in the direction of "Business Informatics". In: Isaev Y.N., Pavlov I.V. (Eds). *Obrazovanie: opyt i perspektivy razvitiya* (*Education: Experience and Development Prospects*). Cheboksary: Sreda; 2019. P. 107–133 (in Russ.). https://doi.org/10.31483/r-33128

СПИСОК ЛИТЕРАТУРЫ

1. Ермошкин В.И. Предполагаемый механизм возникновения аритмии сердца человека. *Образовательный вестник «Сознание»*. 2013;15(6):4–15.
2. Гетман С.И. Распространенность нарушений ритма сердца и проводимости среди обратившихся за медицинской помощью к кардиологу на амбулаторном этапе. *Кардиология*. 2018;58(6):20–28. https://doi.org/10.18087/cardio.2018.6.10130
3. Арзыкулов Ж.А., Омаров А.А., Китуев Б.Б., Турсунова Ф.А., Ештай А.А., Павлова Н.Г. Инновации в лечении аритмии сердца. *Вестник хирургии Казахстана*. 2012;4(32):4–5.
4. Зиеп Б.М., Таратухин Е.О. Возможности методики вариабельности сердечного ритма. *Российский кардиологический журнал*. 2011;6:69–75.
5. Бабунц И.В., Мириджанян Э.М., Машаех Ю.А. *Азбука анализа вариабельности сердечного ритма*. Ставрополь: Принт-мастер; 2002. 112 р.
6. Баевский Р.М., Иванов Г.Г., Гаврилушкин А.П. и др. Анализ вариабельности сердечного ритма при использовании различных электрокардиографических систем (часть 1). *Вестник аритмологии*. 2002;24:65–86.
7. Бых А.И., Высоцкая Е.В., Порван А.П., Рак Л.И. и др. Использование дискриминантного анализа для диагностики хронической сердечной недостаточности у подростков. *Вестник Национального технического университета Харьковский политехнический институт. Серия: Информатика и моделирование.* 2010;31:16–22.

8. Силкина У.И., Баландин В.А. Дискриминантный анализ параметров вариационной пульсометрии. *Российский технологический журнал*. 2020;8(3):81–91. https://doi.org/10.32362/2500-316X-2020-8-3-81-91
9. Новиков А.А., Смоленский А.В., Михайлова А.В. Подходы к оценке показателей вариабельности сердечного ритма (обзор литературы). *Вестник новых медицинских технологий.* 2023;17(3):85–94. https://doi.org/10.24412/2075-4094-2023-3-3-3
10. Баевский Р.М., Иванов Г.Г. Вариабельность сердечного ритма: теоретические аспекты и возможности клинического применения. *Ультразвуковая и функциональная диагностика*. 2001;3:108–127.
11. Алейникова Т.В. Вариабельность сердечного ритма (обзор литературы). *Проблемы здоровья и экологии*. 2012;1:17–23. https://doi.org/10.51523/2708-6011.2012-9-1-3
12. Беседина С.А., Баландин В.А. Корреляция показателей вариабельности сердечного ритма. *Научный диалог: Молодой ученый*. 2017. С. 33–37. https://doi.org/10.18411/spc-22-11-2017-11
13. Куликов А.Л., Бездушный Д.И., Осокин В.Ю. Применение линейного дискриминантного анализа для классификации аварийных режимов электрической сети. *Вестник Ивановского государственного энергетического университета*. 2020;5:38–47. https://doi.org/10.17588/2072-2672.2020.5.038-047
14. Сукиасян А.Г., Маркина В.С., Митрофанов Д.П., Шабалина У.М. Кластеризация подразделений интегрированной группы предприятий по уровню риска на основе методов многомерного статистического анализа. *Фундаментальные исследования*. 2019;5:115–125.
15. Будько О.Н., Сенько Е.В. Классификационные функции для экспресс-диагностики степени заболевания артериальной гипертензией. В сб.: *BIG DATA и анализ высокого уровня: материалы Четвертой Международной научно-практической конференции.* 2018. С. 360–365. URL: https://elib.grsu.by/doc/48339
16. Павленков М.Н., Смирнова Н.А. Разработка технологии оценки устойчивости предприятия химического комплекса. *Статистика и Экономика.* 2013;3:66–69.
17. Сизых Д.С., Сизых Н.В. Особенности преподавания методов дискриминантного анализа для подготовки специалистов по направлению «Бизнес-информатика». В кн.: *Образование: опыт и перспективы развития*; под ред. Ю.Н. Исаева, И.В. Павлова. Чебоксары: ИД «Среда»; 2019. С. 107–133. https://doi.org/10.31483/r-33128

About the authors

Polina A. Sakharova, Bachelor, Institute of Artificial Intelligence, MIREA – Russian Technological University (78, Vernadskogo pr., Moscow, 119454 Russia). E-mail: polinka6777@gmail.com. https://orcid.org/0009-0008-1323-9308

Vyacheslav A. Balandin, Cand. Sci. (Phys.-Math.), Assistant Professor, Department of Biocybernetics Systems and Technologies, Institute of Artificial Intelligence, MIREA – Russian Technological University (78, Vernadskogo pr., Moscow, 119454 Russia). E-mail: admiral49@mail.ru. Scopus Author ID 7003691025, RSCI SPIN-code 1288-9918

Об авторах

Сахарова Полина Александровна, бакалавр, Институт искусственного интеллекта, ФГБОУ ВО «МИРЭА – Российский технологический университет» (119454, Россия, Москва, пр-т Вернадского, д. 78). E-mail: polinka6777@gmail.com. https://orcid.org/0009-0008-1323-9308

Баландин Вячеслав Алексеевич, к.ф.-м.н., доцент, кафедра биокибернетических систем и технологий, Институт искусственного интеллекта, ФГБОУ ВО «МИРЭА – Российский технологический университет» (119454, Россия, Москва, пр-т Вернадского, д. 78). E-mail: admiral49@mail.ru. Scopus Author ID 7003691025, SPIN-код РИНЦ 1288-9918

Translated from Russian into English by Lyudmila O. Bychkova
Edited for English language and spelling by Thomas A. Beavitt

MIREA – Russian Technological University.
78, Vernadskogo pr., Moscow, 119454 Russian Federation.
Publication date January 30, 2025.
Not for sale.

МИРЭА – Российский технологический университет.
119454, РФ, г. Москва, пр-т Вернадского, д. 78.
Дата опубликования 30.01.2025 г.
Не для продажи.